The Role of Wnt/Planar Cell Polarity Signaling in Mouse Facial Branchiomotor Neuron Migration

---

A Dissertation Presented to
the Faculty of the Graduate School
at the University of Missouri

In Partial Fulfillment
of the Requirements for the Degree

Doctor of Philosophy

---

by
DERRICK M. GLASCO

Dr. Anand Chandrasekhar, Dissertation Advisor

JULY 2011

The undersigned, appointed by the Dean of the Graduate School, have examined the dissertation entitled

The Role of Wnt/Planar Cell Polarity Signaling in
Mouse Facial Branchiomotor Neuron Migration

presented by Derrick M. Glasco,

a candidate for the degree of Doctor of Philosophy of Biological Sciences,

and hereby certify that, in their opinion, it is worthy of acceptance.

_____

Professor Anand Chandrasekhar

_____

Professor Elizabeth Bryda

_____

Professor Dawn Cornelison

_____

Professor Samuel Waters

_____

Professor Richard Tsika

ACKNOWLEDGEMENTS

I could easily write a book detailing how so many people have been instrumental in my graduate training and research over the past six years. But let me instead briefly acknowledge the following people who I am greatly indebted to:

***Anand Chandrasekhar**, my mentor, Division of Biological Sciences* – There is a reason that I started my rotations in your lab but never left: You are an outstanding scientist and a kind mentor. You have challenged me in countless ways, and are a great example of success through resourcefulness, dedication, and persistence. Thank you for always looking out for my best interests, and for your generous financial and personal support.

*The members of my graduate committee: **Sam Waters** and **D. Cornelison**, Division of Biological Sciences; **Elizabeth Bryda**, Department of Veterinary Pathobiology; and **Richard Tsika**, Department of Biochemistry* – Each of you has contributed uniquely to my training and development as a scientist. Your expertise and perspectives on developmental biology and the mouse model have been invaluable. Thank you for being challenging, yet merciful, in the review process.

***Anagha Sawant**, former lab colleague, currently in the Department of Veterinary Pathobiology* – We started our graduate journey together and made it out alive! You are a dear friend. Thank you for your everyday help and support, and for making those mundane tasks of daily lab work more exciting.

***Vinoth Sittaramane**, Division of Biological Sciences* – There has never been a question I've had for which you haven't been willing to go through great lengths to find an answer. You are a man of great scientific ideas. Thank you for your friendship and support.

***Gary Vanderlaan**, former lab colleague, Division of Biological Sciences* – Thank you for taking me under your wing when I was a beginning graduate student. You challenged me intellectually every day. I have come to realize just how valuable those times at the whiteboard were, where you explained and re-explained concepts to me.

***Xiufang Pan**, Division of Biological Sciences* – You are an inspiration as to how productive a focused, quietly working scientist can be. Thank you for your support.

***Bernd Fritzsch**, Department of Biology, University of Iowa* – The many visits to your lab were challenging and productive. Thank you for the countless hours you spent one-on-one giving me a crash course in neuroanatomy and tying my seemingly miscellaneous bits of scientific knowledge into an exciting narrative.

***Angelo Iulianella**, Department of Anatomy and Neurobiology, Dalhousie University* – It may have seemed small to you, but the week we spent together in Paul Trainor's lab at the Stowers Institute for Medical Research was invaluable to me. You taught me the basics about mouse dissections, embryology, and *in situ* hybridization, and I've carried those skills with me ever since.

***Jon Dehaven**, Office of Animal Resources* – Thank you for your diligent and knowledgeable care of the mouse colony. It has been a pleasure working with you.

***Julia Rodriguez**, C. S. Bond Life Sciences Center* – Thank you for your joyful assistance through three rounds of NRSA Predoctoral Fellowship applications. You taught me a lot about the process.

***Maureen Kemp**, C. S. Bond Life Sciences Center* – I never imagined graduate school would involve so much paperwork and administrative tasks. Thank you for helping me through it all.

And last, but not least…

Crystal, my wife – You have given me a wonderfully balanced and enjoyable life, not just a career. Thank you for being there every day, listening to me explain my latest findings, and for always encouraging me. I love you!

TABLE OF CONTENTS

LIST OF TABLES

LIST OF FIGURES

ABSTRACT

Neuronal migration is a developmental process essential to the formation of distinct neural layers and functional neural networks in the central nervous system. Defective neuronal migration is an underlying cause of several human diseases; therefore, it is important to better understand the mechanisms regulating this process. As a model, we study the migration of facial branchiomotor neurons (FBMNs) in the developing mouse hindbrain. These neurons, which control facial expressions, migrate caudally during development from rhombomere 4 (r4) to r6. Several components of the Wnt/planar cell polarity (PCP) pathway have been demonstrated to regulate FBMN migration in zebrafish, but a role for Wnt/PCP signaling in mouse FBMN migration had not been previously tested. Therefore, we analyzed whether FBMN migration was affected in Wnt/PCP mutant mice.

Vangl2 encodes a four-pass transmembrane protein and is a core component of Wnt/PCP signaling. It is expressed in the ventricular zone of the neural tube and in FBMNs throughout their migration. In *Vangl2*$^{Lp/+}$ embryos, FBMNs failed to migrate caudally from r4 into r6, instead forming elongated facial motor nuclei spanning r4 and r5. FBMNs in *Vangl2*$^{Lp/Lp}$ embryos were arrested in r4 and most FBMNs failed to migrate radially to the pial surface of the neural tube. However, hindbrain patterning and FBMN progenitor specification were intact, and FBMNs did not transfate into other neuron types, indicating a specific role for *Vangl2* in neuronal migration. Consistent with this, FBMNs failed to migrate in *Vangl2* knockout embryos.

Studies in zebrafish suggest that FBMN migration is regulated independent of the Wnt/PCP pathway, since some, but not all, Wnt/PCP genes regulate FBMN migration. We tested whether this was also the case in mammals. Embryos null for *Ptk7*, a regulator of PCP signaling, had severe defects in caudal FBMN migration. However, FBMNs migrated normally in *Dishevelled (Dvl) 1/2* double mutants, and in zebrafish embryos with disrupted *dvl* signaling, indicating *Dvl* function is largely dispensable for FBMN migration. Consistent with this, loss of *Dvl2* function in $Vangl2^{Lp/+}$ embryos did not exacerbate the $Vangl2^{Lp/+}$ FBMN migration phenotype. Together, these results suggest strongly that the caudal migration of FBMNs is controlled by multiple components of the Wnt/PCP pathway, yet may not require the central signaling molecule Dishevelled.

Celsr1 encodes a cell adhesion molecule that is expressed broadly in the developing hindbrain, including the floor plate and ventricular zones, but not in differentiated FBMNs. In $Celsr1^{Crsh}$ mutants, many FBMNs migrated in the wrong direction, moving rostrally into r2 instead of caudally into r6. This aberrant migration was not a consequence of defects in hindbrain patterning, axon guidance, or misspecification of FBMNs. Interestingly, caudal FBMN migration was largely unaffected, indicating a specific role for *Celsr1* in the directionality of FBMN migration. Defects in migration directionality have not been previously described in any zebrafish or mouse mutants, and these results demonstrate that directionality of migration is a distinctly regulated process.

To better understand how *Celsr1* regulates the directionality of FBMN migration, we investigated the spatial requirement for *Celsr1* function using several tissue-specific Cre lines whose activities overlap with the *Celsr1* expression domain. Since *Celsr1* is strongly expressed in the floor plate, we first examined whether the floor plate itself is necessary for migration. In *Gli2* mutants, which lack a floor plate, FBMNs failed to migrate caudally, signifying a role for the floor plate. However, deletion of *Celsr1* function in the floor plate did not generate any FBMN migration defects. On the other hand, inactivation of *Celsr1* in r3/r5 and r4 each resulted in the rostral migration of FBMNs, but in differing severities. Using anterograde labeling with lipophilic dyes, we found that the position of individual FBMNs within r4 correlated with the direction of migration in *Celsr1*$^{Crsh/+}$ mutants. Together, these results indicate that *Celsr1* is required in the ventricular zone of multiple rhombomeres to regulate the direction of FBMN migration, and provides insight as to how only a subset of FBMNs is affected in *Celsr1* mutants.

These findings have led to new insight as to how FBMN migration is regulated in mammals. The requirement for many Wnt/PCP components such as *Vangl2*, *Ptk7*, and *Celsr1*, but not *Dvl*, suggests that FBMN migration is not a PCP dependent process and that some Wnt/PCP components may possess novel functions outside of Wnt/PCP signaling. Our analysis of *Celsr1* mutants has also revealed that the directionality of FBMN migration and the ability to migrate caudally are differentially regulated. Since rostrally migrating FBMNs in *Celsr1*$^{Crsh/+}$ embryos emanate exclusively from the rostral part of r4, and *Celsr1* functions non-cell autonomously in r3 and r4 to regulate FBMN

directionality, we suspect that *Celsr1* may regulate guidance cues in the anterior hindbrain. Future studies will seek to elucidate potential guidance cues mediated by *Celsr1*, and will aim to determine whether Wnt/PCP components are broadly required for the migration of other neuron types in the central nervous system.

CHAPTER 1: Introduction

Directed cell migration is a fundamental process in physiology and disease. To renew skin tissue, for example, precursor cells continuously migrate up from the basal layer of the epidermis. As part of immune surveillance, leukocytes exit the bloodstream and migrate into tissues to eliminate infectious pathogens. In metastatic cancer, tumor cells acquire the ability to migrate into the bloodstream and form secondary tumors upon invading other tissues. Other chronic diseases, such as atherosclerosis and arthritis, are also a consequence of aberrant cell migration (Horwitz and Webb, 2003).

Cell migration is also a critical process during embryonic development. During gastrulation, blastula cells migrate extensively to establish a multi-layered body plan (Gilbert et al., 2006). Later, cell migration underlies convergence and extension cell movements during neurulation, body axis elongation, and organogenesis (Wallingford et al., 2002). During brain development, the migration of neurons within the central nervous system is essential for the formation of the complex neural circuitry. The distance of neuronal migration can vary considerably, and in humans, some neurons can migrate several centimeters (hundreds of cell body distances) within the cortex. Since defective neuronal migration is associated with several human disorders, it is important to understand this process and its fundamental role in assembling the nervous system.

1.1. Overview of Neuronal Migration

1.1.1. Cellular dynamics of migrating neurons

The cellular dynamics of neuronal migration (**Figure 1.1 A-C**) have been well described in cortical neurons, where migration can be divided into three separate phases. First, directional determination is made by filopodia and lamelipodia interpreting signals from the environment, resulting in the extension of one or more leading processes. Next, nucleokinesis occurs when the nucleus and perinuclear material translocate towards the leading process. Finally, the trailing process is retracted (Lambert de Rouvroit and Goffinet, 2001). Though little is understood about the process of retraction, it is clear that leading process extension and nucleokinesis occur asynchronously (Tsai and Gleeson, 2005), suggesting that they are each regulated distinctly. Furthermore, different classes of neurons may alter this basic migratory cycle depending upon location and time (Valiente and Marin, 2010), indicating that neuronal migration is a highly dynamic process.

Leading Process Dynamics

Leading processes have distinct morphologies in different neuron classes. In general, radially migrating neurons extend single processes, whereas the processes of tangentially migrating neurons are elaborately branched. The stabilization and retraction of these branches, as well as their orientation, are based on signals received from guidance cues in the environment (Valiente and Marin, 2010). Their stability is

also dependent upon longitudinally arranged microtubules extending along the process into the soma, which provides structural support and enables vesicular transport vital for intracellular communication. The signaling mechanisms underlying leading process branching are obscure, but recent studies suggest that branching is partly determined by environmental guidance cues which affect intracellular Ca^{2+} and cAMP levels. At least in cerebellar granule cells, increased intracellular Ca^{2+} levels stimulate branching, whereas reducing the intracellular Ca^{2+} concentration reduces the frequency of branching (Kumada et al., 2009).

Nucleokinesis

Nucleokinesis, the movement of the nucleus and perinuclear material towards the leading process, utilizes many of the same signaling molecules and cytoskeletal components used in mitosis (Morris et al., 1998; Tsai and Gleeson, 2005). In a migrating neuron, a swelling first appears at the proximal end of the leading process, into which the centrosome (microtubule organizing center) and Golgi move (Tsai and Gleeson, 2005). Microtubules emanating from the centrosome extend anteriorly into the leading process and posteriorly to encase the nucleus. This encasing of the nucleus is accompanied by enrichment of the actin cytoskeleton at the anterior and posterior poles. The centrosome then moves up the leading process and is followed by the nucleus and perinuclear material. There is some evidence to indicate that the centrosome exhibits a pulling force on the nucleus; however, in organotypic slices of migrating granule cells, nuclei can be observed migrating past the centrosome

(Umeshima et al., 2007), suggesting that other mechanisms are also possible. Dynein motor proteins are known to be critical for pulling the nucleus towards the centrosome and leading process (Tsai and Gleeson, 2005); however, it is unclear whether dynein acts at the nuclear membrane or leading edge. In either case, coupling of the nucleus and centrosome is a key event in neuronal migration.

Figure 1.1. Cellular dynamics and modes of radial neuronal migration in the cortex.

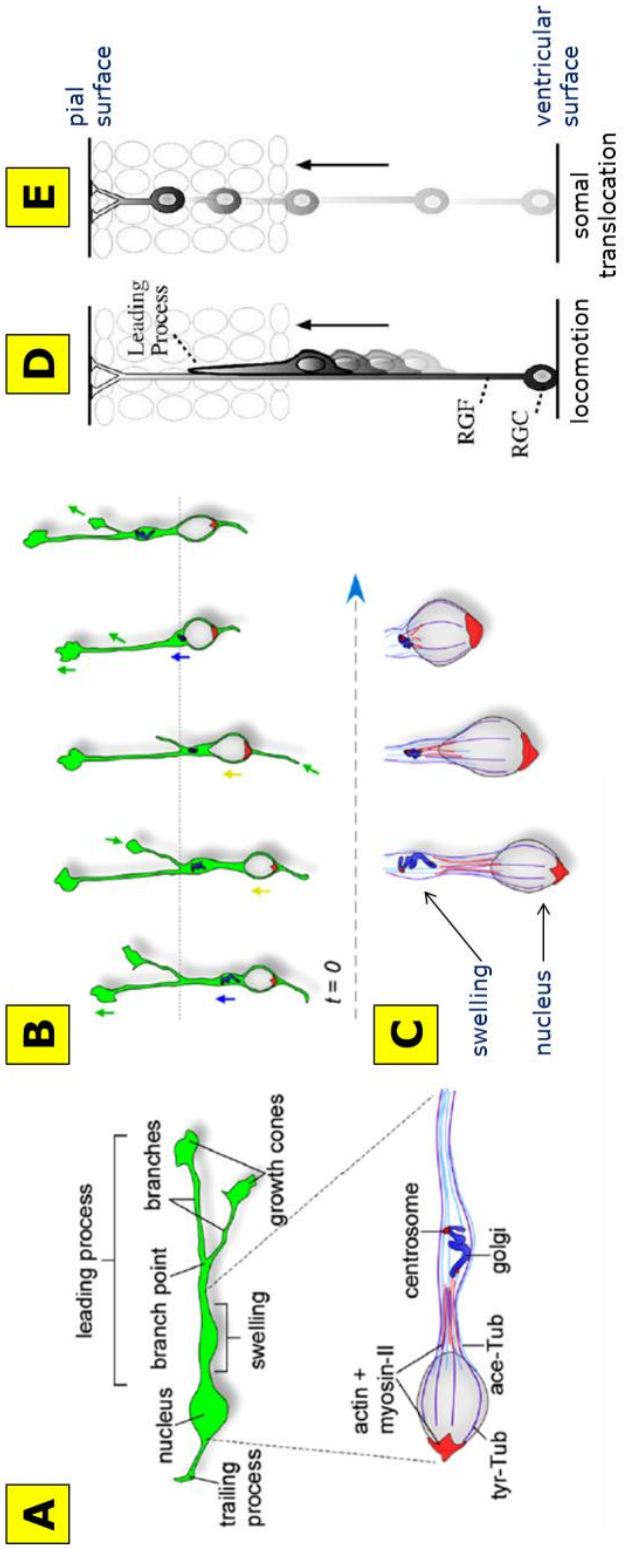

Figure 1.1. Cellular dynamics and modes of radial neuronal migration in the cortex.

A, Structures in a migrating interneuron, with a higher magnification image of the nucleus, centrosome, and Golgi pictured below. **B**, The cycle of migration in cortical interneurons. First, the leading process (green arrow) branches, and the swelling, containing the nucleus and Golgi, move forward (blue arrow). Next, one branch of the leading process is selected, and the nucleus moves forward to the branch point (yellow arrow). The cycle repeats beginning with the growth of a new process. **C**, A high magnification view of nucleokinesis, showing the cytoskeletal connections between the swelling (and leading process) and the nucleus. **D-E**, Two modes of radial neuronal migration in the neocortex, locomotion and somal translocation. **D**, Neurons undergoing locomotion use radial glial fibers as a substrate and maintain a lengthy leading process throughout their migration (black arrow) towards the pial surface. **E**, Neurons undergoing somal translocation have a radial fiber connected to the pial surface and migrate considerably faster than locomoting cells (65 µm/hr vs. 30 µm/hr). Abbreviations: tyr-Tub, tyrosinated tubulin; ace-tub, acetylated tubulin; t, time; RGC, radial glial cell; RGF, radial glial fiber. **A-C** modified from: Manuel Valiente and Oscar Marín. Neuronal migration mechanisms in development and disease. *Current Opinion in Neurobiology* 20:68-78 (2010). **D-E** modified from: Takao Honda *et al.* Cellular and molecular mechanisms of neuronal migration in neocortical development. *Seminars in Cell & Developmental Biology* 14:169-174 (2003).

1.1.2. Radial neuronal migration

Radial migration accompanies the maturation of all neurons in the CNS and involves the translocation of the cell body from the ventricular proliferative zone towards the outer (pial) surface of the brain (**Figure 1.1 D-E**). At the earliest stages of cortical layer formation, most radially-migrating neurons extend a projection to connect to the pial surface of the brain, then undergo somal translocation towards the pial surface independent of a guiding substrate (Nadarajah and Parnavelas, 2002). Upon thickening of the brain tissue, 80-90% of all radially-migrating neurons in the cortex attach to and migrate along radially-oriented glial cells (Anton et al., 1996; Hatten, 1999, 2002; Nadarajah and Parnavelas, 2002). Whether a neuron undergoes somal translocation or locomotion is not cell type-specific, because many cortical neurons change from locomotion to somal translocation once their leading processes reach the pial surface (Nadarajah et al., 2001). Radial glial cells, though serving as a substrate for migrating neurons, can divide and produce neuronal precursors (Miyata et al., 2001; Noctor et al., 2001). The daughter cell inheriting the pia-connected radial glial fiber can then undergo somal translocation towards the pial surface and differentiate into a neuron (Miyata et al., 2001; Miyata et al., 2002). When migration across the glial scaffold is finished, neurons are locked into position as radial glial cells begin to transform into stellate astrocytes and axonal connections are formed (Hatten, 1999).

Radial migration is of special significance in the cortex, where it produces the highly laminated “inside out” arrangement of neurons. In mice, the earliest groups of postmitotic neurons migrate to form the preplate directly above the ventricular zone.

This preplate contains afferent and efferent fibers as well as Cajal-Retzius neurons. Next, more neurons exit the cell cycle and migrate radially from the ventricular zone to invade the preplate, forming the cortical plate. This divides the preplate into a superficial marginal zone, which contains Cajal-Retzius neurons, and a subplate near the ventricular zone. As a result of this migration sequence, the earliest born neurons are located more near the ventricular zone, whereas the later born neurons are located more superficially (Hatten, 1999; Honda et al., 2003; Pearlman et al., 1998). This "inside-out" arrangement is partly controlled by Reelin, a large glycoprotein secreted by superficial Cajal-Retzius neurons but not migratory neurons (D'Arcangelo et al., 1995; Ogawa et al., 1995). In *Reeler* (*Reelin* -/-) mice, later migrating neurons fail to invade the preplate and instead accumulate beneath the marginal zone and subplate cells. Later generated cells then continue to accumulate beneath preexisting neurons superficially (Hatten, 1999; Honda et al., 2003; Pearlman et al., 1998).

When secreted by Cajal-Retzius neurons of the marginal zone, Reelin dimerizes then binds to one of three receptor complexes: Very Low Density Lipoprotein Receptor (VLDLR) and Apolipoprotein E receptor-2 (ApoER2), Cadherin-related Neural Receptor (Cnr), or Integrin-α3β1 (Guerrini and Parrini, 2010). In cultured primary embryonic neurons, binding of Reelin to either VLDLR/ApoER2 or Cnr subsequently leads to the phosphorylation and activation of the cytoplasmic protein Dab1 (Hiesberger et al., 1999; Senzaki et al., 1999), which interacts with targets that alter microtubule function to promote nuclear and soma migration. On the other hand, binding of Reeler to Integrin-α3β1 generates a stop signal that halts migration (Dulabon et al., 2000).

Overall, these results indicate that we have a fairly comprehensive understanding of the mechanisms that regulate radial neuronal migration.

1.1.3. Tangential neuronal migration

Tangential migration is the glia-independent migration of neurons orthogonal to the direction of radial migration. In contrast to radial migration which establishes distinct neural layers, tangential migration generates neuronal diversity within a given brain region (Marin and Rubenstein, 2003). Tangentially migrating neurons attach to diverse substrates. Migrating olfactory interneurons appear to use neighboring neurons as a substrate, whereas neurons expressing Gonadtropin-releasing hormone attach to axons as they migrate (Marin and Rubenstein, 2003). Substrates for GABAergic interneurons and facial branchiomotor neurons are less clear (Hatten, 2002; Marin and Rubenstein, 2003; Pearlman et al., 1998).

1.1.4. Consequences of defective neuronal migration

Several human disorders are associated with defective neuronal migration and typically affect specific neuron types or brain regions. Lissencephaly, heterotopia, polymicrogyria, Aicardi syndrome, and focal cortical dysplasia are all considered neuronal migration disorders. Grouped together, the most common symptoms include cognitive impairment, motor impairment, and epilepsy, which can range in severity

(Copp and Harding, 1999; Gleeson and Walsh, 2000; Guerrini and Parrini, 2010; Pearlman et al., 1998). Since both lissencephaly and periventricular heterotopia affect cortical neuron migration and are well described genetically, they are discussed below.

Lissencephaly

Classic (type I) lissencephaly is characterized by a thickened cortex accompanied by absent or decreased cortical convolutions. Patients exhibit severe mental retardation, developmental delays, seizures, and often shortened life spans. Due to the incomplete migration of cortical neurons, the lissencephalic cortex is severely disorganized with four non-organized layers instead of six highly organized layers (Copp and Harding, 1999; Gleeson and Walsh, 2000; Guerrini and Parrini, 2010; Hatten, 2002; Mochida, 2009; Pearlman et al., 1998). Most genes implicated in lissencephaly are directly related to microtubule function. TUBA1A is an isoform of α-tubulin expressed in the brain (Poirier et al., 2007), whereas LIS1 and doublecortin (DCX) are regulators of microtubule dynamics in neurons. LIS1 interacts with dynein motors, which are critically involved in nucleus/centrosome movements during migration, and DCX binds directly to microtubules and stabilizes them (Mochida, 2009). Reelin (RELN) and VLDLR have also been associated with lissencephaly, but to a lesser extent. Interestingly, LIS1 forms a complex with phosphorylated DAB1 (Mochida, 2009), which is a central molecule in RELN/VLDLR signaling.

Cobblestone (type II) lissencephaly is characterized by the appearance cobblestone-like nodules on the surface of the cortex. In this disorder, the integrity of

the pial surface of the cortex is compromised, resulting in the over-migration of cortical neurons across the pial surface (Mochida, 2009). Six different genes have been associated with this disorder (Guerrini and Parrini, 2010).

Periventricular nodular heterotopia

Periventricular nodular heterotopia (PNH) is characterized by the presence of nodules lining the ventricle walls of the cortex. These nodules contain differentiated neurons which failed to initiate migration to the pial surface (Gleeson and Walsh, 2000). Though many genes associated with PNH are scattered throughout the genome, nearly 100% of families and 26% of individual PNH patients exhibit mutations in *Filamen A (FLNA)* (Parrini et al., 2006). FLNA is an actin-binding protein important for the orthogonal branching of actin filaments and helps sustain actin networks at the leading edge of migratory cells. It is expressed in the ventricular zone of the cortex during development and is strongly expressed in the soma and leading edge projections of migrating neurons (Fox and Walsh, 1999). Since *FLNA* is on the X chromosome, mutations in *FLNA* are embryonic lethal for males, whereas females exhibit a mosaic phenotype due to random X-inactivation. In females, many neurons migrate normally and the cortex has an otherwise normal appearance and layer formation; they are epileptic but often of normal intelligence (Gleeson and Walsh, 2000; Guerrini and Parrini, 2010; Parrini et al., 2006).

Defective neuronal migration has severe health consequences. Therefore, it is important to understand the mechanisms underlying this process. To gain better insight

into neuronal migration mechanisms, our work focuses on facial branchiomotor neurons (FBMNs) in the hindbrain. FBMNs undergo both tangential and radial migrations within the hindbrain and are easily visualized. Therefore, they are an excellent model system for understanding the mechanisms of neuronal migration.

1.2. Facial Branchiomotor Neuron Migration

1.2.1. Neural anatomy of the developing mouse hindbrain

The hindbrain is an embryonic structure which develops into the cerebellum, pons, and medulla (Gilbert et al., 2006). During development, the hindbrain is divided into transient segments called rhombomeres, each which express unique combinations of Hox genes and other transcription factors (Lumsden and Krumlauf, 1996). Different rhombomeres are also distinguished by differential cell adhesion and cell mobility, as cells from adjacent rhombomeres do not mix (Guthrie and Lumsden, 1991; Lumsden, 2004).

The hindbrain contains an array of somatomotor, visceromotor, and branchiomotor neurons (**Figure 1.2**) which are organized similarly in many vertebrates such as mouse, zebrafish, and chicken (Chandrasekhar, 2004). Somatomotor neurons, such as the abducens (nVI) motor nuclei, innervate skeletal muscle; visceromotor neurons, including the superior salivatory nuclei (part of nVII), innervate glands and smooth muscles; and branchiomotor neurons (BMNs) innervate muscles derived from

the branchial arches (Wilson-Pauwels et al., 1988). Trigeminal (nV) BMNs in r2/r3 send their axons out of r2 and innervate muscles involved in mastication. FBMN (nVII) axons exit r4 and innervate muscles involved in voluntary facial expression. In most vertebrates, excluding chicken, FBMN cell bodies are located caudal to r4, and their axons wrap around the abducens (nVI) nuclei to form the internal genu of the facial nerve (Chandrasekhar, 2004; Wilson-Pauwels et al., 1988). This unique route of the facial nerve is a consequence of the caudal migration of FBMN cell bodies from r4 to more caudal locations during development.

Figure 1.2. Organization of cranial motor neurons in r2 – r6 of the developing mouse hindbrain.

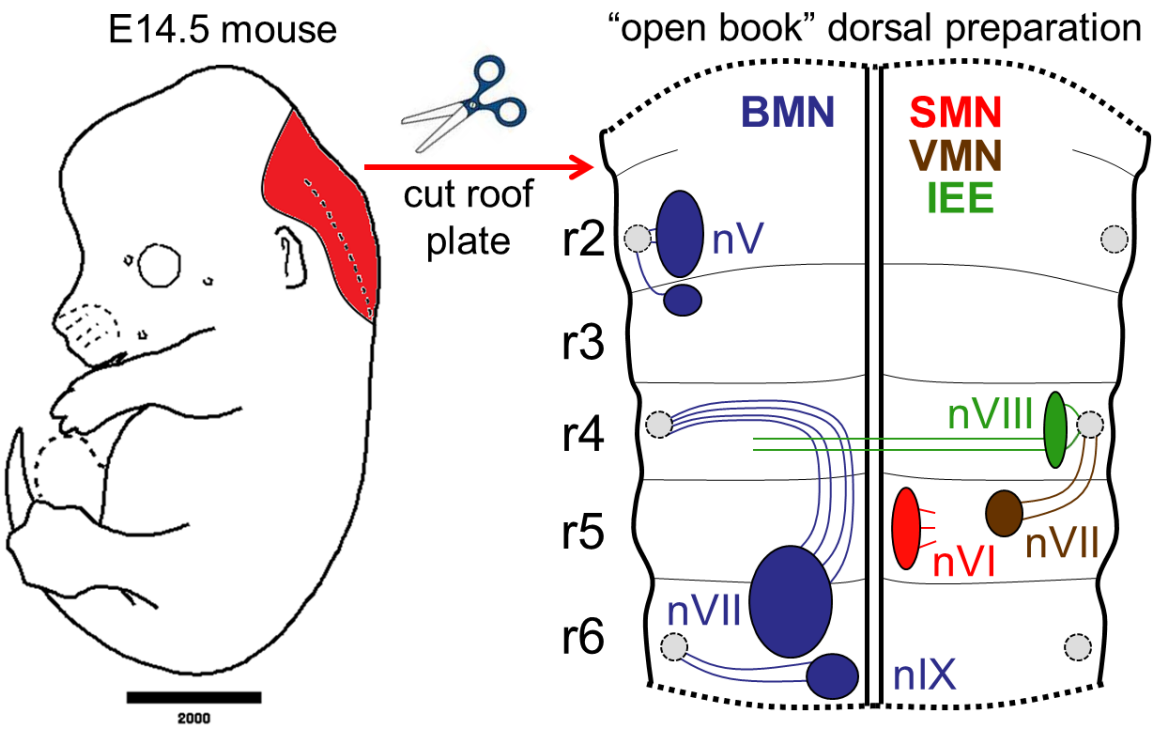

Figure 1.2. Organization of cranial motor neurons in r2 – r6 of the developing mouse hindbrain.

To visualize cranial neuron populations in embryos, the hindbrain region (red) is removed, cut along the roof plate of the fourth ventricle, and flat mounted to create an "open book" preparation. Branchiomotor neuron (BMN, blue), somatomotor neuron (SMN, red), visceromotor neuron (VMN, brown), and inner ear efferent neuron (IEE, green) populations are color coded and shown only on one side for clarity. Axon exit points are indicated by dotted circles. Rhombomere (r) boundaries are no longer clear by E14.5 but are shown for clarity. *Image of whole mouse embryo modified from the Emap Edinburgh Mouse Atlas (http://genex.hgu.mrc.ac.uk).* Scale bar for mouse embryo = 2000 µm.

1.2.2. FBMN migration in the mouse hindbrain

FBMN progenitors are born within the ventricular zone in r4, and move into the mantle layer as they become mature motor neurons by E9.5. With axons already projected out of the r4 exit point into the second branchial arch, the somas undergo a dynamic caudal migration from r4 into r5/r6, followed by a radial migration within r6 to form the facial motor nucleus (FMN) (**Figure 1.3**). FBMN migration takes place between E10.5 – E14.5; however, FBMNs do not initiate migration simultaneously. The earliest-migrating FBMNs complete their migration by E12.0, but the latest-migrating FBMNs do not leave r4 until after E12.5.

At E10.5, some FBMNs begin to migrate caudally (tangentially) within the mantle layer from r4 into r5, adjacent to the floor plate (FP) and in close association with the medial longitudinal fascicle (MLF). By E11.5, many FBMNs have reached r6 and migrate dorsolaterally, away from the FP. At the approximate boundary of the alar and basal plates in r6, they initiate radial migration towards the pial surface to form the FMN. At E12.5, FBMNs at different stages of migration span from r4 to the pial surface of r6. Only a subset of FBMNs is still undergoing migration at E13.5, and by E14.5, migration for all FBMNs is complete.

FBMN migration is an excellent model system to study the complexities of neuronal migration. As FBMNs migrate through multiple rhombomeres, they encounter environments with different cell adhesion properties and gene expression profiles. In accordance, FBMNs regulate the expression of their own receptors and cell adhesion molecules in a rhombomere-specific manner (**Figure 1.4**). As they switch from

tangential to radial migration within r6, their interactions with substrates likely change as well, presumably as they detach from the floor plate and/or MLF to attach to radial glial fibers. Although the molecular cues have yet to be elucidated, it is clear that FBMNs must receive attractive cues from more caudal rhombomeres in order to migrate caudally (Studer, 2001). In addition, our research has demonstrated that FBMNs encounter *directionality* cues, and that mechanisms dictating the directionality of migration and general ability to migrate are independently regulated (**Chapters 3 & 4**). FBMN migration is a complex process involving a plethora of signaling pathways (**Chapter 1.3-1.4**), shares similarities to other types of neuronal migration, and is easily visualized in the zebrafish and mouse models.

Figure 1.3. Overview of trigeminal and facial BMN migration in mice.

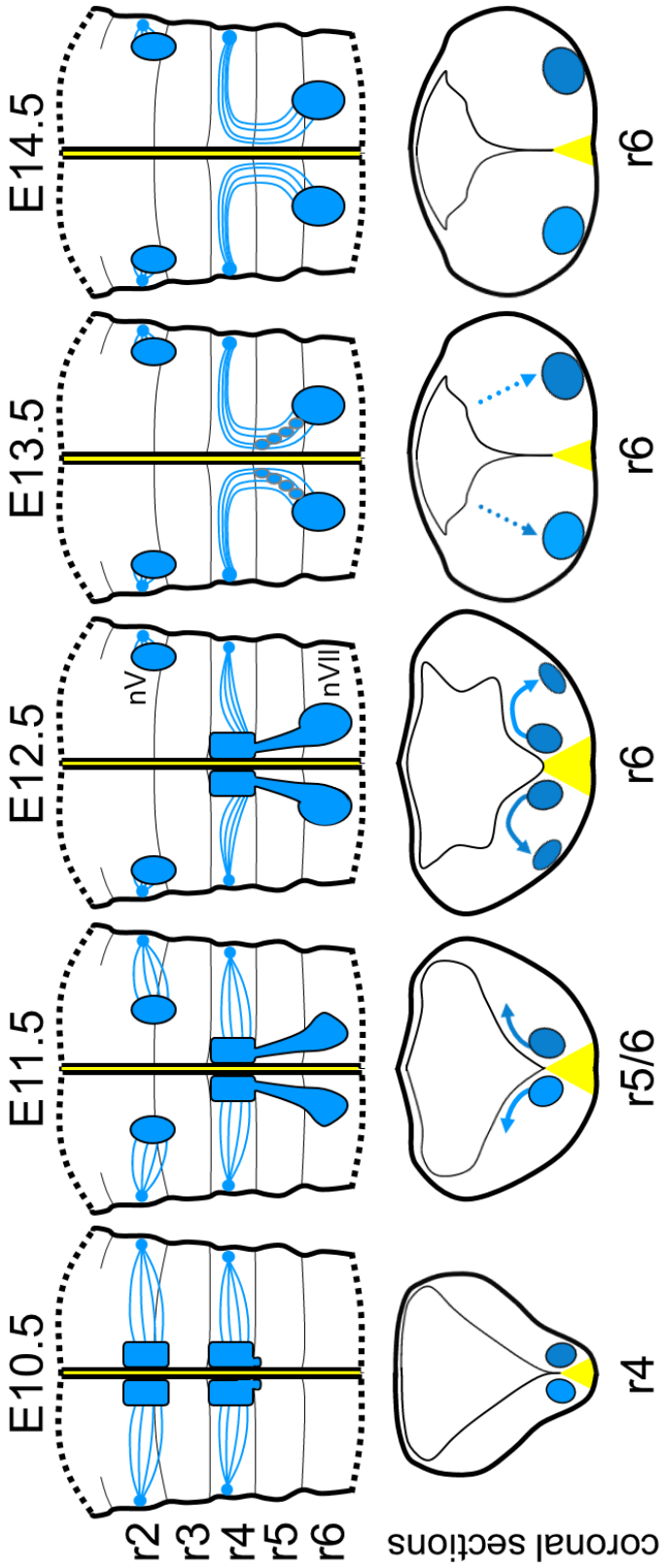

Figure 1.3. Overview of trigeminal and facial BMN migration in mice.

Trigeminal BMNs are specified in rhombomere 2 (r2) and the rostral portion of r3. From E10.5 to E12.5, they migrate dorsolaterally away from the floor plate (yellow) to form trigeminal motor nuclei (nV) in r2/r3. Facial branchiomotor neurons (FBMNs) are specified in r4 and begin to migrate caudally (tangentially) into r5, adjacent to the floor plate. By E11.5, FBMNs in caudal r5 begin to migrate dorsolaterally away from the floor plate and continue caudally into r6. At E12.5, the earliest migrating FBMNs have migrated radially within r6 to begin forming the facial motor nucleus (nVII) at the pial surface of the neural tube. By E13.5, only a small subset of FBMNs has yet to complete the course of migration, and none remain in r4. Migration of all FBMNs is complete by E14.5.

1.3. Molecular Mechanisms Regulating Facial Branchiomotor Neuron Migration

A number of molecular markers can be used to monitor FBMNs throughout their migration or in a rhombomere-specific manner (**Figure 1.4**). Transcription factors involved in either FBMN specification or migration such as *Phox2b* (Pattyn et al., 2000; Pattyn et al., 1997)*, Nkx6.1* (Muller et al., 2003; Pattyn et al., 2003)*, Isl1* (Garel et al., 2000; Hafezparast et al., 2003; Muller et al., 2003; Pfaff et al., 1996; Schwarz et al., 2004; Song et al., 2006), and *Tbx20* (Kraus et al., 2001; Song et al., 2006), are expressed by FBMNs throughout r4-r6. Some cell adhesion molecules are expressed by FBMNs only in certain rhombomeres, as is the case with the switch from *TAG-1* in r4/r5 to *Cdh8* expression in r6 (Garel et al., 2000). Cell surface receptors implicated in axon guidance, such as *Ret7*, *Unc5h3*, and *Neo1* are expressed only in FBMNs undergoing dorsolateral and radial migrations in r5 and/or r6 (Garel et al., 2000; Muller et al., 2003). These intricate changes in gene expression hint at the complex molecular mechanisms which regulate FBMN migration. Next, we will examine the functions of various genes expressed by mouse FBMNs, and discuss the roles of those implicated in regulating FBMN migration.

Figure 1.4. Expression of selected FBMN markers in the mouse.

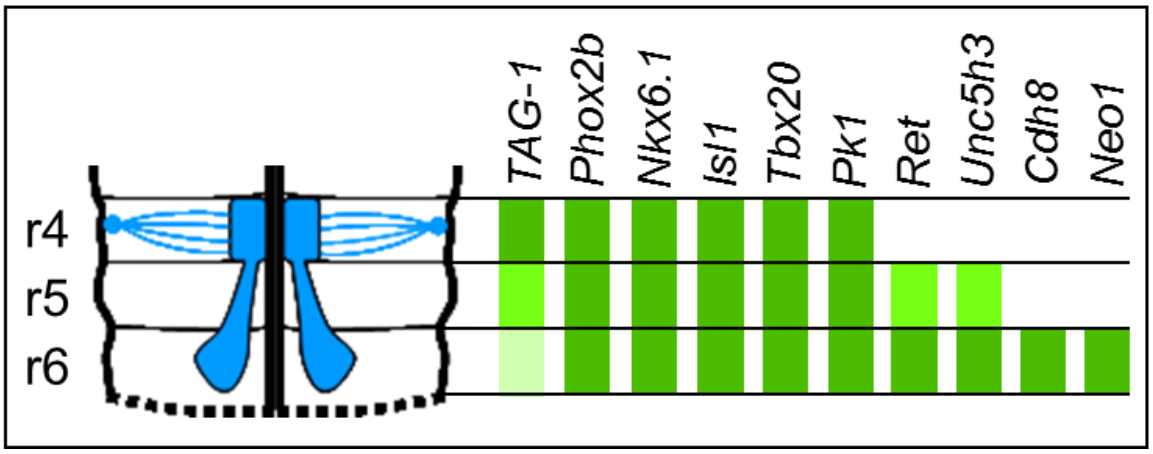

Figure 1.4. Expression of selected FBMN markers in the mouse.

Left: A snapshot of the migration path of FBMNs at E11.5. **Right:** Selected genes with specific expression in FBMNs are shown. Relative RNA expression levels as determined by *in situ* hybridization are noted, as well as any rhombomere-specific expression patterns.

1.3.1. Transcription factors

Ebf1

Early b-cell factor 1 (*Ebf1*) encodes a transcription factor with a novel HLH-related DNA-binding domain and an atypical zinc finger structure important for DNA recognition (Hagman et al., 1993; Hagman et al., 1995). *Ebf1* is well-studied for its role in β-lymphocyte development, where it is typically activated by homodimerization but also heterodimerization with other *Ebf* family members (Garcia-Dominguez et al., 2003). In the hindbrain, *Ebf1* is stongly expressed along the entire rostral-caudal axis from the midbrain through the spinal cord during early stages of development, but by E10.5 is localized mainly to the facial and trigeminal BMN somas as well as inter-rhombomeric boundaries (Garel et al., 1997). *Ebf1* is needed for the proper maturation of neurons, and importantly, only *Ebf1* (not *Ebf2* or *Ebf3*) is expressed in migrating FBMNs (Garel et al., 2000; Garel et al., 1997).

In *Ebf1* mutant embryos, many FBMNs undergo a premature dorsolateral migration within r5. Normal expression of early differentiation markers such as *Isl1*, *Phox2b*, and other *Ebf* genes in mutants suggest that early FBMN development is normal (Garel et al., 2000). However, FBMNs in *Ebf1* mutants are unable to properly regulate the expression of several cell adhesion molecules and receptors such as *TAG-1* (premature downregulation within r5), *Ret* (ectopic activation in r4), and *Cdh8* (ectopic activation in r4/r5) (Garel et al., 2000). These results suggest that *Ebf1* helps FBMNs properly interpret environmental cues present within certain rhombomeres, possibly by preventing an r6-specific gene expression pattern in FBMNs until they have reached r6.

Gata2* & *Gata3

Gata2 and *Gata3* encode zinc finger transcription factors named for the (A/T)GATA(A/G) sequence they recognize. Both genes are expressed in nearly identical patterns in the ventral neural tube and are mostly excluded from the ventricular zone (Nardelli et al., 1999; Pata et al., 1999). In r4, *Hoxb1* activates *Gata2* which subsequently activates *Gata3* (Nardelli et al., 1999; Pata et al., 1999). Though both *Gata2* and *Gata3* are expressed in inner ear efferent (IEE) neurons, the adjacent FBMNs do not express either gene (Nardelli et al., 1999; Pata et al., 1999).

Interestingly, both *Gata2*- and *Gata3*-deficient embryos have defective FBMN migration. In *Gata3* mutants, IEE neurons fail to send projections contralaterally across the floor plate, and FBMNs fail to complete their caudal migration (Pata et al., 1999). The *Gata2* mutant phenotype is nearly identical (Nardelli et al., 1999). Additionally, in *Gata2* mutants, *Isl1* and *Nkx6.1* expression levels are reduced. The reduced *Isl1* signal in r4 may indicate that *Gata2* affects early FBMN specification, which could result in defective migration. *Nkx6.1*, on the other hand, is not required for early FBMN specification but is necessary for their caudal migration (Muller et al., 2003); therefore, loss of *Gata2* could affect FBMN migration indirectly by reducing *Nkx6.1* expression levels.

Hoxb1

Homeobox (*Hox*) genes encode an array of homeodomain transcription factors that are involved in the regionalization of the embryo, whether in segmentation or in limb formation (Alberts, 1994). In the hindbrain, each rhombomere is characterized by the expression of a unique combination of *Hox* genes, which activate region-specific developmental programs and allow for the generation of diverse populations of cranial neurons. *Hoxb1* in particular is expressed robustly within r4 (Goddard et al., 1996; Studer et al., 1996), and interacts with *Hoxa1* in an auto- and para-regulatory loop to maintain r4-specific *Hoxb1* expression (Studer et al., 1998; Studer et al., 1996). *Hoxb1* also lies upstream of or is a positive regulator of numerous genes expressed in r4-derived neurons, including *Isl1*, *Phox2a/b*, and *Gata2/3* (Chandrasekhar, 2004; Gaufo et al., 2000; Pata et al., 1999; Samad et al., 2004).

In *Hoxb1* mutants, r4 patterning is initiated but not maintained. The expression of early r4 markers before E8.5 shows that r4 clearly is formed in *Hoxb1* mutants, but after E8.5 these genes are downregulated significantly and r4 shows an r2-like mixed identity (Goddard et al., 1996; Studer et al., 1996). This mixed identity is demonstrated by the migratory defects of FBMNs. Putative FBMNs correctly project their axons out of the r4 exit point, but do not migrate caudally; instead, they migrate dorsolaterally within r4 much like the trigeminal BMNs in r2/r3, and downregulate *Isl1* expression by E12.5 (Studer et al., 1996). The facial motor nucleus cannot be detected postnatally, indicating that these cells cannot either receive or interpret important signals for their survival (Goddard et al., 1996; Studer et al., 1996). Many *Hoxb1* mutant mice are viable,

but display facial paralysis and facial muscle degeneration due to the loss of several branches of the facial nerve (Goddard et al., 1996).

Isl1

Islet 1 (*Isl1*) encodes a transcription factor containing a C-terminal homeodomain and two N-terminal zinc-binding LIM domains (Appel et al., 1995). In the spinal cord, *Isl1* is initially expressed in all motor neurons preceding axonogenesis (Appel et al., 1995; Pfaff et al., 1996), but later the combinatorial expression of LIM homeobox genes including *Isl1*, *Isl2*, *Lim-1*, and *Lim-3* distinguishes different subtypes of motor neurons (Lumsden, 1995). In the hindbrain, *Isl1* is expressed in all motor neuron subtypes, including FBMNs throughout their development and migration (**Figure 1.4**). Thus, *Isl1* is routinely used as a marker to assay hindbrain neural development and migration (Garel et al., 2000; Hafezparast et al., 2003; Muller et al., 2003; Schwarz et al., 2004; Song et al., 2006).

Isl1 does not play a direct role in FBMN migration, but instead in their initial formation. *Isl1* mutants fail to form motor neurons despite normal architecture and dorsal-ventral patterning of the neural tube (Pfaff et al., 1996). Interestingly, *Engrailed 1 (En1)*-positive interneurons fail to form in the *Isl1* mutant spinal cord, which can be reversed in the presence of *Isl1*-positive motor neurons, suggesting that motor neuron generation is necessary for the differentiation of some interneuron types as well (Pfaff et al., 1996).

Kreisler

Kreisler (also known as *Mafb*) encodes a bZIP transcription factor that is expressed in r5 and r6 during early development. It functions as a transcriptional activator of *Hoxa3* and *Hoxb3* (Manzanares et al., 1999), prevents the caudal expansion of *Hoxb1* and rostral expansion of *Hoxb4* (Sadl et al., 2003), and is likely necessary for the maintenance of *Krox20* expression (Sadl et al., 2003).

Analysis of mouse strains with altered *Kreisler* expression demonstrates the influence of the environment in FBMN migration. In *Kreisler*^{KO} mice, r5 is completely absent (Manzanares et al., 1999; Sadl et al., 2003). Nevertheless, FBMNs in *Kreisler* mutants are able to migrate normally into r6, normally express molecular markers, but break up into several streams upon undergoing dorsolateral and radial migrations (Garel et al., 2000). This implies that putative cues in the hindbrain that attract FBMNs caudally originate caudal to r5, but that r5 is needed to maintain an organized stream of migrating FBMNs. Interestingly, in transgenic mice with prolonged *Kreisler* expression within r5 but normal r6 *Kreisler* expression, FBMNs are specified correctly but are unable to migrate cross the r4/r5 boundary and instead become clustered in posterior r4 (Theil et al., 2002). In these mice, the r5 region fails to expand and the mantle layer of r5 does not form properly (Theil et al., 2002). This demonstrates that the early downregulation of *Kreisler* is necessary for proper r5 development, including the specification and migration of neurons that form the r5 mantle layer. In these embryos, FBMNs fail to migrate because the layer in which they migrate is not present in r5.

Krox20

Kruppel box 2 (*Krox20*), also known as *Early growth response 2* (*Egr2*), encodes a C_2H_2 zinc finger transcription factor that is necessary for the formation of r3 and r5 and their derivatives, which are completely eliminated in *Krox20* mutants (Schneider-Maunoury et al., 1997; Swiatek and Gridley, 1993). Prior to hindbrain segmentation, *Krox20* is expressed in two vertical stripes indicating the future locations of r3 and r5, where it activates expression of several *Hox* genes and also *Sek1*, a receptor tyrosine kinase (Seitanidou et al., 1997).

Krox20 mutant mice fail to form r5. Nevertheless, FBMNs in these mutants are able to migrate caudally into r6; but as in *Kreisler* mutants, FBMNs break up into multiple streams within r6. This suggests that the r5 environment is critical for the formation of an organized caudal stream of FBMNs.

Nkx6.1

NK6 transcription factor related, locus 1 (*Nkx6.1*) encodes a homeodomain-containing transcription factor that functions as an activator but also a potent repressor of transcription (Mirmira et al., 2000). The presence of its own C-terminus interferes with its N-terminal repression activity, so it likely has to be modified by other factors in order to bind DNA efficiently and repress transcription (Mirmira et al., 2000). Nkx6.1 is expressed in the ventral neural tube and FBMNs (**Figure 1.4**), and is induced by *Sonic hedgehog* (*Shh*) expression from the floor plate (Briscoe et al., 2000). In order to properly pattern the neural tube along the dorsal-ventral axis, Nkx6.1 and other ventral

class II transcription factors (i.e. Nkx2.2) undergo cross-repressive interactions with dorsal class I factors (Dbx2, Pax6) to establish boundaries of expression; the specific combination of transcription factor expression determines neuronal fate (Briscoe et al., 2000). Interestingly, although the combination of *Nkx6.1* and *Pax6* expression in the ventral neural tube specifies motor neuron progenitor identity, *Nkx6.1* is only necessary for the induction of somatomotor neurons in the hindbrain, and the spinal cord phenotype varies along the rostral-caudal axis (Muller et al., 2003; Sander et al., 2000).

In the hindbrain, *Nkx6.1* is dispensable for early FBMN specification, but is important for their subsequent development and migration. FBMNs in *Nkx6.1* mutants fail to migrate, with only a few cells crossing into r5 (Muller et al., 2003). Although these cells express early differentiation markers such as *Isl1* and *Phox2b*, they fail to properly control the expression of cell surface receptors (Muller et al., 2003). Both *Ret*, a GDNF receptor tyrosine kinase, and *Unc5h3*, a netrin receptor, are expressed in FBMNs in r4 instead of exclusively in r5 and r6 (Muller et al., 2003). This data, along with the strong expression of *Nkx6.1* in migrating FBMNs (Muller et al., 2003), argues for a cell-autonomous function for *Nkx6.1* in FBMN migration. It is likely that under normal conditions, *Nkx6.1* represses the activation of both *Ret* and *Unc5h3* until FBMNs within r5 and r6 are exposed to signals which release this repression.

Phox2b

Paired-like homeobox 2b (*Phox2b*) encodes a homeodomain transcription factor that is expressed in all branchiomotor and visceromotor neurons of the CNS, as well as

many sensory ganglia of the PNS (Pattyn et al., 1997). Both *Phox2b* and *Phox2a* have widely overlapping expression patterns and identical homeodomains, and *Phox2b* expression in FBMNs is dependent upon the presence of *Phox2a*, and vice versa (Pattyn et al., 1997). *Phox2b* is expressed as early as E9.5 throughout the midline and is upregulated in r2 and r4, corresponding to the locations of the trigeminal and facial branchiomotor nuclei; lateral stripes of expression are also present from the r1/r2 boundary to the r6/r7 boundary from E10.5 onward (Pattyn et al., 1997). *Phox2b* is expressed in FBMNs throughout their migration (**Figure 1.4**), and can be detected postnatally in the facial motor nucleus (Pattyn et al., 1997).

Phox2b mutants are characterized by the absence of all branchiomotor and visceromotor (but not somatomotor) neurons (Pattyn et al., 2000). BMN/VMN precursors fail to exit the cell cycle and undergo apoptosis instead, resulting in a depleted mantle layer (Dubreuil et al., 2000). *Phox2b* also has a late-acting role in FBMN migration. When a knock-in mouse was created expressing *Phox2a* in place of *Phox2b*, *Isl1*-positive FBMNs were generated in lower numbers, but failed to migrate caudally (Coppola et al., 2005). These FBMNs appeared to be properly specified, as indicated by normal expression of *Npn1*, *Ebf1*, and *Ret* (Coppola et al., 2005). These results show that *Phox2a* can sustain motor neuron differentiation in the absence of *Phox2b*, and that the post-differentiation function of *Phox2b* is necessary for FBMN migration.

Tbx20

T-box (Tbx) transcription factors are aptly named for their binding to the T-box consensus sequence, TCACACCT (Wilson and Conlon, 2002). Over 50 *Tbx* genes have been described in a variety of organisms, yet few have been characterized and little is known about protein-protein interactions (Wilson and Conlon, 2002). In the brain, *Tbx20* expression is initiated by E9 in ventral r2 and r4, but by E10.5 is present as two ventral stripes running parallel to the midline from r2 through the cervical spinal cord (Kraus et al., 2001). This mimics the *Isl1* expression pattern as both *Tbx20* and *Isl1* label BMNs (**Figure 1.4**), VMNs, and IEE neurons in the developing hindbrain (Kraus et al., 2001; Song et al., 2006; Varela-Echavarria et al., 1996).

In *Tbx20* conditional mutants (with disrupted *Tbx20* in neural tissues), both trigeminal and facial BMNs fail to migrate and instead remain near the floor plate in r2/r3 and r4, respectively (Song et al., 2006). Interestingly, *Tbx20*-deficient FBMNs are correctly differentiated, as indicated by normal expression of genes such as *Hoxb1*, *Math3*, *Mash1*, *Phox2a/b*, and exclusion of *Gata2* expression (Song et al., 2006). However, *Tbx20*-deficient FBMNs in r4 ectopically express the *Ret* and *Neo1* receptors which are normally expressed in r5 and/or r6. Furthermore, Wnt/PCP genes such as *Wnt11*, *Fzd7*, *Pk1*, and *Vangl1/2* are downregulated (Song et al., 2006). Together, these results indicate that *Tbx20* acts downstream of FBMN differentiation steps, possibly activating a transcriptional cascade necessary for their migration (including some Wnt/PCP genes) and inhibiting the expression of certain cell surface receptors until encountering the proper caudal environment.

1.3.2. Secreted molecules

Ntn1

Netrins encode small secreted proteins containing two extracellular laminin-like domains and an intracellular C-terminal domain unique to the netrin family (Lauderdale et al., 1997). Netrin (Ntn) 1 in the mouse is secreted at high levels from the floor plate and adjacent cells in the ventral neural tube (Serafini et al., 1996). Though *Ntn1* has demonstrated roles in both attracting and repelling axon growth cones in several model systems (Finger et al., 2002; Hong et al., 1999; Keleman and Dickson, 2001; Lauderdale et al., 1997; Serafini et al., 1996), it likely has a function in neuronal migration as well. *Ntn1* mutant embryos fail to form pontine nuclei in the cerebellum, a structure formed by the migration of pontine precursor cell bodies ventrally across the floor plate, a similar path as commissural axons travel (Serafini et al., 1996). A role for *Ntn1* in FBMN migration has not been directly investigated, but interestingly, migration of FBMNs away from the floor plate coincides with the onset of the expression of the netrin receptors *Unc5h3* and *Neo1* (Muller et al., 2003). Therefore, netrin and its receptors likely coordinate the repulsion of FBMNs away from the floor plate.

Reelin

The *Reelin* (*Reln*) gene encodes a secreted extracellular matrix protein with eight reeler repeats and eight EGF repeats (D'Arcangelo et al., 1995). It is expressed almost exclusively in the brain, where it is first detected at E11.5 and its levels increase steadily up through birth (D'Arcangelo et al., 1995). By E14.5 in the hindbrain, *Reln* is expressed

mostly in the area surrounding the facial motor nucleus, with lower levels of expression in FBMNs themselves (Ohshima et al., 2002). In the *reeler* (*Reln*$^{-/-}$) mutant, there are defects specifically in radial FBMN migration. Until E14, FBMNs of wild-type and *reeler* mutant embryos are indistinguishable, but by E14, the facial motor nuclei of *reeler* embryos are harder to distinguish from surrounding structures (Fontaine-Perus and Cheraud, 2005). FBMNs appear to migrate caudally (tangentially), but interact abnormally with either radial fibers or other FBMNs, resulting in a less compact and unorganized facial motor nucleus (Goffinet, 1984).

Though *Reln* has been extensively studied for its roles in cortical layer formation, the mechanism by which it regulates FBMN migration is less clear. It is likely that the Reln protein may be secreted by other post-migratory neurons, where it then transduces a signal within FBMNs which helps stabilize the architecture of the facial motor nucleus (Goffinet, 1995). It is also likely that *Reln* functions in a common or parallel pathway with both *Cdk5* and *Disabled homolog 1* (*Dab1*), an intracellular tyrosine-phosphorylated adaptor protein specifically expressed in FBMNs (Ohshima et al., 2002). *Dab1* mutants display a phenotype mostly indistinguishable from *reeler* mutants, with both inverted cortical layers and defective FBMN migration (Howell et al., 1997; Ohshima et al., 2002). Double mutants for both *Dab1* and *p35* (a regulatory subunit of Cdk5) have greater FBMN migration defects (Ohshima et al., 2002). These results suggest a connection between pathways involving *Reelin*, *Dab1*, and *Cdk5*.

VEGF164

VEGF164 is one of three isoforms of *Vascular endothelial growth factor* (*VEGF*) in mice (Ng et al., 2001; Soker, 2001). Each isoform has demonstrated roles in blood vessel formation, particularly in the lungs, but 80% of all *VEGF* in brain tissue is the *VEGF164* isoform (Ng et al., 2001). In the E12.5 hindbrain, *VEGF164* is expressed in both medial and lateral stripes on the ventral side of the neural tube (Schwarz et al., 2004). Its receptor, *Neuropilin 1* (*Npn1*), is expressed in the floor plate and FBMNs during migration (Kitsukawa et al., 1995; Schwarz et al., 2004; Takagi et al., 1995). The complementary expression patterns of *VEGF164* and *Npn1* suggest that the ligand/receptor combo may regulate aspects of FBMN migration.

In $VEGF^{120/120}$ mutants, which express *VEGF120* at the expense of the *VEGF164* isoform, FBMNs break up into several streams within r5 and r6, forming an anteriorly shifted facial motor nucleus (Schwarz et al., 2004). In explanted hindbrains, FBMNs fail to migrate when exposed to VEGF function-blocking antibodies, and VEGF164-coated beads attract FBMNs (Schwarz et al., 2004). While no obvious peripheral axon guidance defects are seen in *VEGF164*-deficient embryos, both *Npn1* and *Sema3A* mutants display defasciculation of the facial nerve in the second branchial arch (Schwarz et al., 2004). Together, these results suggest that FBMN migration and axon pathfinding may be regulated independently through *Nrp1* via two separate ligands, *Sema3A* and *VEGF164*.

1.3.3. Receptors

Neo1

Neogenin (*Neo1*) encodes a netrin receptor that is part of the immunoglobulin superfamily of proteins (Vielmetter et al., 1994). Though it is expressed in a variety of embryonic tissues (Keeling et al., 1997), it is notably expressed in FBMNs in r6 and trigeminal (nV) motor nuclei during their dorsolateral migration away from the midline (Muller et al., 2003) (**Figure 1.4**). *Neo1* is similar in structure to another netrin receptor, *Deleted in colorectal carcinoma* (*DCC*) (Vielmetter et al., 1994). In *Drosophila*, co-expression of *unc5* and *DCC* (analogous to mouse *Unc5h3* and *Neo1*/*DCC*) induces a long-range chemorepulsive response to netrin (Keleman and Dickson, 2001). Since mouse *Ntn1* is expressed along the midline during FBMN migration and both *Unc5h3* and *Neo1* are specifically expressed in dorsolaterally migrating FBMNs (Muller et al., 2003), it is likely that this ligand-receptor combination is involved in FBMN repulsion from the midline within r6.

In both *Nkx6.1* and *Tbx20* mutants, FBMNs fail to migrate out of r4 (Muller et al., 2003; Song et al., 2006). In *Tbx20* mutants, but not in *Nkx6.1* mutants, *Neo1* is ectopically expressed within the r4-located FBMNs (Muller et al., 2003; Song et al., 2006). These results suggest that *Neo1* expression is likely repressed within r4 and r5 until encountering a signal within r6 that releases this repression, and that *Tbx20* may be involved in this process.

Npn1

Neuropilin1 (*Npn1*) encodes a receptor for multiple VEGF isoforms and class 3 Semaphorins, and can function as a co-receptor with Plexins (Schwarz et al., 2004; Soker, 2001). In the hindbrain, *Npn1* is expressed in the floor plate and FBMNs throughout migration (Kitsukawa et al., 1995; Schwarz et al., 2004; Takagi et al., 1995).

In *Npn1* mutant embryos, FBMNs are generated normally, initiate migration, but break up into several migratory streams within r5 and r6, resulting in an anteriorly-shifted facial motor nucleus (Schwarz et al., 2004). However, FBMNs migrate normally in *Sema3A* and *Sema3C* mutants, and also in a separate *Npn1* mutant with abolished binding to class 3 Semaphorins (Schwarz et al., 2004), suggesting that the Npn1/Sema3 combo does not regulate FBMN migration. On the contrary, FBMN migration is defective in $VEGF^{120/120}$ mutants, suggesting that the Npn1/VEGF pair may function together to regulate FBMN migration (Schwarz et al., 2004).

Ret

Ret proto-oncogene (*Ret*) encodes a functional receptor tyrosine kinase for Glial cell line derived neurotrophic factor (Gdnf) (Durbec et al., 1996; Trupp et al., 1996). It is a member of the TGF-β superfamily of kinases, which are typically serine-threonine kinases. *Ret* is commonly used as an FBMN marker, since it expressed by FBMNs undergoing dorsolateral and radial migrations in r5-r6 (**Figure 1.4**), and is maintained in the facial motor nucleus (Garel et al., 2000).

Surprisingly, FBMNs migrate normally in the absence of functional *Ret* (Song et al., 2006), indicating that *Ret* is dispensable for migration. However, functional redundancy with other genes cannot be ruled out. Given its rhombomere-specific expression pattern and timing of the onset of expression, *Ret* likely has a function in the dorsolateral or radial migration of FBMNs. Interestingly, *Ret* is misexpressed in non-migrated FBMNs in r4 in both *Nkx6.1* and *Tbx20* mutants (Muller et al., 2003; Song et al., 2006). These results indicate that both the *Nkx6.1* and *Tbx20* transcription factors may repress *Ret* expression in r4 until encountering a positive signal within r5 which promotes *Ret* expression.

Unc5c

Unc5 homolog C (*Unc5c*, also known as *Unc5h3*) encodes a netrin receptor that is part of the immunoglobulin superfamily of proteins (Ackerman et al., 1997; Engelkamp, 2002). It is widely expressed in the brain throughout mid-gestation and has a demonstrated role in neuronal migration, as *Unc5h3* mutants have a dramatic reduction in cerebellar size due defective migration of Purkinje and granule cells (Przyborski et al., 1998). In *Drosophila*, Unc5 functions as a netrin receptor and induces either short- or long-range repulsion of axons depending on the context (Keleman and Dickson, 2001). In the developing mouse hindbrain, *Netrin1* is expressed in the floor plate and *Unc5h3* is expressed in FBMNs during dorsolateral and radial migrations within r5 (Muller et al., 2003; Przyborski et al., 1998) (**Figure 1.4**), suggesting a role for Netrin/Unc5h3 in repulsion of FBMNs away from the floor plate. However, this has not been investigated.

In assaying for a phenotype, one could not rule out possible functional redundancy with other genes, since *Unc5h1*, a normally chemorepulsive netrin receptor is also expressed by BMN/VMNs as early as E11 (Barrett and Guthrie, 2001).

In *Nkx6.1* mutants, *Unc5h3* is aberrantly expressed in FBMNs which fail to migrate caudally out of r4, and is turned on somewhat earlier than normal (E11.5 in mutants compared to E12 in WT) (Muller et al., 2003). This suggests that *Nkx6.1* may play a role in repressing *Unc5h3* expression in FBMNs until proper signals are encountered in r5, or that only fully mature FBMNs can properly regulate *Unc5h3* expression.

1.3.4. Cell adhesion molecules

Cdh8

Cadherin 8 (*Cdh8*) encodes a cell adhesion molecule of the type II cadherin subfamily. Type II cadherins are very similar to classical cadherins, with five extracellular cadherin repeats and a comparable cytoplasmic C-terminus, but share more similarity with each other than with classical cadherins (Kido et al., 1998; Suzuki et al., 1991). Like other cadherins, *Cdh8* participates in Ca^{2+}-dependent cell-cell adhesion (Kido et al., 1998), but its exact function is unknown. *Cdh8* is highly expressed in the brain (Suzuki et al., 1991), particularly in FBMNs at the onset of radial migration in r6 (Garel et al., 2000) (**Figure 1.4**). Therefore, it is tempting to speculate that *Cdh8* is involved in the transition from dorsolateral to radial migration, perhaps in attaching to glial substrates needed for

radial migration. In the *Ebf1* mutant, where FBMNs break up into several migratory streams within r5 and r6 but still complete radial migration, *Cdh8* is ectopically expressed in FBMNs from r4 through r6 (Garel et al., 2000).

Tag1

Transient axonal glycoprotein 1 (Tag1) encodes a GPI-anchored cell adhesion molecule of the immunoglobulin superfamily, containing six Ig domains and four fibronectin type III domains (Freigang et al., 2000; Furley et al., 1990). It can mediate cell-cell contact through either hemophilic or heterophilic interactions, and also indirectly mediates intracellular signaling. For example, Tag1 serves as a ligand for amyloid precursor protein (APP), resulting in the γ-secretase-dependent cleavage of components leading to the suppression of neurogenesis (Ma et al., 2008a; Ma et al., 2008b).

In zebrafish, *tag1* is expressed in the earliest-migrating ("pioneer") FBMNs and their axons, and morpholino knockdown of *tag1* largely blocks the migration of FBMNs out of r4 (Sittaramane et al., 2009). *tag1*, *laminin**α**1*, and *stbm/vangl2* (a Wnt/PCP component) genetically interact to regulate FBMN migration, and FBMNs in single morphants behave similarly, suggesting these genes regulate FBMN migration via a common mechanism (Sittaramane et al., 2009).

In mice, *Tag1* is necessary for the migration of neurons in the neocortex and the superficial migratory stream that form the reticular and external cuneate nuclei in the hindbrain (Denaxa et al., 2001; Denaxa et al., 2005; Kyriakopoulou et al., 2002). *Tag1* is

strongly expressed in FBMNs within r4, but is progressively downregulated upon migrating into r5 and r6 (Garel et al., 2000; Kyriakopoulou et al., 2002) (**Figure 1.4**). However, *Tag1* is not necessary for the caudal migration of FBMNs (Michèle Studer, personal communication). This suggests that *Tag1* may function redundantly with other genes to regulate FBMN migration, or that mice utilize an alternative pathway independent of *Tag1* function.

1.3.5. Enzymes

Cdk5

Cyclin-dependent kinase 5 (*Cdk5*) is a member of the serine/threonine cyclin-dependent kinase family by sequence homology alone, since its activity is not cyclin-dependent and it has no known role in cell cycle regulation (Dhavan and Tsai, 2001). It phosphorylates a variety of substrates involved in cytoskeletal activity, cell adhesion, and axon guidance (Dhavan and Tsai, 2001; Ohshima and Mikoshiba, 2002), so it is no surprise that *Cdk5* mutants display an array of neuronal migration defects. *Cdk5* is ubiquitously expressed throughout development, but at much higher levels in the brain, specifically in terminally-differentiated neurons in the marginal zone (Tsai et al., 1993; Zheng et al., 1998). Its two regulatory subunits, p35 (NCK5a, Neuronal CDK5 activator) and p39 (NCK5ai, Neuronal CDK5 activator isoform), are expressed exclusively in the marginal zone (Zheng et al., 1998), which limits Cdk5 activity to post-mitotic neurons.

Cdk5 mutant mice have defects in cortical layer and inferior olive formation, similar to *reeler* (*Reln*$^{-/-}$) and *scrambler* (*Dab1*$^{-/-}$) mutants (Ohshima et al., 2002), suggesting that these genes may function in a similar pathway. FBMNs in *Cdk5* mutants fail to migrate out of r4, yet express markers characteristic of terminally differentiated FBMNs and correctly project axons into the periphery (Ohshima et al., 2002). This phenotype can rescued via expression of a neuron-specific *Cdk5* transgene (Ohshima et al., 2002). These results suggest that regulation of Cdk5 activity by its p35/p39 subunits promotes neuronal migration in a cell-autonomous manner via interactions with proteins involved in cell adhesion and cytoskeletal changes.

Dync1h1

Dynein cytoplasmic 1 heavy chain 1 (*Dync1h1*) encodes a head domain of the dynein motor protein. The dynein head domains bind to microtubules upon homodimerization, and "walks" towards the minus end of microtubules via energy from its own ATPase activity; the specificity of its cargo, such as organelles and other cellular components, is determined by light chains on its tail domain (Alberts, 1994). It is considered a housekeeping gene since *Dync1h1* homozygous knockout mice die before E8.5 with impaired mitosis and a highly fragmented Golgi (Harada et al., 1998).

Interestingly, two independent point mutations in *Dync1h1* result in a neuron-specific phenotype. In both the *Legs at odd angles* (*Loa*) and *Cramping 1* (*Cra1*) mice, heterozygotes are viable but have a dramatic decrease in α-motor neurons in the spinal cord; *Loa*/*Loa* and *Cra1*/*Cra1* homozygotes show a 50-80% reduction in spinal anterior

horn cells (Hafezparast et al., 2003). In *Loa*/*Loa* mutants, whose mutation lies at the *Dync1h1* homodimerization site and binding site for dynein intermediate chains, FBMN migration is affected. FBMNs initiate migration, but it appears to be delayed and many FBMNs prematurely migrate away from the midline in r5, resulting in an elongated facial motor nucleus (Hafezparast et al., 2003). The precise mechanism behind the neuron-specific phenotype and migration defect in *Loa*/*Loa* mice is not clear. In neurons, dynein motors are mainly responsible for carrying cargo from the axon back to the soma (Alberts, 1994). It is thought that the *Loa* mutation may specifically impair neuron-specific subunits from being recruited to a dynein complex, yet allow for functional dynein in other cell types (Hafezparast et al., 2003).

Psen1

Presenilin 1 (*Psen1*) is a gene best known for its role, if mutated, in early onset Alzheimer's Disease. It encodes an eight-pass transmembrane protein that is a component of the γ-secretase complex and possesses the active site which cleaves the amyloid-β precursor protein (APP) and other type I integral membrane proteins (Medina and Dotti, 2003). *Psen1* is expressed in FBMNs and is widespread in the brain throughout mid-gestation (Tanimukai et al., 1999). Interestingly, Psen1 is necessary for the cleavage of classical cell adhesion molecules of the immunoglobulin superfamily (including cadherins), and can modulate Notch signaling (Medina and Dotti, 2003). Interactions of Psen1 with similar target molecules with proposed functions in FBMN migration, such as Neo1, Unc5c, Cdh8, Celsr1, and TAG-1 have not been investigated.

In *Psen1* mutant embryos, neuronal migration defects are widespread. Both radial and tangential migrations are affected in mutants, as cortical layer formation is defective, midline fusion of the cerebellum is incomplete, and cranial motor neurons in the hindbrain are disorganized (Louvi et al., 2004). Both FBMNs and inner ear efferent (IEE) neurons in r4 fail to migrate properly, and the abducens (nVI) and hypoglossal (XII) somatomotor neurons are fragmented and displaced (Louvi et al., 2004).

The mechanism by which *Psen1* regulates neuronal migration is unclear. Since Psen1 is involved in the essential cleavage of diverse membrane proteins which translocate to the nucleus upon cleavage (Medina and Dotti, 2003), Psen1 may regulate gene transcription in multiple pathways. Also, Psen1 interacts directly with multiple cytoskeletal components (Medina and Dotti, 2003), the mechanism by which it may direct cell movement.

1.3.6. Non-canonical Wnt/PCP signaling

A general function of planar cell polarity (PCP) signaling is to create morphological asymmetries in tissues by first creating molecular asymmetries that align cells along a plane (Goodrich, 2008). For example, in the *Drosophila* wing, the PCP component Frizzled is enriched on the distal side of the cell, and this is the only side of the cell from which bristles subsequently emerge. Throughout development, PCP also functions to properly orient cells within a constantly changing environment. In the zebrafish neural tube, for instance, PCP signaling polarizes neural progenitors along the

rostral-caudal axis, maintains the alignment of newborn neurons after division (Ciruna et al., 2006), and is required for the posterior tilting of primary motile cilia (Borovina et al., 2010). Not surprisingly, many PCP components also regulate the caudal migration of FBMNs. Next, we will discuss the mechanisms by which Wnt/PCP signaling establishes cell polarity, and the role of Wnt/PCP signaling in FBMN migration in zebrafish.

1.4. Non-Canonical Wnt/PCP Signaling in Zebrafish FBMN Migration

1.4.1. Role of Wnt/PCP signaling in establishing cell polarity

Wnts are secreted glycoproteins that bind to Frizzled (Fzd) seven-pass transmembrane receptors, activating either a canonical pathway that allows β-catenin to mediate transcriptional changes, or a non-canonical pathway where downstream factors such as Rho or Jun kinases alter the cytoskeleton or cell polarity (**Figure 1.5**) (Veeman et al., 2003). In the canonical pathway, Wnt/Fzd binding causes the stabilization of β-catenin, which is normally targeted for proteosomal degradation by a complex containing axin, adenomatosis polyposis coli (APC), and glycogen synthase kinase 3 (GSK3) (Cadigan and Liu, 2006). Inactivation of this complex is accomplished through interactions between axin and LRP (a Wnt co-receptor) and through Dishevelled (Dvl) phosphorylation. With the axin/APC/GSK3 complex inactive, β-catenin accumulates and enters the nucleus, where it activates transcription upon binding to TCF.

The non-canonical Wnt/PCP pathway has been extensively studied in *Drosophila*, where it is responsible for proper orientation of the ommatidial and wing bristle cells through its formation of polarized complexes of PCP proteins (Barrow, 2006; Das et al., 2004). In *Xenopus* and zebrafish, Wnt/PCP signaling components are required for proper convergence and extension cell movements during gastrulation (Darken et al., 2002; Park and Moon, 2002; Tada et al., 2002; Wallingford and Harland, 2002). In mice, Wnt/PCP proteins are additionally implicated in hair follicle orientation, stereocilia orientation in the inner ear, and neural tube closure (Devenport and Fuchs, 2008; Doudney and Stanier, 2005; Kallay et al., 2006; Montcouquiol et al., 2003; Ravni et al., 2009; Torban et al., 2004a; Torban et al., 2004b; Ybot-Gonzalez et al., 2007).

Feedback mechanisms leading to the formation of polarized complexes of PCP proteins were first described in the *Drosophila* wing. Frizzled (Fz) recruits Dishevelled (Dsh) to the membrane (Wong et al., 2003), which leads to the accumulation of Van-gogh (Vang)/Prickle (Pk) complexes at the adjacent membrane of a neighboring cell. The Vang/Pk complex then prevents Fz/Dsh complex formation, so that Vang/Pk and Fz/Dsh complexes segregate to opposite sides of the cell. Overall, this results in the polarized formation of Vang/Pk (proximal) and Fz/Dsh (distal) complexes on opposing membranes throughout the wing field, and ensures that the wing hairs point distally (Barrow, 2006). Since PCP signaling in *Drosophila* does not require the Wnt ligand (Barrow, 2006), the upstream initiator of Fz activity has not been identified. However, in addition to presumed secreted cues, feedback mechanisms between cells are also

important in maintaining PCP, since mispolarized cells negatively affect the polarization of adjacent cells (Klein and Mlodzik, 2005; Ma et al., 2003).

Recently, the mechanisms underlying polarized PCP complex formation in mice are beginning to be revealed from experiments in a variety of contexts. In commissural axon growth cones, Wnt binds to Fzd3 which binds to Dvl1 and activates PCP signaling through the phosphorylation of Jun kinase (Shafer et al., 2011). Dvl1, in turn, promotes the phosphorylation of Fzd3 which leads to the accumulation of Fzd3 at the membrane and constrains PCP signaling. Vangl2, which becomes active upon phosphorylation downstream of Wnt/Ror2 binding (Gao et al., 2011), diminishes Fzd3 phosphorylation, leading to endocytosis of Fzd3 and an increase in PCP signaling output (Shafer et al., 2011). Therefore, in the presence of active Vangl2, Fzd3 is not stably localized to the plasma membrane. Interestingly, Celsr1 may play a role in Vangl2 membrane stabilization on an adjacent membrane. In cultured keratinocytes, Vangl2 is distributed diffusely throughout the cell and only becomes membrane localized when Celsr1 is expressed in an adjacent cell (Devenport and Fuchs, 2008). Thus, while membrane localization of Fzd3 is inhibited in a cell autonomous fashion by Vangl2, the non-cell autonomous promotion of Vangl2 membrane localization by Celsr1 may allow Fzd3 to accumulate at the membrane of an adjacent cell. More insight into how Vangl2/Pk complex formation may be inhibited in the presence of Fzd/Dvl comes from experiments where mouse PCP components were transfected into HEK cells (Narimatsu et al., 2009). When Fzd is activated by Wnt binding, it leads to the phosphorylation of Dvl2 as part of a Dvl2/Par6 complex. This activated Dvl2/Par6 complex recruits Smurf2

(a ubiquitin ligase), and targets Pk for proteosomal degradation in a local fashion (Narimatsu et al., 2009). The end result is the segregation of Fzd/Dvl on one membrane and Vangl2/Pk on the opposing membrane, as seen in *Drosophila*.

Figure 1.5. The non-canonical Wnt/planar cell polarity signaling pathway in FBMN migration.

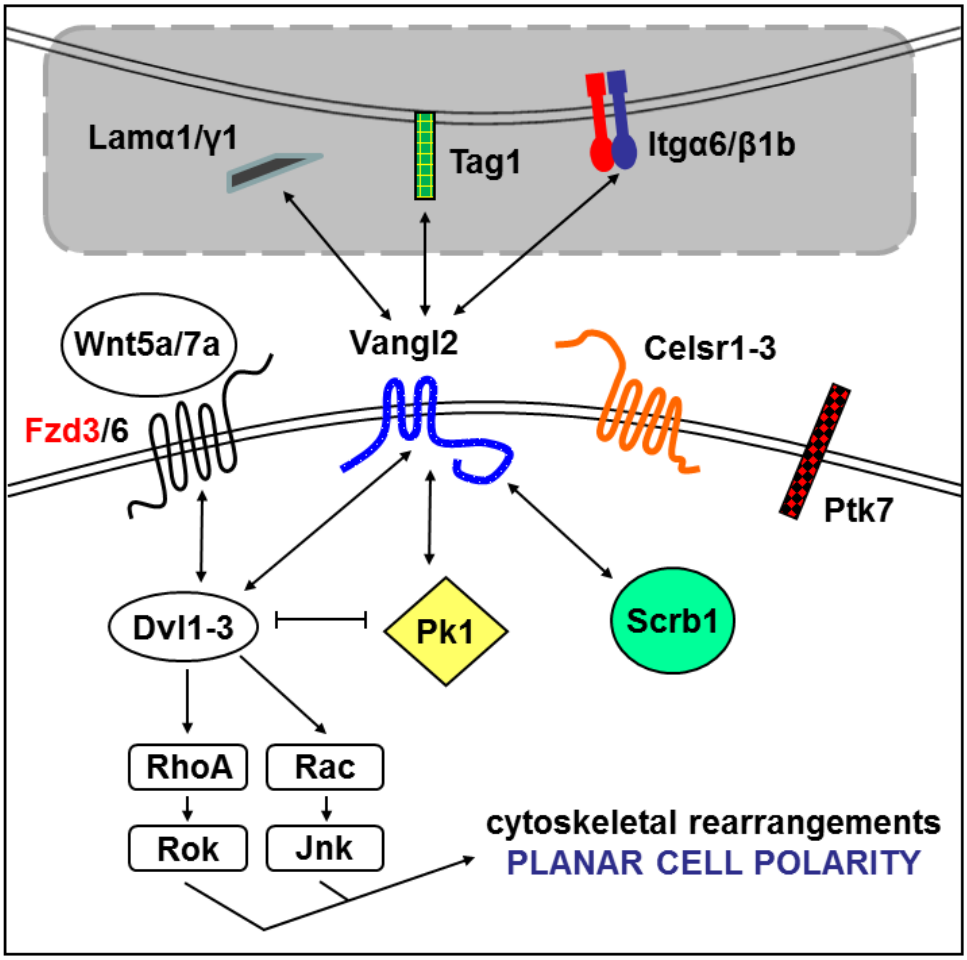

Figure 1.5. The non-canonical Wnt/planar cell polarity signaling pathway in FBMN migration.

Wnt/PCP molecules relevant to FBMN migration studies are shown, along with genetically interacting components (e.g. Laminins, Tag1). Colored molecules have demonstrated roles in FBMN migration in zebrafish, mice, or both. Molecules in the shaded box are required for FBMN migration in zebrafish and genetically interact with *stbm/vangl2*.

1.4.2. Role of Wnt/PCP signaling in zebrafish FBMN migration

Interesting insight into Wnt/PCP signaling has emerged from examining its role in neuronal migration in zebrafish. While Wnt/PCP molecules are required for processes such as convergence and extension, not all of them are necessary for caudal FBMN migration (**Table 1.1**). Many of the core Wnt/PCP genes including *stbm/vangl2*, *celsr1a/1b/2*, *pk1a/1b*, and *fzd3a*, are required for caudal FBMN migration (Bingham et al., 2002; Carreira-Barbosa et al., 2003; Mapp et al., 2010; Wada et al., 2006). However, *wnt5a/11* and *dsh* are not required (Jessen et al., 2002). This suggests that some Wnt/PCP genes function independently of other Wnt/PCP components in a novel pathway to regulate FBMN migration. Intriguingly, PCP-interacting genes from diverse pathways have demonstrated roles in FBMN migration (**Table 1.1**). Tag1, a cell adhesion molecule expressed in early-migrating FBMNs but not the environment, is necessary for FBMN migration and genetically interacts with *stbm/vangl2* (Sittaramane et al., 2009). Though physical interactions between tag1 and Wnt/PCP protein complexes have not been shown, this suggests a mechanism by which FBMNs can interpret migratory cues established by Wnt/PCP proteins, which typically function non-cell autonomously (Jessen et al., 2002; Wada et al., 2006). Furthermore, some laminins (Sittaramane et al., 2009) and integrins (Vinoth Sittaramane, unpublished data), which can function in cell adhesion and migration, are necessary FBMN migration and genetically interact with *stbm/vangl2*, indicating they may participate in a common mechanism to regulate FBMN migration.

Prior to this work, regulation of FBMN migration by non-canonical wnt/planar cell polarity (PCP) signaling molecules had only been demonstrated in zebrafish (*Danio rerio*). Therefore, we investigated whether Wnt/PCP molecules regulate FBMN migration in mammals. In addition to *Vangl2* and *Ptk7* **(Chapter 3)**, and *Celsr1* **(Chapters 4 and 5)**, other Wnt/PCP genes such as *Pk1* (Bernd Fritzsch, unpublished data), *Celsr2-3* and *Fzd3* (Qu et al., 2010), and *Scrb1* (Vivancos et al., 2009) have now been shown to be involved in FBMN migration in mice. We also investigated whether mouse FBMN migration is regulated independent of Dishevelled signaling **(Chapter 3)**, as analysis in zebrafish suggests.

Table 1.1. Wnt/PCP genes and *stbm/vangl2*-interacting genes required for FBMN migration in zebrafish (*Danio rerio*).

Gene	Encoded Protein	Reference
Wnt/PCP genes REQUIRED for FBMN migration		
celsr1a/1b	Atypical cadherin, CAM	(Wada et al., 2006)
celsr2	Atypical cadherin, CAM	(Wada et al., 2006)
fzd3a	Wnt receptor	(Wada et al., 2006)
pk1a	Cytoplasmic protein	(Carreira-Barbosa et al., 2003)
pk1b	Cytoplasmic protein	(Mapp et al., 2010)
scrb1	PDZ-rich cytoplasmic protein	(Wada et al., 2005)
stbm/vangl2	Four-pass transmembrane protein	(Bingham et al., 2002)
PCP genes NOT required for FBMN migration		
dsh	Cytoplasmic protein; downstream of fzd	(Jessen et al., 2002)
glypican4/6	heparan sulfate proteoglycan	(Bingham et al., 2002)
wnt5a	Secreted glycoprotein; ligand for wnt/PCP pathway	(Jessen et al., 2002)
wnt11	Secreted glycoprotein; ligand for wnt/PCP pathway	(Jessen et al., 2002)
stbm/vangl2-interacting genes REQUIRED for FBMN migration		
itgα6	Heterotrimeric receptor component	Chandrasekhar lab, unpublished
itgβ1b	Heterotrimeric receptor component	Chandrasekhar lab, unpublished
hdac1	Histone deacetylase	(Nambiar et al., 2007)
lamα1	Extracellular matrix glycoprotein	(Sittaramane et al., 2009)
lamγ1	Extracellular matrix glycoprotein	Chandrasekhar lab, unpublished
tag1	Glycoprotein CAM; ligand for APP	(Sittaramane et al., 2009)

Table 1.1. Wnt/PCP genes and *stbm/vangl2*-interacting genes required for FBMN migration in zebrafish (*Danio rerio*).

Data was compiled from both mutant and morphant zebrafish FBMN migration studies from published and unpublished sources. A non-PCP gene was termed "*stbm/vangl2*-interacting" if a genetic interaction with *stbm/vangl2* has been demonstrated specifically in the regulation of FBMN migration. Physical interactions with *stbm/vangl2* have not yet been tested in zebrafish. Abbreviations: APP, amyloid precursor protein; CAM, cell adhesion molecule; PCP, planar cell polarity.

CHAPTER 2: Protocols & Techniques

In each protocol described, reagents are referred to in their abbreviated forms (e.g. TBST, TEA). Please see section 2.7 for a detailed list of components and instructions on how to prepare each reagent.

2.1. Adult Mice

2.1.1. Colony maintenance

Mouse (*Mus musculus*) colonies were maintained using standard protocols approved by the Animal Care and Use Committee at the University of Missouri. A 12-hour day/night cycle, 72 – 73 °C room temperature, and 30 – 70% humidity were maintained. Mice were kept in conventional housing with corn cob bedding and at least one source of housing enrichment. For social enrichment, they were housed in groups with the exception of designated breeder males used for timed matings.

To best maintain and reduce the risk of losing specific mouse lines in the colony, a minimum of one breeding trio (one male plus two females), plus one stock cage each of genotyped males and females under 10 months old were kept in the facility at all times. At least every two generations, lines were outcrossed to wild type mice of the appropriate genetic background (e.g. C57BL/6NCrl, BALB/cAnNCrl, 129S2/SvPasCrl) newly purchased from Charles River Laboratories.

2.1.2. ID tagging

All mice in the colony were ID tagged at or before weaning age (P21) for purposes of tracking and genotyping. Each mouse was restrained by hand, and then a small animal ear tag (National Band & Tag, catalog number 1005-1, paint-filled) was applied using a stainless steel applicator (National Band & Tag, catalog number 1005s1). Ear tags were soaked in 70% ethanol immediately before use, and tags were applied midway down the pinna in order to avoid puncturing cartilaginous tissue.

2.1.3. Tissue collection and genomic DNA isolation

For genotyping purposes, DNA was purified from tail clips of mice at postnatal day 21 (P21) or younger. Each mouse was restrained by hand, and 0.5 cm of the tail was removed using a clean razor blade. To stop the bleeding, pressure was applied to the wound and Kwik Stop® Styptic Powder with Benzocaine (Fisher, catalog number NC9482281) was applied to the tip of the tail. If tail clips were collected at P21, the mice were immediately weaned; if before P21, they were placed back into the parent cage until weaning at P21.

Genomic DNA purification was carried out using the DNeasy® Blood & Tissue Kit (QIAGEN, catalog number 69504) per the manufacturer's instructions with the following modifications: 1.) Columns were washed in buffers AW1 and AW2 twice each instead of once; 2.) DNA was resuspended in 100 µL of buffer AE. The typical yield for a 0.5-cm tail clip is approximately 50 ng/µL. This method of purification is critical for the success

of genotyping assays for the *Celsr1*^{KO} and *Celsr1*^{floxed} alleles. However, assays for alleles such as *SE1::gfp*, *Dvl1*^{KO}, and *Dvl2*^{KO} are more robust and work well when using DNA purified by phenol-chloroform extraction.

Tail clips to be processed by phenol-chloroform extraction were digested overnight at 55 °C in 500 µL of lysis buffer with occasional vortexing. Subsequent steps were carried out at room temperature. After adding 700 µL of 1:1 phenol:chloroform (Fisher, catalog number BP1752), samples were mixed on a nutator for 30 minutes, followed by a 5 minute centrifugation at 18,704 x g (14,000 rpm on an Eppendorf 5424 centrifuge). 500 µL of the upper phase was transferred to a new tube and 1 mL of 100% ethanol added, followed by one minute mixing on a nutator to allow a pellet to form. DNA was pelleted for 5 minutes at 18,704 x g, followed by washing in 70% ethanol. After air drying, the purified DNA was resuspended in 100 µL of QIAGEN buffer EB.

2.1.4. Timed matings

Male studs were housed individually and designated as breeders for timed matings. To each male breeder, up to two ID-tagged, female mice were introduced in the afternoon and left overnight to allow mating. Each morning thereafter, females were examined for copulation plugs (hardened semen) as evidence of mating (Papaioannou and Behringer, 2005). Copulation plugs are often externally visible, but a seeker mall probe (Fisher, catalog number S17380) was used to probe internally in all unobvious cases. Each plugged female was transferred from the stud male's cage back

into her home cage and embryo collection was arranged for the desired date. Noon on the day in which a copulation plug was found, the embryos were considered to be staged at E0.5 (Nagy, 2003).

2.1.5. Euthanasia

Adult mice were euthanized by asphyxiation in 100% CO_2. Each mouse was placed in an uncharged, empty container spacious enough for it to assume its normal posture. The container was then covered and slowly flooded with 100% CO_2 until loss of consciousness. A cervical dislocation was then performed to assure death after an appropriate time in the CO_2 chamber. For female mice used for embryo collections, two minutes is sufficient since the freshest embryonic tissue is required. However, mice euthanized for other reasons (e.g. age, colony size reduction) were left in the CO_2 chamber for 10 – 20 minutes before performing cervical dislocation.

All procedures performed on live mice were approved by the University of Missouri Animal Care and Use Committee, and underwent periodic review.

2.2. Embryos

2.2.1. Dissection and staging

Pregnant females were euthanized via CO_2 asphyxiation and cervical dislocation. The mouse was then laid on its back and its abdomen soaked in 70% ethanol in order to minimize hair contamination in the dissection media. The uterus was removed using standard technique (Nagy, 2003) and placed in ice-cold PBS in a 100 mm x 15 mm petri dish (Fisher, catalog number 0875712). After rinsing in this dish, the intact uterus was transferred to a fresh PBS dish where the dissection was initiated. The method of removing embryos from the uterus varies greatly depending upon age. For E10.5 and younger, the uterine swellings were cut individually and the muscle layer removed with forceps (Nagy, 2003). For E11.5 and older, a single incision was made down the muscle layer using surgical scissors to release the pressure of the contracting uterus. Embryos were removed from their decidua (Nagy, 2003) and transferred to a fresh PBS dish for staging and tissue dissection, if desired.

The approximate age of each clutch was already known based on the day of copulation, but was confirmed using Thieler staging since some inbred strains can develop more slowly (Nagy, 2003).

2.2.2. Fixation and storage

The method and length of time for embryo tissue fixation varies greatly depending upon the application (e.g. *in situ* hybridization, immunohistochemistry, neuronal tract tracing, cross sections); however, some general guidelines should be followed since quality tissue is essential for good staining and imaging. The time between sacrificing of the mother and fixation of embryos must be minimized. All steps should be carried out with ice-cold media and fixative, and the fixative should be freshly thawed or freshly made. Subsequent steps in fixation – PFA to methanol dehydration for *in situ* hybridization – should be done quickly and consistently. Lastly, the storage time for fixed embryos should be minimized for best results.

2.2.3. Tissue collection and genomic DNA isolation

For embryos requiring genotyping, a small amount of tissue was collected during dissection for genomic DNA isolation. To minimize contamination between samples, clean forceps were used and wiped down with 70% ethanol between each sample. A small amount of tissue – the size of an E12.5 handplate – was collected into a 1.5-mL microcentrifuge tube filled with PBS. The PBS was removed, replaced with 100 µL of lysis buffer, and incubated at 55 °C for two hours with occasional mixing. DNA was precipitated by adding 1 µL of glycogen (Roche, catalog number 10901393001) plus 200 µL of 100% ethanol per sample, gently mixed, then stored at -20 °C overnight. The following day, the DNA was pelleted at 14,000 rpm for 5 minutes, washed in 250 µL of

70% ethanol, air dried at 37 °C, and resuspended in 35 µL of QIAGEN buffer EB (available in QIAGEN PCR purification kits).

Optimally, the lysis buffer should be added to all tissue samples immediately after dissection of each clutch of embryos. Alternatively, tissue samples can be fixed in 4% PFA and held indefinitely, then rinsed with PBS before incubating in the lysis buffer. This method also works well to re-genotype, if needed, tissue samples previously processed for *in situ* hybridization.

Generally, small tissue samples from the handplate or tail are convenient for genomic DNA isolation. *When using the Cre-loxP system, however, one must only collect DNA from tissues that are Cre-negative. Otherwise, false genotyping results can occur due to the excision of a floxed allele (resulting in a KO allele) by the active Cre recombinase in those tissues.*

2.2.4. Embedding in O. C. T. for frozen sectioning

Embryos can be prepared for frozen sectioning either post-staining or in preparation for staining on sections. In either case, embryos are first incubated in 30% sucrose in PBS-DEPC at 4 °C overnight or until the tissue sinks. This step protects the tissue from freezing damage due to ice formation. Each embryo was subsequently transferred to peel away embedding molds (Electron Microscopy Sciences, catalog number 70182), excess sucrose was removed, and the mold was filled halfway with O. C. T. compound (Tissue-Tek, catalog number 4583). After swirling to disperse any

remaining sucrose, the tissue was oriented as desired adjacent to a flat wall of the mold, then the mold was transferred into a dry ice/100% ethanol bath. With constant monitoring under a dissection scope, each sample was flash frozen in the bath, individually wrapped and labeled, and stored at -80 °C indefinitely. It is important to label the precise location of the embryo in the frozen block, as the block must be glued to the cryostat chuck on the side opposite from the sample.

2.3. Mouse Lines & Genotyping

An overview of mouse lines maintained by our lab and used in this study is shown in **Table 2.1**.

Table 2.1. Mouse lines used in this study.

Mouse Line	MGI #	Source	Maintained in Genetic Background	Referred To As	Described in Section
Vangl2$^{Lp\text{-}m1Jus}$	1934175	Olivier Pourquié (IGBMC; France)	C57BL/6NCrl	*Vangl2*^{Lp}	2.3.1
Celsr1^{Crsh}	2668337	Murdoch (MRC; UK)	BALB/cAnNCrl	*Celsr1*^{Crsh}	2.3.2
Celsr1^{floxed}		Fadel Tissir (Univ. of Louvain; Belgium)	C57BL/6NCrl	*Celsr1*^{floxed}	2.3.3
Celsr1^{tm1Fati}	4430217	Fadel Tissir (Univ. of Louvain; Belgium)	C57BL/6NCrl	*Celsr1*^{KO}	2.3.4
Dvl1^{tm1Awb}	2137230	The Jackson Laboratory (stock #007965)	129S2/SvPasCrl	*Dvl1*^{KO}	2.3.5
Dvl2^{tm1Awb}	2429760	The Jackson Laboratory (stock #008001)	129S2/SvPasCrl	*Dvl2*^{KO}	2.3.6
r4-Cre		Michèle Studer (Univ. of Nice; France)	C57BL/6NCrl	r4-Cre	2.3.7
Egr2$^{tm2(cre)Pch}$	1931056	Susan Dymecki (Harvard Univ.)	C57BL/6NCrl	*Krox20*^{Cre}	2.3.8
Shh$^{tm1(EGFP/cre)Cjt}$	3053959	The Jackson Laboratory (stock #005622)	C57BL/6NCrl	*Shh*^{Cre}	2.3.9
Tg(Isl1-EGFP)2Slp	3779017	Samuel Pfaff (Salk Institute)	C57BL/6NCrl	*SE1::gfp*	2.3.10
Gt(ROSA)26Sor$^{tm4(ACTB\text{-}tdTomato,\text{-}EGFP)Luo}$	3716464	Dawn Cornelison (Univ. of Missouri)	C57BL/6NCrl	*ROSA26*^{mTmG}	2.3.11

2.3.1. *Vangl2 Looptail*^{D255E} mutant mouse line

The *Lp*^{D255E} mutation was created by ENU mutagenesis (Kibar et al., 2001). It contains an T1228A missense mutation in the fifth exon of *Vangl2* (GenBank accession #BC052195.1), which generates a D255E mutation in the C-terminal cytoplasmic portion of the protein adjacent to the plasma membrane (Torban et al., 2004b). Homozygous embryos and heterozygous adults exhibit the same array of phenotypes as *Lp*^{S464N} mice (Kibar et al., 2001).

Embryos were genotyped by PCR amplifying a 243-bp sequence surrounding the point mutation, followed by standard sequencing of the PCR product. PCR conditions are as follows (50 µL reaction):

(The following abbreviation is used: mM = millimolar concentration)

Component	[Stock]	[Final]	µL/reaction
nuclease-free water	--	--	18
GoTaq Green Master Mix (Promega M7123)	2X	1X	25
Forward primer 5'-GGTTCAGTTTGCCGTTTCTC-3'	10 µM	0.5 µM	2.5
Reverse primer 5'-CCCTCCTTCCCCTAAACCTT-3'	10 µM	0.5 µM	2.5
genomic DNA	--	--	2

Thermocycler conditions: 95 °C, 5 min; [(95 °C, 45 sec), (56.2 °C, 30 sec), (72 °C, 1 min)] x 30 cycles; 72 °C, 10 min; hold at 4 °C.

The resulting PCR product is purified using the QIAquick PCR Purification Kit (QIAGEN 28104) per the manufacturer's instructions, resuspending the DNA in the lowest recommended volume. A purified PCR product as dilute as 5 ng/µL can be used successfully, though the typical yield is 25 – 35 ng/µL. The product is submitted for sequencing using forward primer 5'-GGTTCAGTTTGCCGTTTCTC-3'. The genotyping results are determined by examining the sequence chromatogram for the presence of the point mutation within the region of 5'-GATCCACAGA(T/A)GGGGCCAGCC-3'. The wild-type allele is T and the mutant allele reads A (**Figure 2.1 A**). For heterozygous mice, the base will most often display N, although sometimes the software may call T or A. The actual peaks must be examined closely to verify that both T and A are present and that their peaks are approximately equal in height.

Figure 2.1. Sequence genotyping assays for the *Vangl2*^{Lp} and *Celsr1*^{Crsh} alleles.

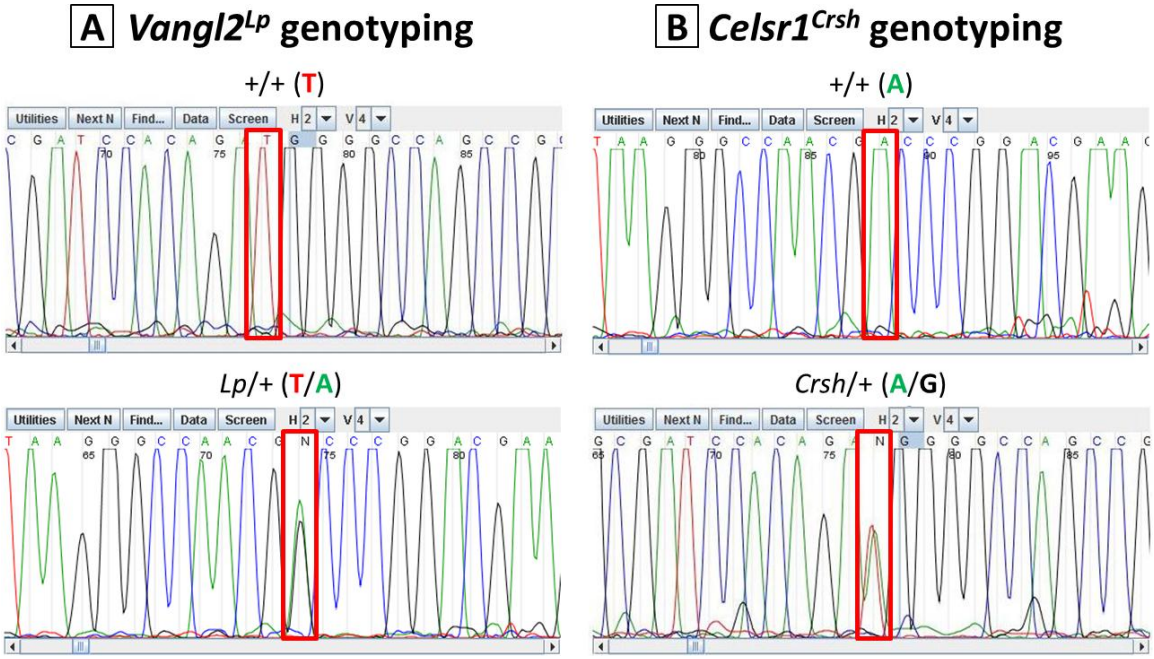

Figure 2.1. Sequence genotyping assays for the *Vangl2*^{Lp} and *Celsr1*^{Crsh} alleles.

A-B, Snapshots of sequence chromatograms around the region of the *Vangl2*^{Lp} (**A**) and *Celsr1*^{Crsh} (**B**) missense mutations. Each nucleotide of interest is boxed in red. **A**, At nucleotide 1228 of *Vangl2* (GenBank accession #BC052195.1), WT mice display T, whereas *Lp*/+ mice display approximately equal sized peaks of T and A. **B**, At nucleotide 1040 of *Celsr1* (GenBank accession #AF031572.1), WT mice display A, whereas *Crsh*/+ mice display approximately equal sized peaks of A and G.

2.3.2. *Celsr1*^{Crash} mutant mouse line

The *Crash (Crsh)* mutant line was created by ENU mutagenesis (Curtin et al., 2003). It contains an A3119G missense mutation in the first exon of *Celsr1* (GenBank accession #AF031572.1), which generates a D1040G mutation in the eighth cadherin repeat of the protein. Homozygous mutants exhibit perinatal lethality, but heterozygous animals are viable and fertile (Curtin et al., 2003). Adult heterozygous *Crsh* mice are easily identifiable, exhibiting head shaking behavior and uncontrollable spinning during tail suspension, making genotyping of adult mice unnecessary. The severity of this phenotype lessens, however, when outcrossed from BALB/c into other genetic backgrounds (D.G., unpublished observations).

Embryos were genotyped by PCR amplifying a 214-bp sequence surrounding the point mutation, followed by standard sequencing of the PCR product. PCR conditions are as follows (50 µL reaction):

Component	[Stock]	[Final]	µL/reaction
nuclease-free water	--	--	35
ThermoPol buffer (NEB M0267S)	10X	1X	5
dNTP mix	10 mM	0.2 mM	1
forward primer 5'-AATTCAGGTGAGTGTGTTGGA-3'	10 µM	0.5 µM	2.5
reverse primer 5'-GTCACCACTCAGTAGGTCCAG-3'	10 µM	0.5 µM	2.5
Taq DNA polymerase (NEB M0267S)	5 U/µL	0.2 U/µL	2

genomic DNA -- -- 2

Thermocycler conditions: 95 °C, 5 min; [(95 °C, 1 min), (65.1 °C, 30 sec), (72 °C, 1 min)] x 30 cycles; 72 °C, 5 min; hold at 4 °C.

The resulting PCR product is purified using the QIAquick PCR Purification Kit (QIAGEN 28104) per the manufacturer's instructions, resuspending the DNA in the lowest recommended volume. A purified PCR product as dilute as 5 ng/μL can be used successfully, though the typical yield is 25 – 35 ng/μL. The product is submitted for sequencing using forward primer 5'-AATTCAGGTGAGTGTGTTGGA-3'. The genotyping results are determined by examining the sequence chromatogram for the presence of the point mutation within the region of 5'-AGGGCCAACG(A/G)CCCGGACGAA-3'. The wild-type allele is A and the mutant allele reads G (**Figure 2.1 B**). For heterozygous mice, the base will most often display N, although sometimes the software may call A or G. The actual peaks must be examined closely to verify that both A and G are present and that their peaks are approximately equal in height.

2.3.3. *Celsr1*^{floxed} mouse line

To create *Celsr1* conditional mutant mice, loxP sites were introduced into introns 25 and 29 of the *Celsr1* gene (Ravni et al., 2009). Thus, in the presence of Cre recombinase, exons 26 through 29 are deleted, which corresponds to transmembrane domains 5 through 7 of the Celsr1 protein.

Genotyping of the *Celsr1*^{floxed} allele was performed by PCR amplification of intron 29. The *Celsr1*^{floxed} allele produces a larger product size than the WT allele due to the introduction of the loxP sequence (Ravni et al., 2009). PCR conditions are as follows (20 µL reaction):

Component	[Stock]	[Final]	µL/reaction
nuclease-free water	--	--	14.8
FastStart buffer with Mg^{2+} (Roche 03553426001)	10X	1X	2
dNTP mix	10 mM	0.2 mM	0.4
forward primer 5'- CCACTCTGCTAACGGTAGG-3'	10 µM	0.375 µM	0.8
reverse primer 5'- GAAAGAGACTGTTGGTGAGC-3'	10 µM	0.375 µM	0.8
FastStart DNA polymerase blend (Roche 03553426001)	5 U/µL	0.05 U/µL	0.2
genomic DNA (purified via QIAGEN DNeasy Blood & Tissue Kit)	--	--	1

Thermocycler conditions: 95 °C, 5 min; [(94 °C, 30 sec), (58 °C, 30 sec), (72 °C, 30)] x 30 cycles; 72 °C, 10 min; hold at 4 °C.

The resulting product is analyzed on a 0.7% agarose 0.5X TBE gel. WT mice (no floxed alleles) are characterized by a 389-bp band, whereas homozygous (*Celsr1*$^{floxed/floxed}$) mice yield a 596-bp band. Heterozygous mice yield bands of both 389 bp and 596 bp (**Figure 2.2 A**).

It is important to note that this primer set will not amplify the *Celsr1*^{KO} allele since the forward primer anneals to a portion of intron/exon 29 of *Celsr1* that has been

deleted in the *Celsr1*^{KO} allele. For crosses generating individuals with the genotype *Celsr1*$^{KO/floxed}$, it is necessary to perform both the *Celsr1*^{floxed} assay and the *Celsr1*^{KO} assay. These animals will appear to be *Celsr1*$^{floxed/floxed}$ and *Celsr1*$^{KO/KO}$ in the respective genotyping assays.

Figure 2.2. PCR genotyping assays for mutant and transgenic mouse lines.

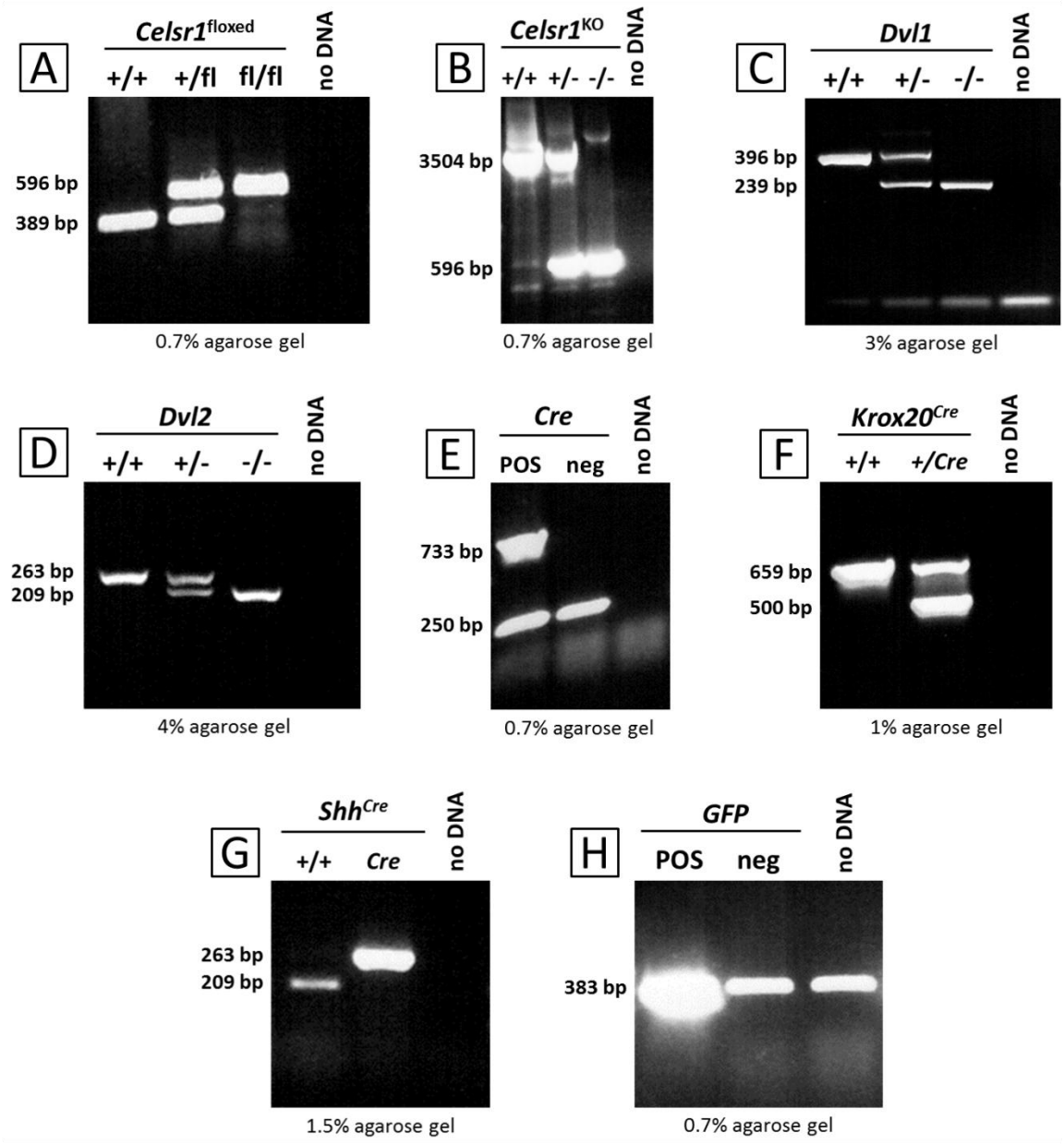

Figure 2.2. PCR genotyping assays for mutant and transgenic mouse lines.

Typical results for standard PCR genotyping assays used in this analysis. For each assay, the expected band sizes, corresponding genotypes, and type of gel are indicated. Negative control lanes (no DNA template) are included to show the presence of primer bands, if any. Complete protocols for the assays are described in their respective sections.

2.3.4. *Celsr1*^{KO} mutant mouse line

To create the *Celsr1*^{KO} line, *Celsr1*^{floxed} mice were crossed with PGK-Cre mice to ubiquitously delete exons 26 through 29 of *Celsr1*, which corresponds to transmembrane domains 5 through 7 (Ravni et al., 2009). *Celsr1* mRNA transcripts are five-fold lower in *Celsr1*$^{KO/KO}$ mice compared to WT and are predicted to result in a truncated protein that is also lacking its cytoplasmic portion (Ravni et al., 2009). Homozygous embryos have varying degrees of neural tube morphology, ranging from normal in appearance to complete craniorachischisis. Some *Celsr1*$^{KO/KO}$ mice are viable but are smaller and noted by their obvious defects in hair follicle orientation (Ravni et al., 2009).

Genotyping of the *Celsr1*^{KO} allele was performed by PCR amplifying the region between introns 25 and 29 of *Celsr1*. The *Celsr1*^{KO} allele produces a much smaller band compared to the WT allele due to the deletion of exons 26 through 29. PCR conditions are as follows (25 µL reaction):

Component	[Stock]	[Final]	µL/reaction
nuclease-free water	--	--	19.745
Long Template buffer #1 (Roche 11681834001)	10X	1X	2.5
dNTP mix	10 mM	0.35 mM	0.875
forward primer 5'- CTCTGTTGACTTCTGACTGG-3'	10 µM	0.3 µM	0.75
reverse primer 5'- GAAAGAGACTGTTGGTGAGC-3'	10 µM	0.3 µM	0.75

Long Template polymerase blend (Roche 11681834001)	5 U/µL	0.076 U/µL	0.38
genomic DNA (purified via QIAGEN DNeasy Blood & Tissue Kit)	--	--	1

Thermocycler conditions: 95 °C, 4 min; [(94 °C, 1 min), (55 °C, 1 min), (72 °C, 4 min 30 sec)] x 40 cycles; 72 °C, 15 min; hold at 4 °C.

The resulting product is analyzed on a 0.7% agarose 0.5X TBE gel. The WT allele is characterized by a 3504-bp band, whereas the *Celsr1*^{KO} allele produces a 596-bp band. Heterozygous mice show both 3504 bp and 596 bp bands (**Figure 2.2 B**).

It is important to note that this primer set will not amplify the *Celsr1*^{floxed} allele since the forward primer anneals to a portion of intron 25 of *Celsr1* that has been replaced by the loxP sites and Neo cassette. For crosses generating individuals with the genotype *Celsr1*$^{KO/floxed}$, it is necessary to perform both the *Celsr1*^{floxed} assay and the *Celsr1*^{KO} assay. These animals will appear to be *Celsr1*$^{floxed/floxed}$ and *Celsr1*$^{KO/KO}$ in the respective genotyping assays.

2.3.5. *Dishevelled 1* mutant mouse line

Dishevelled (*Dvl*) *1* mutant mice lack part of exon 2 and all of exons 3 and 4, and no protein can be detected on Western blots (Lijam et al., 1997). No gross anatomical or motor defects have been reported in these mutants; however, *Dvl1*$^{-/-}$ adults display a variety of social abnormalities and have sensorimotor gating defects (Lijam et al., 1997; Long et al., 2004).

Genotyping was performed by standard PCR as follows (50 µL reaction) (http://jaxmice.jax.org/protocolsdb/f?p=116:2:1048897077745801::NO:2:P2_MASTER_PROTOCOL_ID,P2_JRS_CODE:3480,007965):

Component	[Stock]	[Final]	µL/reaction
nuclease-free water	--	--	15.5
GoTaq Green Master Mix (Promega M7123)	2X	1X	25
Forward primer (mutant allele) 5'- GCCAGAGGCCACTTGTGTAG-3'	10 µM	0.5 µM	2.5
Forward primer (WT allele) 5'- GACAACATAGCAGGGGCCTA-3'	10 µM	0.5 µM	2.5
Reverse primer 5'- CACAGGGGCTAGGAGTACCA-3'	10 µM	0.5 µM	2.5
genomic DNA (purified via phenol/chloroform extraction)	--	--	2

Thermocycler conditions: 95 °C, 5 min; [(95 °C, 45 sec), (60.4 °C, 1 min), (72 °C, 1 min)] x 35 cycles; 72 °C, 2 min; hold at 4 °C.

The resulting product is analyzed on a 2-3% agarose 0.5X TBE gel. The WT allele is characterized by a 396-bp band, whereas the mutant allele produces a 239-bp band. Heterozygous mice show both 396 bp and 239 bp bands (**Figure 2.2 C**).

2.3.6. *Dishevelled 2* mutant mouse line

Dishevelled (*Dvl*) *2* mutant mice lack exons 3 - 6, and no protein can be detected on Western blots (Hamblet et al., 2002). For 50% of *Dvl2* homozygous mutants, this

results in perinatal lethality due to cardiac defects (Hamblet et al., 2002). Neural tube defects are present in 2 – 3% of *Dvl2* mutants, and most surviving adults have kinked tails (Hamblet et al., 2002), consistent with a role for *Dvl2* in the Wnt/PCP pathway.

Genotyping was performed by standard PCR as follows (50 µL reaction) (http://jaxmice.jax.org/protocolsdb/f?p=116:2:4281157126504667::NO:2:P2_MASTER_PROTOCOL_ID,P2_JRS_CODE:1482,008001):

Component	[Stock]	[Final]	µL/reaction
nuclease-free water	--	--	15.5
GoTaq Green Master Mix (Promega M7123)	2X	1X	25
Forward primer (mutant allele) 5'-GCCAGAGGCCACTTGTGTAG-3'	10 µM	0.5 µM	2.5
Forward primer (WT allele) 5'-CCACCTCCAAATGCTATGCT-3'	10 µM	0.5 µM	2.5
Reverse primer 5'-GAATCGGTGACACTGCTGAA-3'	10 µM	0.5 µM	2.5
genomic DNA (purified via phenol/chloroform extraction)	--	--	2

Thermocycler conditions: 95 °C, 5 min; [(95 °C, 45 sec), (55 °C, 1 min), (72 °C, 1 min)] x 35 cycles; 72 °C, 2 min; hold at 4 °C.

The resulting product is analyzed on a 3% agarose 0.5X TBE gel. The WT allele is characterized by a 263-bp band, whereas the mutant allele produces a 209-bp band. Heterozygous mice show both 263 bp and 209 bp bands (**Figure 2.2 D**).

2.3.7. r4-Cre mouse line

r4-Cre transgenic mice express Cre recombinase under the control of a *Hoxb1* r4 enhancer. By E9.0, Cre expression is confined solely to r4-derived tissues, whereas endogenous *Hoxb1* at E9.0 is widespread in trunk tissues (Studer et al., 1998).

Genotyping was performed by PCR amplification of the *Cre* allele as follows (25 µl reaction):

Component	[Stock]	[Final]	µL/reaction
nuclease-free water	--	--	6.5
GoTaq Green Master Mix (Promega M7123)	2X	1X	12.5
Forward primer (Cre) 5'-TTGCCGGTCGTGGGCGGCATGGTGC-3'	10 µM	0.5 µM	1.25
Reverse primer (Cre allele) 5'-CACGGGCACTGTGTCCAGACCAGGC-3'	10 µM	0.5 µM	1.25
Forward primer (Actin) 5'-CAACCGAGACCTTCCTGTTC-3'	10 µM	0.5 µM	1.25
Reverse primer (Actin) 5'-ATGTGGATGGAGAGGAGTCG-3'	10 µM	0.5 µM	1.25
genomic DNA (purified via QIAGEN DNeasy Blood & Tissue Kit)	--	--	1

Thermocycler conditions: 95 °C, 5 min; [(95 °C, 45 sec), (60 °C, 1 min), (72 °C, 1 min)] x 35 cycles; 72 °C, 2 min; hold at 4 °C.

The resulting product is analyzed on a 0.7% agarose 0.5X TBE gel. The presence of a 250-bp actin band verifies the quality of the DNA template, and the presence of Cre

is characterized by a 733-bp band (**Figure 2.2 E**). This assay will not distinguish between mice carrying one or two copies of Cre.

2.3.8. *Krox20^{Cre}* mouse line

Krox20^{Cre} mice were generated by replacing, via homologous recombination, a portion of exons 1 and exon 2 with nls-*Cre*. This places *Cre* under the control of the *Krox20* regulatory elements but renders *Krox20* a null allele (Voiculescu et al., 2000). *Cre* expression is consistent with normal *Krox20* gene expression (Voiculescu et al., 2000; Voiculescu et al., 2001).

Genotyping was performed by standard PCR amplification as follows (25 µl reaction):

Component	[Stock]	[Final]	µL/reaction
nuclease-free water	--	--	7.75
GoTaq Green Master Mix (Promega M7123)	2X	1X	12.5
Common reverse primer 5'-CTTTACACAGCATCGCCAAG-3'	10 µM	0.5 µM	1.25
Forward primer (WT allele) 5'-TTGACCAGATGAACGGAGTG-3'	10 µM	0.5 µM	1.25
Forward primer (*Krox20^{Cre}* allele) 5'-ATCAGGACATAGCGTTGGCT-3'	10 µM	0.5 µM	1.25
genomic DNA (purified via QIAGEN DNeasy Blood & Tissue Kit)	--	--	1

Thermocycler conditions: 95 °C, 5 min; [(95 °C, 45 sec), (53 °C, 1 min), (72 °C, 1 min)] x 35 cycles; 72 °C, 2 min; hold at 4 °C.

The resulting product is analyzed on a 1% agarose 0.5X TBE gel. The WT *Krox20* allele is characterized by a 659-bp band, whereas the *Krox20*^{Cre} allele produces a 500-bp band. Heterozygous mice show both the 659-bp and 500-bp bands (**Figure 2.2 F**).

2.3.9. *Shh*$^{EGFP\text{-}Cre}$ mouse line

Shh$^{EGFP\text{-}Cre}$ mice were generated by inserting an *EGFP-Cre* cassette at the ATG of the *Shh* locus, rendering *EGFP-Cre* under the control of *Shh* regulatory elements (Harfe et al., 2004). *Cre* expression recapitulates the *Shh* expression pattern in these mice, and *Shh* is non-functional due to the deletion of bases 1 – 35 of the *Shh* open reading frame (Harfe et al., 2004).

Genotyping was performed by standard PCR amplification as follows (25 µl reaction)

(http://jaxmice.jax.org/protocolsdb/f?p=116:2:3138008314039253::NO:2:P2_MASTER_PROTOCOL_ID,P2_JRS_CODE:1073,005622):

Component	[Stock]	[Final]	µL/reaction
nuclease-free water	--	--	6.625
GoTaq Green Master Mix (Promega M7123)	2X	1X	12.5
Common forward primer 5'-GGGACAGCTCACAAGTCCTC-3'	10 µM	0.5 µM	1.25

Reverse primer (WT allele) 5'-CTCGGCTACGTTGGGAATAA-3'	10 µM	0.5 µM	1.25
Reverse primer (*Shh*$^{EGFP-Cre}$ allele) 5'-GGTGCGCTCCTGGACGTA-3'	10 µM	0.5 µM	1.25
Perfect Match PCR Enhancer (Stratagene 600129)	1 U/µL	0.04 U/µL	0.125
genomic DNA (purified via QIAGEN DNeasy Blood & Tissue Kit)	--	--	2

Thermocycler conditions: 94 °C, 3 min; [(94 °C, 30 sec), (64 °C, 45 sec), (72 °C, 1 min)] x 35 cycles; 72 °C, 2 min; hold at 4 °C.

The resulting product is analyzed on a 1.5% agarose 0.5X TBE gel. The WT *Shh* allele is characterized by a 200-bp band, whereas the *Shh*$^{EGFP-Cre}$ transgene produces a 350-bp band. Heterozygous mice show both the 200-bp and 350-bp bands (**Figure 2.2 G**).

2.3.10. *SE1::gfp* mouse line

SE1::gfp mice transgenic mice were generated by using a motor neuron-specific enhancer element (SE1, CREST1) normally located 3' to the *Isl1* gene to drive GFP expression (Shirasaki et al., 2006). As a result, GFP is expressed in the cell bodies and axons of *Isl1*-expressing neurons (Qu et al., 2010; Shirasaki et al., 2006; Song et al., 2006). GFP expression in the hindbrain region is robust until E14.5.

Genotyping was performed by standard PCR amplification as follows (25 µl reaction):

Component	[Stock]	[Final]	µL/reaction
nuclease-free water	--	--	9
GoTaq Green Master Mix (Promega M7123)	2X	1X	12.5
Forward primer 5'-CGCACCATCTTCTTCAAGGACGAC-3'	10 µM	0.5 µM	1.25
Reverse primer 5'-AACTCCAGCAGGACCATGTGATCG-3'	10 µM	0.5 µM	1.25
genomic DNA (purified via QIAGEN DNeasy Blood & Tissue Kit)	--	--	1

Thermocycler conditions: 94 °C, 3 min; [(94 °C, 30 sec), (60 °C, 30 sec), (72 °C, 1 min)] x 35 cycles; 72 °C, 10 min; hold at 4 °C.

The resulting product is analyzed on a 0.7% agarose 0.5X TBE gel. Presence of the GFP transgene is characterized by a 383-bp band; however, GFP-negative samples and samples lacking a DNA template will produce a primer band at approximately 400 bp. The primer band is less intense; therefore, samples with more intense bands are deemed to be GFP-positive (**Figure 2.2 H**). This assay cannot distinguish between mice carrying one or two copies of GFP.

2.3.11. ROSA26^{mTmG} mouse line

ROSA26^{mTmG} mice express membrane-targeted tdTomato (mT) under the control of the strong and ubiquitous CMV enhancer/chicken β-actin core promoter (pCA) at the ROSA26 locus (Muzumdar et al., 2007). In the presence of Cre recombinase, the mT

cassette is excised, allowing for the expression of membrane-targeted EGFP (mG) located downstream. The robust expression of mT/mG makes these mice an effective Cre reporter strain and useful for lineage tracing applications.

In lieu of PCR genotyping, ROSA26^{mTmG} mice are easily identified by the examining tail clips for red fluorescence. This can be accomplished using a rhodamine emission filter on a stereomicroscope at 25X total magnification. Likewise, embryos carrying the ROSA26^{mTmG} allele show red fluorescence in all Cre-negative tissues.

2.4. *In Situ* Probe Synthesis

2.4.1. DNA preparation

To generate DNA to be used for *in situ* hybridization probe synthesis, primers were designed to amplify a unique region of the gene of interest. For optimal penetration of the probe during the hybridization step, fragments between 400 – 800 bp were used. The resulting PCR product was kit-purified (QIAGEN, catalog number 28104) and cloned into a plasmid carrying one or more of the T7, SP6, or T3 promoters (e.g. pGEM-T Easy, pBluescript). The plasmid was linearized just downstream of the gene fragment to allow for transcription termination, and purified via phenol-chloroform extraction as described (Maniatis et al., 1982).

2.4.2. Synthesis of labeled RNA

Probe synthesis was carried out using a DIG RNA labeling kit (Roche, catalog number 11175025910) as follows:

Component	[Stock]	[Final]	µL/reaction
nuclease-free water	--	--	31.8
Transcription buffer	10X	1X	5
dig (or flu) labeled NTP mix	10X	1X	5
Protector RNAse inhibitor	20 U/µL	0.8 U/µL	2
Linearized template DNA	1 µg/µL	0.02 µg/µL	1.2
RNA polymerase (T7, SP6, T3)	10 µM	0.5 µM	2.5

The reaction was incubated for two hours at 37 °C. To precipitate the probe RNA, 1 µL of 20 µg/µL glycogen (Roche, catalog number 10901393001), 5 µL of 0.2 M EDTA, 6.3 µL of 4 M LiCl, and 190 µL of 100% ethanol were added, and the sample was allowed to precipitate overnight at -20 °C. The following day, the RNA was pelleted at 15,000 rpm at 4 °C for 10 minutes, washed with 250 µL of 70% ethanol, and resuspended in 30 µL of nuclease-free water. Probes were stored at -20 °C for up to several years, and *in vitro* transcript quality was assessed on an RNA gel (**Figure 2.3**).

Figure 2.3. Sample quality assessment of synthesized *in situ* riboprobes.

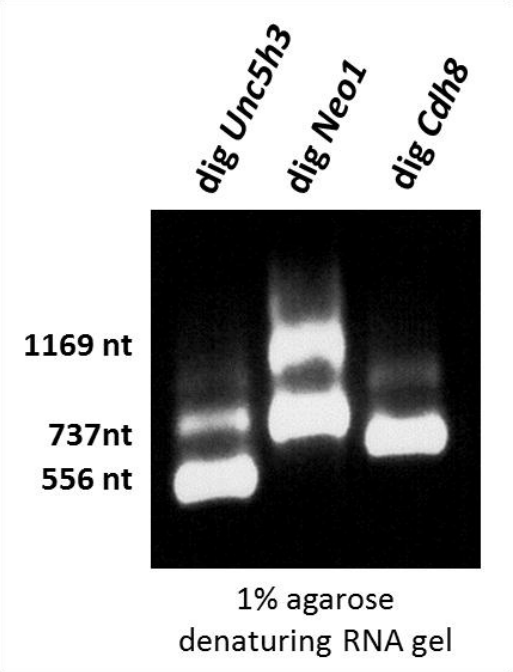

Figure 2.3. Sample quality assessment of synthesized *in situ* riboprobes.

Typical appearance of high-quality *in situ* riboprobes on a denaturing RNA gel. Synthesis of each riboprobe shows multiple bands, but generally produces satisfactory *in situ* hybridization results. Abbreviations: dig, digoxygenin-labeled; nt, nucleotides.

2.4.3. RNA gel electrophoresis

RNA probes were assessed on a denaturing gel to minimize secondary structure formation and allow for accurate size determination. In a 500-mL conical flask, 1 g of agarose was dissolved in 84.8 mL of dH_2O. Under a fume hood on a swirling hot plate, 5.2 mL of 37% formaldehyde (Fisher, catalog number BP531) was added, followed by 10 mL of 10X MOPS. The gel was cast immediately, and after solidifying, the chamber was flooded with 1X MOPS running buffer.

Each lane was loaded with 2 µL of RNA probe, 1 µL of 0.1% ethidium bromide (Fisher, catalog number BP1302), and 15 µL of 1.25X RNA loading buffer. Distinct bands on the gel indicate a high-quality synthesis (**Figure 2.3**), whereas a smear indicates a low-quality synthesis or degradation. Multiple bands for one probe is normal and usually produces good *in situ* results.

2.5. Expression Analysis

Multiple techniques for the *in situ* detection of RNA and protein were utilized and are detailed below. The optimal dilutions for riboprobes and antibodies used in this work are listed in **Table 2.2**.

Table 2.2. Antibody and *in situ* probe dilutions.

PROBE	DILUTION	METHOD	PROBE	DILUTION	METHOD
ALDH5A1	1:625	section ISH	*Neo1*	1:500	whole-mount ISH
Cdh8	1:500	whole-mount ISH	*Nkx6.1*	1:500	whole-mount ISH
Celsr1	1:500	whole-mount ISH	*Phox2b*	1:500	whole-mount ISH
Foxa2	1:500	whole-mount ISH	*Plxna1*	1:500	whole-mount ISH
Gad1	1:625	section ISH	*Ptk7*	1:250	whole-mount ISH
Gata3	1:250	whole-mount ISH	*Ret7*	1:250	whole-mount ISH
Hb9	1:500	whole-mount ISH	*Sek1*	1:500	whole-mount ISH
Hoxa2	1:500	whole-mount ISH	*Sema3a*	1:250	whole-mount ISH
Hoxb1	1:500	whole-mount ISH	*SLC6A4*	1:625	section ISH
Isl1	1:500	whole-mount ISH	*TAG-1*	1:500	whole-mount ISH
Krox20	1:500	whole-mount ISH	*Tbx20*	1:500	whole-mount ISH
Mash1	1:250	whole-mount ISH	*Unc5h3*	1:500	whole-mount ISH
Math1	1:500	whole-mount ISH	*Vangl2*	1:500	whole-mount ISH
Math3	1:500	whole-mount ISH	*Wnt5a*	1:250	whole-mount ISH

ANTIBODY	DILUTION	METHOD	VENDOR	CATALOG NUMBER
Primary ABs				
mouse α-NF	1:100	whole-mount IHC	DSHB	2H3
mouse α-NF-160	1:300	whole-mount IHC	Sigma	N5264
rabbit α-GFP	1:400	whole-mount IHC	Invitrogen	A11122
mouse α-Isl1	1:500	section IHC	DSHB	39.4d5
rabbit α-GFP	1:500	section IHC	Invitrogen	A11122
Secondary ABs				
goat α-mouse HRP	1:300	whole-mount IHC	Sigma	A3682
goat α-mouse 568 nm	1:250	section IHC	Invitrogen	A11004
chicken α-rabbit 488 nm	1:250	section IHC	Invitrogen	A21441

Table 2.2. Antibody and *in situ* probe dilutions.

The optimal dilutions for *in situ* probes, primary antibodies, and secondary antibodies successfully used in the lab are listed. The appropriate detection method, vendor, and catalog number are also included. Abbreviations: ISH, *in situ* hybridization; IHC, immunohistochemistry; AB, antibody; α, anti; HRP, horseradish peroxidase; nm, nanometer; DSHB, Developmental Studies Hybridoma Bank (University of Iowa).

2.5.1. Whole mount *in situ* hybridization

Mouse hindbrain tissue can be effectively processed for whole mount *in situ* hybridization provided the reagents, including the large riboprobe, are able to adequately penetrate the tissue. Failure to consider the unique requirements for each age and tissue type can lead to poor staining results. E8.5 – 9.5 embryos can be processed whole as long as the E9.5 embryos have holes poked in their brain ventricles. E10.5 embryos are best processed with the trunks removed and small holes poked; some trapping in the brain ventricles is unavoidable. For E11.5 and older, thorough dissection of the hindbrain away from the pial membrane and surrounding tissues – an "open book" preparation – is essential for high quality staining and images. For embryos E11.5 – 12.5, the removal of the pial membrane can be performed before or after staining, whereas hindbrains at E13.5 and older should be fully dissected before fixation. These considerations allow for the penetration of reagents and properly applied proteinase K permeabilization of the tissue.

Tissue for *in situ* hybridization was fixed in freshly thawed 4% PFA-DEPC overnight at 4 °C. The next day, it was dehydrated to 100% methanol for permeabilization and long-term storage. To dehydrate, PFA-fixed embryos were washed twice in PBS-DEPC for 5 minutes at room temperature, followed by 10-minute washes in 25%, 50%, 75% and 100% methanol washes diluted in PBS-DEPC. After the wash in 100% methanol, the methanol was replaced and the tissue stored at -20 °C. Strong staining can be achieved with embryos stored in methanol for eight months or less, and up to two years in some cases.

All reagents up to and including the post-hybridization washes at 70 °C should be DEPC treated to avoid RNA degradation in the samples. A clean workspace is also necessary to minimize the possibility of RNAse contamination. Samples should be rocked continually during the procedure for best reagent penetration, and 20-mL scintillation vials with 5 mL of solution should be used, with the exception of the hybridization step.

To begin the *in situ* hybridization procedure, embryos were bleached in 5:1 methanol:30% hydrogen peroxide at room temperature for 30 minutes. Next, they were rehydrated via 10-minute washes each in 66% and 33% methanol in PBT, followed by two five-minute washes in PBT. To permeabilize the tissues, embryos were treated with 20 µg/mL proteinase K in PBT for one minute per embryonic day of development; for example, an E12.5 hindbrain is treated for 12.5 minutes. After two five-minute PBT washes, the embryos were re-fixed in 4% PFA/0.25% glutaraldehyde for 20 minutes, followed by two more five-minute PBT washes. After transferring the embryos to 2-mL *screwcap* tubes, samples were washed with pre-warmed hybridization buffer at 70 °C for 5 minutes, and then incubated with new buffer for at least two hours at 70 °C. To hybridize the probe, samples were incubated in diluted probe (usually 1:500) in pre-warmed hybridization buffer at 70 °C overnight with gentle rocking.

The next day, the probe solution was removed and stored at -20 °C. *It can be reused up to three times.* The embryos were transferred to new 20-mL scintillation vials and incubated twice for 45 minutes each with 2X SSC/0.1% CHAPS, then 0.2X SSC/0.1 CHAPS for 30 minutes at 70 °C. Next, samples were brought to room temperature with

two five-minute washes in TBST. To remove any remaining non-hybridized probe, embryos were incubated in 50 µg/mL RNAse A in TBST for 30 minutes at 37 °C, followed by two five-minute washes in TBST at room temperature. For the blocking step, samples were incubated in 2 mL of 20% heat-inactivated goat serum in TBST for at least one hour at 4 °C. The secondary antibody, anti-digoxygenin or anti-fluorescein conjugated to alkaline phosphatase (Roche, catalog number 11093274910 or 1426338) was then added directly to the vial at 1:1500 and incubated overnight at 4 °C.

The next day, unbound antibody was washed away with at least four to six washes in TBST at 4 °C, followed by an overnight wash in a larger volume at 4 °C.

On the final day, embryos were washed three times for 30 minutes each with TBST at 4 °C. To create optimal conditions for the alkaline phosphatase enzyme, samples were washed twice for 15 minutes in AP buffer, and transferred to 12-well tissue culture plates (Falcon 353043). To initiate the color reaction, samples were incubated *in the dark* at 37 °C with the substrates NBT (2.34 µg/mL) and BCIP (1.75 µg/mL) diluted in AP buffer. A typical color reaction takes one hour to be visible and is usually complete by three to four hours, though some probes (e.g. *Celsr1*, *Foxa2*) can take several days at room temperature. Once the color reaction was satisfactory, samples were washed twice in PBS for 5 minutes, followed by an overnight fixation in 4% PFA.

To prepare for imaging after fixation, embryos were washed twice in PBS for 5 minutes, followed by 25%, 50%, then 70% glycerol for 10 minutes each. Samples were

mounted on slides in 70% glycerol and imaged. Samples stored in glycerol are good for many years if kept at 4 °C.

2.5.2. Two-color whole mount *in situ* hybridization

Two-color staining, though difficult, can be achieved with mouse samples. The initial protocol is identical to the single-color technique (**Chapter 2.5.1**), except that *both* probes are added at the hybridization step. One probe must contain the dig hapten and the other must contain the fluorescein hapten. The initial color reaction must be with the NBT/BCIP substrates, but can be used to detect either the dig or fluorescein probe.

For two-color staining, the NBT/BCIP color reaction was stopped by washing twice with 0.1% Tween, followed by 0.1 M glycine-HCl (pH 2.2) for 30 minutes at room temperature to deactivate alkaline phosphatase. *It is vital to not fix in PFA at this step.* After transferring the embryos to new scintillation vials, they were washed twice with TBST at room temperature. Thereafter, the blocking step, antibody incubation, and post-antibody washes were performed as in the single-color *in situ* protocol (**Chapter 2.5.1**).

To prepare samples for the second color reaction, they were moved to 12-well culture plates and washed rapidly three times with Tris-HCl (pH 8.2). The Fast Red substrate was prepared according to the manufacturer's instructions (Sigma, catalog number F4648), using 1 mL per well. Embryos were incubated in the dark at room temperature for as long as necessary, usually several days. The Fast Red substrate can

be replaced up to four times per day. When the desired color intensity was reached, the samples were rinsed twice in PBS for five minutes, followed by an overnight fixation in 4% PFA at 4 °C. The embryos were brought to 70% glycerol and imaged.

2.5.3. *In situ* hybridization of embryo cross-sections

30 µm frozen sections of O. C. T.-embedded embryos (**Chapter 2.2.4**) were prepared at a -19 °C cryostat chamber temperature using standard techniques (Harlow and Lane, 2006c). Sections were transferred onto Fisher Superfrost® Plus slides (catalog number 12-550-15), which are treated to electrostatically adhere to tissue sections. Slides were marked with a hydrophobic barrier around the samples using a PAP pen (Abcam, catalog number ab2601) and dried for 15 - 30 minutes at 50 °C.

All steps were carried out in a humidified chamber at room temperature unless otherwise indicated. Sections were rinsed in PBS, fixed in 4% PFA for 10 minutes, then washed thrice in PBS for five minutes each. To permeabilize the tissue, sections were exposed to 3 µg/mL proteinase K for no longer than five minutes, then re-fixed in 4% PFA for 5 minutes. After three five-minute PBS washes, sections were incubated in TEA for 10 minutes, permeabilized with 1% Triton X-100 for 30 minutes, then washed in PBS three times for five minutes each. To prepare the sections for probe hybridization, they were incubated in 500 µL of hybridization solution for a minimum of two hours at 68 °C. 150 µL of the diluted probe solution (typically 1:625 in hybridization solution) was

added, coverslips were applied using forceps soaked in 0.4 M NaOH, and the slides were incubated overnight at 68 °C.

The following day, the coverslips were carefully removed by allowing them to naturally fall off in a fluid environment. Unbound probe was washed away with 1X SSC/50% formamide at 68 °C three times for 45 minutes each. Slides were rinsed in B1 solution back at room temperature for five minutes, then blocked in 10% HIGS in B1 for one hour. The secondary antibody, anti-digoxygenin conjugated to alkaline phosphatase (Roche, catalog number 11093274910) was diluted 1:2500 in HIGS/B1 and applied to the sections overnight at 4 °C.

On the final day, slides were washed three times with B1 solution for 10 minutes each, then with B3 solution for 5 minutes to create optimal conditions for alkaline phosphatase. BM Purple substrate (Roche, catalog number 11442074001) was added and the color reaction was monitored for several hours until complete. When satisfactory, each slide was rinsed with PBS multiple times then mounted in 175 µL of Mowiol mounting medium (Harlow and Lane, 2006b) and imaged as desired.

2.5.4. Whole mount immunohistochemistry

Neurofilament staining of whole mount embryos was carried out using a different protocol optimized for each primary antibody, as described below.

Protocol A: Anti-NF-160 antibody (Sigma, catalog number N-5264)

Whole embryos at E10.5, E11.5, or dissected E12.5 hindbrains, were fixed in ice-cold Dent's (4:1 methanol:DMSO) and stored at 4 °C overnight up to 3 months.

All steps in the nine day staining procedure were carried out at room temperature in a glass vial on an orbital rocker. First, embryos were bleached in 2:1 Dent's:30% hydrogen peroxide overnight, followed by three washes in TBS for a minimum of 15 minutes each. The primary antibody was diluted 1:300 in blocking serum (4:1 HIGS:DMSO) and incubated overnight. Samples were then washed in TBS four times for one hour each, followed by two overnight washes. The goat anti-mouse HRP-conjugated secondary antibody (Sigma, catalog number A-3682) was then applied for two nights at 1:300 in blocking serum. As in after the primary antibody incubation, samples were washed in TBS four times for one hour each, followed by two overnight washes. For the color reaction, embryos were incubated in the DAB working solution (0.05% DAB, 0.02% hydrogen peroxide in TBS) for 30 minutes to overnight until the desired staining was achieved. The color reaction was stopped by quick rinses in PBS, followed by overnight fixation in 4% PFA. Samples were then cleared to 70% glycerol and imaged as desired.

Protocol B: 2H3 antibody (Developmental Studies Hybridoma Bank)

Whole embryos at E10.5, 11.5, or dissected E12.5 hindbrains, were fixed in ice-cold Dent's (4:1 methanol:DMSO) overnight at 4 °C, then brought to 100% methanol and stored at -20 °C for up to several months (Joyner and Wall, 2008).

All steps in this protocol were carried out on an orbital rocker. To begin, the embryos were rehydrated by incubating in 50% methanol, 15% methanol, then PBS for 30 minutes each at room temperature. For the blocking step, they were incubated in PBSMT at room temperature twice for one hour each. The primary antibody was diluted 1:100 in PBSMT and incubated at 4 °C overnight. To wash, samples were washed in PBSMT twice at 4 °C and three times at room temperature for one hour each. The goat anti-mouse HRP-conjugated secondary antibody (Sigma, catalog number A-3682) was then diluted at 1:200 and applied overnight at 4 °C. Samples were washed in PBSMT in the same manner as after the 2H3 incubation, then washed in PBT for 20 minutes at room temperature. To prepare for the color reaction, samples were incubated in 0.3 mg/mL DAB in PBT at room temperature for 20 minutes. The reaction was initiated by adding hydrogen peroxide to 0.03% and was monitored continuously under a dissecting microscope until the desired color intensity was achieved. To stop the reaction, embryos were washed several times in PBS, then fixed in 4% PFA. Imaging was performed in 70% glycerol.

Protocol C: Other antibodies (αIsl1, αGFP)

Embryos were fixed in 4% PFA and stored at 4 °C overnight or up to several months. All steps were carried out at room temperature unless otherwise noted. Samples were washed in IB four times for 30 minutes each, followed by one wash containing 5% horse serum in IB (blocking solution), then incubated overnight with the diluted primary antibody in blocking solution. Samples were washed with IB twice for

30 minutes each, blocking solution for 30 minutes, and then incubated overnight with the diluted secondary antibody at 4 °C (1:200 for AlexaFluor secondary antibodies). After three thirty-minute washes in IB, samples were incubated with A/B solution (Avidin/Biotin, Vector Laboratories, catalog number PK6102) overnight. The next day, samples were washed with 1% DMSO in PBS six times for 15 minutes each followed by 15 minutes in 0.5 mg/mL DAB substrate in 1% DMSO. To initiate the peroxidase reaction, hydrogen peroxide was added to a final concentration of 0.003% and the color reaction was continually monitored. Once the reaction was satisfactory, the enzyme was inactivated 0.1% sodium azide in PBS, followed by rapid PBS washes and overnight fixation in 4% PFA at 4 °C. For imaging, samples were cleared to 70% glycerol.

2.5.5. Immunostaining of embryo cross-sections

Frozen tissue sections have several advantages for immunostaining, including preservation of antigens, tissue structure, and ease of preparation (Harlow and Lane, 2006c). In general, immunostaining on tissues E11.5 and younger is less problematic.

Frozen tissue sections were prepared as described (**Chapter 2.5.3**) except that the slides were dried for 30 – 60 minutes at room temperature. Subsequent steps were carried out in a humidified chamber (Harlow and Lane, 2006a). The sections were first permeabilized with PBT (1% Triton X-100 in PBS) three times for 10 minutes each. Non-specific binding was blocked with 10% filtered HIGS in PBT for one hour at room temperature. The diluted primary antibody was applied overnight at 4 °C. Following

three ten-minute washes in PBT at room temperature, the sections were incubated in the diluted secondary antibody for a minimum of five hours at room temperature or overnight at 4 °C. After three more ten-minute PBT washes at room temperature, samples were mounted in 175 µL of Mowiol mounting medium (Harlow and Lane, 2006b) per slide and imaged as desired.

If more transparent tissue is desired, the samples can be dehydrated in an ethanol series (25%, 50%, 75%, 100%) followed by two four-minute xylene washes before mounting with Mowiol.

2.6. Neuronal Tract Tracing With Lipophilic Dyes

Retrograde labeling of neurons with fluorescent lipophilic dyes has been used extensively to characterize FBMN migration defects in both zebrafish and mouse mutants (Bingham et al., 2002; Muller et al., 2003; Pata et al., 1999; Qu et al., 2010; Studer, 2001; Studer et al., 1996; Tiveron et al., 2003). Lipophilic tracers such as DiI and DiO (Invitrogen) are often used; however, multiple color analysis is difficult due to varying diffusion rates for the different dyes. NeuroVue™ dyes (Molecular Targeting Technologies), on the other hand, have similar diffusion rates for simultaneous application of different colors (Fritzsch et al., 2005). Since dye-coated filters are used, tissue damage from microinjection is eliminated and the filters can be cut to any desired size and shape and positioned precisely.

Embryos were prepared by fixing in 4% PFA at 4 °C for three days or up to one year. Extreme care was taken during each stage of dissection and fixation to avoid poking damage to the embryos, as peripheral nerves can be inadvertently severed and ruin the analysis. Embryos should be fixed whole unless otherwise required for a specific application. Optimally, perfusion fixation of the pregnant female (and thus the embryos) should be performed, especially for >E12.5 embryos (would need ACUC approval). To prepare for dye placement, embryos were transferred with forceps into PBS-filled petri dishes coated with Sylgard® silicone elastomer (Dow Corning, prepared using manufacturer's instructions). *If in situ hybridization will be performed later on the tissue, 0.4% PFA should be used instead of PBS to reduce RNA degradation.* Depending on the application, small incisions were made at the desired site of dye placement using microscissors, with care taken not to damage the tissue.

Under a dissecting microscope, placement sites were examined to determine the appropriate size and shape needed for the dye. *At the same magnification*, microscissors were used to cut triangles of desired size from the 1 cm^2 dye-coated filter. To avoid cross contamination of dyes, a separate set of instruments was used for each color dye, and were kept free of residual ethanol or moisture. A cut triangle was picked up with dedicated forceps then placed into the injection site (**Figure 2.4**), and additional pieces were inserted as needed. Using forceps, each embryo was transferred back into its original tube (filled with 4% PFA) to allow for dye diffusion.

Time and temperature needed for dye diffusion must be empirically determined based on the target tissue, age of the embryo, and length of fixation. An E12.5 embryo

with hindbrain labeling typically requires two days at 37 °C, whereas an E10.5 embryo should be incubated at room temperature overnight or up to two days. Dye diffusion was monitored occasionally under a fluorescent stereomicroscope, *without removing the embryo from the tube*, by viewing the dye fluorescence through the tube wall. Once sufficiently diffused, the tissue was dissected and moved immediately to a slide covered with a small amount of 100% glycerol, and imaged via confocal microscopy. In order to avoid dye diffusion in mounted samples, images were obtained with a small number of samples as quickly as possible. For E10.5-11.5 embryos, images must be taken immediately after mounting in glycerol to avoid dye diffusion. Samples >E12.5 can be stored at up to overnight, if needed. When a dye-injected sample has diffused sufficiently, it is easiest to store at 4 °C (which stops the diffusion) until ready to image rather than to mount it in 100% glycerol and store the slide.

In situ hybridization can be performed 4 °C on tissue samples after labeling with NeuroVue dyes using the same protocol as methanol-fixed embryos. After imaging in 100% glycerol, the sample should be placed back into its original tube in 4% PFA and stored at 4 °C until *in situ* hybridization experiments are carried out.

Figure 2.4. Dye placement sites for retrograde labeling of cranial nerves.

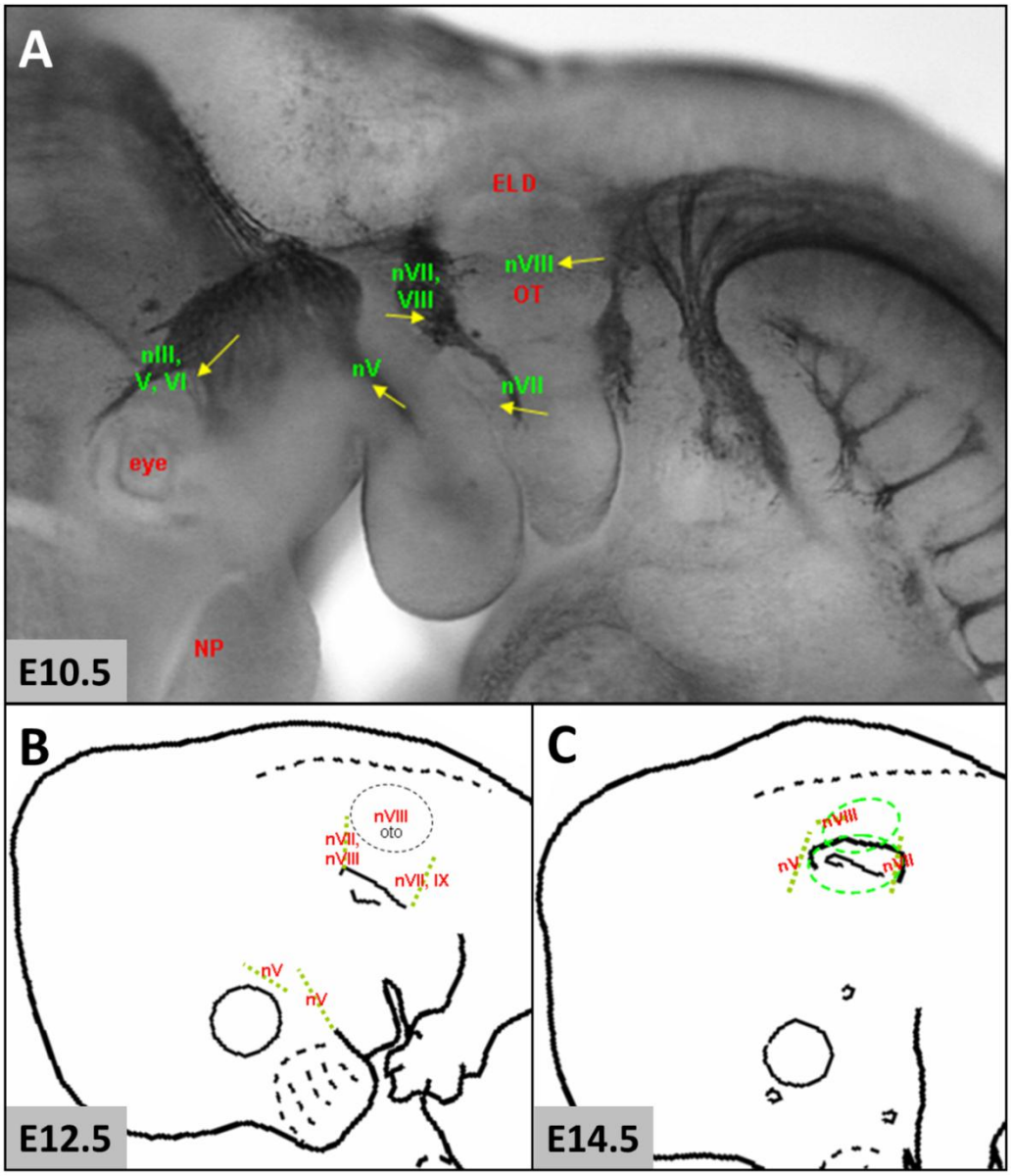

Figure 2.4. Dye placement sites for retrograde labeling of cranial nerves.

Lateral views of E10.5, E12.5, and E14.5 embryos with rostral to the left. **A**, E10.5 embryo stained with an anti-neurofilament (NF-160) antibody to show cranial nerve routes. Arrows indicate the precise locations of dye wedge placement for retrograde labeling of cranial nerves, either individually or in combination. NP, nasal pit; OT, otic vesicle; ELD, endolymphatic duct. **B – C**, Diagrams of E12.5 (**B**) and E14.5 (**C**) embryos. Dotted lines indicate the angles and positions of dye placement for cranial nerve labeling. Dotted circles indicate the locations of developing inner ear structures which are exposed after superficial dissection. Oto, otic vesicle.

2.7. Solution Recipes

2.7.1. Common use solutions

1X PBS (4 L)

Component	Amount	[Stock]	[Final]
NaCl (M.W. 58.44)	32 g	100%	136.89 mM
KCl (M.W. 74.56)	0.8 g	100%	2.68 mM
$Na_2HPO_4 \bullet 7\ H_2O$ (M.W. 268.07)	640 mL	0.1 M	16 mM
$NaH_2PO_4 \bullet H_2O$ (M.W. 137.99)	160 mL	0.1 M	4 mM
ddH_2O	to 4 L	-	-

Add enough ddH_2O to dissolve solids, then bring up to 4 L with ddH_2O in a 4-L beaker. Aliquot into 4 x 1 L and 8 x 500 mL bottles and autoclave.

4% PFA-PBS (1 L)

Component	Amount	[Stock]	[Final]
Paraformaldehyde (M.W. variable)	41.67 g	96%	4%
1X PBS-DEPC	to 1 L	-	-

In a fume hood, add the solid paraformaldehyde and approximately 800 mL of 1X PBS to a 2-L conical flask. Cover the opening of the flask with plastic wrap and stir with medium heat for 20 minutes or up to an hour to dissolve. Add 6 to 8 drops of 10 N NaOH to clear the solution. Filter the solution though a funnel fitted with filter paper

into a 1-L graduated cylinder, then bring up to 1 L with 1X PBS-DEPC. Aliquot into 15- or 50-mL tubes and store at -20 °C.

30% sucrose in PBS-DEPC (50 mL)

Component	Amount	[Stock]	[Final]
Sucrose (Fisher S5)	15 g	100%	30%
PBS-DEPC	to 50 mL	-	-

Do not autoclave. Make in a 50-mL tube and store at 4 °C. Sterile filter if desired.

10X TBE Buffer (1 L)

Component	Amount	[Stock]	[Final]
Tris base (M.W. 121.14)	108 g	100%	0.88 M
Boric acid (M.W. 61.83)	55 g	100%	0.88 M
EDTA, pH 8.0	40 mL	0.5 M	0.2 M
ddH_2O	to 1 L	-	-

This reagent does not need to be autoclaved. Dilute to 0.5X – 1X concentration for use in electrophoresis.

TE Buffer, pH 8.0 (100 mL)

Component	Amount	[Stock]	[Final]
Tris-HCl, pH 8.0	1 mL	1 M	10 mM
EDTA, pH 8.0	0.2 mL	0.5 M	1 mM

ddH_2O	98.8 mL	-	-

10X MOPS Buffer (1L)

Component	Amount	[Stock]	[Final]
MOPS (M.W. 209.26)	46.3 g	100%	0.2 M
EDTA • 2 H_2O (M.W. 372.24)	3.72 g	100%	0.01 M
ddH_2O	to 1 L	-	-

Adjust to pH 7.0 before bringing to final volume of 1 L. Autoclave for 20 minutes.

1.25X RNA Loading Buffer (1.5 ml)

Component	Amount	[Stock]	[Final]
Deionized formamide	720 µL	100%	48%
MOPS buffer	160 µL	10X	1.1X
Formaldehyde	260 µL	37%	6.4%
Glycerol	80 µL	100%	5.3%
Bromophenol blue	20 µL	100%	1.3%
Xylene cyanol	20 µL	100%	1.3%
Sodium acetate (M.W. 82.03)	6.8g	100%	0.17 mM
ddH_2O	240 µL	-	-

Heat inactivation of serum

Heat-inactivated serum is desirable for some protocols and applications. To prepare for heat inactivation, thaw unopened serum at 4 °C. Bring a waterbath to 56 °C. Then, bring the unopened container of serum to 56 °C, swirling every five minutes to assure even heating. *Instead of placing a thermometer in the serum container, the temperature must be monitored in a separate container. This container should be of comparable size and volume to the serum container, and filled with 4 °C water.* Once at 56 °C, incubate the serum for precisely 30 minutes. Immediately after incubation, place the serum on ice, separate into aliquots, and store at -20 °C. Multiple freeze-thaw of serum should be avoided.

Treatment of solutions with diethyl pyrocarbonate (DEPC)

DEPC treatment of solutions is desirable in applications where RNAse contamination and degradation of RNA is of concern (e.g. *in situ* hybridization). To inactivate RNAse, DEPC can be added directly to a previously autoclaved or freshly made solution. Add 1 mL of 100% DEPC (Sigma, catalog number D-5758) per 1 L of solution (0.1% final concentration). Shake vigorously, incubate overnight in a fume hood with loosened caps, then autoclave the following day.

2.7.2. Genomic DNA isolation

Lysis Buffer (97.7 mL)

Component	Amount	[Stock]	[Final]
Tris-HCl, pH 8.0	5 mL	1 M	50 mM
EDTA	1 mL	0.5 M	5 mM
NaCl	10 mL	1 M	100 mM
SDS	2.5 mL	20%	0.5%
ddH_2O	79.2 mL	-	-

Mix each of the components in a sterile 100-mL bottle and store at room temperature. Proteinase K (Sigma P4850, >800 U/mL) is added fresh to each aliquot during use. To make a 1-mL working aliquot, combine 977 µL of the stock lysis buffer and 23 µL of proteinase K into a 1.5-mL tube. The working concentration of proteinase K for digestion is >18.4 U/mL.

2.7.3. Whole mount *in situ* hybridization

To eliminate RNAse contamination during *in situ* hybridization, use diethyl pyrocarbonate (DEPC)-treated reagents for all steps up to and including the hybridization of the riboprobe. After hybridization, either DEPC-treated or untreated solutions may be used.

PBT (50 mL)

Component	Amount	[Stock]	[Final]
Triton X-100 (in PBS-DEPC)	500 µL	10%	0.1%
PBS-DEPC	45.5 mL	-	-

Do not autoclave. Make fresh during *in situ* hybridization procedure.

Proteinase K Solution (5 mL)

Component	Amount	[Stock]	[Final]
Proteinase K (Sigma P4850)	4 µL	800 U/mL	0.64 U/mL
PBS-DEPC	4.996 mL	-	-

Do not autoclave. Make fresh during *in situ* hybridization procedure.

PFA/Glutaraldehyde Solution (5 mL)

Component	Amount	[Stock]	[Final]
Glutaraldehyde (EMD GX015305)	50 µL	25%	0.25%
PBS-DEPC	4.95 mL	-	-

Do not autoclave. Make fresh during *in situ* hybridization procedure.

20X SSC (1 L)

Component	Amount	[Stock]	[Final]
NaCl (M.W. 58.44)	175.3 g	100%	2.99 mM
88.2 g sodium citrate	88.2 g	100%	290 mM

ddH_2O	to 1 L	-	-

Dissolve solids in approximately 800 mL of ddH_2O. Adjust to pH 7.0 with 10 N NaOH, then bring to final volume. Autoclave for 20 minutes.

Hybridization Buffer (50 mL)

Component	Amount	[Stock]	[Final]
Formamide (Fisher BP228)	25 mL	100%	50%
SSC-DEPC	12.5 mL	20X	5X
EDTA-DEPC, pH 8.0	500 µL	0.5 M	5 mM
Triton X-100	500 µL	10%	0.1%
CHAPS (Sigma C3023)	500 µL	10%	0.1%
Heparin (Sigma H3393)	50 µL	50 mg/mL	100 µg/mL
Yeast tRNA (Roche 10109223001)	50 mg	-	-
Blocking reagent (Roche 1096176)	1 g	-	-
ddH_2O-DEPC	to 50 mL	-	-

Prepare this buffer in a 50-mL tube, inverting frequently during preparation. Incubate in 55 °C water bath to help dissolve. Seal the cap with laboratory film and store at -20 °C.

2X SSC/0.1% CHAPS Post-Hybridization Wash (50 mL)

Component	Amount	[Stock]	[Final]
SSC-DEPC	5 mL	20X	2X
CHAPS (Sigma C3023)	50 mg	100%	0.1%

ddH_2O-DEPC	45 mL	-	-

Do not autoclave. Prepare this solution at the end of day 1 of the *in situ* hybridization procedure, and incubate overnight in the hybridization oven.

0.2X SSC/0.1% CHAPS Post-Hybridization Wash (50 mL)

Component	Amount	[Stock]	[Final]
SSC-DEPC	500 µL	20X	0.2X
CHAPS (Sigma C3023)	50 mg	100%	0.1%
ddH_2O-DEPC	49.5 mL	-	-

Do not autoclave. Prepare this solution at the end of day 1 of the *in situ* hybridization procedure, and incubate overnight in the hybridization oven.

RNAse A Solution (10 mL)

Component	Amount	[Stock]	[Final]
Ribonuclease A (Sigma R4642)	50 µL	30 mg/mL	50 µg/mL
TBST	9.950 mL	-	-

Do not autoclave. Make fresh during *in situ* hybridization procedure.

TBST (100 mL)

Component	Amount	[Stock]	[Final]
Tris-HCl, pH 7.5	5 mL	1 M	50 mM
NaCl	15 mL	1 M	150 mM

KCl	1 mL	1 M	1 mM
Triton X-100 (Fisher BP151)	1 mL	100%	1%
ddH_2O	78 mL	-	-

Do not autoclave. Make fresh during *in situ* hybridization procedure.

Maleic Acid Buffer (1 L)

Component	Amount	[Stock]	[Final]
Maleic acid (M.W. 116.07)	11.61 g	100%	100 mM
NaCl (M.W. 58.44)	8.77 g	100%	150 mM
NaOH (pellets, M.W. 40.00)	6 g	100%	150 mM
ddH_2O	to 1 L	-	-

Dissolve solids in 800 mL of ddH_2O. Adjust to pH 7.5 with 10 N NaOH, then bring to final volume. Autoclave for 20 minutes.

20% Goat Serum in TBST (10 mL)

Component	Amount	[Stock]	[Final]
Heat inactivated goat serum	2 mL	100%	20%
(Invitrogen 16210, not filtered, heat inactivated at 56 °C)			
TBST	8 mL	-	-

Do not autoclave. Make fresh during *in situ* hybridization procedure and store on ice until use.

Alkaline Phosphatase (AP) Buffer (50 mL)

Component	Amount	[Stock]	[Final]
Tris-HCl, pH 9.5	5 mL	1 M	100 mM
NaCl	5 mL	1 M	100 mM
$MgCl_2$	2.5 mL	1 M	50 mM
Tween-20 (Sigma P9416)	50 µL	100%	0.1%
ddH_2O	37.45 mL	-	-

Do not autoclave. Make fresh during *in situ* hybridization procedure.

NBT/BCIP Color Reaction Solution (~5 mL)

Component	Amount	[Stock]	[Final]
NBT (Roche 1383213001)	16.88 µL	100 mg/mL	2.34 µg/mL
BCIP (Roche 1383221001)	17.5 µL	50 mg/mL	1.75 µg/mL
AP buffer	5 mL	-	-

Fast Red Color Reaction Solution (~1 mL)

Component	Amount	[Stock]	[Final]
Fast red (Sigma 11496549001)	1 tablet	-	-
Tablet components:			
Naphthol substrate	0.5 mg	-	0.5 mg/mL
Fast red chromogen	2 mg	-	2 mg/mL
Levamisole	0.4 mg	-	0.4 mg/mL

ddH_2O	1 mL	-	-

Dissolve 1 tablet in 1 mL of ddH_2O by vortexing vigorously. Use 1 mL of solution per well of embryos.

2.7.4. Section *in situ* hybridization

Proteinase K Solution (5 mL)

Component	Amount	[Stock]	[Final]
Proteinase K (Sigma P4850)	0.6 µL	800 U/mL	0.096 U/mL
PBS-DEPC	5 mL	-	-

Do not autoclave. Make fresh during *in situ* hybridization procedure.

Triethanolamine-HCl (TEA) Solution (200 mL)

Component	Amount	[Stock]	[Final]
Triethanolamine (Fisher T407)	2.7 mL	100%	1.35%
Hydrocholoric acid (Fisher A144)	350 µL	37.4%	0.065%
Acetic anhydride (Fisher A10)	500 µL	100%	0.25%
ddH_2O-DEPC	196.45 mL	-	-

Do not autoclave. Make fresh during *in situ* hybridization procedure. To ddH_2O-DEPC, add the triethanolamine first and let stir. Next, add the hydrochloric acid and mix well. Just before use, add the acetic anhydride.

Triton Permeabilizing Solution in PBS (5 mL)

Component	Amount	[Stock]	[Final]
Triton X-100	500 µL	10%	1%
PBS-DEPC	4.5 mL	-	-

Do not autoclave. Make fresh during *in situ* hybridization procedure.

Hybridization Buffer (50 mL)

Component	Amount	[Stock]	[Final]
Formamide (Fisher BP228)	25 mL	100%	50%
SSC-DEPC	12.5 mL	20X	5X
Denhardt's reagent (Fisher BP515)	5 mL	50X	5X
Yeast tRNA	1.25 mL	10 λ/λ	250 µg/mL
ssDNA from salmon testes (Sigma D7656)	2.4 mL	10.4 λ/λ	500 µg/mL
ddH_2O-DEPC	to 50 mL	-	-

Prepare this buffer in a 50-mL tube, inverting frequently during preparation. Dissolve thoroughly, then seal the cap with laboratory film and store at -20 °C.

NaOH Forcep-Soaking Solution (1 mL)

Component	Amount	[Stock]	[Final]
Sodium hydroxide (Fisher SS255)	40 µL	10 M	0.4 M
ddH_2O-DEPC	960 µL	-	-

Post-Hybridization Wash (50 mL)

Component	Amount	[Stock]	[Final]
Formamide (Fisher BP228)	25 mL	100%	50%
SSC-DEPC	2.5 mL	20X	1X

Do not autoclave. Make fresh during *in situ* hybridization procedure.

B1 Solution (50 mL)

Component	Amount	[Stock]	[Final]
Tris-HCl, pH 7.5	5 mL	1 M	0.1 M
NaCl	7.5 mL	1 M	0.15 M
Tween-20 (Sigma P9416)	25 µL	100%	0.05%
ddH_2O	to 50 mL	-	-

Do not autoclave. Make fresh during *in situ* hybridization procedure.

10% Serum in B1 Solution (10 mL)

Component	Amount	[Stock]	[Final]
Heat inactivated goat serum	1 mL	100%	10%
(Invitrogen 16210, not filtered, heat inactivated at 56 °C)			
B1 Solution	9 mL	-	-

Do not autoclave. Make fresh during *in situ* hybridization procedure and store on ice until use.

B3 Solution (50 mL)

Component	Amount	[Stock]	[Final]
Tris-HCl, pH 9.5	5 mL	1 M	0.1 M
NaCl	5 mL	1 M	0.1 M
$MgCl_2$	2.5 mL	1 M	50 mM
Tween-20 (Sigma P9416)	50 µL	100%	0.1%
Levamisole	3-4 drops	30 mg/mL	-
ddH_2O	to 50 mL	-	-

Do not autoclave. Make fresh during *in situ* hybridization procedure, and filter before use.

2.7.5. Whole mount immunohistochemistry

Dent's Fixative (10 mL)

Component	Amount	[Stock]	[Final]
Methanol (Fisher A412)	8 mL	100%	80%
DMSO (Fisher BP231)	2 mL	100%	20%

Make fresh and use immediately, or over a few day period while stored at 4 °C.

Diaminobenzidine (DAB) Stock Solution (66 mL)

Component	Amount	[Stock]	[Final]
DAB (Sigma D9015)	100 mg	>96%	1.5 mg/mL

ddH_2O	66 mL	-	-

DAB is toxic and light sensitive. In low light conditions, remove the aluminum tear seal from the ISOPAC© container. The container will be under pressure, so release the pressure by injecting a syringe needle into the rubber stopper. With a second syringe and needle, inject 66 mL of ddH_2O into the container and swirl to dissolve. With the container on ice, aliquot into tubes, then store at -20 °C in a foil-covered box.

Protocol A: Anti-NF-160 antibody (Sigma, catalog number N-5264)

Bleaching Solution (9 mL)

Component	Amount	[Stock]	[Final]
Hydrogen Peroxide (Fisher H325)	3 mL	30%	10%
Dent's Fixative	6 mL	-	-

Make fresh and use immediately.

TBS (50 mL)

Component	Amount	[Stock]	[Final]
Tris-HCl, pH 8.0	500 µL	1 M	10 mM
NaCl	7.5 mL	1 M	150 mM
ddH_2O	to 50 mL	-	-

Make fresh and use immediately.

Blocking Serum (5 mL)

Component	Amount	[Stock]	[Final]
Heat-inactivated goat serum	4 mL	100%	80%
DMSO (Fisher BP231)	1 mL	100%	20%
Thimerosal (Sigma T-5125)	5 µL	100%	0.1%

Make fresh and use immediately. Addition of thimerosal (an anti-fungal agent) is optional.

Working DAB Substrate Solution (5 mL)

Component	Amount	[Stock]	[Final]
DAB	1.67 mL	1.5 mg/mL	0.5 mg/mL
Hydrogen Peroxide (Fisher H325)	3.25 µL	30%	0.02%

Make fresh and keep in the dark until use.

Protocol B: 2H3 antibody (Developmental Studies Hybridoma Bank)

Embryo Bleaching Solution (12 mL)

Component	Amount	[Stock]	[Final]
Methanol (Fisher A412)	8 mL	100%	66.7%
DMSO (Fisher BP231)	2 mL	100%	16.7%
Hydrogen Peroxide (Fisher H325)	2 mL	30%	5%

Make fresh and use immediately.

PBSMT (50 mL)

Component	Amount	[Stock]	[Final]
Instant Skim Milk Powder	1 g	100%	2%
Triton X-100 (Fisher BP151)	50 µL	100%	0.1%
PBS	to 50 mL	-	-

Make fresh at the beginning of the procedure and as needed throughout. Refrigerate or store on ice when not in use.

PBT (50 mL)

Component	Amount	[Stock]	[Final]
BSA (Sigma A7906)	100 mg	100%	2%
Triton X-100 (Fisher BP151)	50 µL	100%	0.1%
PBS	to 50 mL	-	-

Make fresh and use immediately.

Working DAB Substrate Solution (5 mL)

Component	Amount	[Stock]	[Final]
DAB	1 mL	1.5 mg/mL	0.3 mg/mL
PBT	4 mL	-	-

Make fresh and keep in the dark until use.

Protocol C: Non-neurofilament antibodies

Incubation Buffer, IB (50 mL)

Component	Amount	[Stock]	[Final]
BSA (Sigma A7906)	500 mg	100%	10 mg/mL
Triton X-100 (Fisher BP151)	500 µL	100%	1%
DMSO (Fisher BP231)	500 µL	100%	1%
1X PBS	48.5 mL	-	-

Make fresh and use immediately, or over a few day period while stored at 4 °C.

Horse Serum in IB (10 mL)

Component	Amount	[Stock]	[Final]
Horse serum (Vector Labs S-2000)	500 µL	100%	5%
IB	4.5 mL	-	-

Make fresh, store on ice, and use immediately.

Avidin-Biotin (A/B) Solution (5 mL)

Component	Amount	[Stock]	[Final]
Reagent A (Vector Labs PK6102)	50 µL	1%	0.01%
Reagent B (Vector Labs PK6102)	50 µL	1%	0.01%
IB	4.9 mL	-	-

Make fresh for immediate use.

1% DMSO Solution (50 mL)

Component	Amount	[Stock]	[Final]
DMSO (Fisher BP231)	500 µL	100%	1%
1X PBS	45.5 mL	-	-

Make fresh for immediate use.

Working DAB Substrate Solution (12 mL)

Component	Amount	[Stock]	[Final]
DAB	4 mL	1.5 mg/mL	0.5 mg/mL
1% DMSO Solution	8 mL	-	-

Make fresh for immediate use.

Working Peroxide Substrate Solution (1 mL)

Component	Amount	[Stock]	[Final]
Hydrogen Peroxide (Fisher H325)	1 µL	30%	0.03%
1% DMSO Solution	999 µL	-	-

Make fresh and use immediately.

HRP Reaction Stopper Solution (10 mL)

Component	Amount	[Stock]	[Final]
Sodium azide	90.91 µL	11%	0.1%
1% DMSO Solution	9.91 mL	-	-

Make fresh using *cold* 1X PBS and use immediately.

2.7.6. Section immunohistochemistry

PBT (50 mL)

Component	Amount	[Stock]	[Final]
Triton X-100 (in PBS-DEPC)	5 mL	10%	1%
PBS-DEPC	45 mL	-	-

Do not autoclave. Make fresh during procedure.

Block Solution (10 mL)

Component	Amount	[Stock]	[Final]
Filtered (0.22 µm) HIGS	1 mL	100%	10%
PBS	9 mL	-	-

Do not autoclave. Make fresh during procedure and keep on ice. The filtered heat-inactivated goat serum (HIGS) can be made fresh or taken from stored aliquots at -20 °C.

2.7.7. Neuronal tract tracing with lipophilic dyes

0.4% PFA Solution (50 mL)

Component	Amount	[Stock]	[Final]
PFA-DEPC	5 mL	4%	0.4%

PBS-DEPC	45 mL	-	-

Make and store this solution in 50-mL tubes. Pour into petri dishes in lieu of PBS-DEPC during dissection or injection of embryos that will be subsequently processed for *in situ* hybridization. The low concentration of PFA will minimize RNAse activity but is safer to use than 4% PFA.

2.7.8. Plasmid miniprep

AES I (100 mL)

Component	Amount	[Stock]	[Final]
glucose	5 mL	1 M	50 mM
Tris, pH 8.0	2.5 mL	1 M	25 mM
EDTA, pH 8.0	2 mL	0.5 M	10 mM
ddH_2O	90.5 mL	-	-

Make from previously autoclaved stock solutions. Filter and store in a sterile container long term at 4 °C.

AES II (10 mL)

Component	Amount	[Stock]	[Final]
SDS	500 µL	20%	1%
NaOH	200 µL	10 M	200 mM
ddH_2O	9.3 mL	-	-

Do not autoclave. Make fresh during the procedure.

AES III (100 mL)

Component	Amount	[Stock]	[Final]
Potassium acetate (KAc)	60 mL	5 M	3 M
Glacial acetic acid	11.5 mL	-	-
ddH_2O	9.3 mL	-	-

Do not autoclave. Store in a sterile container long term at room temperature.

CHAPTER 3: The Wnt/PCP Protein Vangl2 is Necessary for the Migration of Facial Branchiomotor Neurons in Mice, and Functions Independent of Dishevelled Function

3.1. Introduction

A fundamental process in brain development involves the migration of facial branchiomotor neurons (FBMNs) in the embryonic brain stem across several rhombomeres (r) to their final locations. Several components of the Wnt/planar cell polarity (PCP) pathway, including the transmembrane protein vangl2, have been shown to regulate FBMN migration in zebrafish. Therefore, we analyzed FBMN migration in the *Vangl2* mouse mutant, *Looptail (Lp)*. In *Vangl2*$^{Lp/+}$ embryos, FBMNs failed to undergo their characteristic caudal migration from r4 into r6 and instead formed elongated facial motor nuclei spanning r4 and r5. FBMNs in *Vangl2*$^{Lp/Lp}$ embryos were arrested in r4 and most FBMNs failed to migrate radially to the pial surface of the neural tube. However, hindbrain patterning and FBMN progenitor specification were intact, and FBMNs did not transfate into other non-migratory neuron types, indicating a specific role for *Vangl2* in neuronal migration. Consistent with this, FBMNs failed to migrate in *Vangl2* knockout embryos.

Studies in zebrafish suggest that FBMN migration is regulated independent of the Wnt/PCP pathway, since some, but not all, Wnt/PCP genes regulate FBMN migration. We tested whether this was also the case in mammals. Embryos null for *Ptk7*, a regulator of PCP signaling, had severe defects in caudal FBMN migration.

However, FBMNs migrated normally in *Dishevelled (Dvl) 1/2* double mutants, and in zebrafish embryos with disrupted *dvl* signaling, indicating *Dvl* function is largely dispensable for FBMN migration. Consistent with this, loss of *Dvl2* function in *Vangl2*$^{Lp/+}$ embryos did not exacerbate the *Vangl2*$^{Lp/+}$ FBMN migration phenotype. Together, these results suggest strongly that caudal migration of FBMNs is controlled by multiple components of the Wnt/PCP pathway, yet may not require the central signaling molecule Dishevelled.

3.2. Results

3.2.1. *Vangl2* is expressed in FBMNs and adjacent cell types in the developing hindbrain

To investigate the role of *Vangl2* in FBMN migration, we first examined its expression pattern in mouse embryos using *in situ* hybridization. In the mouse, FBMNs are born in the ventricular zone of r4 and specified by E9.5, then begin to migrate caudally at E10.5 within the mantle layer. At the onset of migration (**Figure 3.1 A**), *Vangl2* was expressed in FBMNs as well as the ventricular zone of r4 and at all axial levels (**Figure 3.1 C, E**, n=6). This pattern of expression was maintained at E11.5, when the first FBMNs reached fully into r6 (**Figure 3.1 D, F**, n=7) and as late as E12.5 (**data not shown**, n=9), when the earliest FBMNs migrate radially within r6 to begin forming the facial motor nucleus (**Figure 3.1 B**). This expression pattern is in striking contrast to

zebrafish *vangl2*, which is expressed ubiquitously throughout the hindbrain (Park and Moon, 2002; Sittaramane et al., 2009).

Figure 3.1. *Vangl2* expression in the developing hindbrain and FBMNs.

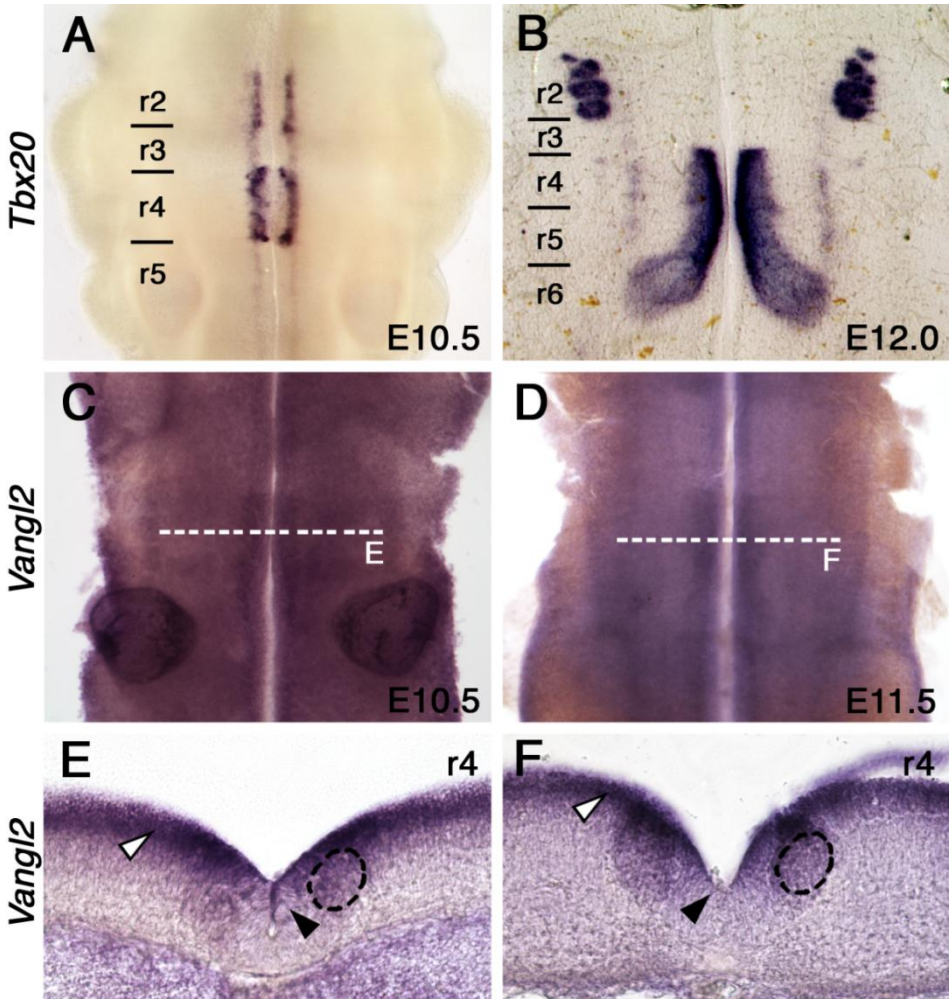

Figure 3.1. *Vangl2* expression in the developing hindbrain and FBMNs.

A-D, Ventricular views of flat-mounted hindbrains processed for ISH with digoxigenin-labeled *Tbx20* (**A-B**) and *Vangl2* (**C-D**) probes. At E10.5 (**A**), *Tbx20* mRNA is expressed in trigeminal BMNs in r2-r3 and FBMNs in r4. By E12.0 (**B**), *Tbx20* expression is maintained in laterally-migrated trigeminal BMNs in r2-r3 and caudally migrating FBMNs spanning r4-r6. At the onset of FBMN migration, E10.5 (**C**) and E11.5 (**D**), *Vangl2* mRNA is expressed at all axial levels of the hindbrain. Punctate staining is seen near the midline where the FBMNs are located. **E-F**, 50 µm coronal sections at the r4 level of the *Vangl2*-stained embryos in **C** and **D**. At E10.5 (**E**), *Vangl2* is expressed in the ventricular zone (white arrowhead) and the FBMN domain (dotted circle), with little to no expression in the floor plate (black arrowhead). By E11.5 (**F**), *Vangl2* expression is maintained in the ventricular zone (white arrowhead) and the FBMN domain (dotted circle), but is excluded from floor plate cells (black arrowhead).

3.2.2. FBMNs fail to migrate caudally in *Vangl2* mutants

Previous studies in zebrafish and mice have demonstrated roles for several Wnt/PCP genes in FBMN migration (Bingham et al., 2002; Carreira-Barbosa et al., 2003; Qu et al., 2010; Vivancos et al., 2009; Wada et al., 2006). Since *Vangl2* is expressed in and around FBMNs (**Figure 3.1 C-F**), we tested whether their migration was affected in *Looptail* (*Lp*) embryos harboring a D255E mutation in the C-terminal cytoplasmic domain of Vangl2 (Torban et al., 2004b) which abolishes localization to the plasma membrane (Torban et al., 2007).

We first examined FBMN migration in $Vangl2^{Lp}$ embryos in the *SE1::gfp* background, in which all cranial MNs express GFP (Song et al., 2006). In WT embryos at E11.5 and E12.5, FBMNs were seen as a longitudinal stream of migrating cells spanning r4 to r6, then migrating dorsolaterally within r6 (**Figure 3.2 A, Figure 3.3 A**, 10/10 embryos). In contrast, FBMNs largely failed to migrate caudally out of r4 in both $Vangl2^{Lp/+}$ and $Vangl2^{Lp/Lp}$ embryos (**Figure 3.2 B-C**, 17/17 and 8/8 embryos), and some neurons migrated dorsolaterally, especially in the vicinity of the r4/r5 boundary (**Figure 3.3 B-C**). Interestingly, a few FBMNs also migrated into r3 in both $Vangl2^{Lp/+}$ and $Vangl2^{Lp/Lp}$ embryos, but never in WT embryos (**Figure 3.3**). *In situ* hybridization with *Tbx20*, a BMN/VMN marker, revealed that by E12.5, WT FBMNs migrated radially towards the pial surface within r6 to form the facial motor nucleus (**Figure 3.2 D; Figure 3.4 A-A"**, 7/7 embryos), which was complete by E14.5 (**Figure 3.2 G**, 3/3 embryos). In contrast, FBMNs in $Vangl2^{Lp/+}$ remained mostly confined to r4 but still underwent their dorsolateral and radial migrations to form aberrant, elongated nuclei spanning r3 to r5

(**Figure 3.2 E, H; Figure 3.4 B-B"**, 8/8 at E12.5 and 4/4 at E14.5). In *Vangl2*$^{Lp/Lp}$ mutants, FBMNs remained within r4 and most failed to migrate radially to the pial surface of the neural tube (**Figure 3.2 F, I; Figure 3.4 C-C"**, 3/3 at E12.5 and 6/6 at E14.5).

Since the *Vangl2*^{Lp} allele encodes a protein that fails to reach the membrane and may act in a dominant negative fashion (Torban et al., 2007), we also examined FBMN migration in *Vangl2* knockout mice (*Vangl2*$^{del/del}$), where no Vangl2 protein is detected (Song et al., 2010). FBMNs largely failed to migrate out of r4 in both *Vangl2*$^{del/+}$ (4/4 embryos) and *Vangl2*$^{del/del}$ embryos (4/4 embryos), and interestingly, a subset of FBMNs in *Vangl2*$^{del/+}$ embryos appeared to migrate into r3 (**Figure 3.5 A-C**, 1/4 embryos).

Interestingly, craniorachischisis (open neural tube) occurs in *Vangl2*$^{Lp/Lp}$, but not *Vangl2*$^{Lp/+}$ embryos (Murdoch et al., 2001; Torban et al., 2004b; Ybot-Gonzalez et al., 2007), indicating that the FBMN migration phenotype is not a secondary consequence of neural tube defects.

Figure 3.2. FBMNs fail to migrate caudally in *Vangl2*^{Lp} embryos.

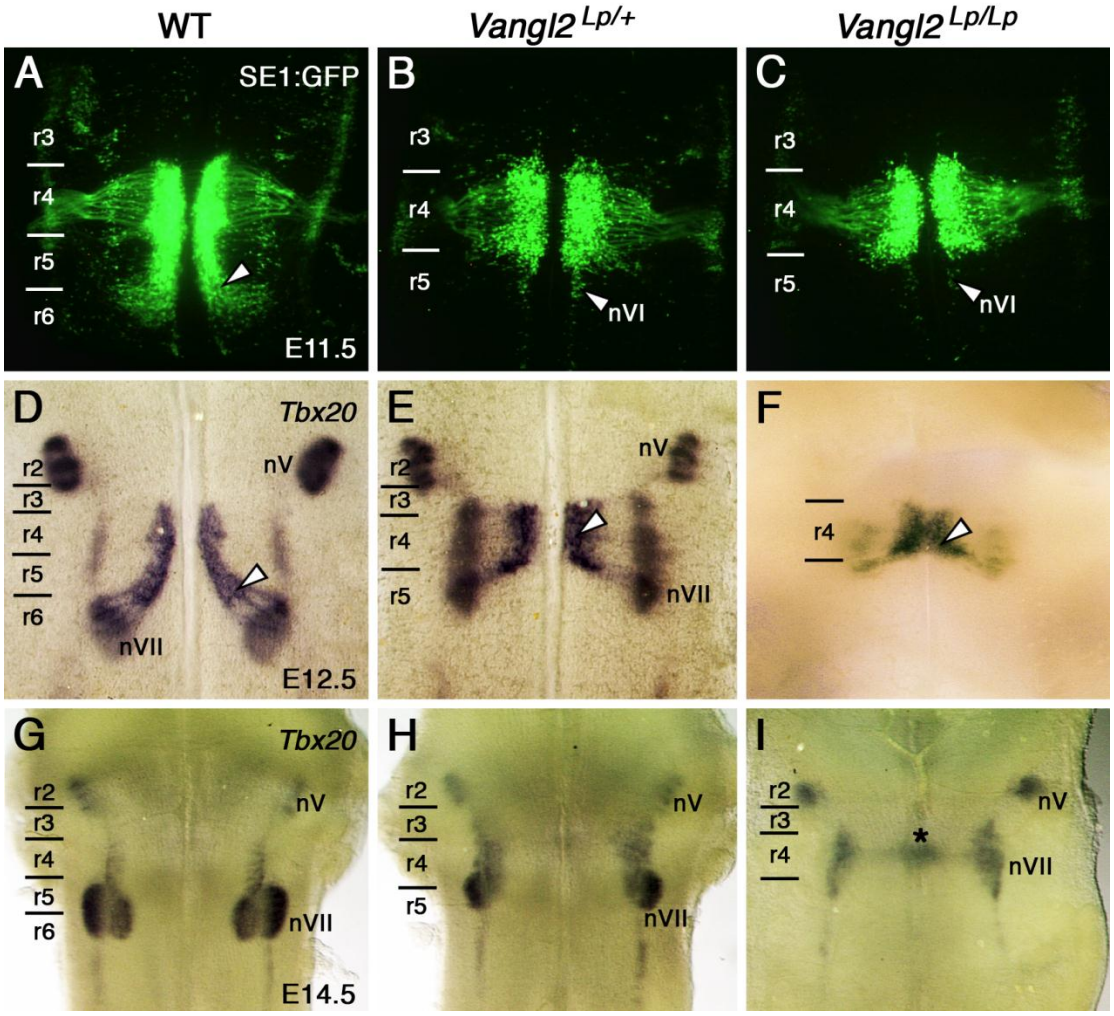

Figure 3.2. FBMNs fail to migrate caudally in *Vangl2*^{Lp} embryos.

A-C, Ventricular views of live *SE1::gfp* flat-mounted hindbrains, imaged via confocal microscopy to detect GFP. At E11.5, FBMNs in WT embryos (**A**) migrate caudally from r4 into r6 and dorsolaterally away from the midline (white arrowhead). In *Vangl2*$^{Lp/+}$ (**B**) and *Vangl2*$^{Lp/Lp}$ embryos (**C**), FBMNs fail to migrate out of r4. Neurons seen in r5 are from the abducens (nVI) nuclei (white arrowheads) and are not FBMNs. **D-F**, Ventricular views of flat-mounted hindbrains processed for *Tbx20* ISH. At E12.5, FBMNs in WT embryos (**D**) are seen migrating caudally from r4 into r6 (white arrowhead), then migrate radially to form the facial motor nucleus (nVII) in r6. In *Vangl2*$^{Lp/+}$ (**E**) embryos, some *Tbx20*-expressing cells are seen in r5, but are more confined to r4 in *Vangl2*$^{Lp/Lp}$ embryos (**F**). **G-I**, Pial views of flat-mounted hindbrains processed for *Tbx20* ISH. At E14.5, *Tbx20*-expressing FBMNs in WT embryos (**G**) have completed migration into r5/r6 to form the facial motor nucleus (nVII). In *Vangl2*$^{Lp/+}$ embryos (**H**), the facial motor nucleus (nVII) is elongated within r4/r5 and is confined entirely to r4 in *Vangl2*$^{Lp/Lp}$ embryos (**I**).

Figure 3.3. Confocal analysis of the *Vangl2*^{Lp} FBMN migration phenotype.

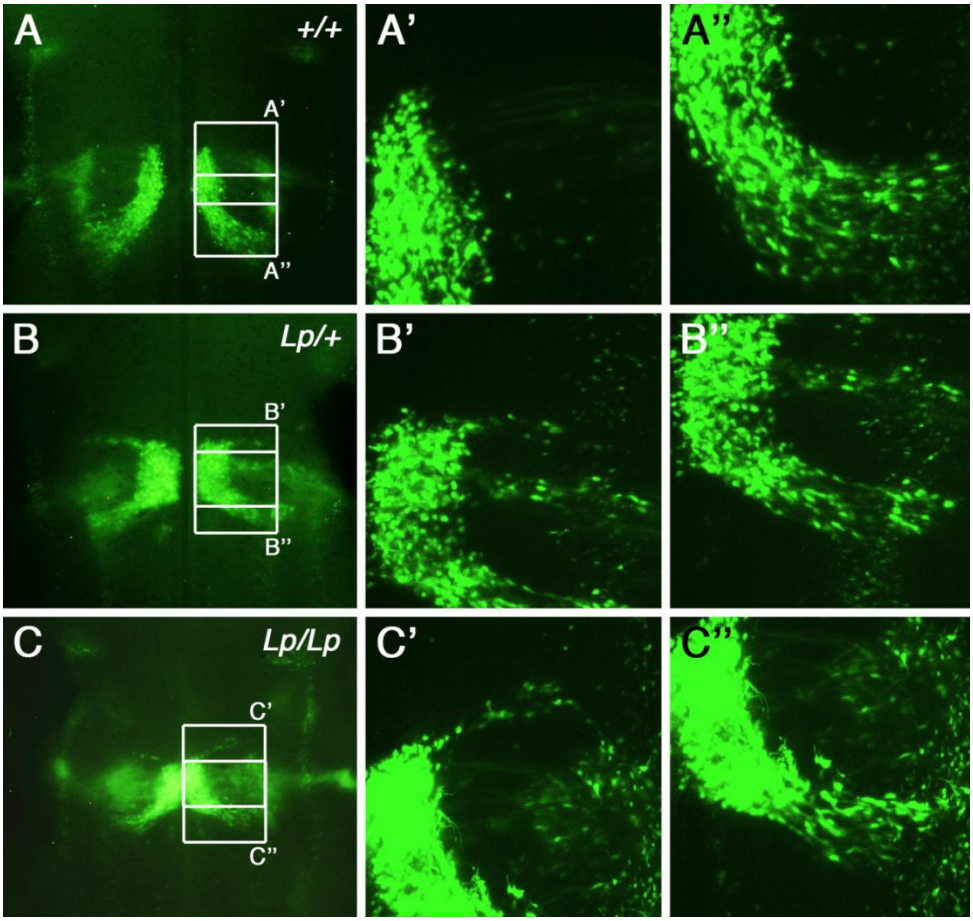

Figure 3.3. Confocal analysis of the *Vangl2*^{Lp} FBMN migration phenotype.

A-C, Live confocal imaging of GFP-expressing FBMNs from the *SE1::gfp* line. In WT embryos (**A-A"**), FBMNs form an organized stream while migrating from r4 to r6. In *Vangl2*$^{Lp/+}$ (**B-B"**) and *Vangl2*$^{Lp/Lp}$ (**C-C"**) embryos, FBMNs are generally less organized and break up into multiple streams migrating laterally within r4 and r5.

Figure 3.4. Tangential and radial FBMN migration defects in *Vangl2*^{Lp} embryos.

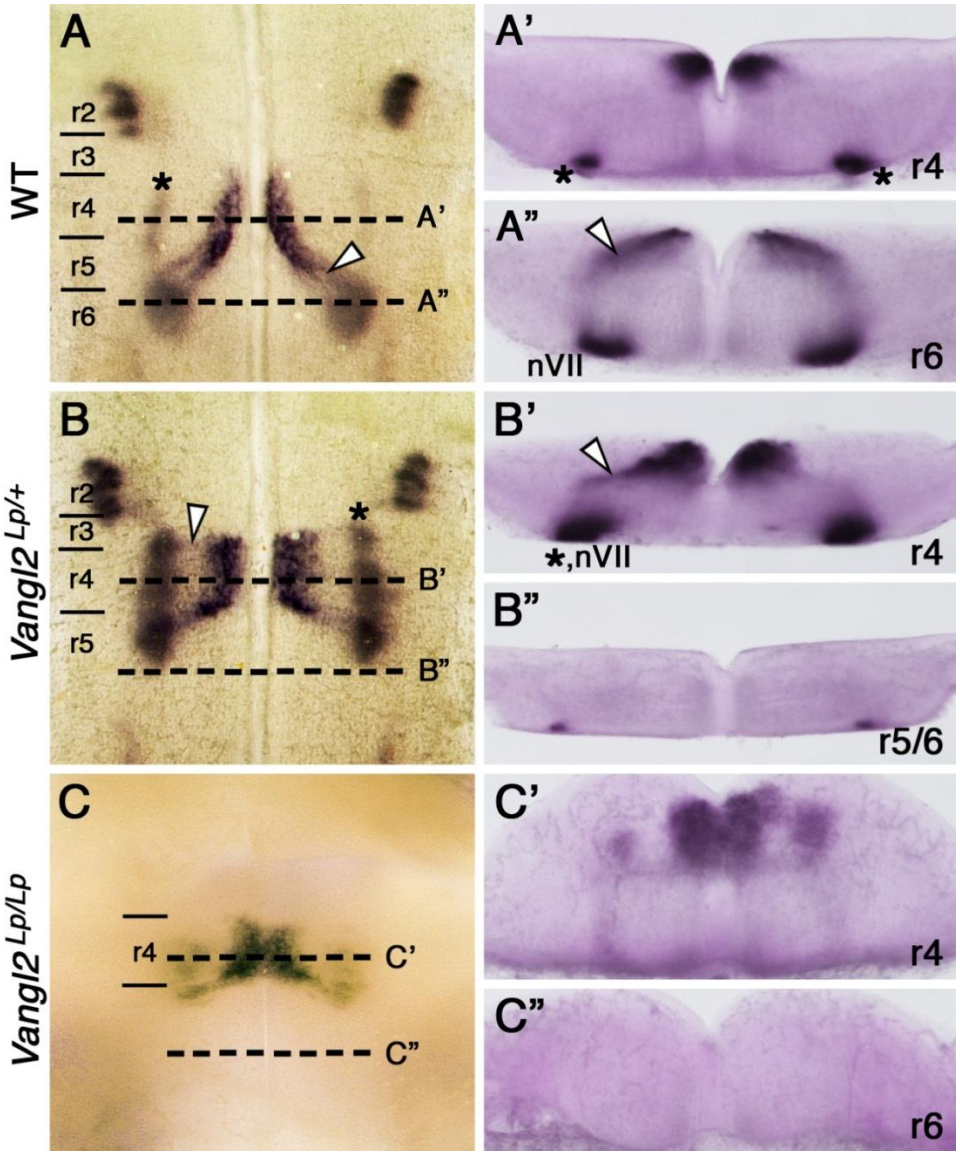

Figure 3.4. Tangential and radial FBMN migration defects in *Vangl2*^{Lp} embryos.

A-C, E12.5 embryos processed for *Tbx20* ISH. In WT embryos (**A-A"**), *Tbx20*-expressing FBMNs migrate caudally from r4 into r6, then migrate radially (white arrowheads) to the pial surface of the neural tube and form the facial motor nucleus (nVII). Inner ear efferent (IEE) neurons at the r4 pial surface also express *Tbx20* (asterisks). In *Vangl2*$^{Lp/+}$ embryos (**B-B"**), FBMNs are displaced caudally but undergo their radial migration (white arrowheads) normally. FBMNs in *Vangl2*$^{Lp/Lp}$ embryos (**C-C"**) are confined to r4, and fail to migrate radially, remaining near the ventricular surface.

Figure 3.5. FBMNs fail to migrate caudally in *Vangl2*^{KO} embryos.

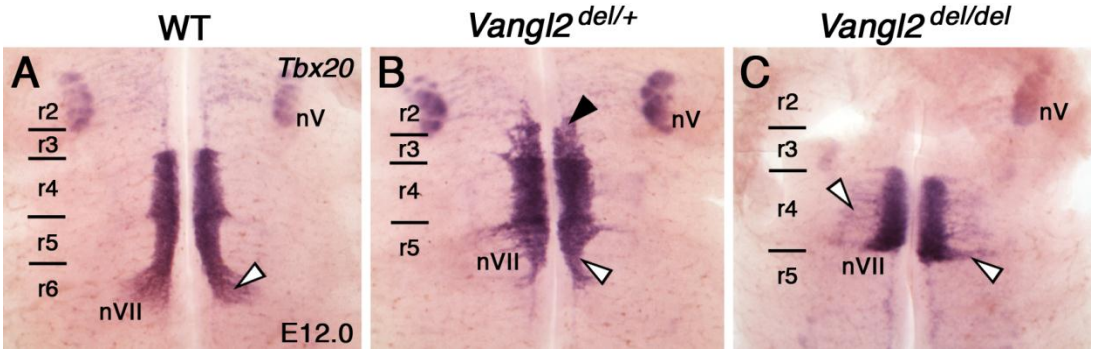

Figure 3.5. FBMNs fail to migrate caudally in *Vangl2*^{KO} embryos.

A-C, Ventricular views of flat-mounted hindbrains processed for *Tbx20* ISH. At E12.0, FBMNs in WT embryos (**A**) migrate caudally from r4 into r6, then migrate dorsolaterally and radially within r6 (white arrowhead) to form the facial motor nucleus (nVII). In *Vangl2*$^{del/+}$ embryos (**B**), *Tbx20*-expressing cells are seen spanning r3 (black arrowhead) to r5 (white arrowhead) but do not migrate into r6. In *Vangl2*$^{del/del}$ embryos (**C**), FBMNs are confined to r4, with enlarged populations of *Tbx20*-expressing cells in lateral r4 (white arrowheads) compared to WT.

3.2.3. FBMNs are specified and differentiate normally in *Vangl2^{Lp}* mutants

We further characterized the *Vangl2^{Lp}* phenotype at E12.5, the midpoint of FBMN migration, using multiple approaches. FBMNs in both WT and *Vangl2^{Lp}* mutants expressed *Phox2b* (**Figure 3.6 A-C**, 8/8 WT, 8/8 *Lp*/+, 3/3 *Lp/Lp*), a BM/VM neuron differentiation marker (Pattyn et al., 2000), indicating that the non-migrating cells in the *Vangl2^{Lp}* mutants differentiated correctly. Using NeuroVue dyes to retrogradely label FBMNs from their innervation site in the second branchial arch (Fritzsch et al., 2005), we tested whether *Vangl2^{Lp}* mutant FBMN axons properly projected into the facial nerve. Intriguingly, FBMNs were labeled in *Vangl2$^{Lp/+}$* (4/4) and *Vangl2$^{Lp/Lp}$* (2/2) embryos but appeared reduced in number in *Vangl2$^{Lp/Lp}$* mutants (**Figure 3.6 D-F**, 2/2 embryos). *Ret7*, a Gdnf receptor, is normally expressed in FBMNs upon entering r6 (Garel et al., 2000). However, FBMNs in *Vangl2$^{Lp/+}$* and *Vangl2$^{Lp/Lp}$* embryos aberrantly expressed *Ret7* in r4 (**Figure 3.6 G-I**, 4/4 *Lp*/+ and 2/2 *Lp/Lp*).

We wondered whether FBMN migration defects in *Vangl2$^{Lp/+}$* mutants were a consequence of improper progenitor specification. *Mash1* and *Mash3* encode transcription factors that are essential for FBMN progenitor specification and their subsequent migration, and are expressed in longitudinal domains in the ventricular zone, corresponding to the pMN domain (Ohsawa et al., 2005; Tiveron et al., 2003). These expression domains were not affected in *Vangl2$^{Lp/+}$* and *Vangl2$^{Lp/Lp}$* embryos (**Figure 3.7 A-F**; *Mash1*: 2/2 *Lp*/+ and 2/2 *Lp*/*Lp*; *Math3*: 3/3 *Lp*/+ and 2/2 *Lp/Lp*), suggesting that mutant FBMN progenitors were specified normally. Neurofilament

staining of peripheral nerves revealed normal projection patterns for the trigeminal (nV) and facial (nVII) nerves at E11.5 (**Figure 3.7 G-I**, 3/3 *Lp*/+ and 2/2 *Lp/Lp*), indicating that despite the failure of FBMN migration, their axonal projections branch and innervate peripheral targets. In addition, the rhombomere markers *Hoxb1* (r4) and *Krox20* (r3/r5) were expressed normally in *Vangl2*^{Lp} mutants (**Figure 3.8 A-C**, 7/7 *Lp*/+ and 2/2 *Lp/Lp*), arguing against the phenotype being a consequence of hindbrain patterning defects.

Rhombomere 4 generates both FBMNs and inner ear efferent (IEE) neurons. Whereas FBMNs migrate caudally out of r4, IEE neurons, which express *Gata3* (Karis et al., 2001), are confined to r4. In adjacent r5, the non-migratory abducens neurons express the homeobox transcription factor *Hb9* (Thaler et al., 1999), indicative of somatomotor neurons (SMNs). Therefore, we tested whether *Vangl2*^{Lp} FBMNs were misspecified as either IEE neurons or SMNs, which could account for the caudal migration phenotype. In WT embryos, *Gata3* was present in a high-expressing medial domain near the floor plate and a weaker-expressing lateral domain, but was excluded from the FBMNs (**Figure 3.8 D-D'**, 6/6 embryos). This expression pattern was unaffected in *Vangl2*$^{Lp/+}$ and *Vangl2*$^{Lp/Lp}$ embryos (**Figure 3.8 E-E', F-F'**, 8/8 *Lp*/+ and 1/1 *Lp*/*Lp*). Similarly, *Hb9* was not misexpressed in FBMNs within r4 (**Figure 3.8 H-I**, 10/10 *Lp*/+ and 5/5 *Lp/Lp*). Together, these results indicate that the FBMN migration phenotype in *Vangl2*^{Lp} mutants is not due to misspecification into non-migratory neurons.

Figure 3.6. Analysis of FBMN migration in *Vangl2*^{Lp} embryos.

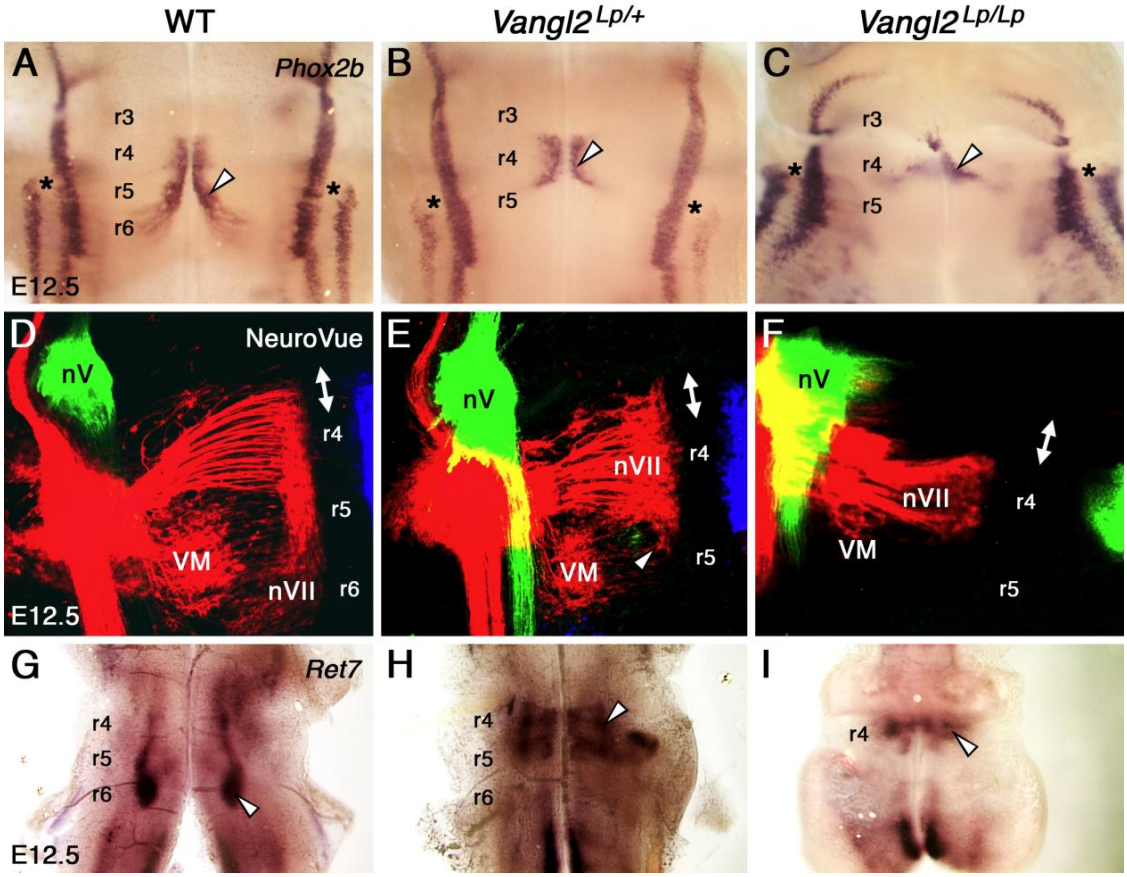

Figure 3.6. Analysis of FBMN migration in *Vangl2*^{Lp} embryos.

A-I, Ventricular views of flat-mounted hindbrains at E12.5 processed for *Phox2b* ISH (**A-C**), NeuroVue retrograde labeling (**D-F**), or *Ret7* ISH (**G-I**). **A-C**, *Phox2b* labeling. In WT embryos (**A**), *Phox2b* labels BM/VM neurons, including FBMNs along their migratory route from r4 to r6 (white arrowhead). In *Vangl2*$^{Lp/+}$ (**B**) and *Vangl2*$^{Lp/Lp}$ (**C**) embryos, *Phox2b* labeled FBMNs confined to r4, while a dorsal stripe of *Phox2b*-expressing cells in *Vangl2*$^{Lp/Lp}$ embryos appeared shifted rostrally (asterisks, compare **C** to **A**). **D-F**, Retrograde labeling of hindbrain motor neurons with lipophilic NeuroVue dyes. Red dye applied to the facial nerve in WT (**D**) labels FBMNs (nVII) spanning r4 through r6, and facial visceromotor neurons of the superior salivatory nucleus (VM) within r5. Green dye applied to the trigeminal nerve labels trigeminal (nV) BMNs in r2 and rostral r3. In *Vangl2*$^{Lp/+}$ (**E**) and *Vangl2*$^{Lp/Lp}$ (**F**) embryos, VM nuclei appear reduced, and FBMNs are confined almost exclusively to r4. Some FBMNs cross into r5 in *Vangl2*$^{Lp/+}$ embryos (**E**) as shown by the position of the abducens (nVI) nuclei (green in r5). **G-I**, *Ret7* labeling. In WT embryos (**G**), *Ret7* is expressed by FBMNs in r6 (arrowhead) but not r4. Aberrant *Ret7* expression occurs in both *Vangl2*$^{Lp/+}$ (**H**) and *Vangl2*$^{Lp/Lp}$ (**I**) embryos (white arrowheads). Midline positions are indicated by double-headed arrows.

Figure 3.7. FBMN progenitor specification and peripheral nerve projections are normal in *Vangl2*^{Lp} embryos.

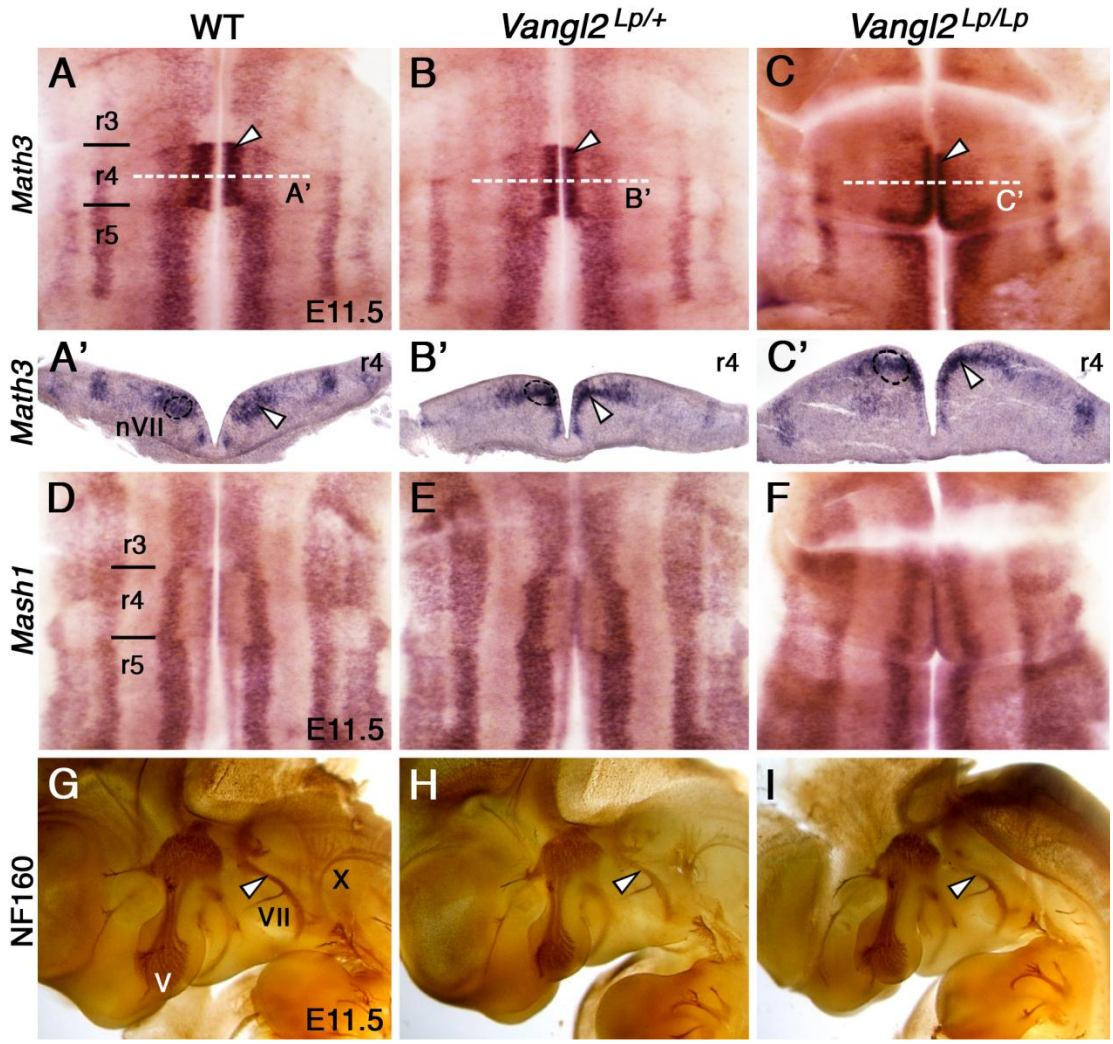

Figure 3.7. FBMN progenitor specification and peripheral nerve projections are normal in *Vangl2*^{Lp} embryos.

A-I, E11.5 embryos processed for ISH for *Math3* (**A-C**, **A'-C'**) or *Mash1* (**D-F**). Embryos were imaged via ventricular views of flat-mounted hindbrains (**A-F**) or 50 µm coronal sections (**A'-C'**). At E11.5, *Math3* expression within r4 (white arrowheads) is limited to the pMN domain (dotted circles) in WT (**A**, **A'**), *Vangl2*$^{Lp/+}$ (**B**, **B'**), and *Vangl2*$^{Lp/Lp}$ (**C**, **C'**) embryos. *Mash1* expression within r4 is limited to an overlapping, but distinct portion of the pMN domain in WT (**D**), *Vangl2*$^{Lp/+}$ (**E**), and *Vangl2*$^{Lp/Lp}$ (**F**) embryos. **G-I**, Lateral views, rostral to the left, of E11.5 embryos processed for anti-neurofilament (NF-160) immunohistochemistry. In WT embryos (**G**), the trigeminal (V) and facial (VII, white arrowhead) nerves project into the first and second branchial arches, respectively, and the vagus (X) nerve is seen exiting the caudal hindbrain. No noticeable differences in these projections are seen in *Vangl2*$^{Lp/+}$ (**H**) or *Vangl2*$^{Lp/Lp}$ (**I**) embryos.

Figure 3.8. ***Vangl2*^{Lp} mutants have normal hindbrain patterning and are not transfated to non-migratory neuron types.**

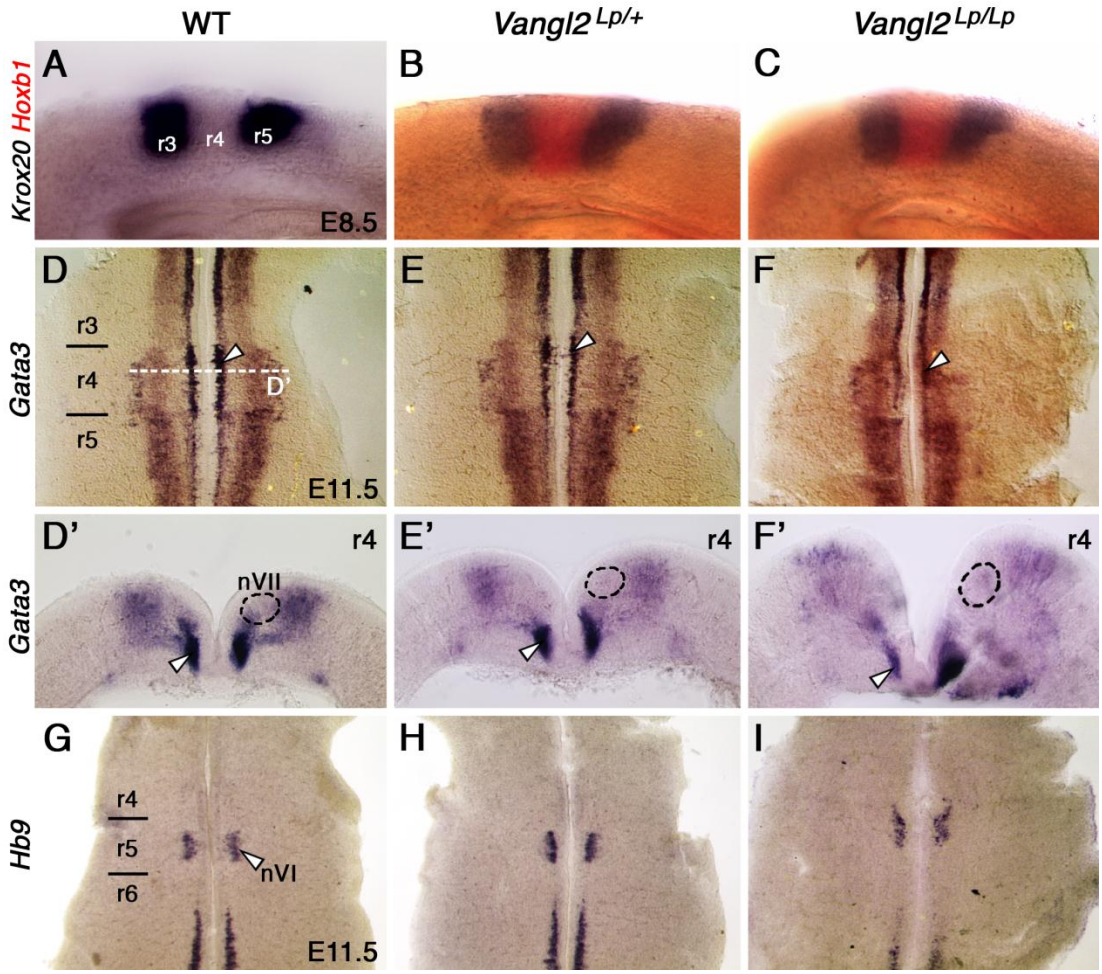

Figure 3.8. *Vangl2*^{Lp} mutants have normal hindbrain patterning and are not transfated to non-migratory neuron types.

A-C, Lateral views, rostral to the left, of E8.5 embryos processed for *Krox20* and *Hoxb1* ISH. *Krox20* (r3/r5 marker) and *Hoxb1* (r4 marker) are expressed in the appropriate rhombomeres in *Vangl2*^{Lp} embryos (compare **B** and **C** to **A**). **D-F**, Dorsal views and cross sections at the r4 level (**D'-F'**) of E11.5 embryos processed for *Gata3* ISH. In WT embryos (**D**), *Gata3* is expressed in a high-expression medial domain (arrowhead) and a lower-expression lateral domain. A cross section (**D'**) at the r4 level reveals that *Gata3* expression is limited to inner ear efferent (IEE) neurons but excluded from the FBMN domain (nVII, dotted circle). This expression pattern is intact in *Vangl2*$^{Lp/+}$ (**E**, **E'**) and *Vangl2*$^{Lp/Lp}$ (**F**, **F'**) embryos, and *Gata3* is not expressed in the FBMN domain. **G-I**, Dorsal views of E11.5 embryos processed for *Hb9* ISH. In WT embryos (**G**), *Hb9* is expressed in somatomotor nuclei, including the non-migratory abducens (nVI) nuclei in r5 (arrowhead), but is not expressed in FBMNs. In *Vangl2*$^{Lp/+}$ (**H**) and *Vangl2*$^{Lp/Lp}$ (**I**) embryos, the *Hb9* expression pattern is intact and remains excluded from FBMNs.

3.2.4. Wnt/PCP genes are expressed normally in *Vangl2^{Lp}* mutants

We next examined the expression of Wnt/PCP genes in *Vangl2^{Lp}* mutants. In mouse *Tbx20* mutants, FBMNs fail to migrate caudally and misexpress numerous Wnt/PCP genes, including *Prickle1 (Pk1)* and *Wnt11* (Song et al., 2006). In zebrafish, *pk1* is necessary for FBMN migration and genetically interacts with *vangl2* (Carreira-Barbosa et al., 2003). *Wnt5a*, which encodes a secreted glycoprotein of the Wnt/PCP pathway, is expressed outside of FBMNs but may serve as an attractive cue to migrating FBMNs (Song et al., 2006; Vivancos et al., 2009). Therefore, we examined the expression of these genes in *Vangl2^{Lp}* mutants. In E12.5 WT embryos, *Wnt5a* is only expressed in the floor plate from r2 to r4, then broadly from r5 and caudally in a rostral^{low} to caudal^{high} gradient (**Figure 3.9 A**, 2/2 embryos) (Vivancos et al., 2009). A sharp boundary of expression occurs at the r4/r5 boundary. In *Vangl2$^{Lp/Lp}$* mutants (**Figure 3.9 C**, n=2), the boundary was less clear and overall expression levels appeared lower. However, *Wnt5a* expression in *Vangl2$^{Lp/+}$* embryos (**Figure 3.9 B**, 2/2 embryos) was indistinguishable from WT (despite an FBMN migration phenotype), signifying that the caudal migration defect in *Vangl2$^{Lp/Lp}$* mutants was not due to aberrant *Wnt5a* expression. *Pk1* expression, as expected, corresponded to the location of FBMNs in both WT and *Vangl2^{Lp}* mutants (**Figure 3.9 D-F**), suggesting that overall Wnt/PCP gene expression patterns are likely normal in *Vangl2^{Lp}* mutants.

Figure 3.9. Wnt/PCP gene expression in *Vangl2*^{Lp} embryos.

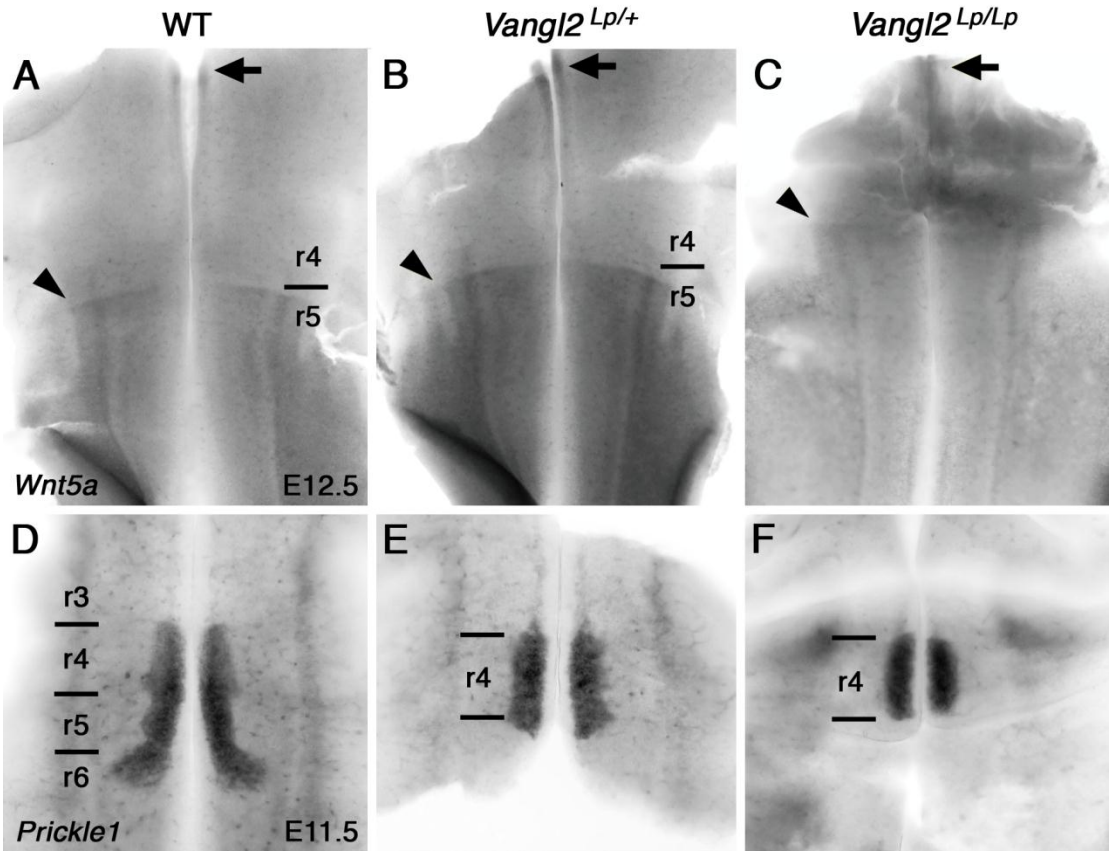

Figure 3.9. Wnt/PCP gene expression in *Vangl2*^{Lp} embryos.

A-F, Ventricular views of flat-mounted hindbrains processed for *Wnt5a* (**A-C**) or *Prickle1* (**D-F**) ISH. In E12.5 WT embryos (**A**), *Wnt5a* is expressed in a stepwise caudal^{high} to rostral^{low} gradient, with no expression in r4 and a sharp boundary between r4 and r5 (black arrowhead). No noticeable difference is seen in *Vangl2*$^{Lp/+}$ embryos (**B**), and a sharp boundary between r4 and r5 is intact in *Vangl2*$^{Lp/Lp}$ embryos (**C**) despite neural tube defects. In E11.5 WT embryos (**D**), *Prickle1* is expressed in FBMNs along their migratory route spanning r4 through r6. *Prickle1* remains expressed in *Vangl2*$^{Lp/+}$ (**E**) and *Vangl2*$^{Lp/Lp}$ (**F**) FBMNs confined to r4. *Images courtesy of Mi-Ryoung Song, Gwangju Institute of Science and Technology, Republic of Korea. D.M. Glasco provided the embryos for these experiments.*

3.2.5. FBMN migration is regulated independent of *Dishevelled* function

In mice, Wnt5a and Wnt7a can act as chemoattractants for FBMNs in a bead assay; however, their *in vivo* roles are less clear since FBMNs migrate out of r4 in *Wnt5a* mutants, with a slight defect in dorsolateral migration in r5/r6 (Vivancos et al., 2009). In zebrafish, previous studies have shown that FBMN migration is regulated by multiple Wnt/PCP genes, but PCP-specific Wnt ligands appear dispensable (Bingham et al., 2002; Carreira-Barbosa et al., 2003; Jessen et al., 2002; Wada et al., 2006). Furthermore, injection of a dominant negative form of *dishevelled (Dvl)*, the central downstream signaling component of the Wnt/PCP pathway, does not affect FBMN migration (Jessen et al., 2002). Therefore, to determine whether FBMNs can migrate independent of PCP signaling, we examined FBMN migration in *Dvl*-deficient mouse and zebrafish embryos.

Combinatorial deletion of two to three copies of mouse *Dvl* genes did not disrupt caudal FBMN migration (**Figure 3.10 A-C; Figure 3.11 A-C**), including in *Dvl1*+/-; *Dvl2*-/- embryos with high penetrance of hindbrain neural tube defects (3/6 embryos). Most importantly, FBMNs also migrated caudally into r6 in *Dvl1/2* double mutants (**Figure 3.10 D; Figure 3.11 D**), which exhibit classic PCP defects including a fully open neural tube and misorientation of stereociliary bundles in the inner ear (Etheridge et al., 2008; Hamblet et al., 2002; Wang et al., 2005). Similar to *Vangl2*$^{Lp/Lp}$, the bilateral populations of FBMNs in r4 initially appeared fused at the midline (**Figure 3.10 D**). By E14.5, however, these populations were segregated to form an FMN on either side of the midline (**Figure 3.11 A-D**), indicating that they were still able to undergo radial migration to the pial surface.

We further examined the requirement for Dvl signaling by disrupting the function of *dvl* and downstream effectors in *Tg(isl1:gfp)* zebrafish embryos, which express GFP in branchiomotor neurons (Higashijima et al., 2000). Similar to mice, zebrafish FBMNs are born in r4 and migrate caudally into r6 and r7 (Chandrasekhar, 2004; Chandrasekhar et al., 1997; Higashijima et al., 2000). Overexpression of a dominant negative *dvl* construct *(Xdd1*, *Dvl-delPDZ)* (Jessen et al., 2002) resulted in a convergence and extension (CE) defect and shortened body axis; however, FBMNs migrated caudally into r6 and r7 (**Figure 3.10 F**). Similarly, injection of C- and N-terminal deletion constructs *(Dvl-delC* and *Dvl-delN)*, mutant *Daam1 (Daam1-delN),* and WT *dvl1* overexpression, generated CE defects, but failed to disrupt caudal FBMN migration (**Figure 3.10 G-H**, data not shown).

If FBMN migration is *Dvl*-independent, we hypothesized that loss of *Dvl* function in *Vangl2*$^{Lp/+}$ embryos would not exacerbate the *Vangl2*$^{Lp/+}$ migration defect. Therefore, we crossed *Vangl2*^{Lp} mice with *Dvl2* mutants (Hamblet et al., 2002). *Dvl2*-/- mice exhibit a mild incidence of PCP defects (Hamblet et al., 2002) yet normal FBMN migration (**Figure 3.12 C**, 11/11 embryos) and would be a sensitized background to test for genetic interaction with *Vangl2*. Many FBMNs migrated into r5 in both *Vangl2*$^{Lp/+}$; *Dvl2*+/- (5/5 embryos) and *Vangl2*$^{Lp/+}$; *Dvl2*-/- embryos (5/5 embryos) (**Figure 3.12 E-F**), comparable to *Vangl2*$^{Lp/+}$ embryos (**Figure 3.12 D**), suggesting that *Vangl2* and *Dvl2* do not genetically interact to regulate caudal FBMN migration. Since *Vangl2*$^{Lp/+}$; *Dvl2*-/- embryos had fully open neural tubes, the clusters of non-migrated FBMNs in r4 were fused across the midline, as in *Vangl2*$^{Lp/Lp}$ embryos (**Figure 3.12 G**). Interestingly,

migration of FBMNs into r3, as seen in some *Vangl2*$^{Lp/+}$ embryos was never seen in *Vangl2*$^{Lp/+}$; *Dvl2*-/- embryos, suggesting that abnormal rostral migration of FBMNs may be Dvl-dependent. To test this further, we crossed *Dvl2* mutants with *Celsr1*^{Crsh} mice, which exhibit FBMN migration directionality defects (Qu et al., 2010). In *Celsr1*$^{Crsh/+}$ embryos, a significant number of FBMNs migrated rostrally into r2/r3, while most migrated caudally into r6 (**Figure 3.12 H**) (Qu et al., 2010). While FBMNs migrated rostrally in *Celsr1*$^{Crsh/+}$; *Dvl2*+/- embryos (**Figure 3.12 I**, 12/14 embryos), this defect was completely rescued in *Celsr1*$^{Crsh/+}$; *Dvl2*-/- embryos (5/5 embryos), and FBMNs migrated caudally despite an open neural tube (**Figure 3.12 J**). These data suggest that while caudal FBMN migration is insensitive to or independent of *Dvl* activity, the aberrant rostral migration seen in *Vangl2*$^{Lp/+}$ and *Celsr1*$^{Crsh/+}$ embryos requires *Dvl* function. Finally, in *Vangl2*$^{Lp/+}$; *Celsr1*$^{Crsh/+}$ transheterozygotes (**Figure 3.12 K**), FBMNs failed to migrate caudally (5/5 embryos), and no rostral migration was noted. The phenotype mimicked the *Vangl2*^{Lp} phenotype, suggesting that the general ability to migrate, regulated by *Vangl2*, is hierarchical to the directionality decision of migrating FBMNs, regulated by *Celsr1*.

Figure 3.10. FBMN migration is regulated independent of *Dishevelled* function in mice and zebrafish.

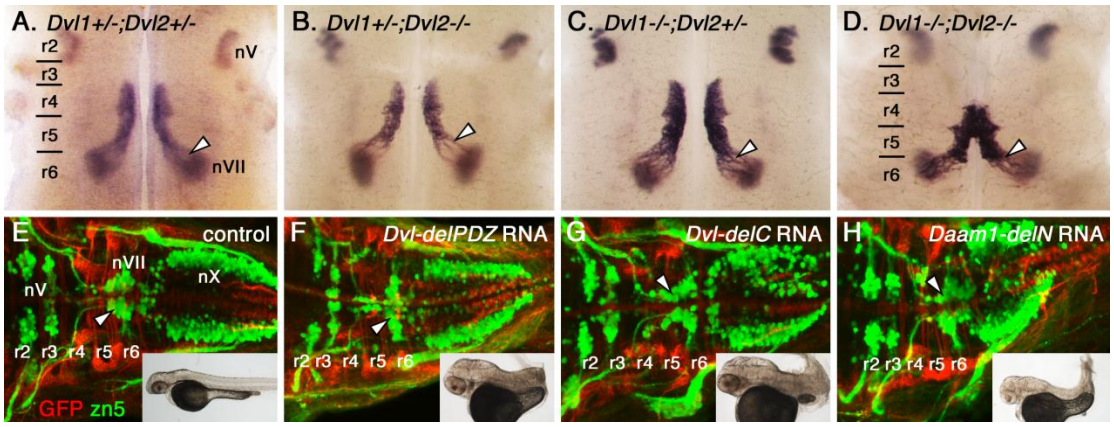

Figure 3.10. FBMN migration is regulated independent of *Dishevelled* function in mice and zebrafish.

A-D, Ventricular views of flat-mounted hindbrains processed for *Tbx20* ISH at E12.5. In control *Dvl1+/-;Dvl2+/-* embryos (**A**, n=3), FBMNs migrate caudally from r4 into r6 (arrowhead) to form the facial motor nucleus (nVII). This migration is intact in *Dvl1+/-;Dvl2-/-* (**B**, 4/4 embryos), *Dvl1-/-;Dvl2+/-* (**C**, 3/3 embryos), and *Dvl1-/-;Dvl2-/-* mutants (**D**, 4/4 embryos). Neural tube defects (CRN) occurred in *Dvl1+/-;Dvl2-/-* (**B**, 2/4 embryos) and *Dvl1-/-;Dvl2-/-* (**D**, 4/4 embryos). **E-H**, Dorsal views of 48 hpf *Tg(isl1:gfp)* zebrafish embryos processed for anti-GFP and zn5 immunohistochemistry. In control embryos (**E**), anti-GFP (green) labels FBMNs migrating caudally from r4 into r6 (arrowhead) and r7. Anti-zn5 labels rhombomere boundaries. Whole embryos (inset) have normal elongation of the body axis. In embryos injected with *Dvl-delPDZ* (**F**), *Dvl-delC* (**G**), and *Daam1-delN* (**H**) RNA, FBMNs are able to migrate caudally (arrowheads) despite convergence and extension defects resulting in a shortened body axes (insets). *Vinoth Sittaramane (Anand Chandrasekhar Lab, University of Missouri) performed the experiments in panels E-H.*

Figure 3.11. FBMN migration in *Dvl1;Dvl2* and *Ptk7*$^{chz/chz}$ mutants at E14.5.

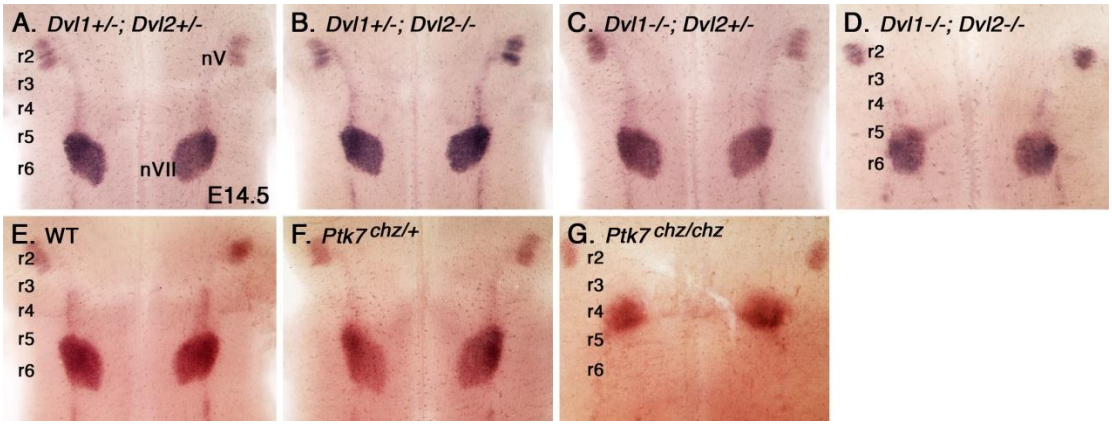

Figure 3.11. FBMN migration in *Dvl1;Dvl2* and *Ptk7*$^{chz/chz}$ mutants at E14.5.

A-G, Pial views of E14.5 embryos processed for *Tbx20* ISH. By E14.5, FBMNs in control embryos (**A**, **E-F**) have completed their caudal and radial migrations to form facial motor nuclei (nVII) in r6. Likewise, these nuclei are formed in r6 in *Dvl*-deficient embryos including *Dvl1+/-;Dvl2-/-* (**B**, 2/2 embryos), *Dvl1-/-;Dvl2+/-* (**C**, 6/6 embryos), and *Dvl1-/-;Dvl2-/-* mutants (**D**, 4/4 embryos). Neural tube defects (CRN) were noted in *Dvl1-/-;Dvl2-/-* mutants (**D**, 4/4 embryos). In *Ptk7*$^{chz/chz}$ mutants (**G**), the facial motor nuclei are rostrally displaced in r4 (8/8 embryos).

Figure 3.12. Genetic interaction studies of *Vangl2*, *Celsr1*, and *Dvl2* in mice.

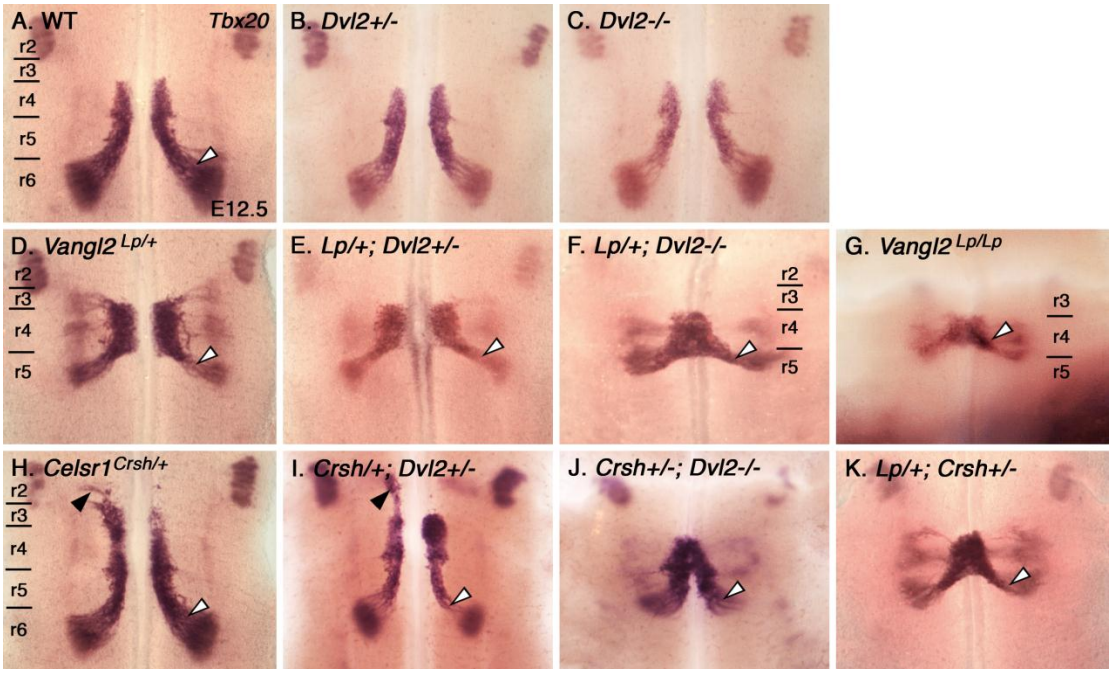

Figure 3.12. Genetic interaction studies of *Vangl2*, *Celsr1*, and *Dvl2* in mice.

A-K, Ventricular views of flat-mounted hindbrains processed for *Tbx20* ISH at E12.5. The caudal aspects of FBMNs are labeled with white arrowheads, while rostrally-migrating neurons in *Celsr1*-deficient embryos are labeled with black arrowheads. Neural tube defects (CRN) occurred in *Vangl2*$^{Lp/+}$; *Dvl2*-/- (**F**, 5/5 embryos), *Vangl2*$^{Lp/Lp}$ (**G**, 6/6 embryos), *Celsr1*$^{Crsh/+}$; *Dvl2*+/- (**I**, 4/14 embryos), *Celsr1*$^{Crsh/+}$; *Dvl2*-/- (**J**, 5/5 embryos), and *Vangl2*$^{Lp/+}$; *Celsr1*$^{Crsh/+}$ (**K**, 2/2 embryos).

3.2.6. *Ptk7* is necessary for FBMN migration in mice

Ptk7 encodes a single-pass transmembrane protein with seven extracellular Ig-like domains and a cytosolic kinase homology domain which lacks catalytic activity (Jung et al., 2004; Mossie et al., 1995). It has demonstrated roles in cancer cell metastasis and convergence and extension cell movements during gastrulation, both of which require the organized polarization of cells. In cancer cell lines, PTK7 is localized to the leading edge of migrating cells and their migration is heavily dependent on cleavage of PTK7 from a full-length to soluble form by the matrix metalloprotease MT1-MMP (Golubkov et al., 2010). The mouse *Ptk7* mutant *Chuzhoi*, in which the level of soluble Ptk7 is greatly reduced, displays classic PCP phenotypes (Paudyal et al., 2010), suggesting a role for *Ptk7* in PCP signaling. Given this, and the genetic interactions between $Ptk7^{Chz}$, $Vangl2^{Lp}$, and $Celsr1^{Crsh}$ in neural tube closure (Paudyal et al., 2010), we examined FBMN migration in $Ptk7^{Chz}$ mutant mice.

In $Ptk7^{Chz/Chz}$ mutants, most FBMNs failed to migrate caudally out of r4 (**Figure 3.13**). In some embryos (4/6), a small subset of FBMNs migrated caudally to a similar extent as WT (compare **Figure 3.13 C to A-B**) and formed the FMN in r6 by E14.5 (**Figure 3.11 E-G**). Nevertheless, the vast majority of FBMNs failed to migrate caudally to any extent, demonstrating a clear role for *Ptk7* in FBMN migration in mice.

Figure 3.13. FBMN migration is impaired in the *Ptk7* mutant *Chuzhoi*.

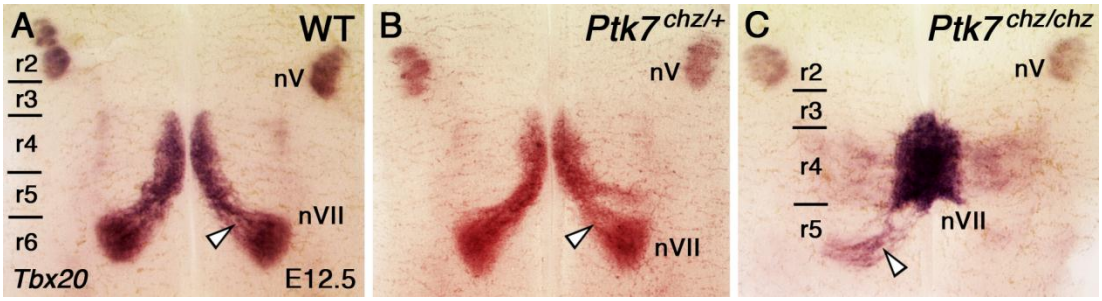

Figure 3.13. FBMN migration is impaired in the *Ptk7* mutant *Chuzhoi*.

A-C, Ventricular views of flat-mounted hindbrains processed for *Tbx20* ISH at E12.5. In WT (**A**) and *Ptk7*$^{chz/+}$ (**B**) embryos, FBMNs migrate caudally from r4 into r6 (arrowheads) to form the facial motor nucleus (nVII). In *Ptk7*$^{chz/chz}$ mutants (**C**), FBMNs are confined to r4, except for a small subset which is able to leave r4 (white arrowhead, 4/6 embryos). In 2/6 *Ptk7*$^{chz/chz}$ mutants (not shown), all FBMNs were confined to r4.

3.3. Discussion

3.3.1. FBMN migration defects in *Vangl2* mutants

An intriguing aspect of the FBMN migration defects in *Vangl2* mutants is the fully penetrant phenotype in heterozygous embryos. In both *Vangl2*$^{del/+}$ and *Vangl2*$^{Lp/+}$ embryos, FBMNs fail to migrate caudally, with some rostrally migrating FBMNs seen in *Vangl2*$^{del/+}$ embryos (**Figures 3.2, 3.5**). Since no Vangl2 protein is detected in *Vangl2*$^{del/del}$ mice (Song et al., 2010), it suggests that the *Vangl2*$^{del/+}$ phenotype may be due to haploinsufficiency and that a minimal threshold level of Vangl2 is required for proper FBMN migration. Conversely, the *Vangl2*^{Lp} allele likely functions as a dominant negative. The mutant protein encoded by *Vangl2*^{Lp} is unable to be recruited into COPII vesicles by Sec24b (Merte et al., 2010) and thus fails to reach the plasma membrane (Merte et al., 2010; Torban et al., 2007), possibly competing with the WT protein for intracellular binding partners, though mutant Vangl2 cannot bind Dvl (Torban et al., 2004b). Interestingly, phosphorylation of Vangl2 is essential for its function and is regulated by Wnt5a/Ror2 signaling at the plasma membrane (Gao et al., 2011). Moreover, the presence of mutant Vangl2 protein decreases the phosphorylation of WT Vangl2, strongly suggesting that *Vangl2*^{Lp} functions as a dominant negative.

Overall, our evidence suggests that FBMN migration is more sensitive to levels of Vangl2 than other processes such as neural tube closure and CE. Despite relatively normal neural tube morphology, FBMNs in *Vangl2*$^{Lp/+}$ embryos fail to migrate out of r4 (**Figure 3.2**). Therefore, while PCP phenotypes such as neural tube closure require

complete loss of *Vangl2*, FBMN migration appears to have a higher threshold requirement for *Vangl2* function. Since FBMNs can migrate caudally in an open neural tube environment (*Dvl1/2* mutants), it further suggests that FBMN migration and neural tube closure are regulated independently.

3.3.2. Cellular autonomy of Vangl2 function

In zebrafish embryos, *vangl2* is ubiquitously expressed and functions non-cell autonomously to regulate FBMN migration (Jessen et al., 2002). In contrast, mouse *Vangl2* is restricted to the ventricular zone and differentiated FBMNs arising from such (**Figure 3.1 C-F**). Therefore, it is tempting to speculate a cell autonomous role for *Vangl2* in mice. Consistent with this idea, some difference in gene expression was seen between WT and *Vangl2*^{Lp} mutants. *In situ* hybridization with the FBMN marker *Tbx20* in *Vangl2*$^{Lp/+}$ heterozygotes labeled multiple streams of putative FBMNs migrating away from the midline, forming elongated nuclei spanning r3 to r5 (**Figure 3.2 E**). Similar streams of cells are seen in *Islet1 (Isl1)*-labeled *Vangl2*$^{Lp/+}$ heterozygotes (Vivancos et al., 2009). *Phox2b*- and *Prickle1*-expressing neurons, however, were arranged compactly near the midline in r4 (**Figure 3.6 B**, **Figure 3.9 E**). Retrograde labeling experiments revealed that those streams of *Tbx20*- and *Isl1*-expressing cells do not send their axons into the facial nerve (**Figure 3.6 E**); therefore, they could not physiologically function as FBMNs. Since IEE neurons also express *Tbx20* and *Isl1*, these aberrant nuclei could reflect an enlarged population of IEE neurons. However, *Gata3* expression levels in

Vangl2$^{Lp/+}$ heterozygotes were indistinguishable from WT (compare **Figure 3.8 D-E**), arguing against this.

WT and *Vangl2*$^{Lp/+}$ embryos also showed gross differences in the expression of rhombomere-specific FBMN cell surface markers. *Ret7* (**Figure 3.6 G-I**) was aberrantly expressed in r4 in *Vangl2*^{Lp} mutants, but only upon entering r6 in WT. This may reflect an inability of mutant FBMNs to regulate expression of rhombomere-specific cell surface molecules (Muller et al., 2003), or alternatively, indicate that *Ret7* is expressed in FBMNs at the appropriate time point, regardless of location (Song et al., 2006). Since *Ret7* function is dispensable for FBMN migration (Song et al., 2006), *Ret7* misexpression alone cannot account for the *Vangl2*^{Lp} migration phenotype; but it implies a difference in gene expression between WT and *Vangl2*-deficient FBMNs. It would be instructive to compare gene expression profiles of FBMNs isolated from r4 in WT and *Vangl2*^{Lp} mutants.

Alternatively, *Vangl2* may function non-cell autonomously to regulate FBMN migration as in zebrafish, albeit by different mechanisms. In zebrafish, FBMNs use the laminin-expressing basement membrane as a substrate for their caudal migration from r4 to r6/r7 (Grant and Moens, 2010). Mouse FBMNs, on the contrary, migrate caudally adjacent to the ventricular zone from r4 into r6 (**Figure 3.4 A'-A"**), where they dive down radially to the pial surface near the basement membrane. Interestingly, some Laminin genes such as *Laminin*α*5* are expressed along the ventricular zone in the hindbrain (Coles et al., 2006), unlike in zebrafish, where laminins are restricted to the basement membrane (Grant and Moens, 2010). Mouse *Laminin*α*5* expression overlaps

with the expression domains of *Vangl2* (**Figure 3.1 C-F**) and *Celsr1* (Qu et al., 2010), and in zebrafish, *lamα1* genetically interacts with *vangl2* to regulate FBMN migration (Sittaramane et al., 2009). Therefore, a mechanism may exist by which Vangl2 and Celsr1 interact with Laminins and other molecules at the ventricular surface to guide the caudal migration of FBMNs.

3.3.3. Potential role for Dishevelled in FBMN migration

Though FBMN migration defects have been described in multiple Wnt/PCP mutants (Bingham et al., 2002; Carreira-Barbosa et al., 2003; Qu et al., 2010; Vivancos et al., 2009; Wada et al., 2006), whether FBMN migration is truly a PCP-dependent process has been somewhat unclear. In hindbrain explant cultures, some FBMNs are attracted to *Wnt5a*- and *Wnt7a*-coated beads; however, FBMNs still migrate caudally in *Wnt5a* and *Wnt7a* mutant embryos, with only some defects in dorsolateral migration seen in *Wnt5a* mutants (Vivancos et al., 2009). Intriguingly, in *Tbx20* mutants, FBMNs fail to migrate caudally and also misexpress Wnt/PCP genes in the neural tube, including *Fzd7*, *Wnt11*, and *Vangl1/2*; however, *Dvl3* expression is unaffected (Song et al., 2006). This implies that FBMN migration may not be *Dvl*-mediated. Using multiple *in vivo* approaches in both zebrafish and mice, (**Figures 3.10-3.12**), we determined that Dvl function is dispensable for caudal FBMN migration. This is important because mouse *Dvl1/2* double mutants display strong PCP phenotypes including neural tube defects, a shortened body axis, and misorientation of stereocilia in the inner ear (Hamblet et al.,

2002). Similarly, *dvl*-deficient zebrafish embryos have a robust convergence and extension phenotype (**Figure 3.10 E-H**), indicative of defective PCP. Since FBMNs migrate normally in *Dvl*-deficient embryos of either species, this suggests strongly that FBMN migration is regulated independent of Wnt/PCP signaling, and though the migration utilizes many Wnt/PCP components, it is not regulated via the conventional Wnt/PCP pathway. However, with three *Dvl* genes in mice, we cannot rule out that *Dvl3* may be compensating for lack of *Dvl1-2* function in *Dvl1/2* double mutants. *Dvl2/3* double mutants die by E9.5, and *Dvl1/3* double mutants do not have PCP defects (Etheridge et al., 2008), making further studies of *Dvl* mouse mutants unfeasible.

Whereas the general *ability* for FBMNs to migrate appears to be Dvl-independent, our data hints that the *directionality* of migration may be a Dvl-dependent process. A subset of FBMNs in *Celsr1*$^{Crsh/+}$ embryos migrates rostrally instead of caudally; however, most FBMNs migrate in the normal direction, and all FBMNs migrate out of r4 (Qu et al., 2010). Since *Celsr1*, like *Vangl2*, is a "core" PCP molecule, one would expect a similar phenotype in both *Celsr1*$^{Crsh/+}$ and *Vangl2*$^{Lp/+}$ embryos if the *ability* for FBMNs to migrate caudally were a PCP-dependent process. But since loss of *Dvl2* function rescues the rostral migration phenotype in *Celsr1*$^{Crsh/+}$ embryos (**Figure 3.12 H-J**) but does not exacerbate the *Vangl2*$^{Lp/+}$ phenotype (**Figure 3.12 D-F**), it suggests that *directionality* of migration and *ability* to migrate are regulated independently. Such a distinction would explain why the *Vangl2*$^{Lp/+}$; *Celsr1*$^{Crsh/+}$ transheterozygous phenotype mimics the *Vangl2*^{Lp} phenotype (**Figure 3.12 K**) and no rostral migration occurs in those

embryos – perhaps FBMNs must first acquire the ability to be motile (through *Vangl2*) before responding to directionality cues (through *Celsr1*).

3.3.4. Role of *Ptk7* in mouse FBMN migration

Mouse *Ptk7* mutants display CRN and inner ear phenotypes consistent with a role for *Ptk7* in the PCP pathway (Lu et al., 2004; Paudyal et al., 2010; Yen et al., 2009). However, other data suggest that it is a regulator of PCP signaling rather than an integral component. Although *Xenopus* Ptk7 has been shown to localize disheveled to the membrane (Shnitsar and Borchers, 2008), Dvl2 localization is normal in mouse *Ptk7* mutants, and no physical interactions between Ptk7 and other PCP genes have been found in mice (Paudyal et al., 2010). In the context of neural tube closure, *Ptk7* genetically interacts with *Vangl2* and *Celsr1*, as does *Scribble1 (Scrb1)*. Conversely, *Ptk7* and *Scrb1* do not genetically interact, suggesting they both regulate Wnt/PCP signaling, but through distinct mechanisms (Paudyal et al., 2010). Since the vast majority of FBMNs in *Ptk7*^{chuzhoi} mutants failed to migrate, this further suggests that the novel pathway responsible for regulating FBMN migration utilizes core Wnt/PCP components (e.g. *Vangl2*, *Dvl1/2*) as well as Wnt/PCP regulatory molecules (e.g. *Ptk7*, *Scrb1*).

CHAPTER 4: The Atypical Cadherin Celsr1 Regulates the Directionality of Facial Branchiomotor Neuron Migration in the Mouse Hindbrain

Text and figures modified from:

Yibo Qu*, Derrick M. Glasco*, Libing Zhou, Anagha Sawant, Aurélia Ravni, Bernd Fritzsch, Christine Damrau, Jennifer N. Murdoch, Sylvia Evans, Samuel L. Pfaff, Caroline Formstone, André M. Goffinet, Anand Chandrasekhar, and Fadel Tissir (2010). Atypical cadherins Celsr1-3 differentially regulate migration of facial branchiomotor neurons in mice. *Journal of Neuroscience* 30(28):9392-9401. *equal contribution

4.1. Introduction

In the developing central nervous system, post-mitotic neurons leave ventricular zones of precursor proliferation and migrate to their destinations. Several tightly regulated modes of migration have been described, including radial migration of excitatory neurons to the cortex, tangential migration of cortical interneurons, migration to the olfactory bulb in the rostral migratory stream, and migration of rhombic lip derivatives. A unique and intriguing example of neuronal migration is that of facial branchiomotor neurons (FBMNs), which innervate muscles responsible for facial expression derived from the second pharyngeal arch (Chandrasekhar, 2004; Garel et al., 2000; Guthrie, 2007). FBMNs are generated in rhombomere 4 (r4) and extend their axons from dorsal exit points towards muscle targets. Their cell bodies undergo a

complex caudal, tangential migration from r4 to r6. They migrate in the subventricular region, and pass medial to the nucleus abducens (nVI) in r5 (Song et al., 2006), before moving laterally and dorsally in r5-r6. Finally, they undergo a radial, gliophilic, Reelin- and Cdk5- dependent migration in r6 to reach their terminal, subpial location (Chandrasekhar, 2004; Goffinet, 1984; Ohshima et al., 2002). While migrating, FBMNs leave their axons behind which forms the "genu" of the facial nerve, with facial motor axons looping around nVI and the medial longitudinal fasciculus (mlf). Caudal translocation of the soma of FBMNs with looping of axons is seen in both fish and mammals, but not chicken, with some species-specific differences (Gilland and Baker, 2005).

In zebrafish, several planar cell polarity (PCP) genes such as *van gogh-like 2 (vangl2)*, *frizzled3a (fzd3a)*, *celsr2*, *prickle1a*, and *prickle1b* are necessary for the caudal migration of FBMNs (Bingham et al., 2002; Carreira-Barbosa et al., 2003; Jessen et al., 2002; Rohrschneider et al., 2007; Wada et al., 2006). In mice, some Wnt/PCP genes (*Fzd3, Vangl2, Wnt5a*) and downstream signaling events have been recently implicated in regulating FBMN movement (Vivancos et al., 2009). To understand better the role of PCP-related mechanisms in FBMN migration in mice, we studied the role of the atypical cadherin Celsr1. Mouse *Celsr1-3* genes are homologous to *Drosophila flamingo/starry night*, and are expressed in the developing nervous system in complementary patterns (Formstone and Little, 2001; Shima et al., 2002; Tissir et al., 2002). Celsr1 has established roles in PCP-related processes such as neural tube closure, organization of stereocilia of hair cells in the inner ear (Curtin et al., 2003; Montcouquiol et al., 2003;

Wang and Nathans, 2007), and skin hair patterning (Devenport and Fuchs, 2008; Guo et al., 2004; Ravni et al., 2009). Using *Celsr1*^{Crsh} (Curtin et al., 2003) mutant mice, we demonstrate a role for *Celsr1* in regulating the direction of FBMN migration.

4.2. Results

4.2.1. *Celsr1* expression in the developing hindbrain

Celsr1 expression was studied by ISH with a digoxigenin-labeled riboprobe, and immunohistochemistry with anti-Celsr1 antibodies (**Figure 4.1**). At E10.5, *Celsr1* mRNA was expressed in the ventricular zone and floor plate cells at all axial levels (**Figure 4.1 A-B**; 6/6 embryos). By E12.5, *Celsr1* expression in floor plate cells was downregulated in r4 and more anterior regions, but maintained at high levels in and caudal to r5, adjacent to the migrating FBMNs (**Figure 4.1 C-D**; 4/6 embryos).

Our collaborators (Yibo Qu and Fadel Tissir, Institute of Neuroscience, Developmental Neurobiology, Université Catholique de Louvain, Brussels, Belgium) examined Celsr1 expression using an anti-Celsr1 antibody. At the protein level, Celsr1 was strongly expressed in radial neuroepithelial cells located in the paramedian ventricular zone at E9.5-E10.5, with high signal in their pial end-feet (**Figure 4.1 E**). Celsr1-positive cells were intermingled with emerging Islet1-positive FBMNs in r4. Expression was also seen in radial cells in the alar plate. Using confocal imaging (**Figure 4.1 E**, insert), they found that Celsr1 protein may colocalize with Isl1 in some FBMNs at

E9.5. From E10.5 - E11.5, Celsr1 expression was downregulated in neuroepithelial cells, but remained high in floor plate cells (**Figure 4.1 F-G**). Colocalization of Celsr1 and Isl1 in FBMNs was not seen between E10.5 – E11.5.

Figure 4.1. Expression of *Celsr1* in the developing hindbrain.

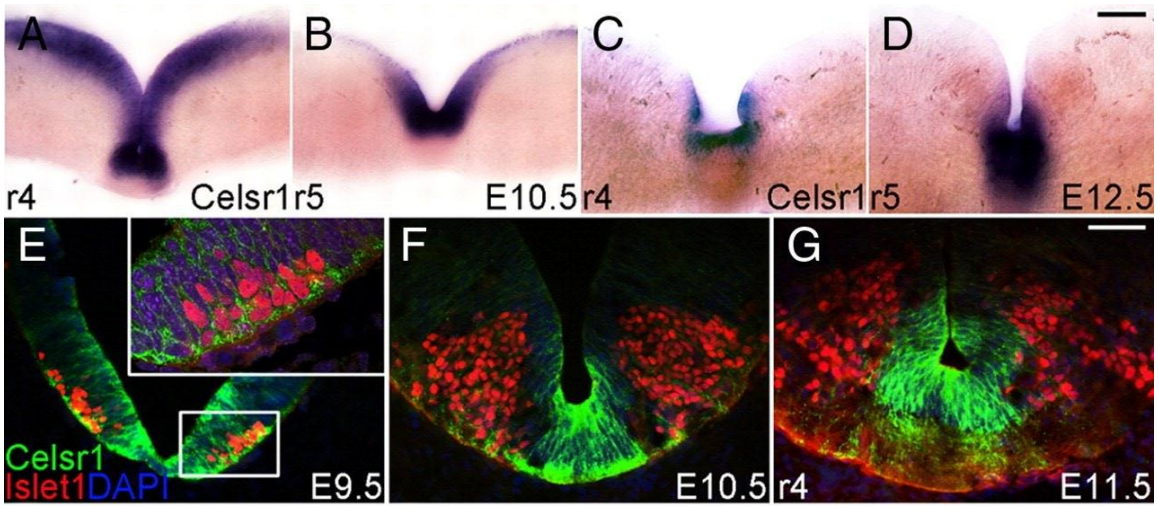

Figure 4.1. Expression of *Celsr1* in the developing hindbrain.

A-D, ISH of *Celsr1* digoxigenin-labeled probe on hindbrain coronal sections. At E10.5 (**A-B**), *Celsr1* mRNA is expressed in the neuroepithelium and the floor plate. At E12.5 (**C-D**), *Celsr1* expression is downregulated in r4 but remains high in the floor plate of r5. **E-G**, Immunofluorescence using anti-Celsr1 (green) and anti-Isl1 (red) in r4. Celsr1 protein expression is found in FBMN precursors in ventricular zones at E9.5, but is restricted to the floor plate from E10.5. Confocal analysis shows that Celsr1 (green) may colocalize with Isl1 (red) in FBMNs at E9.5. Scale bars: (in **D**), 100 μm for **A-D**; (in **G**), 50 μm for **E-G**. *(Panels E-G courtesy of Yibo Qu and Fadel Tissir, Institute of Neuroscience, Developmental Neurobiology, Université Catholique de Louvain, Brussels, Belgium; published in Qu, Glasco et al (2010), J Neurosci 30(28):9392-9401.)*

4.2.2. Inactivation of *Celsr1* perturbs the direction of FBMN migration

Given the intriguing pattern of *Celsr1* expression in the developing hindbrain, we tested its potential role in FBMN migration by analyzing *Celsr1*^{Crsh} mice, which harbor a missense mutation in the *Celsr1* coding sequence resulting in one amino acid substitution in the eighth cadherin repeat (Curtin et al., 2003) (**Figure 4.2**).

In WT embryos, *Tbx20* (Kraus et al., 2001; Song et al., 2006) was expressed by FBMNs throughout their migratory pathway from r4-r6 from E10.5 to E12.5 (**Figure 4.2**; 3/3 embryos). By E14.5, FBMNs had completely migrated and formed the facial (nVII) nucleus in lateral-dorsal r6 (**Figure 4.2 D**; 9/9 embryos). In E12.5 heterozygotes *Celsr1*$^{Crsh/+}$, *Tbx20* ISH revealed abnormal, rostrally migrating columns of putative FBMNs in r2 and r3, in addition to caudally migrating neurons in r5 and r6 (**Figure 4.2 B**; 6/6 embryos). By E14.5, the caudally migrating FBMNs had formed the nVII nucleus in dorsal r6, and the rostrally migrating cells also formed a putative nVII nucleus in dorsolateral r2, adjacent to the trigeminal (nV) nucleus (**Figure 4.2 E**; 6/8 embryos). Such a phenotype of direction reversal has not been seen previously in any vertebrate (Chandrasekhar, 2004; Fritzsch, 1998; Gilland and Baker, 2005). While the rostral migration phenotype was fully penetrant, its expressivity varied among animals and even between the left and right sides of the body (**Figure 4.3**), perhaps reflecting stochastic variations, as proposed for *Fzd6* mutant skin phenotypes (Wang et al., 2006). The phenotype also persisted in embryos collected from *Celsr1*$^{Crsh/+}$ x WT crosses in multiple genetic backgrounds (**Figure 4.3**), arguing against a background-specific phenotype.

In *Celsr1*$^{Crsh/Crsh}$ homozygotes, FBMN migration was greatly reduced compared to heterozygotes at E12.5 and E14.5 (**Figure 4.2 C**, 2/2 embryos; **Figure 4.2 F**; 5/5 embryos). Nevertheless, by E14.5, an ectopic putative nVII nucleus was formed in r3 (**Figure 4.2 F**; 2/5 embryos), or a facial nucleus was seen in r5/r6 (3/5 embryos; data not shown), indicating that FBMNs in *Celsr1*$^{Crsh/Crsh}$ can migrate out of r4 in both directions in a similar fashion to *Celsr1*$^{Crsh/+}$ and *Celsr1*$^{KO/KO}$ mutants (Qu et al., 2010).

We used additional tools and reagents to characterize the FBMN migration defects in *Celsr1*^{Crsh} mutants. Neurofilament NF-160 staining (Tiveron et al., 2003) revealed abnormal, rostrally migrating columns of putative FBMNs in r2 and r3, in addition to caudally migrating neurons in r5 and r6 in *Celsr1*$^{Crsh/+}$, and non-migrated cells in r4 of *Celsr1*$^{Crsh/Crsh}$ (**Figure 4.4 A-C**). Despite aberrant neuronal migration, motor innervation patterns in the periphery were unaffected (**Figure 4.4 D-F**). Retrograde labeling of FBMNs from the second arch using NeuroVue dyes (Fritzsch et al., 2005) stained cell bodies in r2 and r3, confirming that rostrally migrating FBMNs in *Celsr1*$^{Crsh/+}$ embryos project their axons into the facial nerve (**Figure 4.4 H**; 4/6 embryos). In some *Celsr1*$^{Crsh/Crsh}$ embryos, FBMN migration appeared completely blocked, with cells remaining confined to r4 (**Figure 4.4 I**; 3/3 embryos). To investigate further whether FBMNs migrated in *Celsr1*$^{Crsh/Crsh}$ homozygotes, we examined mutant phenotypes in the *SE1::GFP* background, where all cranial motor neurons express GFP (Shirasaki et al., 2006; Song et al., 2006). As expected, rostrally migrating FBMNs were found in *Celsr1*$^{Crsh/+}$ (**Figure 4.2 H; Figure 4.5 A-B**; 12/12 embryos). In *Celsr1*$^{Crsh/Crsh}$, FBMNs migrated rostrally and caudally out of r4 (**Figure 4.2 I; Figure 4.5 C, F**; 5/5 embryos), but

they failed to form orderly streams of migrating cells as in WT (**Figure 4.5 D**) and *Celsr1*$^{Crsh/+}$ embryos (**Figure 4.5 E**). Despite migration into ectopic locations, *Celsr1* mutant FBMNs did not undergo any significant apoptosis (Qu et al., 2010).

Figure 4.2. FBMNs migrate rostrally in *Celsr1*^{Crsh} embryos.

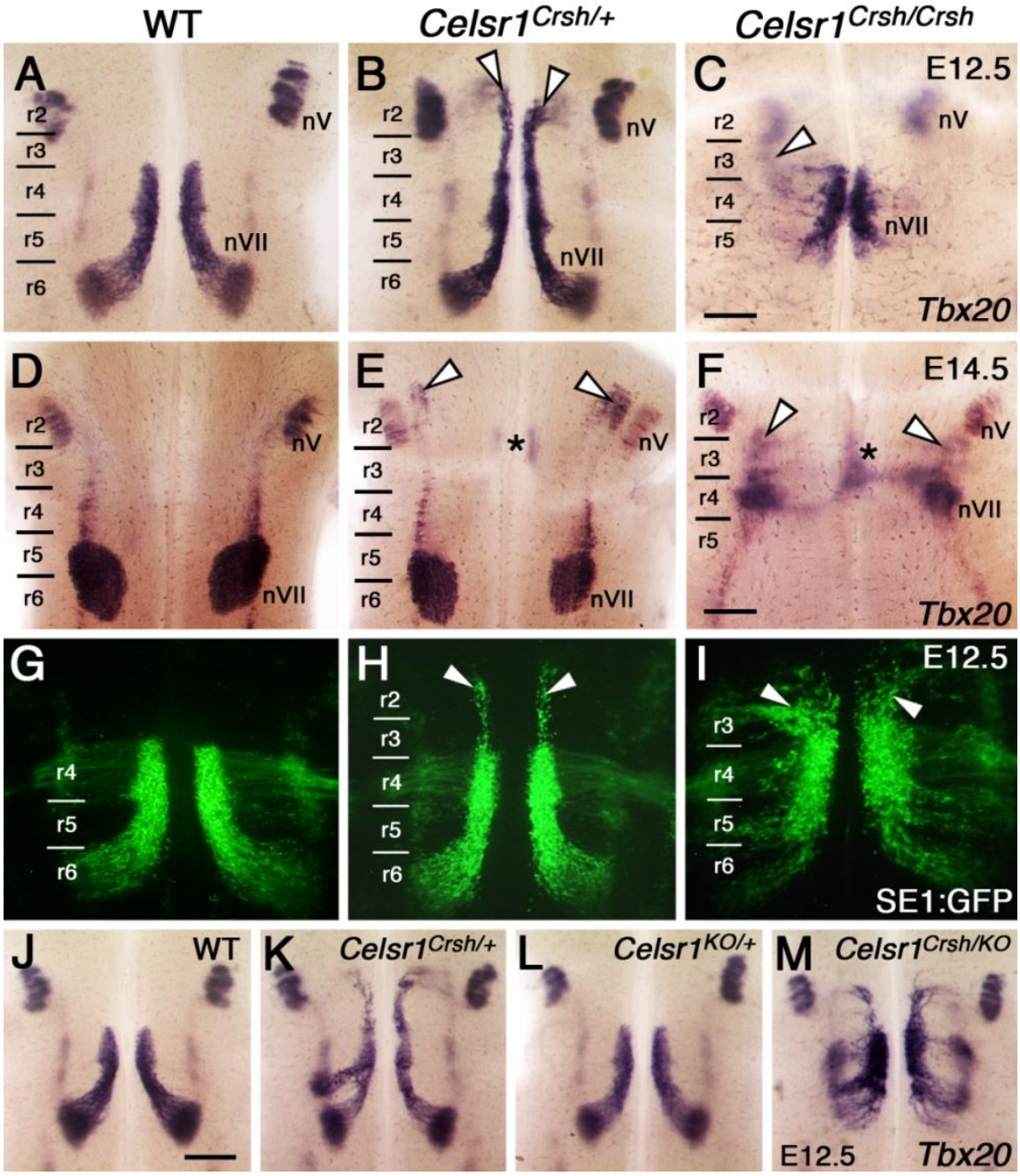

Figure 4.2. FBMNs migrate rostrally in *Celsr1*^{Crsh} embryos.

A-M, Ventricular side (**A-C**, **G-M**) and pial side (**D-F**) views of flat-mounted hindbrains processed for ISH using *Tbx20* (**A-F**, **J-M**) and imaging of neurons in *SE1::GFP* embryos (**G-I**). **A**, In a WT embryo at E12.5, FBMNs are distributed throughout their migratory pathway spanning r4, r5, and r6. Within r6, the neurons migrate radially (laterally in this view) toward the pial surface to form the facial (nVII) nucleus. **B**, In a *Celsr1*$^{Crsh/+}$ embryo, a large number of putative FBMNs (arrowheads) migrate rostrally into r2 and r3. **C**, In a *Celsr1*$^{Crsh/Crsh}$ embryo, putative FBMNs mostly remain in r4 or migrate into r5. A few *Tbx20*-expressing cells are found in r3 (out-of-focus, arrowhead). The trigeminal (nV) nucleus develops normally in all embryos. **D**, In a WT embryo at E14.5, the facial (nVII) nucleus spans r5 and r6, and the trigeminal (nV) nucleus is found in r2. **E**, In a *Celsr1*$^{Crsh/+}$ embryo, the nVII nucleus forms but is smaller than in *Celsr1*$^{+/+}$ siblings. In addition, ectopic *Tbx20*-expressing cells are found in r3 (asterisk) and r2 (arrowheads) adjacent to the nV neurons. **F**, In a *Celsr1*$^{Crsh/Crsh}$ embryo, a putative facial (nVII) nucleus forms in r4. Ectopic *Tbx20*-expressing cells are also found in medial (asterisk) and lateral (arrowheads) locations in the r2-r3 region. **G**, **H**, In *SE1::GFP* transgenic WT and *Celsr1*$^{Crsh/+}$ embryos, the organization of FBMNs is identical to that seen by *Tbx20 in situs* (**A**, **B**), with rostral migration in heterozygotes (arrowheads). **I**, In a *Celsr1*$^{Crsh/Crsh}$ embryo, the *SE1::GFP* reporter reveals extensive rostral FBMN migration into r3 and r2 (arrowheads), and few neurons migrate into r6. **J-M**, Siblings from a *Celsr1*$^{KO/+}$ x *Celsr1*$^{Crsh/+}$ cross. **J**, **L**, FBMNs migrate normally in WT (**J**) and *Celsr1*$^{KO/+}$ (**L**). **K**, Rostral neuron migration in *Celsr1*$^{Crsh/+}$. **M**, In a *Celsr1*$^{Crsh/KO}$ transheterozygote, most FBMNs remain in r4 and r5, with smaller numbers migrating into r2/r3 and r6. This phenotype is very similar to the migration pattern seen in *Celsr1*$^{Crsh/Crsh}$ (**I**) and *Celsr1*$^{KO/KO}$ (Qu et al., 2010). Scale bars: (in **C**), **A-C**, **G-I**, 300 µm; (in **F**) **D-F**, 375 µm; (in **J**), **J-M**, 375 µm.

Figure 4.3. The *Celsr1*^{Crsh} rostral FBMN migration phenotype persists in mixed genetic backgrounds and is often asymmetric.

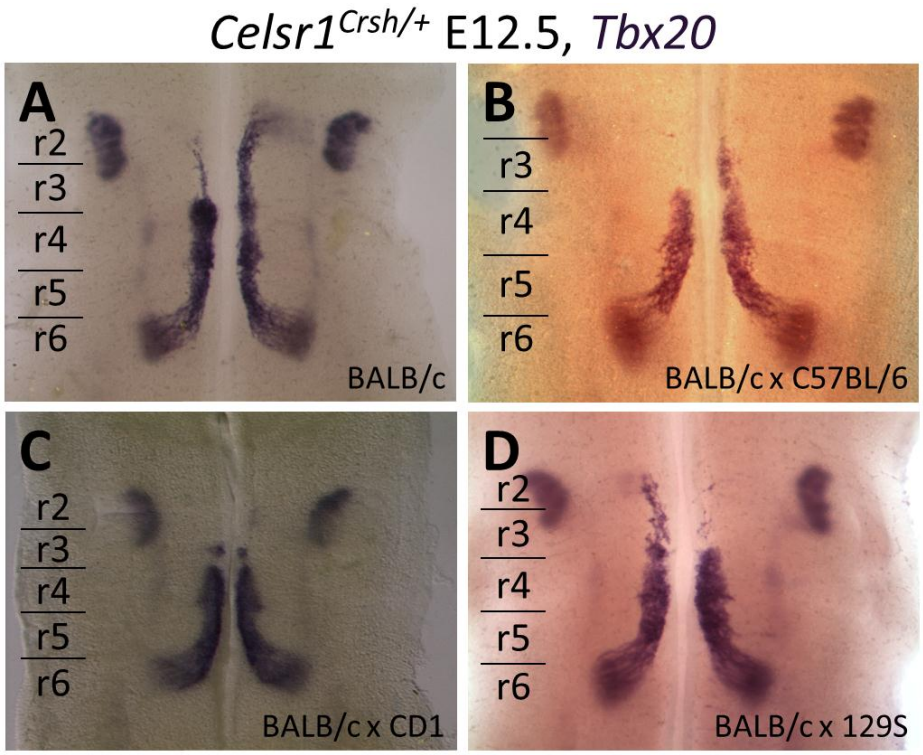

Figure 4.3. The *Celsr1*^{Crsh} rostral FBMN migration phenotype persists in mixed genetic backgrounds and is often asymmetric.

A-D, Ventricular side views of *Celsr1*$^{Crsh/+}$ embryos at E12.5 processed for *Tbx20* ISH. Asymmetries in the rostral FBMN migration phenotype are evident (**B**, **D**), and the extent of rostral FBMN migration sometimes varies (**A**, **C**). The most common phenotype resembles that in **A**. This rostral FBMN migration phenotype persists when a *Celsr1*$^{Crsh/+}$ male (BALB/c) is crossed to a WT female of the C57BL/6 (**B**, 3/3 embryos), CD1 (**C**, 2/2 embryos), and 129S (**D**, 10/11 embryos) genetic backgrounds.

Figure 4.4. FBMNs migrate rostrally in *Celsr1*^{Crsh} embryos.

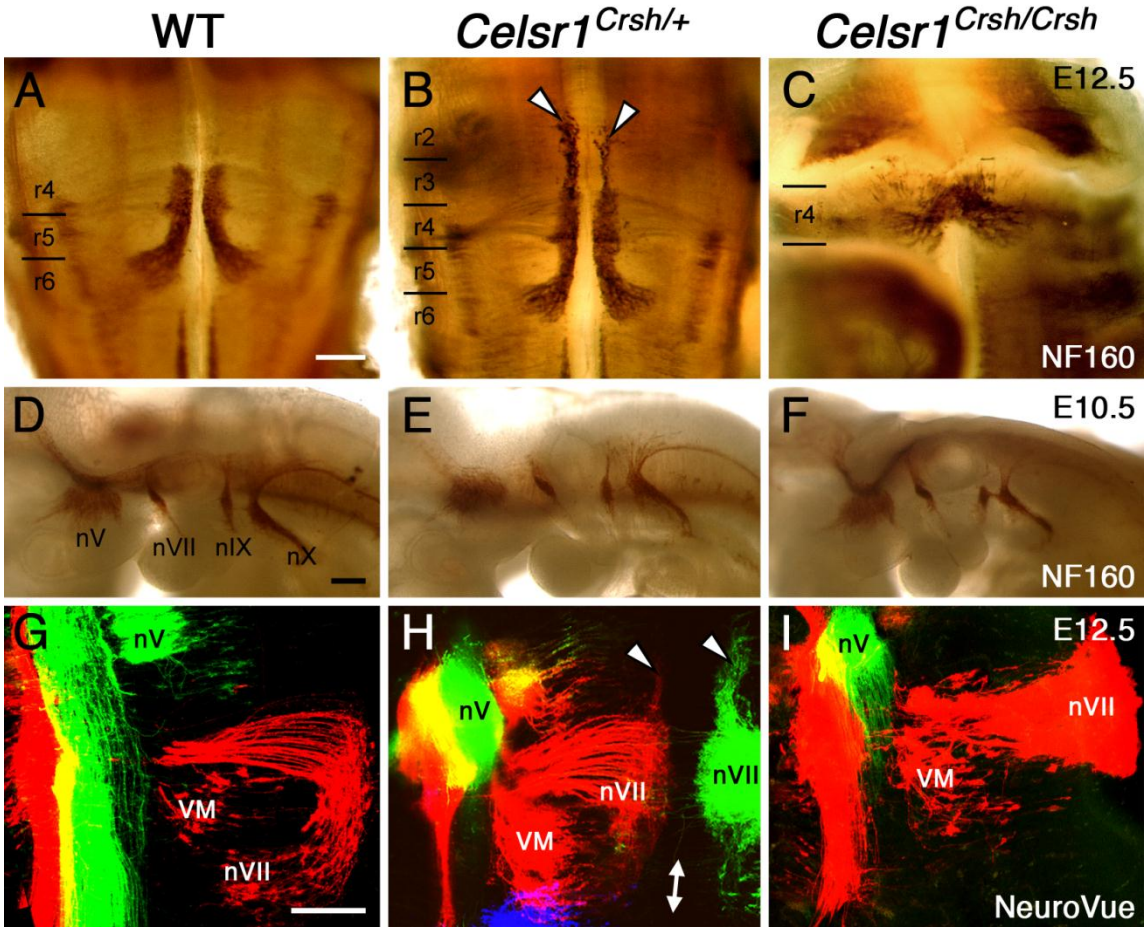

Figure 4.4. FBMNs migrate rostrally in *Celsr1*^{Crsh} embryos.

Ventricular side views of flat-mounted E12.5 hindbrains processed for neurofilament (NF-160) immunostaining (**A-C**) and retrograde labeling with NeuroVue dyes (**G-I**). **A**, In a WT embryo, neurofilament staining labels FBMNs in r4-r6, and their axons exiting the hindbrain from r4. **B**, In a *Celsr1*$^{Crsh/+}$ embryo, putative FBMNs (arrowheads) migrate rostrally into r2 and r3, while a large number of neurons also migrate correctly into r5 and r6. **C**, In a *Celsr1*$^{Crsh/Crsh}$ embryo, putative FBMNs remain in the r4 region. **D-F**, Lateral views, with rostral to the left, of NF-160-stained E10.5 embryos. The peripheral projections of cranial nerves V, VII, IX, and X are very similar between wild-type (**D**) and *Celsr1*-deficient embryos (**E**, **F**). **G-I**, Retrograde labeling of motor neurons using NeuroVue lipophilic dyes applied to nerve exit points. Trigeminal motor neurons (nV, green) were labeled from the r2 exit point. FBMNs (nVII, red) and visceral motor neurons (VM, red) were labeled from the r4 exit point. The positions of nV and VM mark the locations of r2 and r5, respectively. **G**, In a WT embryo, FBMNs migrate through r5 to form nVII in lateral r6. **H**, In a *Celsr1*$^{Crsh/+}$ embryo, many FBMNs (arrowheads) are located in r2 and r3. FBMNs on the right side (nVII, green) were labeled with dye applied at the r4 exit point on the right side. A two-sided arrow indicates the midline. **I**, In a *Celsr1*$^{Crsh/Crsh}$ embryo, the FBMNs (nVII) mostly remain in r4. Scale bars = 250 μm.

Figure 4.5. FBMNs migrate rostrally in *Celsr1*^{Crsh}; *SE1::GFP* embryos.

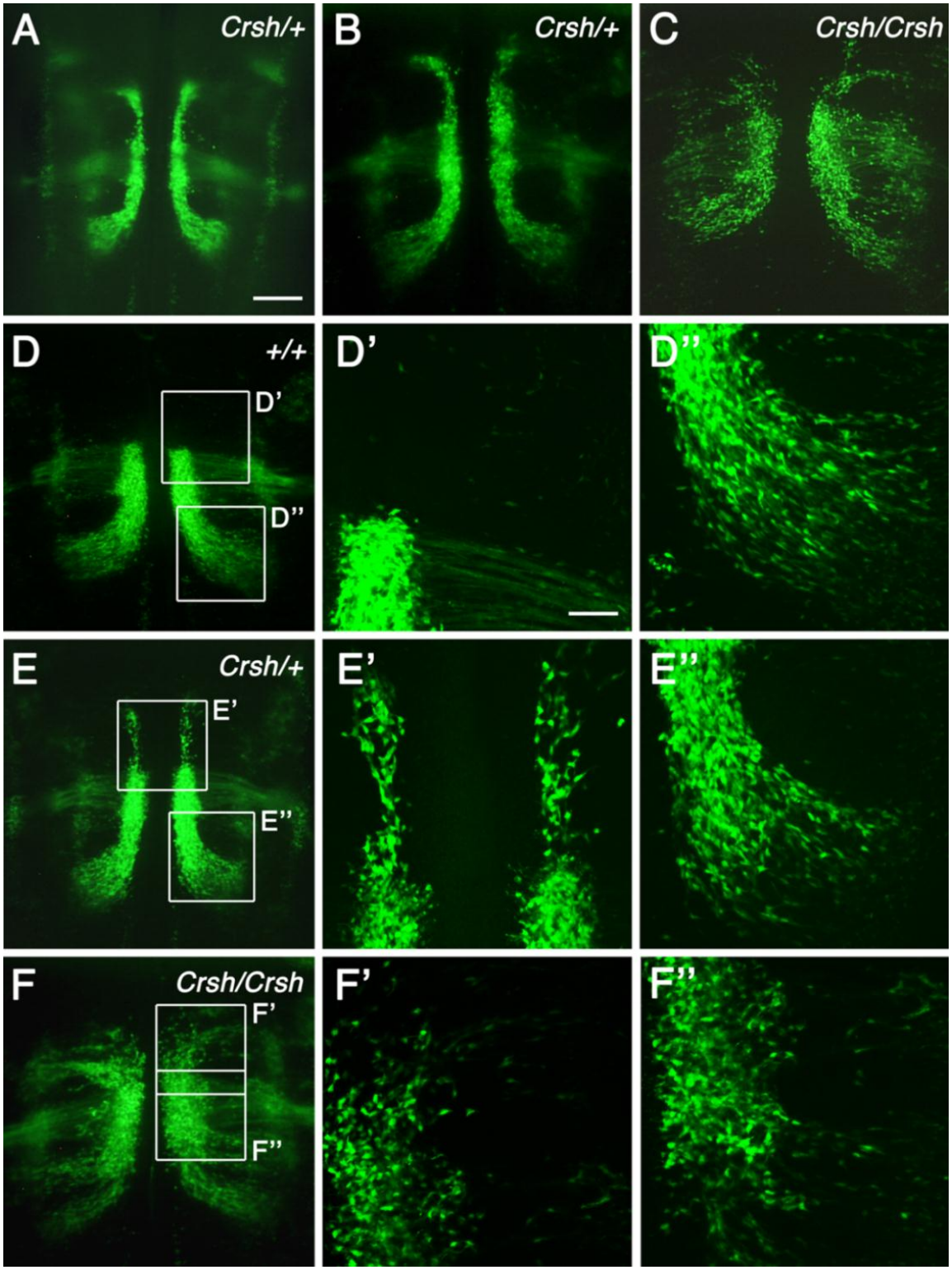

Figure 4.5. FBMNs migrate rostrally in *Celsr1*^{Crsh}; *SE1::GFP* embryos.

Ventricular side views of live, flat-mounted E12.5 hindbrains from *SE1::GFP* embryos. **A**, **B**, Additional examples of *Celsr1*$^{Crsh/+}$ showing rostral FBMN migration into r2 and r3, while a large number of neurons also migrate correctly into r5 and r6. **C**, Additional example of *Celsr1*$^{Crsh/Crsh}$, with FBMNs migrating rostrally and caudally out of r4. **D-F**, Embryos shown in **Figure 4.2 G-I**. For each panel, the right-side panels show higher magnification views of the regions indicated by the boxes. **D"-F"**, In +/+ and *Celsr1*$^{Crsh/+}$ embryos, FBMNs migrate caudally into r6 in orderly streams, but are more disorganized in *Celsr1*$^{Crsh/Crsh}$. **D'-F'**, Whereas FBMNs migrate rostrally out of r4 only in *Celsr1*$^{Crsh/+}$ and *Celsr1*$^{Crsh/Crsh}$ embryos, their movement appears to be disorganized in the latter. Scale bars: (in **A**), **A-F**, 300 µm; (in **D'**), **D'-F'**, **D"-F"**, 100 µm.

4.2.3. Nature of the *Celsr1*^{Crsh} and *Celsr1*^{KO} alleles

The *Celsr1*$^{Crsh/+}$ phenotype is similar to that of homozygous *Celsr1*$^{KO/KO}$ mutant mice (Qu et al., 2010), suggesting that either *Celsr1*^{KO} encodes a hypomorphic allele or *Celsr1*^{Crsh} has a dominant negative effect. In *Celsr1*$^{KO/KO}$ mice, the mRNA level is reduced by 80%, indicating that the mutant RNA may be unstable (Ravni et al., 2009). Moreover, no Celsr1 protein is detected in *Celsr1*$^{KO/KO}$ brain extracts via Western blot analysis, clearly demonstrating that *Celsr1*^{KO} is a null allele (Qu et al., 2010).

Given that the *Celsr1*^{KO} allele is null, the *Celsr1*$^{Crsh/+}$ phenotype could result from haploinsufficiency or a dominant negative effect. To further investigate this, we crossed the *Celsr1*^{Crsh} and *Celsr1*^{KO} strains to examine the FBMN migration phenotype of *Celsr1*$^{Crsh/KO}$ transheterozygotes at E12.5, using *Tbx20* ISH (**Figure 4.2 J-M**). Rostrally and caudally migrating cells were seen in *Celsr1*$^{Crsh/KO}$ embryos (5/5), and the phenotype was very similar to that of *Celsr1*$^{KO/KO}$ mutants. Thus, while the *Crsh* allele behaves like a null in trans with the KO allele, only *Celsr1*$^{Crsh/+}$, but not *Celsr1*$^{KO/+}$, embryos exhibit migration defects, suggesting that the *Celsr1*^{Crsh} allele is dominant negative.

4.2.4. Mutations in *Celsr1* do not affect rhombomere identity or neuronal specification

To test whether mutation of *Celsr1* affects rhombomere specification and patterning, we performed ISH at E8.5 with *Krox20* (**Figure 4.6 A-B**) and *Hoxb1* (**Figure 4.6 C-D**), which label r3/r5 and r4, respectively (Gilardi-Hebenstreit et al., 1992; Murphy

et al., 1989; Swiatek and Gridley, 1993). The specification of r3-r5 and rhombomeric borders appeared normal in all *Celsr1*$^{Crsh/+}$ embryos studied (*Krox20*, 5/5 embryos; *Hoxb1*, 3/3 embryos). Together, these results indicate that defective FBMN migration in *Celsr1*$^{Crsh/+}$ embryos does not result from aberrant specification of rhombomere identity.

Another possibility is that many FBMNs fail to migrate properly in *Celsr1*^{Crsh} mutants because they become misspecified as non-migratory neurons. To test this, we examined the expression of *Gata3*, which marks inner ear efferent neurons that are specified in, but do not migrate out of r4 (Karis et al., 2001), and *Hb9*, which identifies somatic motor neurons such as the abducens (nVI) neurons in r5 (Thaler et al., 1999). In r4 of E11.5 WT embryos, there was a medial domain of high *Gata3*-expressing cells adjacent to the floor plate, a lateral domain of weaker expressing cells, and a narrow domain ventral to the FBMNs connecting the two (**Figure 4.7 A, A'**). In all three backgrounds with defective FBMN migration (*Celsr1*$^{Crsh/+}$, *Celsr1*$^{Crsh/Crsh}$, and *Celsr1*$^{KO/KO}$ mutants), there was a marked increase in the number of *Gata3*-expressing cells in r4 (**Figure 4.7 B-D**). However, cross-sections revealed that the excess cells were located either in the lateral domain or the connecting domain, but not within the FBMN domain (**Figure 4.7 B'-D'**), suggesting that non-migratory FBMNs are not misspecified as *Gata3*-expressing cells. Similarly, *Hb9* was not expressed ectopically in r4 in non-migratory FBMNs in any of the mutant backgrounds (**Figure 4.7 E-H**), suggesting that the neuronal migration defects are not caused by transdifferentiation of FBMNs into non-migratory cell types.

Figure 4.6. Normal hindbrain patterning in Celsr1^{Crsh} mutants.

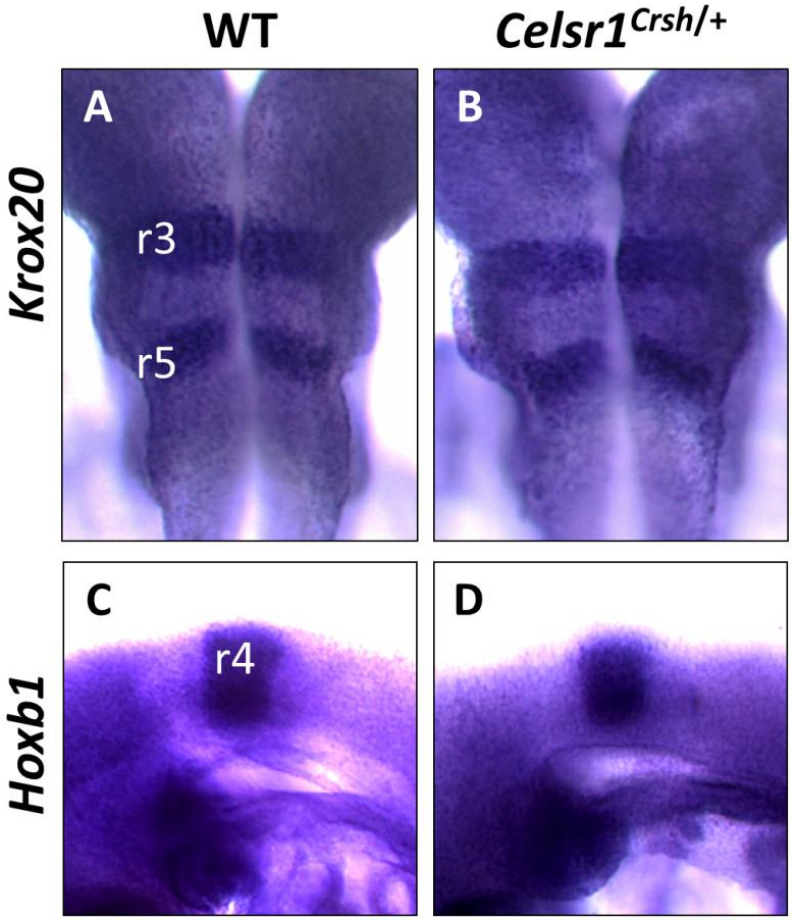

Figure 4.6. Normal hindbrain patterning in Celsr1^{Crsh} mutants.

A-D, Hindbrains at E8.5 were processed by ISH with *Krox20* (**A-B**) to label r3 and r5 and *Hoxb1* (**C-D**) to label r4. **A-B**, Dorsal views of *Krox20*-stained hindbrains. No difference was seen between WT (**A**) and *Celsr1*$^{Crsh/+}$ (**B**). **C-D**, Lateral views of *Hoxb1*-stained hindbrains, showing identical expression patterns in WT (**C**) and *Celsr1*$^{Crsh/+}$ (**D**).

Figure 4.7. Normal neuronal specification in Celsr1^{Crsh} mutants.

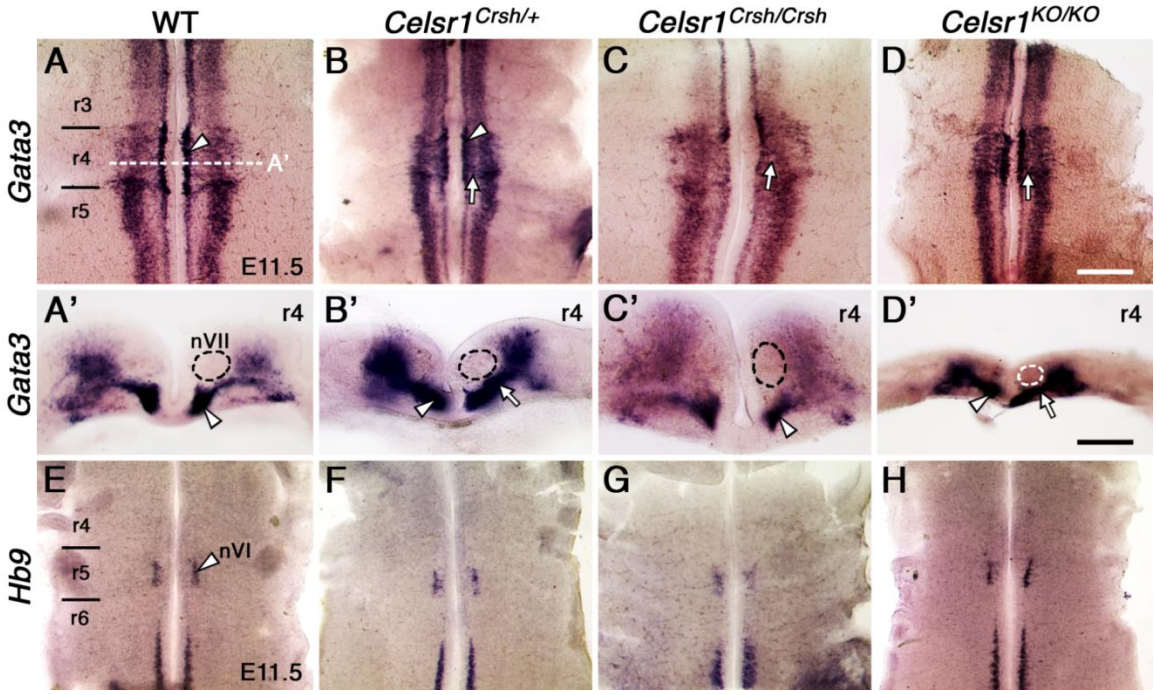

Figure 4.7. Normal neuronal specification in Celsr1^{Crsh} mutants.

Ventricular side views (**A-H**) and cross-sections (**A'-D'**) of flat-mounted E11.5 hindbrains processed for ISH of *Gata3* (**A-D**, **A'-D'**) and *Hb9* (**E-H**) expression. **A'-D'** show cross-sections in r4 of the respective embryos (**A-D**) at the approximate level indicated in **A**. Thickness of the hindbrain tissue varied considerably between embryos (compare **C'** and **D'**) due to genotype and slight stage differences. **A**, In a WT embryo, two domains of *Gata3* expression are evident, a high expression medial domain (arrowhead), and a weaker-expressing lateral domain. The cross-section at the r4 level (**A'**) shows the inner ear efferent (IEE) neurons (arrowhead) with the position of FBMNs (nVII) outlined in black, adjacent to the *Gata3*-expressing cells. **B**, In a *Celsr1*$^{Crsh/+}$ embryo, many *Gata3*-expressing cells (arrow) bridge the gap between the two expression domains in r4. Cross-section in r4 (**B'**) reveals a continuous column (arrow) connecting the IEE domain (arrowhead) to the lateral domain, but these cells are outside the region of FBMNs (black outline). **C**, **D**, In *Celsr1*$^{Crsh/Crsh}$ and *Celsr1*$^{KO/KO}$ embryos, *Gata3*-expressing cells (arrows) found in between the two expression domains are located outside the region of the FBMNs (outlines in **C'** and **D'**). **E-H**, There is a bilateral cluster of *Hb9*-expressing cells (arrowhead) in r5, corresponding to the abducens motor (nVI) nucleus in WT (**E**) and *Celsr1*-deficient embryos (**F-H**). Importantly, there are no ectopic *Hb9*-expressing cells in r4 in the mutants (**G**, **H**), even though there are a large number of non-migrated FBMNs in these embryos. Scale bars: (in **D**) **A-H**, 400 μm; (in **D'**), **A'-D'**, 200 μm.

4.2.5. FBMNs migrate normally in *Celsr3*^{KO} mutant mice

In zebrafish, *celsr1a* and *celsr1b* function redundantly with *celsr2* to regulate caudal FBMN migration (Wada et al., 2006). However, a potential role for *celsr3* had not been investigated. In the mouse, *Celsr3* is expressed prominently in the developing brain and is restricted to r2 and r4 (Formstone and Little, 2001; Shima et al., 2002), corresponding to the birthplaces of trigeminal (nV) and facial (nVII) branchiomotor neurons, respectively. Many neuronal precursors express *Celsr1*, but switch to *Celsr3* upon specification (Shima et al., 2002; Song et al., 2006; Tissir and Goffinet, 2006). *Celsr3* mutant mice display defective axonal tract formation due to disrupted interactions between axons and guidepost cells (Tissir et al., 2005; Zhou et al., 2008). Therefore, we investigated FBMN migration in *Celsr3* mutants, which encodes a version of Celsr3 lacking all seven transmembrane domains and the C-terminal cytoplasmic domain, rendering it incapable of signaling (Tissir et al., 2005).

In WT embryos at E12.5, *Phox2b* was expressed in FBMNs throughout their migratory pathway from r4-r6 (**Figure 4.8 A**). Surprisingly, in *Celsr3*$^{KO/KO}$ embryos, FBMN migration was normal (**Figure 4.8 B**). The absence of a phenotype in *Celsr3*^{KO} mice suggests that either *Celsr3* does not regulate FBMN migration, or that other genes such as *Celsr2* may compensate for the loss of *Celsr3*.

Indeed, it was later reported that in *Celsr2*^{KO} mice, FBMNs migrate prematurely into lateral r4/r5, an effect that is exacerbated in *Celsr2/3* double mutant embryos (Qu et al., 2010). This suggests that *Celsr2* and *Celsr3* function redundantly to regulate FBMN migration. Since the phenotypes of *Celsr2/3* double mutants and *Fzd3*^{KO} are

identical (Qu et al., 2010), *Celsr2/3* and *Fzd3* probably function together to regulate FBMN migration.

Figure 4.8. FBMNs migrate normally in *Celsr3*^{KO} mutant mice.

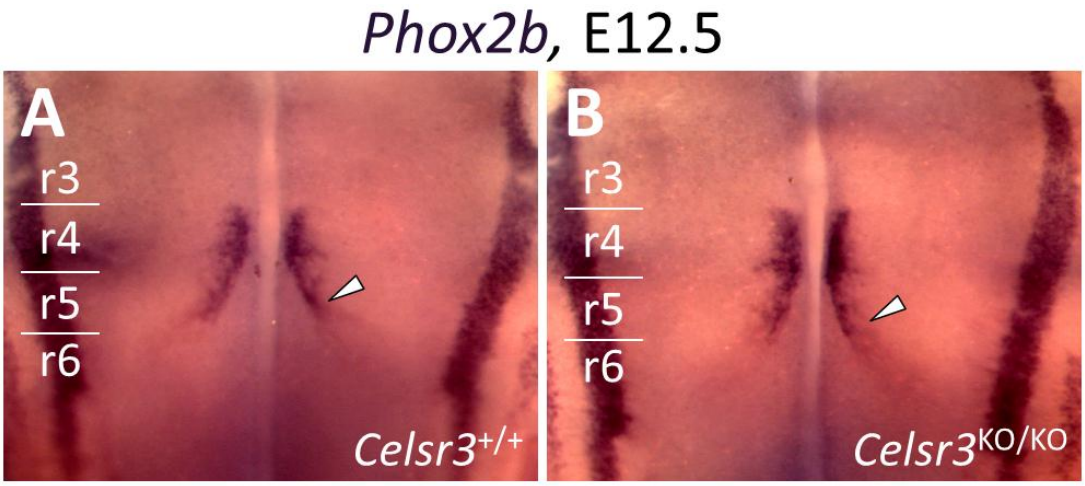

Figure 4.8. FBMNs migrate normally in *Celsr3*^{KO} mutant mice.

Dorsal views of flat-mounted hindbrains at E12.5 processed for *Phox2b* ISH (**A**-**B**). **A**, In a WT embryo, *Phox2b* labels FBMNs in r4 and throughout migration into r5/r6 (arrowhead). **B**, In a Celsr3$^{KO/KO}$ embryo, FBMNs migrate normally into r5/r6 (arrowhead).

4.3. Discussion

In zebrafish, *celsr2*, *celsr1a* and *celsr1b* regulate FBMN migration out of r4, such that combined loss of function results in a block of caudal FBMN migration, with all neurons confined to r4 (Wada et al., 2006). In contrast, we show that, in the mouse, *Celsr1* helps specify the *directionality* of FBMN migration and that *Celsr3* function is dispensable for this process.

Celsr1 regulates the directionality of FBMN migration

When *Celsr1* function is compromised, FBMNs can still migrate caudally out of r4, but many move rostrally. *Isl1*- and *Tbx20*-expressing cells display a continuous distribution in medial r2-r4. The size of the facial nucleus in r6 is diminished when the number of these cells increases, whereas that of the trigeminal motor nucleus is comparable to its wild-type counterpart (Qu et al., 2010). Altogether, these data suggest that *Isl1*- or *Tbx20*-positive cells located in medial r2-r4 are not transfated trigeminal motor neurons. All mouse and zebrafish mutants studied thus far exhibit complete or partial block of FBMN caudal migration, but never direction reversal (Chandrasekhar, 2004; Cooper et al., 2005; Nambiar et al., 2007; Rohrschneider et al., 2007; Song, 2007; Wada et al., 2005). Interestingly, only a subset of FBMNs migrates rostrally in *Celsr1* mutants. One possibility is that *Celsr1* functions redundantly with other molecules to specify directionality. Alternatively, the *Celsr1* mutant phenotype may reflect heterogeneity within the FBMN population such that only a subset depends

on *Celsr1* for specification of caudal direction of migration. Intriguingly, in zebrafish, only the earliest migrating FBMNs express the Tag1 protein (Sittaramane et al., 2009), suggesting that there may be molecular heterogeneity among FBMNs. Whether such heterogeneity could underlie differential responses to *Celsr1* remains to be explored. Nevertheless, the role for *Celsr1* in regulating the caudal direction of migration is particularly significant, given that no other gene has been shown to perform a similar function.

Our observations suggesting that the *Celsr1*^{Crsh} allele encodes a protein with a dominant negative activity is supported by analysis of the skin and cultured keratinocytes in *Celsr1*^{Crsh} mutant mice (Devenport and Fuchs, 2008). In the skin, homophilic interactions between Celsr1 molecules appear to drive PCP signaling. The mutant protein encoded by *Celsr1*^{Crsh} is produced but no longer polarized along the anterior-posterior axis, which perturbs the subcellular distribution of the PCP proteins Stbm/Vangl2 and Fzd6. Furthermore, Celsr1 and Vangl2 interact physically (Devenport and Fuchs, 2008), and this interaction is abolished by the *Looptail* mutation in *Vangl2*, which disrupts PCP (Kibar et al., 2001; Montcouquiol et al., 2003; Murdoch et al., 2001), and blocks FBMN migration (Vivancos et al., 2009) (**Chapter 3**). Altogether, our observations in *Celsr1* mutants suggest that PCP genes of the *Celsr*, *Fzd* and *Vangl* families may regulate interactions between cells, and thereby specify directionality in cell migration along the rostrocaudal axis (Goodrich, 2008). It would be instructive to examine the subcellular distribution of PCP proteins in FBMN precursors in WT and

Celsr1 mutant mice, as well as the role of other PCP genes such as *Fzd6* in FBMN migration.

Celsr1 regulates the migration of FBMNs in a non-cell autonomous manner

Celsr1 is expressed broadly in ventricular zone precursors of the developing hindbrain (Tissir et al., 2002), and our data demonstrate a particularly high expression in the ventricular zone where FBMNs are generated. To probe the cell autonomy of Celsr1 function in FBMN migration, our collaborators (Yibo Qu and Fadel Tissir, Institute of Neuroscience, Developmental Neurobiology, Université Catholique de Louvain, Brussels, Belgium) used the *Isl1-Cre* line (Srinivas et al., 2001) to specifically inactivate Celsr1 in these cells. In contrast to $Celsr1^{KO/KO}$ and $Celsr1^{Crsh/+}$ mice, FBMNs migrated normally in *Celsr1*|*Isl1* mice (Qu et al., 2010). Although an FBMN-autonomous effect of residual Celsr1 protein inherited from precursors cannot be formally excluded, the fact that no Celsr1 protein is detected in early FBMNs (Qu et al., 2010) clearly indicates non-cell autonomous action. Thus, Celsr1 specifies caudal movement of FBMNs indirectly, by acting in neuroepithelial precursors or in radial cells, both of which have their cell bodies in ventricular zones. In line with this, in zebrafish, PCP proteins Frizzled3a and Celsr2 also regulate migration of FBMNs non-cell autonomously, probably through their function in the neuroepithelium (Wada et al., 2006). Although the role of radial neuroepithelial cells as a substrate to guide radially migrating neurons is well known, it is more difficult to figure out how they could regulate tangential migration. The non-FBMN autonomous action of Celsr1 implies that Celsr1, expressed in radial cells but not

in FBMNs, would mediate heterophilic interactions, which runs counter to evidence implicating Celsr and Flamingo cadherins in homophilic interactions (Takeichi, 2007).

Since *Celsr1* functions non-cell autonomously to regulate FBMN migration, one possibility is that it may function in floor plate cells. Consistent with this, *Celsr1* expression is maintained in the floor plate even after expression in the ventricular zone dissipates, and is downregulated in r4 but maintained in r5-r6 midway through FBMN migration (**Figure 4.1 A-D**). We tested this hypothesis in **Chapter 5** by deleting *Celsr1* solely in floor plate cells using the Shh^{Cre} line. Another possibility is *Celsr1* acts in a rhombomere-specific manner to regulate FBMN migration. We examined this hypothesis in **Chapter 5** using the r4-Cre and $Krox20^{Cre}$ lines to delete *Celsr1* in r4 and r3/r5, respectively.

CHAPTER 5: *Celsr1* Functions Non-Cell Autonomously in Rhombomeres 3 and 4 to Regulate the Directionality of Facial Branchiomotor Neuron Migration in Mice

5.1. Introduction

In *Celsr1* mutant mice, a subset of FBMNs migrates in the wrong direction (**Chapter 4**). This type of migration defect has not been seen previously in any zebrafish or mouse mutant, and provides a handle to investigate the mechanisms regulating directionality of cell migration. *Celsr1* is expressed in a dynamic fashion in the hindbrain, but is excluded from migrating FBMNs. During the initial stages of FBMN migration (E10.5 – 12.0), *Celsr1* is expressed in the ventricular zone and floor plate along all axial levels. Later, *Celsr1* is downregulated in the ventricular zone, but persists in the floor plate (Qu et al., 2010). To understand how *Celsr1* regulates the directionality of FBMN migration, we investigated the spatial requirement for *Celsr1* function by taking advantage of several tissue-specific Cre lines whose activities overlap with the *Celsr1* expression domain. We demonstrate here that even though the floor plate itself is necessary for FBMN migration, deletion of *Celsr1* function in the floor plate does not generate FBMN migration defects. On the other hand, inactivation of *Celsr1* in r3/r5 and r4 each result in the rostral migration of FBMNs, but in differing severities. Using anterograde dye labeling, we found that the position of individual FBMNs within r4 correlated with the direction of migration in *Celsr1*^{Crsh} mutants. Together, these results

indicate that *Celsr1* is required in the ventricular zone of multiple rhombomeres to regulate the direction of FBMN migration, and provides insight as to how only a subset of FBMNs is affected in *Celsr1* mutants.

5.2. Results

5.2.1. Floor plate cells are essential for the caudal migration of FBMNs

Celsr1 mRNA is present in the ventricular zone before E12, and is strongly expressed in floor plate cells throughout the period of FBMN migration. Likewise, Celsr1 protein is robustly expressed in floor plate (Formstone et al., 2010; Qu et al., 2010). By E12.5, when most FBMNs have left r4, floor plate *Celsr1* is maintained in r5 and caudally but downregulated more anteriorly, suggesting a possible role for *Celsr1* in the floor plate.

We first tested whether floor plate cells in general regulate FBMN migration by examining *Gli2* mutant mice, which lack a floor plate but still generate motor neurons in normal numbers (Matise et al., 1998). Since previous analyses on *Gli2* mutants were performed on the spinal cord (Ding et al., 1998; Matise et al., 1998), we first analyzed the hindbrain region in these mutants. *Gli2* mutant hindbrains lacked the typical V-shaped medial hinge point (Greene et al., 1998) and did not express the floor plate marker *Foxa2* (**Figure 5.1 A-D**), confirming the absence of a floor plate. Nonetheless, *Tbx20*-expressing cells were born in r4 but failed to migrate caudally into r6.

By E12.5, *Tbx20 in situs* show that FBMNs in WT embryos span r4 to r6, and many have undergone radial migration within r6 to the pial surface of the neural tube to form the facial motor nucleus (**Figure 5.1 E, I-J**). In *Gli2* mutants, however, FBMNs fail to migrate caudally yet still undergo radial migration within r4 (**Figure 5.1 G, K-L**). This suggests that the loss of the floor plate specifically affects the tangential, but not radial, migration of FBMNs. Consistent with this, FBMNs are found at the pial surface by E14.5 in both WT (r6 region) and *Gli2* mutants (r4 region) (**Figure 5.1 M-P**).

Additionally, using NeuroVue lipophilic dyes and anti-neurofilament immunostaining, we found that FBMN axons in *Gli2* mutants send their axons out of the r4 exit points in a disorganized fashion (**Figure 5.2 A-C**) and are mildly defasiculated in the second branchial arch (**Figure 5.2 D-F, D'-F'**), but ultimately reach their peripheral targets.

Overall, despite some axon guidance defects in *Gli2* mutants, FBMNs appear to be specified yet fail to migrate caudally out of r4. This implicates the floor plate as an important regulator of FBMN migration in mice.

Figure 5.1. FBMNs fail to migrate caudally in *Gli2* mutants lacking a floor plate.

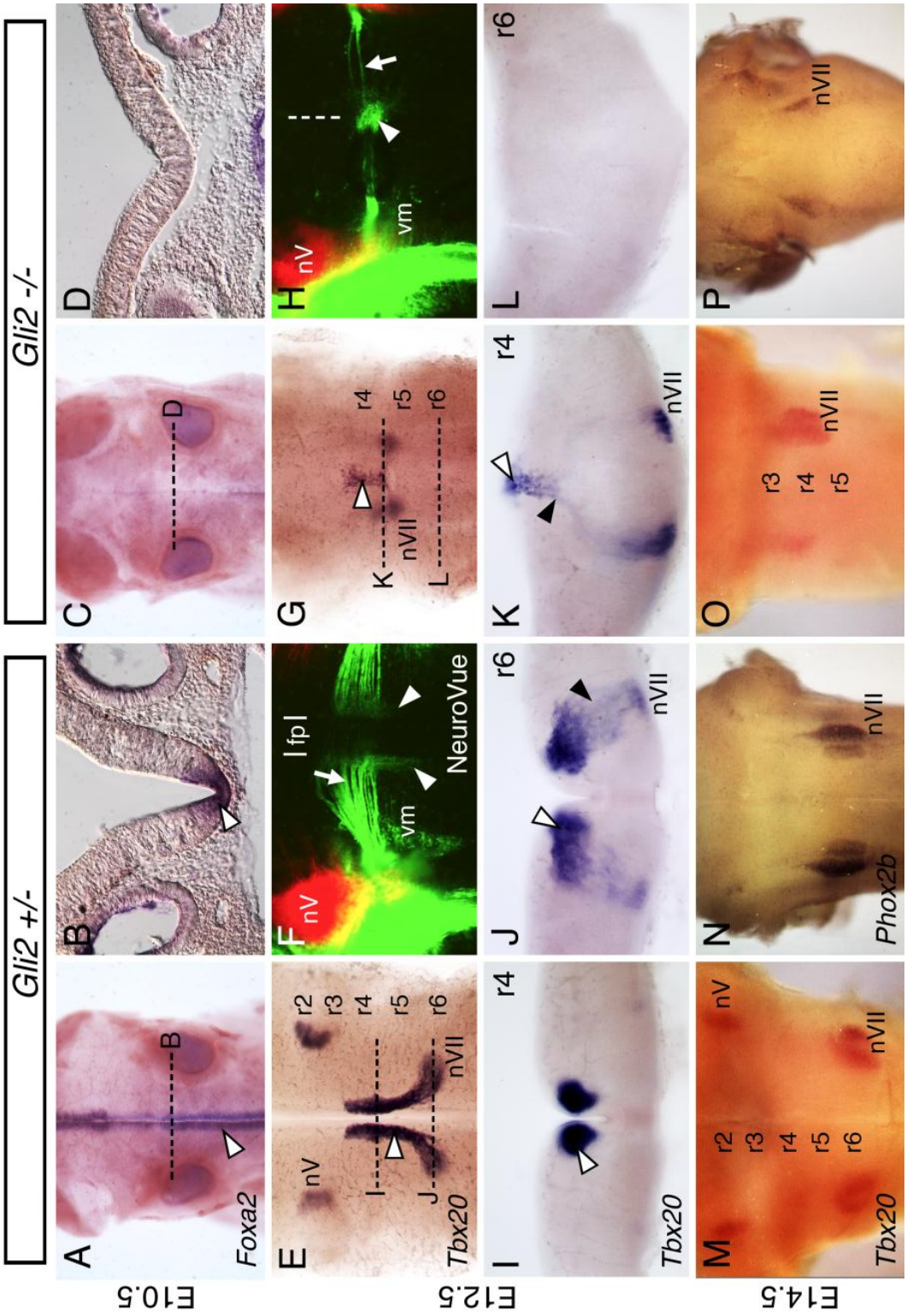

Figure 5.1. FBMNs fail to migrate caudally in *Gli2* mutants lacking a floor plate.

A-D, Hindbrains at E10.5 processed by ISH with *Foxa2* to label floor plate cells. In a *Gli2* +/- embryo (**A-B**), *Foxa2* is expressed along the midline, corresponding to the floor plate (white arrows), as seen in a dorsal view (**A**) and a 30 μm coronal section at the r5 level (**B**). In a *Gli2* -/- embryo (**C-D**), *Foxa2* is absent from the midline, indicating the absence of a floor plate. **E-L**, Hindbrains at E12.5 processed for *Tbx20* ISH (**E, G, I-L**) or injected with NeuroVue lipophilic dyes in the V and VII peripheral nerves (**F, H**). **E-H** are dorsal views and **I-L** are approximately 100 μm coronal sections at the r4 or r6 level. In a *Gli2* +/- embryo (**E-F, I-J**), FBMNs adjacent to both sides of the floor plate (fp) migrate caudally from r4 into r6 (white arrowheads), then undergo radial migration to the pial surface of the neural tube in r6 (black arrowhead). FBMN axons (white arrow) span the rostral-caudal length of r4 more medially, but converge into the r4 exit point within lateral r4. In a *Gli2* -/- embryo (**G-H, K-L**), FBMNs are found in a single cluster (white arrowheads) near the midline (dotted line) and fail to migrate caudally out of r4. The FBMN axons which project out of the r4 exit point (white arrow) appear reduced. **M-P**, Dorsal views of E14.5 hindbrains processed for *Tbx20* (**M, O**) or *Phox2b* (**N, P**) ISH. In *Gli2* +/- embryos (**M-N**), the facial motor nuclei (nVII, FMN) are located at the pial surface of r6. In *Gli2* -/- (**O-P**), the FMN are displaced rostrally and reduced in size.

Figure 5.2. Axons of the facial and vestibulocochlear nerves are defasciculated in *Gli2* mutants.

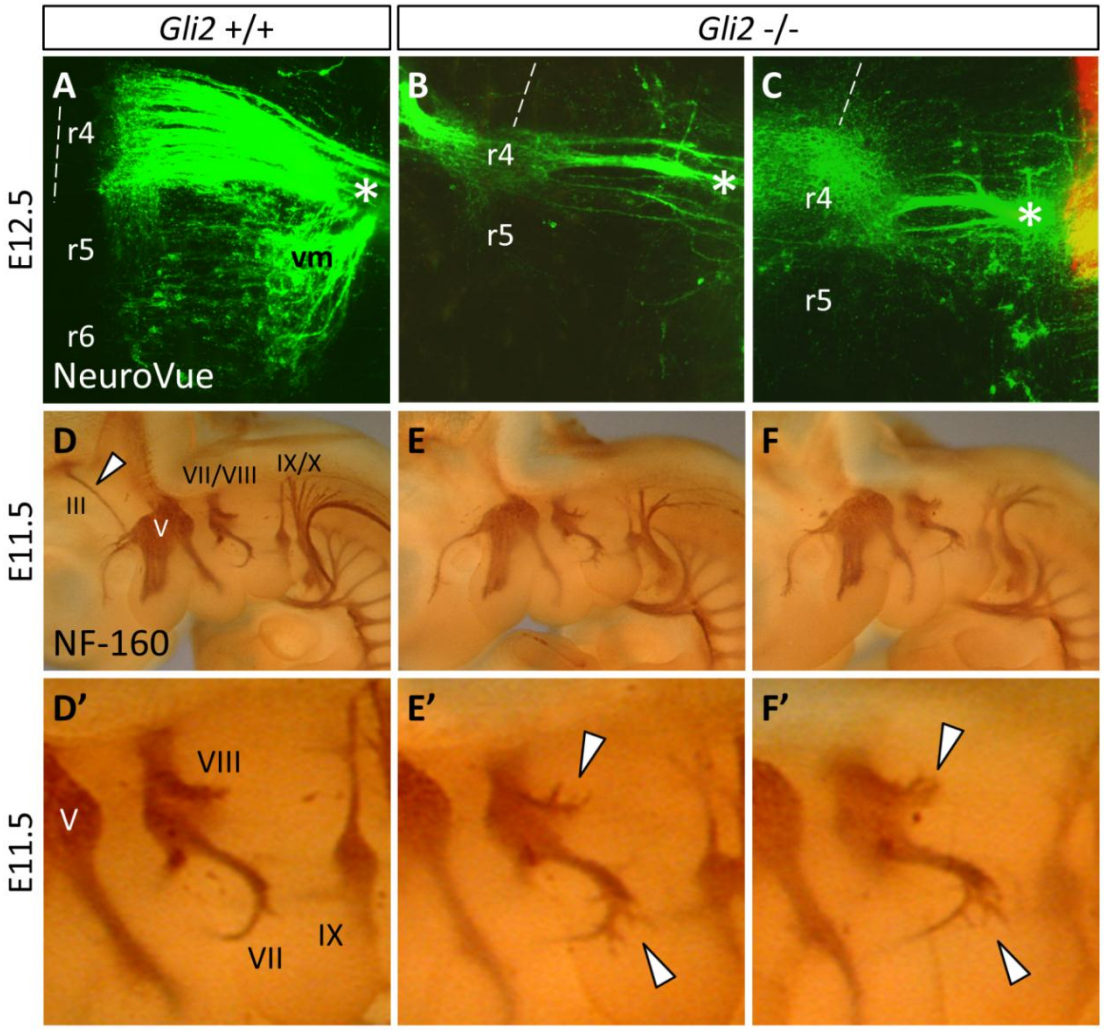

Figure 5.2. Axons of the facial and vestibulocochlear nerves are defasciculated in *Gli2* mutants.

A-C, Dorsal views of E12.5 hindbrains after facial nerve injection of NeuroVue lipophilic dyes. FBMNs on only one side of the midline (dotted line) are shown. In a WT embryo (**A**), FBMNs migrate caudally from r4 into r6. The facial visceromotor (vm) neurons are stationary in r5. FBMN axons span the entire rostral-caudal length of r4 and converge to exit the brain through the r4 exit point (asterisk). Facial VM axons also exit through the r4 exit point. In *Gli2* -/- embryos (**B-C**, examples from two different embryos shown), FBMN axons are grossly disorganized and fewer in number, and the facial VM neurons are either missing or greatly reduced in number. **D-F**, Lateral views, rostral to the left, of whole E11.5 embryos processed for anti-neurofilament (NF-160) IHC. In a WT embryo (**D**), the cranial nerves shown innervate their targets in the maxillary process and branchial arches. The oculomotor (III) nerve innervates the developing eye. In a magnified view of the same embryo (**D'**), the facial (VII) nerve is hook-shaped and splits into two branches at its distal end. The vestibulocochlear (VIII) nerve innervates the developing ear with a single projection. In *Gli2* -/- embryos (**E-F**, **E'-F'**, examples from two different embryos shown), both the VII and VIII nerves maintain their general shapes but defasciculate into multiple branches (white arrowheads). The III nerve is missing, as previously reported (Matise et al., 1998). All other nerves studied appear to have normal branching patterns.

5.2.2. Disruption of *Celsr1* function in the floor plate does not affect FBMN migration

Since the floor plate appears to be necessary for caudal FBMN migration (**Figure 5.1**), and *Celsr1* is expressed in the floor plate (Qu et al., 2010), we wondered whether *Celsr1* itself may act from the floor plate to regulate FBMN migration. We tested this hypothesis by specifically inactivating *Celsr1* in floor plate cells using the Shh^{Cre} (**Figure 5.3**) and $Celsr1^{floxed}$ mouse lines.

To confirm that Cre activity was restricted to floor plate cells, we crossed Shh^{Cre} mice (Harfe et al., 2004) with $ROSA26^{mTmG}$ reporter mice (Muzumdar et al., 2007) to generate Shh^{Cre}; $ROSA26^{mTmG}$ embryos expressing membrane-targeted EGFP in tissues with active Cre recombinase. In addition to GFP immunostaining on sections (indicative of the Cre domain), we used the motor neuron marker Islet1 (Isl1) as a reference point along both the dorsal-ventral and rostral-caudal axes. At the onset of FBMN migration (E10.5), Cre-mediated GFP expression was robust in floor plate cells at all axial levels of the hindbrain (**Figure 5.5 A-C**) (3 whole mount, 3 sectioned). Next, we generated *Celsr1* floor plate conditional mutants (FP-cKO) using a breeding strategy designed to produce two FP-cKO genotypes, Shh^{Cre}; $Celsr1^{KO/fl}$ and Shh^{Cre}; $Celsr1^{fl/fl}$ (**Figure 5.4**). We used Shh^{Cre}; $Celsr1^{KO/fl}$ embryos to ensure that Cre-mediated excision only needed to occur for copy of the $Celsr1^{floxed}$ allele, and Shh^{Cre}; $Celsr1^{fl/fl}$ embryos were used to compare possible differences in migration phenotypes due to $Celsr1^{floxed}$ copy number. All embryos were assayed for FBMN migration defects via *Tbx20* ISH. In FP-cKO embryos, FBMNs migrated only in the caudal direction in all embryos tested (n=14) (**Figure 5.5 E-**

F). This demonstrates that *Celsr1* does not function from the floor plate to regulate FBMN migration.

Figure 5.3. Overlap of the *Celsr1* expression pattern with tissue-specific Cre driver domains.

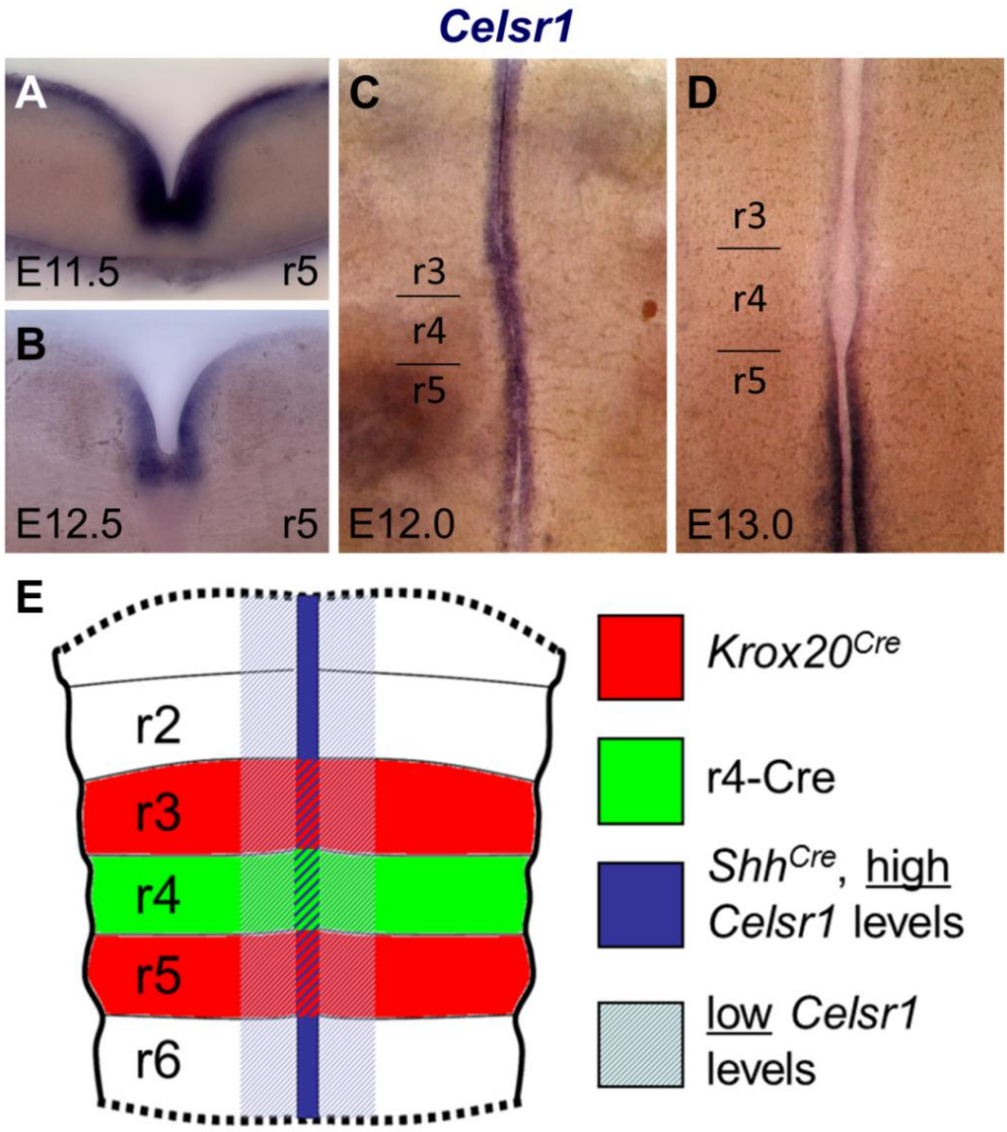

Figure 5.3. Overlap of the *Celsr1* expression pattern with tissue-specific Cre driver domains.

A-D, E11.5-13.0 WT hindbrains processed for *Celsr1* ISH, then sectioned through r5 (**A-B**) or flat-mounted (**C-D**). At E11.5 and earlier (**A**), *Celsr1* is expressed in the floor plate and ventricular surface of the hindbrain at all axial levels. By E12.5 (**B**), expression at the ventricular surface is downregulated but maintained in the floor plate. *Celsr1* expression is also downregulated in the anterior hindbrain between E12.0-13.0 (**C-D**), but is maintained at approximately r5 and caudally. **E**, Overview of the tissue-specific Cre lines used in this study showing overlap of the Cre domains with *Celsr1* expression. The terms "high" and "low" are used to describe the spatial and temporal expression pattern of *Celsr1* in the floor plate versus ventricular zone.

Figure 5.4. Breeding scheme used to generate *Celsr1* conditional mutant embryos.

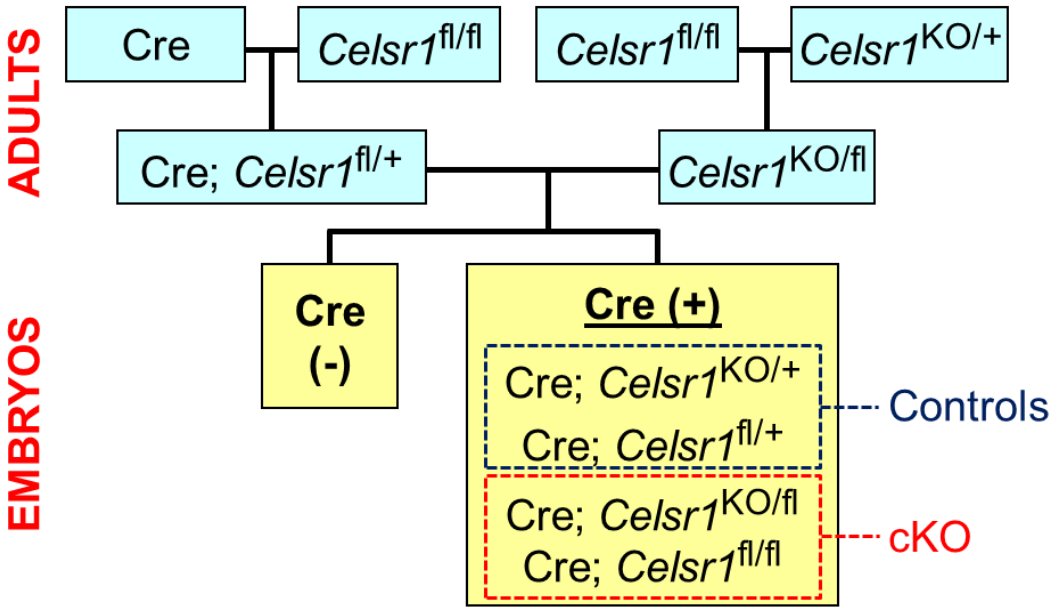

Figure 5.4. Breeding scheme used to generate *Celsr1* conditional mutant embryos.

To produce male stud mice (Cre; *Celsr1*$^{fl/+}$) from which conditional knockout (cKO) embryos could be generated, mice from each Cre line were crossed with *Celsr1*$^{fl/fl}$ mice. Females for timed matings (*Celsr1*$^{KO/fl}$) were produced by crossing *Celsr1*$^{fl/fl}$ and *Celsr1*$^{KO/+}$ mice. For embryo collection, Cre; *Celsr1*$^{fl/+}$ studs were timed mated with *Celsr1*$^{KO/fl}$ females. Cre-negative embryos were disregarded, while Cre-positive embryos were used for analysis. Cre; *Celsr1*$^{KO/+}$ and Cre; *Celsr1*$^{fl/+}$ embryos served as controls against *Celsr1* cKO embryos, which were either of the *Celsr1*$^{KO/fl}$ or Cre; *Celsr1*$^{fl/fl}$ genotype.

Figure 5.5. Disruption of *Celsr1* function in the floor plate does not affect FBMN migration.

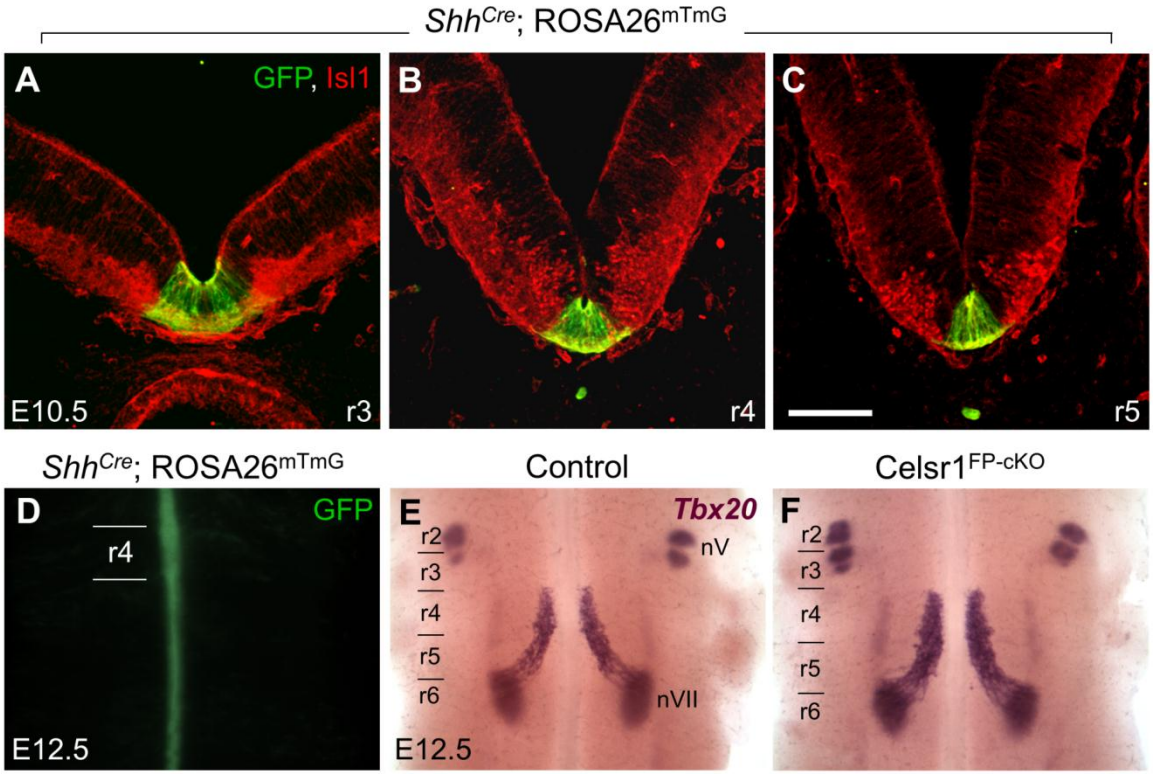

Figure 5.5. Disruption of *Celsr1* function in the floor plate does not affect FBMN migration.

A-C, 30 µm coronal sections of E10.5 embryos processed for anti-GFP (green) and anti-Isl1 (red) IHC. GFP staining indicates the Shh^{Cre} domain, and Isl1 stains for motor neurons. The light red background signal is due to mTomato expression in all tissues of the $ROSA26^{mTmG}$ mouse where Cre is not active. At all axial levels, Cre activity is restricted to floor plate cells. **D-F**, Dorsal views of E12.5 embryos visualized live for GFP (**D**) or processed for *Tbx20* ISH (**E-F**). GFP localization in a Shh^{Cre}; $ROSA26^{mTmG}$ embryo (**D**) indicates where *Celsr1* function is disrupted in floor plate-cKO (FP-cKO) embryos. In control embryos (Shh^{Cre}; $Celsr1^{fl/+}$ or Shh^{Cre}; $Celsr1^{KO/+}$, n=8), *Tbx20* labels trigeminal BMNs (nV) in r2/r3 and FBMNs (nVII) migrating caudally from r4 to r6 (**E**). FBMNs also migrate normally in FP-cKO embryos (**F**) (Shh^{Cre}; $Celsr1^{KO/fl}$ or Shh^{Cre}; $Celsr1^{fl/fl}$, n=14).

5.2.3. *Celsr1* functions in rhombomeres 3 and 5 to regulate FBMN migration

Since *Celsr1* does not function in the floor plate to regulate FBMN migration, we wondered whether it may function in specific rhombomeres. To test this, we conditionally inactivated *Celsr1* in r3 and r5 using the *Krox20*^{Cre} knock-in mouse line, where Cre recombinase is expressed from the endogenous *Krox20* promoter (Voiculescu et al., 2000). To confirm Cre expression in r3 and r5, we crossed *Krox20*^{Cre} mice with ROSA26^{mTmG} reporter mice and immunostained for Isl1 and GFP at E10.5. Cre-mediated GFP expression was seen at all dorsal-ventral levels of r3 and r5 (**Figure 5.6 A-C**) and was expressed uniformly in the floor plate in all embryos tested (5 whole mount, 5 sectioned). Notably, Cre-mediated GFP was excluded from r4-derived FBMNs (Isl1-positive cells) migrating caudally within r5 (**Figure 5.6 C**).

We then generated *Celsr1* r3/r5 conditional mutant embryos (r3/r5-cKO) with the genotypes *Krox20*^{Cre}*; Celsr1*$^{KO/fl}$ or *Krox20*^{Cre}*; Celsr1*$^{fl/fl}$ and assayed for FBMN migration defects via *Tbx20* ISH. In some *Celsr1* r3/5-cKO embryos (3/12), a subset of *Tbx20*-positive FBMNs migrated rostrally into r2 instead of caudally into r6 (**Figure 5.6 E-F**), similar to *Celsr1*^{Crsh} and *Celsr1*^{KO} mutants (Qu et al., 2010). In several r3/r5-cKO embryos (9/12), some caudal migration defects were seen, as aberrant facial nuclei formed in r5 instead of r6.

It was previously reported that *Krox20*^{Cre} male studs can transmit Cre through the germline after eight weeks of age. This would, in our case, allow the *Krox20*^{Cre}; *Celsr1*$^{fl/+}$ male stud to transmit the *Celsr1*^{KO} allele instead of *Celsr1*^{floxed}, resulting in some

Krox20^{Cre}; *Celsr1*$^{KO/KO}$ mutant embryos which would have a rostral migration phenotype. We saw no indication of such in our careful genotyping and morphological analysis of embryos. Nevertheless, to rule out the possibility that the FBMN migration phenotype in r3/r5-cKO embryos might be due *Krox20*^{Cre} activity in the male germ line, we implemented an alternate breeding strategy. We crossed *Krox20*^{Cre}; *Celsr1*$^{KO/+}$ males with *Celsr1*$^{fl/fl}$ females to generate *Krox20*^{Cre}; *Celsr1*$^{KO/fl}$ (r3/r5-cKO) embryos and assayed FBMN migration via *Tbx20* ISH. In most r3/r5-cKO embryos (8/9), FBMNs migrated rostrally (data not shown), confirming that the phenotype was a direct result of conditional deletion of *Celsr1* in r3/r5.

Together, these results indicate that loss of *Celsr1* function in r3/r5 can recapitulate all of the migration defects seen in *Celsr1*^{Crsh} and *Celsr1*^{KO} embryos, albeit at a lower frequency. Since FBMN migration is affected in 100% of *Celsr1*^{Crsh} and *Celsr1*^{KO} mutants (Qu et al., 2010), *Celsr1* function in tissues other than r3 (and/or r5) appears to be necessary for specifying FBMN direction. Based on *Celsr1* expression, these tissues could include ventricular zone cells within r4 itself.

Figure 5.6. FBMNs migrate rostrally following inactivation of *Celsr1* in r3 and r5.

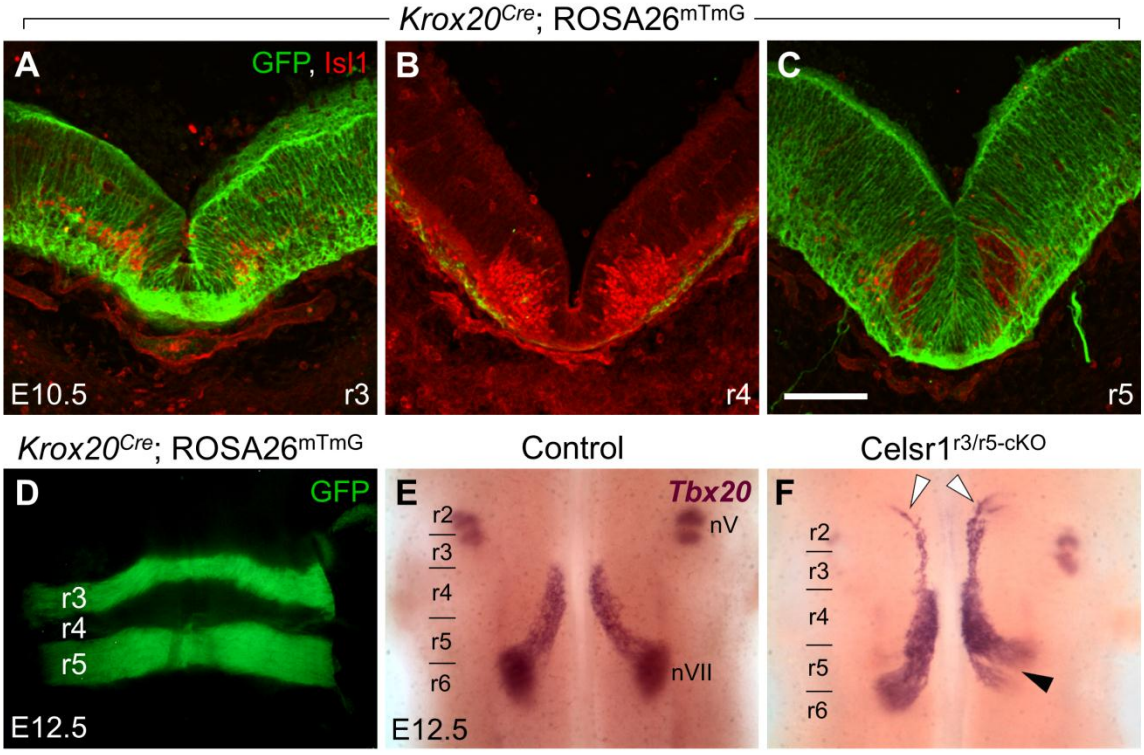

Figure 5.6. FBMNs migrate rostrally following inactivation of *Celsr1* in r3 and r5.

A-C, 30 µm coronal sections of E10.5 embryos processed for anti-GFP (green) and anti-Isl1 (red) IHC. GFP staining indicates the *Krox20*^{Cre} domain, and Isl1 stains for motor neurons. In r3 (**A**) and r5 (**C**), Cre activity is ubiquitous, including in floor plate cells. In r4 (**B**), Cre is inactive except for in a few cells along the pial membrane, which was seen in all sections (5/5 embryos). The light red background signal is due to mTomato expression in the of the ROSA26^{mTmG} mouse in all tissues where Cre is not active. **D-F**, Dorsal views of E12.5 embryos visualized live for GFP (**D**) or processed for *Tbx20* ISH (**E-F**). GFP localization in a *Krox20*^{Cre}; ROSA26^{mTmG} embryo (**D**) indicates where *Celsr1* function is disrupted in r3/r5-cKO embryos. In control embryos (*Krox20*^{Cre}*; Celsr1*$^{fl/+}$ or *Krox20*^{Cre}*; Celsr1*$^{KO/+}$, n=18), *Tbx20* labels trigeminal BMNs (nV) in r2/r3 and FBMNs (nVII) migrating caudally from r4 to r6 (**E**). In r3/r5-cKO embryos (**F**) (*Shh*^{Cre}*; Celsr1*$^{KO/fl}$ or *Shh*^{Cre}*; Celsr1*$^{fl/fl}$), a subset of FBMNs migrate rostrally instead of caudally (white arrowheads) into r2, similar to *Celsr1* mutants (4/12 embryos). Some FBMNs fail to migrate fully into r6, forming a rostrally displaced FMN in r5 (black arrowhead, 8/12 embryos).

5.2.4. *Celsr1* function in rhombomere 4 contributes to regulation of FBMN migration

We conditionally inactivated *Celsr1* in r4 and its derivatives using the r4-Cre mouse line (unpublished, Michèle Studer, Université Nice, France). To confirm Cre expression within r4, we crossed r4-Cre mice with ROSA26^{mTmG} reporter mice and immunostained for Isl1 and GFP at E10.5. Cre-mediated GFP was localized exclusively to r4-derived cells, including FBMNs along their migration route in r4-r6 (**Figure 5.7 A-C**) (2 whole mount, 7 embryos sectioned). Notably, Cre-mediated GFP expression in the floor plate of r4 was inconsistent between different embryos and even adjacent sections of the same embryo. The level of expression ranged from robust to missing altogether, though most sections showed expression in some, but not all, floor plate cells (data not shown). This suggests that *Celsr1* is not fully inactivated in the floor plate in r4 conditional mutant embryos (r4-cKO).

In *Celsr1* r4-cKO embryos, a subset of *Tbx20*-positive FBMNs migrated rostrally instead of caudally (**Figure 5.7 E-F**) (9/12 embryos), as seen in *Celsr1*^{Crsh} and *Celsr1*^{KO} mutants. Interestingly, these aberrantly-migrated FBMNs were found exclusively in r3, typically in clusters near the r3/r4 boundary. Therefore, although FBMNs migrated rostrally in r4-cKO embryos, it less severe than the *Celsr1*^{Crsh} and *Celsr1*^{KO} mutant phenotype, where FBMNs migrate two rhombomeres in the rostral direction and settle in r2 adjacent to the trigeminal motor nuclei (Qu et al., 2010). In combination with the r3/r5-cKO phenotype, this suggests that *Celsr1* functions in multiple rhombomeres, including r4 to regulate FBMN directionality.

Figure 5.7. FBMNs migrate rostrally upon conditional deletion of *Celsr1* in r4.

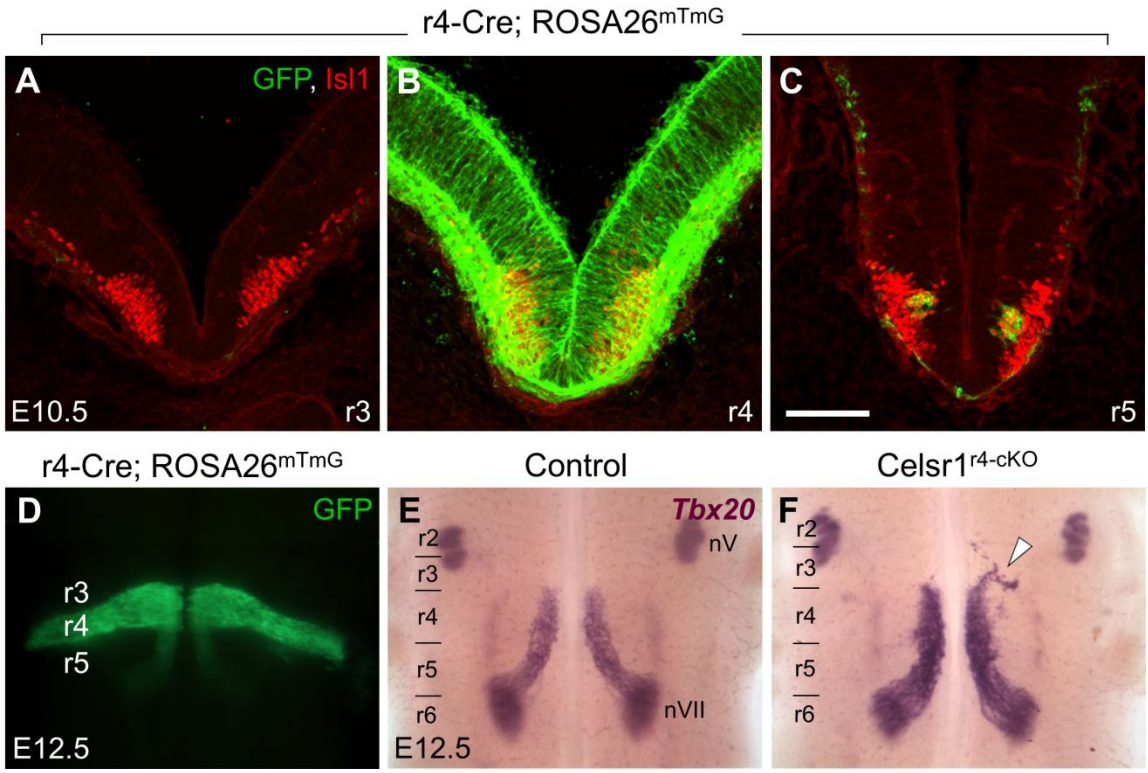

Figure 5.7. FBMNs migrate rostrally upon conditional deletion of *Celsr1* in r4.

A-C, 30 µm coronal sections of E10.5 embryos processed for anti-GFP (green) and anti-Isl1 (red) IHC. GFP staining indicates the r4-Cre domain, and Isl1 stains for motor neurons. Cre activity is absent in r3 (**A**), and the light red background signal is due to mTomato expression in the of the ROSA26^{mTmG} mouse in all tissues where Cre is not active. In r4, Cre activity is found at all dorsal-ventral levels. In the floor plate, however, Cre activity was inconsistent (and occasionally absent) between different r4 sections, even of the same embryo (n=4 embryos). In r5 (**C**), Cre is inactive, except for in FBMNs migrating into r5, which were derived from r4. Other Isl1-positive cells in r5 represent both the facial VMNs and abducens SMNs. **D-F**, Dorsal views of E12.5 embryos visualized live for GFP (**D**) or processed for *Tbx20* ISH (**E-F**). GFP localization in a r4-Cre; ROSA26^{mTmG} embryo (**D**) shows that Cre activity is only detected in r4 and in r4-derived FBMNs migrating through r5 and r6. In control embryos (r4-Cre*; Celsr1*$^{fl/+}$ or r4-Cre*; Celsr1*$^{KO/+}$, n=21), *Tbx20* labels trigeminal BMNs (nV) in r2/r3 and FBMNs (nVII) migrating caudally from r4 to r6 (**E**). In r4-cKO embryos (**F**) (r4-Cre*; Celsr1*$^{KO/fl}$ or r4-Cre*; Celsr1*$^{fl/fl}$), a subset of FBMNs migrate rostrally instead of caudally (white arrowheads) within r3 but do not reach r2 (9/12 embryos).

5.2.5. The position of FBMNs within r4 correlates with their direction of migration in *Celsr1*^{Crsh} embryos

We wondered why, in *Celsr1* mutants, only a *subset* of FBMNs migrate rostrally, while the majority of FBMNs undergo their normal caudal migration. One possibility is a random stochastic event based on suboptimal signaling within r4. In this case, rostrally migrating FBMNs would originate at various positions, spanning the rostral-caudal extent within r4. Alternatively, since disruption of *Celsr1* function in r3 and r4 results in loss of directionality for migrating FBMNs, the directionality decision may be made through the interaction of FBMNs with their environment at the r3/r4 border. In this case, rostrally migrating FBMNs would originate entirely from the region of r4 adjacent to the r3/r4 boundary.

To test whether rostrally migrating FBMNs emanate from the entire rostral-caudal span of r4 or only the anterior boundary of r4, we placed NeuroVue lipophilic dyes into the regions corresponding to both the normal (caudal) and aberrant (rostral) populations of migrating FBMNs in *Celsr1*^{Crsh} mutants. By E9.5, FBMN axons are sent into the r4 exit point at rostral-caudal levels corresponding to their soma positions within r4 (Rossel and Capecchi, 1999; Schneider-Maunoury et al., 1997). Therefore, by anterogradely labeling migrating FBMNs from outside of r4, we could determine their starting positions within r4 prior to migration.

In E12.5 WT embryos, injection into caudally migrating neurons in r5/r6 anterogradely labeled axons projecting across the entire rostral-caudal span of r4 (3/3 embryos) (**Figure 5.8 B, B'**). Dye injection into r2/r3 did not produce any labeling back

into the r4 exit point. The medial longitudinal fascicle and reticular formation were consistently labeled in all embryos, since they run parallel to the floor plate at all axial levels. Interestingly, dye injection into the caudal FBMN population of *Celsr1*$^{Crsh/+}$ embryos labeled a notably smaller number of axons projecting towards the r4 exit point (**Figure 5.8 C, C'**). Injection into the rostral FBMN population in r2/r3 labeled axons projecting into the r4 exit point entirely *rostral* to axons produced by caudally migrating FBMNs. The two axon populations (rostral vs. caudal) were completely segregated, and no intermixing was seen (3/3 embryos) (**Figure 5.8 C, C'**). These results indicate that the ability for FBMNs to migrate rostrally in *Celsr1*^{Crsh} mutants is correlated with their rostral-caudal position in r4.

Figure 5.8. The rostrally migrating subsets of FBMNs in *Celsr1*$^{Crsh/+}$ embryos are born solely in the rostral portion of r4.

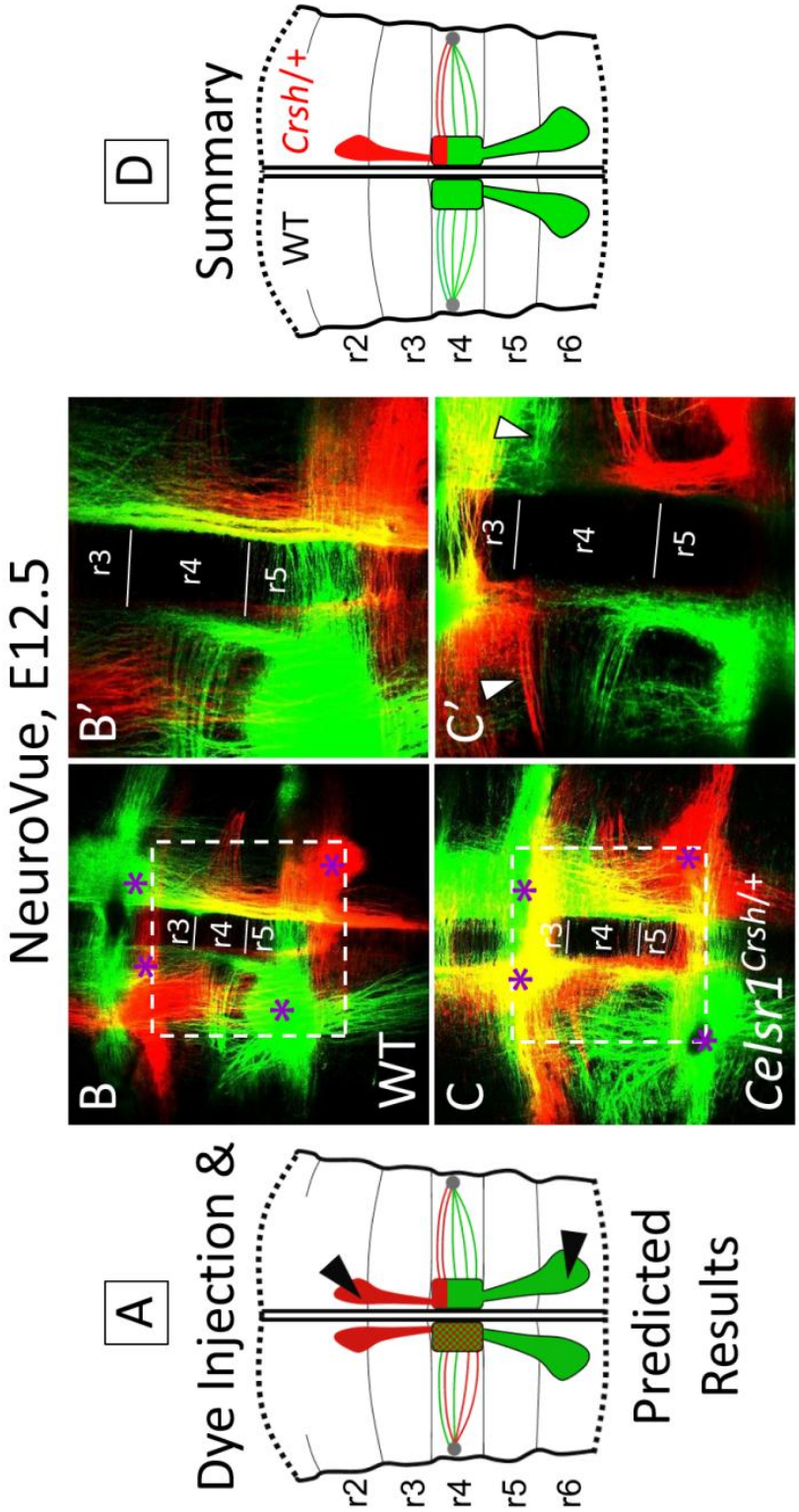

Figure 5.8. The rostrally migrating subsets of FBMNs in *Celsr1*$^{Crsh/+}$ embryos are born solely in the rostral portion of r4.

A, Schematic of a flat-mounted E12.5 hindbrain depicting the dye placement sites for labeling of rostral and caudal subsets of migrating FBMNs. Different colors (NeuroVue Jade, green; NeuroVue Maroon, red) were placed near the rostral and caudal populations. Two possible outcomes are shown on either side of the midline. On the left side, red and green axons are seen along the entire span of r4. On the right side, the rostral and caudal FBMN populations are segregated from birth, as indicated by a sharp separation between red and green axons projecting into the r4 exit point. **B-C**, Low mag views showing lipophilic dye placement sites (purple asterisks) in WT and *Celsr1*$^{Crsh/+}$ embryos. Bilateral populations of both rostral and caudal FBMNs were labeled. **B'-C'**, High mag views of the boxed areas in **B-C**. In a WT embryo (**B'**), dye placement into r5/r6 labels FBMN axons spanning the rostral-caudal extent of r4. Dye placement into r2/r3 does not label anything projecting into the r4 exit points. In a *Celsr1*$^{Crsh/+}$ embryo (**C'**), dye placement into r5/r6 labels FBMN axons spanning most of r4, whereas placement into r2/r3 labels FBMN axons projecting into the r4 exit points along the rostral-most part of r4. **D**, Cartoon summarizing the results shown in **B'-C'**.

5.2.6. *Wnt5a* expression is normal in *Celsr1* cKO embryos

Since the rostrally migrating subset of FBMNs originate from the rostral edge of r4, we wondered whether these FBMNs may receive abnormal levels of migratory cues that cause them to misinterpret their directionality of migration. Wnt5a, one of the ligands for the non-canonical Wnt/PCP signaling pathway, is expressed a rhombomere-specific gradient in the hindbrain and can serve as a chemoattractant for migrating FBMNs (Vivancos et al., 2009). Therefore, we tested whether the *Wnt5a* gradient was shifted or aberrantly expressed in the rostral hindbrain of *Celsr1* conditional mutants, which could account for the rostral migration phenotype.

In E11.5 control embryos, *Wnt5a* was expressed in a caudal^{high} to rostral^{low} gradient caudal to r5, was virtually absent from r4, but strongly expressed in the floor plate rostral to r4 (**Figure 5.9 A, C**) (Vivancos et al., 2009). No difference was seen in r3/r5-cKO or r4-cKO mice, as the sharp boundaries of *Wnt5a* expression were seen in r3-r5 (**Figure 5.9 B, D**), indicating that perturbation of *Wnt5a* signaling is not responsible for the rostral FBMN migration phenotype in *Celsr1* conditional mutants.

Figure 5.9. *Wnt5a* is expressed normally in *Celsr1*$^{r3/r5\text{-}cKO}$ and *Celsr1*$^{r4\text{-}cKO}$ embryos.

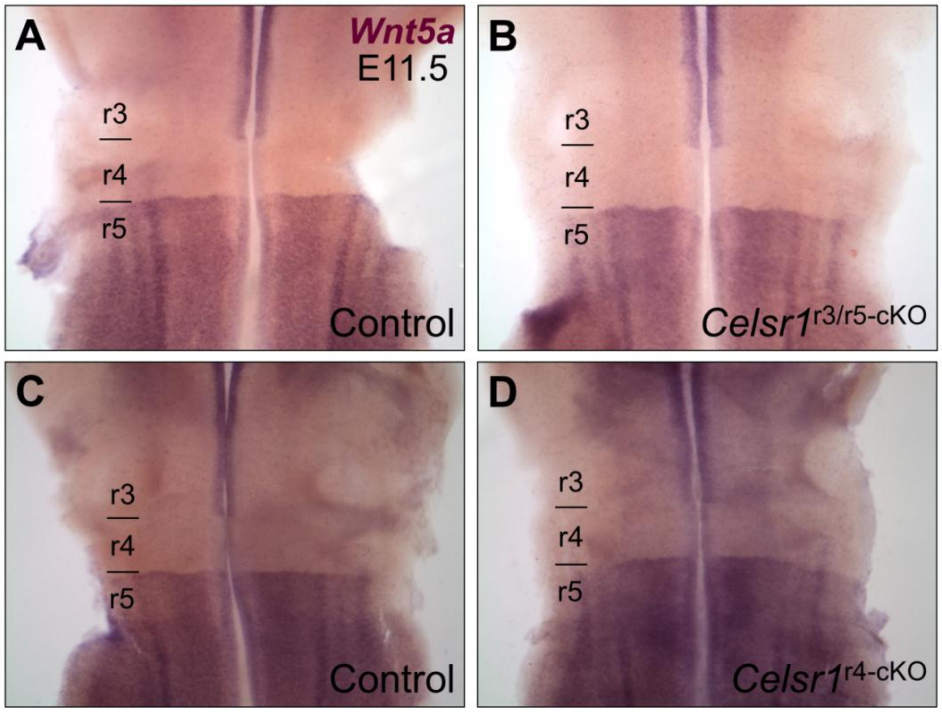

Figure 5.9. *Wnt5a* is expressed normally in *Celsr1*$^{r3/r5\text{-}cKO}$ and *Celsr1*$^{r4\text{-}cKO}$ embryos.

A-D, Dorsal views of flat-mounted E11.5 hindbrains processed for *Wnt5a* ISH. In control embryos (**A, C**) of either *Cre*; *Celsr1*$^{fl/+}$ or Cre*; Celsr1*$^{KO/+}$ genotypes, *Wnt5a* is expressed along the midline rostral to r4, mostly absent from r4, and expressed in a caudal^{high} to rostral^{low} gradient caudal to r4. *Wnt5a* is expressed identically in r4-Cre; *Celsr1*$^{KO/fl}$ (**B**) (n=4) and *Krox20*^{Cre}; *Celsr1*$^{KO/fl}$ (**D**) embryos (n=4), with sharp boundaries intact at the r3/r4 and r4/r5 borders.

5.3. Discussion

The caudal migration of FBMNs in the developing hindbrain is a tightly regulated process involving diverse signaling pathways, including non-canonical Wnt/PCP signaling. Though a large number of genes have been implicated in the caudal migration of FBMNs (**Chapter 1.3-1.4**), our studies with *Celsr1*^{Crsh} mice have indicated for the first time that some genes actively prevent rostral migration. We described here the tissue-specific requirements for *Celsr1* in regulating FBMN migration, and revealed that the rostral and caudal subsets of migrating FBMNs in *Celsr1*^{Crsh} mutants are distinguished based on their rostral-caudal starting positions within r4. This analysis provides a starting point for unlocking the mechanisms behind how *Celsr1* controls the directionality of FBMN migration.

Our analysis of *Celsr1* mutants (Qu et al., 2010) suggests that FBMNs likely possess the ability to migrate in either the rostral or caudal direction, but that *Celsr1* normally mediates directionality cues that steer them caudally. One possibility is that loss of *Celsr1* function results in the random orientation of FBMNs and their environment, therefore enabling FBMNs to migrate rostrally. In that case, one would expect about 50% of FBMNs to migrate rostrally; however, in all *Celsr1* mutants analyzed, the rostrally migrating substream is comprised of substantially less than 50% of FBMNs and is often only a few cells. Redundant function of other genes with *Celsr1* to mediate directionality could account for this, and differing phenotypes between r3/r5-cKO and r4-cKO embryos suggest that polarity of the environment is still of

importance. When *Celsr1* is inactivated solely in r4 (r4-cKO embryos), a subset of FBMNs is able to migrate caudally into r3, but these cells typically become aggregated at the caudal portion of r3. Since r3 is polarized normally in this case, it may create a non-permissive environment that prevents FBMNs from migrating in the rostral direction. In r3/r5-cKO embryos, FBMNs are able to migrate fully into r2, since r3 in this case would be a permissive (depolarized) environment. In addition, loss of *Dvl2* function in *Celsr1*$^{Crsh/+}$ embryos suppresses the rostral FBMN migration phenotype (**Chapter 3.2.5**), suggesting directionality decisions may receive input from the Wnt/PCP pathway.

Other data suggest that *Celsr1* may mediate guidance cues in the rostral hindbrain that normally repel FBMNs in the caudal direction. Since rostrally-migrating FBMNs emanate exclusively from rostral r4 (**Figure 5.8**), it is clear that loss of *Celsr1* function differentially affects FBMNs based on their positions within r4. In *Celsr1* mutants, even small changes in the concentration gradients of secreted guidance cues such as Wnts, Semaphorins, Plexins, and VEGF could in principle affect only the rostral-most FBMNs in r4 and lead to their rostral migration. Alternatively, *Celsr1*-mediated changes in the adhesion properties of r3 (adjacent to FBMNs) could abolish the non-permissive environment, acting in a local fashion to affect only the rostral-most FBMNs in r4. To answer these questions, it would be insightful to assay for differences in gene expression in hindbrain samples isolated from the r3/r4 region of both WT and *Celsr1* mutant embryos.

Given the *Celsr1* expression pattern, it was surprising to find that loss of *Celsr1* function in the floor plate does not affect FBMN migration. *Celsr1* is expressed in the

floor plate at the onset of migration, and persists even after downregulation of *Celsr1* at the ventricular surface (**Figure 5.3**). A partial requirement for *Celsr1* in the floor plate cannot be ruled out, since floor plate *Celsr1* is deleted in a rhombomere-specific manner in both r3/r5-cKO and r4-cKO embryos.

Despite *Celsr1* function in the floor plate being dispensable for FBMN migration, our analysis of *Gli2* mutants demonstrates the importance of the floor plate itself in regulating this process. *Gli2* mutant mice lack a floor plate but still specify motor neurons (Ding et al., 1998). However, mutant FBMNs fail to migrate out of r4 (**Figure 5.1**). FBMN axons ultimately reach the r4 exit point and incorporate into the facial nerve, albeit in a disorganized manner (**Figure 5.2**). Peripheral projections of the VII/VIII nerves are also somewhat disorganized, but likely do not account for the migration phenotype, since FBMN migration and axon guidance are independently regulated (Schwarz et al., 2004). A thorough characterization of *Gli2* mutants was beyond the scope of our analysis, but these data suggest that a functional floor plate is critical for caudal FBMN migration.

Potential roles for *Celsr1* in the floor plate, outside of FBMN migration

Instead of FBMN migration, *Celsr1* in the floor plate could potentially serve to regulate other floor plate-dependent processes such as neural tube closure (Doudney and Stanier, 2005; Greene et al., 1998; Murdoch et al., 2001), orientation of floor plate primary cilia (Borovina et al., 2010; Okada et al., 2005), guidance of commissural axons (Serafini et al., 1996), or migration of inferior olivary, lateral reticular, and external

cuneate nuclei (de Diego et al., 2002). Potential roles for *Celsr1* in these processes have yet to be examined.

CHAPTER 6: Concluding Remarks and Future Directions

Neuronal migration is a critical process in brain development, contributing to the formation of distinct neural layers and diversity of neuronal populations within brain regions (Marin and Rubenstein, 2003). Using mouse FBMNs as a model system, our work has implicated roles for multiple non-canonical Wnt/PCP signaling molecules in the tangential (non-radial) migration of neurons. Similar to zebrafish, FBMNs failed to migrate caudally in some mouse Wnt/PCP mutants (e.g. *Vangl2*^{Lp}, *Ptk7*^{chz}), but not in *Dvl1/2* double mutants, suggesting that some Wnt/PCP genes may function in a novel pathway independent of *Dvl* signaling to regulate FBMN migration (**Chapter 3**). Furthermore, we discovered that *Celsr1*, another Wnt/PCP gene, regulates the direction of FBMN migration along the A-P axis (**Chapter 4**) by functioning non-cell autonomously throughout the ventricular zone of r3-r5 (**Chapter 5**). Interestingly, the direction of migrating FBMNs in *Celsr1* mutants is correlated with their rostral-caudal positions within r4 (**Chapter 5**), suggesting that *Celsr1* may regulate guidance cues in the anterior hindbrain that normally prevent FBMNs from migrating rostrally.

Though our work has shed light on the regulation of FBMN migration in mice, many questions remain unsolved. Future experiments, as detailed below, should aim to determine (1) whether Wnt/PCP molecules are broadly required for neuronal migration, (2) the cell type(s) in which *Vangl2* functions to regulate FBMN migration, (3) the mechanism of *Celsr1* function, including elucidation of signaling cues mediated by *Celsr1*

in the anterior hindbrain, and (4) the subcellular distribution and interaction of Wnt/PCP proteins in the context of cell migration. Therefore, the following aims are proposed:

6.1. Examine whether Wnt/PCP signaling is required for the tangential migration of other neuronal populations during development

In zebrafish *stbm/vangl2* mutants, many neuronal and non-neuronal cell types migrate normally, including noradrenergic locus coeruleus neurons, neural crest cells, adaxial muscle cells, cerebellar granule and Purkinje cells, and lateral line primordium cells (Bingham et al., 2002). Although *vangl2* function is not required for these migrations, it is unclear whether other Wnt/PCP genes are utilized and whether other populations of tangentially migrating neurons in mice require Wnt/PCP signaling. To test this, we will examine three well characterized tangential neuronal migrations in *Vangl2*^{Lp} and *Celsr1*^{Crsh} mutants. The rostral migratory stream of olfactory interneurons will be labeled via *bis*-benzamide staining and anti-BrdU immunohistochemistry (Tucker et al., 2006). Cortical interneuron migration will be assayed via immunostaining using GAD67 (Millipore) and PSA-NCAM (Developmental Studies Hybridoma Bank; University of Iowa) antibodies. GnRH-expressing neurons, which migrate from the vomeronasal organ to the basal forebrain (Bless et al., 2005), will be visualized via immunostaining using a GnRH antibody (Immunostar; Hudson, WI). Aberrant migration of these neuron types would implicate a broader role for Wnt/PCP signaling in tangential neuronal migration. If *Vangl2*^{Lp} and *Celsr1*^{Crsh} mutants exhibit migration defects, it would be

interesting to test whether these migrations are *Dvl*-independent, as is the case with FBMN migration (**Chapter 3.3.3.**).

6.2. Determine the tissue-specific requirement of *Vangl2* in mouse FBMN migration

In zebrafish, *vangl2* is ubiquitously expressed in neural tissue during development (Park and Moon, 2002; Sittaramane et al., 2009). It largely functions non-cell autonomously to regulate FBMN migration (Jessen et al., 2002), and unpublished mosaic analyses from our lab suggest that *vangl2* function in the floor plate is critical. In mice, *Vangl2* is expressed in the floor plate before FBMN migration (E9.5), but is downregulated by the onset of migration (E10.5) (**Chapter 3.2.1.**), consistent with a proposed mutually inhibitory interaction with Shh in floor plate boundary determination (Murdoch et al., 2001). Therefore, it is possible that in mice, *Vangl2* could function from the floor plate at early stages (<E10.5) to regulate FBMN migration. To test this, we will conditionally inactivate *Vangl2* in floor plate cells using the Shh^{Cre} and $Vangl2^{floxed}$ (Song et al., 2010) mouse lines.

On the other hand, *Vangl2* mRNA expression more strongly suggests that it may function cell autonomously to regulate FBMN migration. From E10.5 – 12.5, *Vangl2* is strongly expressed in the ventricular zone at all axial levels of the hindbrain, as well as migrating FBMNs (**Chapter 3.2.1.**). To test whether *Vangl2* functions cell autonomously, we will conditionally inactivate it in differentiated motor neurons using the $Isl1^{Cre}$ mouse

line (Srinivas et al., 2001). If there is no phenotype in either *Vangl2*$^{FP\text{-}cKO}$ or *Vangl2*$^{motor\ neuron\text{-}cKO}$ embryos, it is likely that *Vangl2* functions non-cell autonomously from the ventricular zone to regulate FBMN migration; in which case, we could test this using the *Krox20*^{Cre} and r4-Cre mouse lines.

6.3. Elucidate the FBMN directionality cues mediated by *Celsr1*

Our analyses of *Celsr1* mutants have shown that disruption of *Celsr1* function in r3/r5 and r4 each result in the rostral migration of FBMNs (**Chapter 5.2.3-5.2.4**), and that rostrally migrating FBMNs in *Celsr1*$^{Crsh/+}$ embryos emanate exclusively from the rostral-most portion of r4 (**Chapter 5.2.5**). This suggests that FBMN directionality may be determined by the interaction of FBMNs with their environment near the r3/r4 border, or that *Celsr1* regulates guidance cues that differentially affect the rostral-most population of FBMNs in *Celsr1* mutants. The major questions that need to be answered are (1) By what mechanism does *Celsr1* control the direction of FBMN migration? and (2) Does *Celsr1* regulate chemorepulsive or chemoattractive cues in the anterior hindbrain that normally steer FBMNs in the caudal direction? To answer this, screening for changes in gene expression patterns (WT vs. *Celsr1* mutants) of known axon and neuronal guidance cues would be impractical with a narrow focus. To best understand how *Celsr1* governs FBMN directionality, we will perform RNA-Seq (Wang et al., 2009) on hindbrain tissue samples isolated from WT and *Celsr1* mutant embryos.

To prepare samples for analysis, we will collect 10.5 embryos from WT and *Celsr1*^{KO} mutants in the *SE1::gfp* background. Since *SE1::gfp* mice express EGFP in motor neurons (Shirasaki et al., 2006), we will be able to distinguish between *Celsr1* mutants with weak or strong rostral FBMN migration phenotypes and only isolate tissue samples from the most extreme cases. Rhombomere boundaries are clearly visible at E10.5, and will allow us to accurately isolate individual rhombomeres for analysis. Since *Celsr1* likely regulates cues in the rostral hindbrain, we will dissect out the basal plate of r3 (alternatively, r4 and/or r5) using a tungsten needle, isolate total RNA, and submit it to the DNA Core Facility for RNA-seq analysis. Results will be analyzed to identify RNA transcripts that are upregulated or downregulated in *Celsr1* mutant samples.

6.4. Examine whether the r2/r3 hindbrain region normally repels FBMNs

Previous studies have shown that the caudal hindbrain (r5-r6) can attract FBMNs (Garel et al., 2000; Studer, 2001), but it is not known whether the rostral hindbrain (r2-r3) normally repels FBMNs. It is possible that FBMNs possess the ability to migrate either rostrally or caudally, but that guidance cues originating from r5-r6 attract them in the caudal direction. In this case, the rostral-most FBMNs in r4 *Celsr1*$^{Crsh/+}$ embryos may receive sub-threshold levels of guidance cues and thus migrate rostrally instead of caudally. Alternatively, the r2-r3 region may also repel FBMNs in WT, in which case loss of *Celsr1* function may destabilize the repulsive cue, allowing for some adjacent FBMNs

to migrate rostrally. Answering this question could shed light on how FBMN directionality is regulated.

To test whether the rostral hindbrain normally repels FBMNs, we will establish a system to examine FBMN migration in explanted hindbrain tissue fragments. Previous studies using explants have demonstrated that neural crest cells and MGE-derived neurons can grow out of explanted tissue and respond to guidance cues (Flames et al., 2004; Lopez-Bendito et al., 2008; Sanchez-Alcaniz et al., 2011; Theveneau et al., 2010). Assuming that FBMNs are able to migrate out of explanted r4 fragments, we will explant in close proximity various combinations of r2/r3, r4, and r5/r6 from WT and *Celsr1*^{KO} mutants in the *SE1::gfp* background. We will then examine the extent of attraction or repulsion of FBMNs from each r4 explant towards or away from adjacent explants.

Next, we will use the results of the *Celsr1* mutant RNA-seq analysis (**Chapter 6.3**) to identify potential neuronal guidance cues regulated by *Celsr1*. Promising candidate molecules will be soaked into beads (Vivancos et al., 2009) and placed adjacent to r4 explants, and their potential attractive or repulsive interactions with migrating FBMNs will be tested.

6.5. Examine the subcellular distribution of Wnt/PCP proteins in the context of migration

The subcellular distribution of mouse Wnt/PCP proteins have been examined in a variety of cell types, including skin epidermis and cultured keratinocytes (Devenport

and Fuchs, 2008), neural tube neuroepithelium (Torban et al., 2007), MDCK cells (Kallay et al., 2006), and axon growth cones (Shafer et al., 2011). However, they have not been analyzed in the context of cell migration. We are currently working to establish a cell culture model to investigate the subcellular distribution and interactions between Wnt/PCP proteins in migrating cells. So far, we have identified three human cancer cell lines – OVCA433 and DUV13 (ovarian carcinoma cell lines) and 132n1-P2Y$_2$ (astrocytoma cell line) – which migrate in culture and express Wnt/PCP genes of interest.

First, we will use immunofluorescence with specific antibodies to examine the distribution of expressed Wnt/PCP proteins in each cell line. It would be interesting, for instance, to examine whether Vangl2 is upregulated at the leading edge of migrating cells, as it is in the tips of growth cone filopodia in commissural axons (Shafer et al., 2011). Next, we will test the suitability of each cell line as a model for studying cell migration by inactivating Wnt/PCP genes and examining the potential effects on migration. We have in hand full-length constructs for Vangl2 (WT, *Vangl2*^{Lp}, *Vangl2*$^{\Delta cyto}$) and Celsr1 (WT, *Celsr1*^{Crsh}, *Celsr1*$^{\Delta cyto}$) which are designed for cell transfection (Devenport and Fuchs, 2008).

Similar to the proposed explant experiments (**Chapter 6.4**), we will use the results of the *Celsr1* mutant RNA-seq analysis (**Chapter 6.3**) to test potential guidance cues regulated by *Celsr1*. Promising candidate molecules will be soaked into beads and placed into the culture wells, and their potential attractive or repulsive interactions with migrating cells will be tested.

REFERENCES

Ackerman, S.L., Kozak, L.P., Przyborski, S.A., Rund, L.A., Boyer, B.B., and Knowles, B.B. (1997). The mouse rostral cerebellar malformation gene encodes an UNC-5-like protein. Nature *386*, 838-842.

Alberts, B. (1994). Molecular biology of the cell, 3rd edn (New York, Garland Pub.).

Anton, E.S., Cameron, R.S., and Rakic, P. (1996). Role of neuron-glial junctional domain proteins in the maintenance and termination of neuronal migration across the embryonic cerebral wall. J Neurosci *16*, 2283-2293.

Appel, B., Korzh, V., Glasgow, E., Thor, S., Edlund, T., Dawid, I.B., and Eisen, J.S. (1995). Motoneuron fate specification revealed by patterned LIM homeobox gene expression in embryonic zebrafish. Development *121*, 4117-4125.

Barrett, C., and Guthrie, S. (2001). Expression patterns of the netrin receptor UNC5H1 among developing motor neurons in the embryonic rat hindbrain. Mech Dev *106*, 163-166.

Barrow, J.R. (2006). Wnt/PCP signaling: A veritable polar star in establishing patterns of polarity in embryonic tissues. Semin Cell Dev Biol.

Bingham, S., Higashijima, S., Okamoto, H., and Chandrasekhar, A. (2002). The Zebrafish trilobite gene is essential for tangential migration of branchiomotor neurons. Dev Biol *242*, 149-160.

Bless, E.P., Walker, H.J., Yu, K.W., Knoll, J.G., Moenter, S.M., Schwarting, G.A., and Tobet, S.A. (2005). Live view of gonadotropin-releasing hormone containing neuron migration. Endocrinology *146*, 463-468.

Borovina, A., Superina, S., Voskas, D., and Ciruna, B. (2010). Vangl2 directs the posterior tilting and asymmetric localization of motile primary cilia. Nat Cell Biol *12*, 407-412.

Briscoe, J., Pierani, A., Jessell, T.M., and Ericson, J. (2000). A homeodomain protein code specifies progenitor cell identity and neuronal fate in the ventral neural tube. Cell *101*, 435-445.

Cadigan, K.M., and Liu, Y.I. (2006). Wnt signaling: complexity at the surface. J Cell Sci *119*, 395-402.

Carreira-Barbosa, F., Concha, M.L., Takeuchi, M., Ueno, N., Wilson, S.W., and Tada, M. (2003). Prickle 1 regulates cell movements during gastrulation and neuronal migration in zebrafish. Development *130*, 4037-4046.

Chandrasekhar, A. (2004). Turning heads: development of vertebrate branchiomotor neurons. Dev Dyn *229*, 143-161.

Chandrasekhar, A., Moens, C.B., Warren, J.T., Jr., Kimmel, C.B., and Kuwada, J.Y. (1997). Development of branchiomotor neurons in zebrafish. Development *124*, 2633-2644.

Ciruna, B., Jenny, A., Lee, D., Mlodzik, M., and Schier, A.F. (2006). Planar cell polarity signalling couples cell division and morphogenesis during neurulation. Nature *439*, 220-224.

Coles, E.G., Gammill, L.S., Miner, J.H., and Bronner-Fraser, M. (2006). Abnormalities in neural crest cell migration in laminin alpha5 mutant mice. Dev Biol *289*, 218-228.

Cooper, K.L., Armstrong, J., and Moens, C.B. (2005). Zebrafish foggy/spt 5 is required for migration of facial branchiomotor neurons but not for their survival. Dev Dyn *234*, 651-658.

Copp, A.J., and Harding, B.N. (1999). Neuronal migration disorders in humans and in mouse models--an overview. Epilepsy Res *36*, 133-141.

Coppola, E., Pattyn, A., Guthrie, S.C., Goridis, C., and Studer, M. (2005). Reciprocal gene replacements reveal unique functions for Phox2 genes during neural differentiation. Embo J *24*, 4392-4403.

Curtin, J.A., Quint, E., Tsipouri, V., Arkell, R.M., Cattanach, B., Copp, A.J., Henderson, D.J., Spurr, N., Stanier, P., Fisher, E.M.*, et al.* (2003). Mutation of Celsr1 disrupts planar polarity of inner ear hair cells and causes severe neural tube defects in the mouse. Curr Biol *13*, 1129-1133.

D'Arcangelo, G., Miao, G.G., Chen, S.C., Soares, H.D., Morgan, J.I., and Curran, T. (1995). A protein related to extracellular matrix proteins deleted in the mouse mutant reeler. Nature *374*, 719-723.

Darken, R.S., Scola, A.M., Rakeman, A.S., Das, G., Mlodzik, M., and Wilson, P.A. (2002). The planar polarity gene strabismus regulates convergent extension movements in Xenopus. Embo J *21*, 976-985.

Das, G., Jenny, A., Klein, T.J., Eaton, S., and Mlodzik, M. (2004). Diego interacts with Prickle and Strabismus/Van Gogh to localize planar cell polarity complexes. Development *131*, 4467-4476.

de Diego, I., Kyriakopoulou, K., Karagogeos, D., and Wassef, M. (2002). Multiple influences on the migration of precerebellar neurons in the caudal medulla. Development *129*, 297-306.

Denaxa, M., Chan, C.H., Schachner, M., Parnavelas, J.G., and Karagogeos, D. (2001). The adhesion molecule TAG-1 mediates the migration of cortical interneurons from the ganglionic eminence along the corticofugal fiber system. Development *128*, 4635-4644.

Denaxa, M., Kyriakopoulou, K., Theodorakis, K., Trichas, G., Vidaki, M., Takeda, Y., Watanabe, K., and Karagogeos, D. (2005). The adhesion molecule TAG-1 is required for proper migration of the superficial migratory stream in the medulla but not of cortical interneurons. Dev Biol *288*, 87-99.

Devenport, D., and Fuchs, E. (2008). Planar polarization in embryonic epidermis orchestrates global asymmetric morphogenesis of hair follicles. Nat Cell Biol.

Dhavan, R., and Tsai, L.H. (2001). A decade of CDK5. Nat Rev Mol Cell Biol *2*, 749-759.

Ding, Q., Motoyama, J., Gasca, S., Mo, R., Sasaki, H., Rossant, J., and Hui, C.C. (1998). Diminished Sonic hedgehog signaling and lack of floor plate differentiation in Gli2 mutant mice. In Development, pp. 2533-2543.

Doudney, K., and Stanier, P. (2005). Epithelial cell polarity genes are required for neural tube closure. Am J Med Genet C Semin Med Genet *135*, 42-47.

Dubreuil, V., Hirsch, M.R., Pattyn, A., Brunet, J.F., and Goridis, C. (2000). The Phox2b transcription factor coordinately regulates neuronal cell cycle exit and identity. Development *127*, 5191-5201.

Dulabon, L., Olson, E.C., Taglienti, M.G., Eisenhuth, S., McGrath, B., Walsh, C.A., Kreidberg, J.A., and Anton, E.S. (2000). Reelin binds alpha3beta1 integrin and inhibits neuronal migration. Neuron *27*, 33-44.

Durbec, P., Marcos-Gutierrez, C.V., Kilkenny, C., Grigoriou, M., Wartiowaara, K., Suvanto, P., Smith, D., Ponder, B., Costantini, F., Saarma, M.*, et al.* (1996). GDNF signalling through the Ret receptor tyrosine kinase. Nature *381*, 789-793.

Engelkamp, D. (2002). Cloning of three mouse Unc5 genes and their expression patterns at mid-gestation. Mech Dev *118*, 191-197.

Etheridge, S.L., Ray, S., Li, S., Hamblet, N.S., Lijam, N., Tsang, M., Greer, J., Kardos, N., Wang, J., Sussman, D.J.*, et al.* (2008). Murine dishevelled 3 functions in redundant pathways with dishevelled 1 and 2 in normal cardiac outflow tract, cochlea, and neural tube development. PLoS Genet *4*, e1000259.

Finger, J.H., Bronson, R.T., Harris, B., Johnson, K., Przyborski, S.A., and Ackerman, S.L. (2002). The netrin 1 receptors Unc5h3 and Dcc are necessary at multiple choice points for the guidance of corticospinal tract axons. J Neurosci *22*, 10346-10356.

Flames, N., Long, J.E., Garratt, A.N., Fischer, T.M., Gassmann, M., Birchmeier, C., Lai, C., Rubenstein, J.L., and Marin, O. (2004). Short- and long-range attraction of cortical GABAergic interneurons by neuregulin-1. Neuron *44*, 251-261.

Fontaine-Perus, J., and Cheraud, Y. (2005). Mouse-chick neural chimeras. Int J Dev Biol *49*, 349-353.

Formstone, C.J., and Little, P.F. (2001). The flamingo-related mouse Celsr family (Celsr1-3) genes exhibit distinct patterns of expression during embryonic development. Mech Dev *109*, 91-94.

Formstone, C.J., Moxon, C., Murdoch, J., Little, P., and Mason, I. (2010). Basal enrichment within neuroepithelia suggests novel function(s) for Celsr1 protein. Mol Cell Neurosci *44*, 210-222.

Fox, J.W., and Walsh, C.A. (1999). Periventricular heterotopia and the genetics of neuronal migration in the cerebral cortex. Am J Hum Genet *65*, 19-24.

Freigang, J., Proba, K., Leder, L., Diederichs, K., Sonderegger, P., and Welte, W. (2000). The crystal structure of the ligand binding module of axonin-1/TAG-1 suggests a zipper mechanism for neural cell adhesion. Cell *101*, 425-433.

Fritzsch, B. (1998). Of mice and genes: evolution of vertebrate brain development. Brain Behav Evol *52*, 207-217.

Fritzsch, B., Muirhead, K.A., Feng, F., Gray, B.D., and Ohlsson-Wilhelm, B.M. (2005). Diffusion and imaging properties of three new lipophilic tracers, NeuroVue Maroon, NeuroVue Red and NeuroVue Green and their use for double and triple labeling of neuronal profile. Brain Res Bull *66*, 249-258.

Furley, A.J., Morton, S.B., Manalo, D., Karagogeos, D., Dodd, J., and Jessell, T.M. (1990). The axonal glycoprotein TAG-1 is an immunoglobulin superfamily member with neurite outgrowth-promoting activity. Cell *61*, 157-170.

Gao, B., Song, H., Bishop, K., Elliot, G., Garrett, L., English, M.A., Andre, P., Robinson, J., Sood, R., Minami, Y.*, et al.* (2011). Wnt Signaling Gradients Establish Planar Cell Polarity by Inducing Vangl2 Phosphorylation through Ror2. Dev Cell *20*, 163-176.

Garcia-Dominguez, M., Poquet, C., Garel, S., and Charnay, P. (2003). Ebf gene function is required for coupling neuronal differentiation and cell cycle exit. Development *130*, 6013-6025.

Garel, S., Garcia-Dominguez, M., and Charnay, P. (2000). Control of the migratory pathway of facial branchiomotor neurones. Development *127*, 5297-5307.

Garel, S., Marin, F., Mattei, M.G., Vesque, C., Vincent, A., and Charnay, P. (1997). Family of Ebf/Olf-1-related genes potentially involved in neuronal differentiation and regional specification in the central nervous system. Dev Dyn *210*, 191-205.

Gaufo, G.O., Flodby, P., and Capecchi, M.R. (2000). Hoxb1 controls effectors of sonic hedgehog and Mash1 signaling pathways. Development *127*, 5343-5354.

Gilardi-Hebenstreit, P., Nieto, M.A., Frain, M., Mattei, M.G., Chestier, A., Wilkinson, D.G., and Charnay, P. (1992). An Eph-related receptor protein tyrosine kinase gene segmentally expressed in the developing mouse hindbrain. Oncogene *7*, 2499-2506.

Gilbert, S.F., Singer, S.R., Tyler, M.S., and Kozlowski, R.N. (2006). Developmental biology, 8th edn (Sunderland, Mass., Sinauer Associates, Inc. Publishers).

Gilland, E., and Baker, R. (2005). Evolutionary patterns of cranial nerve efferent nuclei in vertebrates. Brain Behav Evol *66*, 234-254.

Gleeson, J.G., and Walsh, C.A. (2000). Neuronal migration disorders: from genetic diseases to developmental mechanisms. Trends Neurosci *23*, 352-359.

Goddard, J.M., Rossel, M., Manley, N.R., and Capecchi, M.R. (1996). Mice with targeted disruption of Hoxb-1 fail to form the motor nucleus of the VIIth nerve. Development *122*, 3217-3228.

Goffinet, A.M. (1984). Abnormal development of the facial nerve nucleus in reeler mutant mice. J Anat *138 (Pt 2)*, 207-215.

Goffinet, A.M. (1995). Developmental neurobiology. A real gene for reeler. Nature *374*, 675-676.

Golubkov, V.S., Chekanov, A.V., Cieplak, P., Aleshin, A.E., Chernov, A.V., Zhu, W., Radichev, I.A., Zhang, D., Dong, P.D., and Strongin, A.Y. (2010). The Wnt/Planar Cell Polarity Protein-tyrosine Kinase-7 (PTK7) Is a Highly Efficient Proteolytic Target of Membrane Type-1 Matrix Metalloproteinase: IMPLICATIONS IN CANCER AND EMBRYOGENESIS. J Biol Chem *285*, 35740-35749.

Goodrich, L.V. (2008). The plane facts of PCP in the CNS. Neuron *60*, 9-16.

Grant, P.K., and Moens, C.B. (2010). The neuroepithelial basement membrane serves as a boundary and a substrate for neuron migration in the zebrafish hindbrain. Neural Dev *5*, 9.

Greene, N.D., Gerrelli, D., Van Straaten, H.W., and Copp, A.J. (1998). Abnormalities of floor plate, notochord and somite differentiation in the loop-tail (Lp) mouse: a model of severe neural tube defects. Mech Dev *73*, 59-72.

Guerrini, R., and Parrini, E. (2010). Neuronal migration disorders. Neurobiol Dis *38*, 154-166.

Guo, N., Hawkins, C., and Nathans, J. (2004). Frizzled6 controls hair patterning in mice. Proc Natl Acad Sci U S A *101*, 9277-9281.

Guthrie, S. (2007). Patterning and axon guidance of cranial motor neurons. Nat Rev Neurosci *8*, 859-871.

Guthrie, S., and Lumsden, A. (1991). Formation and regeneration of rhombomere boundaries in the developing chick hindbrain. Development *112*, 221-229.

Hafezparast, M., Klocke, R., Ruhrberg, C., Marquardt, A., Ahmad-Annuar, A., Bowen, S., Lalli, G., Witherden, A.S., Hummerich, H., Nicholson, S.*, et al.* (2003). Mutations in dynein link motor neuron degeneration to defects in retrograde transport. Science *300*, 808-812.

Hagman, J., Belanger, C., Travis, A., Turck, C.W., and Grosschedl, R. (1993). Cloning and functional characterization of early B-cell factor, a regulator of lymphocyte-specific gene expression. Genes Dev *7*, 760-773.

Hagman, J., Gutch, M.J., Lin, H., and Grosschedl, R. (1995). EBF contains a novel zinc coordination motif and multiple dimerization and transcriptional activation domains. Embo J *14*, 2907-2916.

Hamblet, N.S., Lijam, N., Ruiz-Lozano, P., Wang, J., Yang, Y., Luo, Z., Mei, L., Chien, K.R., Sussman, D.J., and Wynshaw-Boris, A. (2002). Dishevelled 2 is essential for cardiac outflow tract development, somite segmentation and neural tube closure. Development *129*, 5827-5838.

Harada, A., Takei, Y., Kanai, Y., Tanaka, Y., Nonaka, S., and Hirokawa, N. (1998). Golgi vesiculation and lysosome dispersion in cells lacking cytoplasmic dynein. J Cell Biol *141*, 51-59.

Harfe, B.D., Scherz, P.J., Nissim, S., Tian, H., McMahon, A.P., and Tabin, C.J. (2004). Evidence for an expansion-based temporal Shh gradient in specifying vertebrate digit identities. Cell *118*, 517-528.

Harlow, E., and Lane, D. (2006a). Binding Antibodies to Tissue Sections. Cold Spring Harb Protoc *2006*, pdb.prot4331-.

Harlow, E., and Lane, D. (2006b). Mounting Samples in Gelvatol or Mowiol. Cold Spring Harb Protoc *2006*, pdb.prot4461-.

Harlow, E., and Lane, D. (2006c). Preparing Frozen Tissue Sections for Immunostaining. Cold Spring Harb Protoc *2006*, pdb.prot4328-.

Hatten, M.E. (1999). Central nervous system neuronal migration. Annu Rev Neurosci *22*, 511-539.

Hatten, M.E. (2002). New directions in neuronal migration. Science *297*, 1660-1663.

Hiesberger, T., Trommsdorff, M., Howell, B.W., Goffinet, A., Mumby, M.C., Cooper, J.A., and Herz, J. (1999). Direct binding of Reelin to VLDL receptor and ApoE receptor 2 induces tyrosine phosphorylation of disabled-1 and modulates tau phosphorylation. Neuron *24*, 481-489.

Higashijima, S., Hotta, Y., and Okamoto, H. (2000). Visualization of cranial motor neurons in live transgenic zebrafish expressing green fluorescent protein under the control of the islet-1 promoter/enhancer. J Neurosci *20*, 206-218.

Honda, T., Tabata, H., and Nakajima, K. (2003). Cellular and molecular mechanisms of neuronal migration in neocortical development. Semin Cell Dev Biol *14*, 169-174.

Hong, K., Hinck, L., Nishiyama, M., Poo, M.M., Tessier-Lavigne, M., and Stein, E. (1999). A ligand-gated association between cytoplasmic domains of UNC5 and DCC family receptors converts netrin-induced growth cone attraction to repulsion. Cell *97*, 927-941.

Horwitz, R., and Webb, D. (2003). Cell migration. Curr Biol *13*, R756-759.

Howell, B.W., Hawkes, R., Soriano, P., and Cooper, J.A. (1997). Neuronal position in the developing brain is regulated by mouse disabled-1. Nature *389*, 733-737.

Jessen, J.R., Topczewski, J., Bingham, S., Sepich, D.S., Marlow, F., Chandrasekhar, A., and Solnica-Krezel, L. (2002). Zebrafish trilobite identifies new roles for Strabismus in gastrulation and neuronal movements. Nat Cell Biol *4*, 610-615.

Joyner, A., and Wall, N. (2008). Immunohistochemistry of Whole-Mount Mouse Embryos. Cold Spring Harb Protoc *2008*, pdb.prot4820-.

Jung, J.W., Shin, W.S., Song, J., and Lee, S.T. (2004). Cloning and characterization of the full-length mouse Ptk7 cDNA encoding a defective receptor protein tyrosine kinase. Gene *328*, 75-84.

Kallay, L.M., McNickle, A., Brennwald, P.J., Hubbard, A.L., and Braiterman, L.T. (2006). Scribble associates with two polarity proteins, Lgl2 and Vangl2, via distinct molecular domains. J Cell Biochem *99*, 647-664.

Karis, A., Pata, I., van Doorninck, J.H., Grosveld, F., de Zeeuw, C.I., de Caprona, D., and Fritzsch, B. (2001). Transcription factor GATA-3 alters pathway selection of olivocochlear neurons and affects morphogenesis of the ear. J Comp Neurol *429*, 615-630.

Keeling, S.L., Gad, J.M., and Cooper, H.M. (1997). Mouse Neogenin, a DCC-like molecule, has four splice variants and is expressed widely in the adult mouse and during embryogenesis. Oncogene *15*, 691-700.

Keleman, K., and Dickson, B.J. (2001). Short- and long-range repulsion by the Drosophila Unc5 netrin receptor. Neuron *32*, 605-617.

Kibar, Z., Vogan, K.J., Groulx, N., Justice, M.J., Underhill, D.A., and Gros, P. (2001). Ltap, a mammalian homolog of Drosophila Strabismus/Van Gogh, is altered in the mouse neural tube mutant Loop-tail. Nat Genet *28*, 251-255.

Kido, M., Obata, S., Tanihara, H., Rochelle, J.M., Seldin, M.F., Taketani, S., and Suzuki, S.T. (1998). Molecular properties and chromosomal location of cadherin-8. Genomics *48*, 186-194.

Kitsukawa, T., Shimono, A., Kawakami, A., Kondoh, H., and Fujisawa, H. (1995). Overexpression of a membrane protein, neuropilin, in chimeric mice causes anomalies in the cardiovascular system, nervous system and limbs. Development *121*, 4309-4318.

Klein, T.J., and Mlodzik, M. (2005). Planar cell polarization: an emerging model points in the right direction. Annu Rev Cell Dev Biol *21*, 155-176.

Kraus, F., Haenig, B., and Kispert, A. (2001). Cloning and expression analysis of the mouse T-box gene tbx20. Mech Dev *100*, 87-91.

Kumada, T., Jiang, Y., Kawanami, A., Cameron, D.B., and Komuro, H. (2009). Autonomous turning of cerebellar granule cells in vitro by intrinsic programs. Dev Biol *326*, 237-249.

Kyriakopoulou, K., de Diego, I., Wassef, M., and Karagogeos, D. (2002). A combination of chain and neurophilic migration involving the adhesion molecule TAG-1 in the caudal medulla. Development *129*, 287-296.

Lambert de Rouvroit, C., and Goffinet, A.M. (2001). Neuronal migration. Mech Dev *105*, 47-56.

Lauderdale, J.D., Davis, N.M., and Kuwada, J.Y. (1997). Axon tracts correlate with netrin-1a expression in the zebrafish embryo. Mol Cell Neurosci *9*, 293-313.

Lijam, N., Paylor, R., McDonald, M.P., Crawley, J.N., Deng, C.X., Herrup, K., Stevens, K.E., Maccaferri, G., McBain, C.J., Sussman, D.J.*, et al.* (1997). Social interaction and sensorimotor gating abnormalities in mice lacking Dvl1. Cell *90*, 895-905.

Long, J.M., LaPorte, P., Paylor, R., and Wynshaw-Boris, A. (2004). Expanded characterization of the social interaction abnormalities in mice lacking Dvl1. Genes Brain Behav *3*, 51-62.

Lopez-Bendito, G., Sanchez-Alcaniz, J.A., Pla, R., Borrell, V., Pico, E., Valdeolmillos, M., and Marin, O. (2008). Chemokine signaling controls intracortical migration and final distribution of GABAergic interneurons. J Neurosci *28*, 1613-1624.

Louvi, A., Sisodia, S.S., and Grove, E.A. (2004). Presenilin 1 in migration and morphogenesis in the central nervous system. Development *131*, 3093-3105.

Lu, X., Borchers, A.G., Jolicoeur, C., Rayburn, H., Baker, J.C., and Tessier-Lavigne, M. (2004). PTK7/CCK-4 is a novel regulator of planar cell polarity in vertebrates. Nature *430*, 93-98.

Lumsden, A. (1995). Neural development. A 'LIM code' for motor neurons? Curr Biol *5*, 491-495.

Lumsden, A. (2004). Segmentation and compartition in the early avian hindbrain. Mech Dev *121*, 1081-1088.

Lumsden, A., and Krumlauf, R. (1996). Patterning the vertebrate neuraxis. Science *274*, 1109-1115.

Ma, D., Yang, C.H., McNeill, H., Simon, M.A., and Axelrod, J.D. (2003). Fidelity in planar cell polarity signalling. Nature *421*, 543-547.

Ma, Q.H., Bagnard, D., Xiao, Z.C., and Dawe, G.S. (2008a). A TAG on to the neurogenic functions of APP. Cell Adh Migr *2*, 2-8.

Ma, Q.H., Futagawa, T., Yang, W.L., Jiang, X.D., Zeng, L., Takeda, Y., Xu, R.X., Bagnard, D., Schachner, M., Furley, A.J.*, et al.* (2008b). A TAG1-APP signalling pathway through Fe65 negatively modulates neurogenesis. Nat Cell Biol *10*, 283-294.

Maniatis, T., Fritsch, E.F., and Sambrook, J. (1982). Molecular cloning : a laboratory manual (Cold Spring Harbor, N.Y., Cold Spring Harbor Laboratory).

Manzanares, M., Trainor, P.A., Nonchev, S., Ariza-McNaughton, L., Brodie, J., Gould, A., Marshall, H., Morrison, A., Kwan, C.T., Sham, M.H.*, et al.* (1999). The role of kreisler in segmentation during hindbrain development. Dev Biol *211*, 220-237.

Mapp, O.M., Wanner, S.J., Rohrschneider, M.R., and Prince, V.E. (2010). Prickle1b mediates interpretation of migratory cues during zebrafish facial branchiomotor neuron migration. Dev Dyn *239*, 1596-1608.

Marin, O., and Rubenstein, J.L. (2003). Cell migration in the forebrain. Annu Rev Neurosci *26*, 441-483.

Matise, M.P., Epstein, D.J., Park, H.L., Platt, K.A., and Joyner, A.L. (1998). Gli2 is required for induction of floor plate and adjacent cells, but not most ventral neurons in the mouse central nervous system. Development *125*, 2759-2770.

Medina, M., and Dotti, C.G. (2003). RIPped out by presenilin-dependent gamma-secretase. Cell Signal *15*, 829-841.

Merte, J., Jensen, D., Wright, K., Sarsfield, S., Wang, Y., Schekman, R., and Ginty, D.D. (2010). Sec24b selectively sorts Vangl2 to regulate planar cell polarity during neural tube closure. Nat Cell Biol *12*, 41-46; sup pp 41-48.

Mirmira, R.G., Watada, H., and German, M.S. (2000). Beta-cell differentiation factor Nkx6.1 contains distinct DNA binding interference and transcriptional repression domains. J Biol Chem *275*, 14743-14751.

Miyata, T., Kawaguchi, A., Okano, H., and Ogawa, M. (2001). Asymmetric inheritance of radial glial fibers by cortical neurons. Neuron *31*, 727-741.

Miyata, T., Kawaguchi, A., Saito, K., Kuramochi, H., and Ogawa, M. (2002). Visualization of cell cycling by an improvement in slice culture methods. J Neurosci Res *69*, 861-868.

Mochida, G.H. (2009). Genetics and biology of microcephaly and lissencephaly. Semin Pediatr Neurol *16*, 120-126.

Montcouquiol, M., Rachel, R.A., Lanford, P.J., Copeland, N.G., Jenkins, N.A., and Kelley, M.W. (2003). Identification of Vangl2 and Scrb1 as planar polarity genes in mammals. Nature *423*, 173-177.

Morris, N.R., Efimov, V.P., and Xiang, X. (1998). Nuclear migration, nucleokinesis and lissencephaly. Trends Cell Biol *8*, 467-470.

Mossie, K., Jallal, B., Alves, F., Sures, I., Plowman, G.D., and Ullrich, A. (1995). Colon carcinoma kinase-4 defines a new subclass of the receptor tyrosine kinase family. Oncogene *11*, 2179-2184.

Muller, M., Jabs, N., Lorke, D.E., Fritzsch, B., and Sander, M. (2003). Nkx6.1 controls migration and axon pathfinding of cranial branchio-motoneurons. Development *130*, 5815-5826.

Murdoch, J.N., Doudney, K., Paternotte, C., Copp, A.J., and Stanier, P. (2001). Severe neural tube defects in the loop-tail mouse result from mutation of Lpp1, a novel gene involved in floor plate specification. Hum Mol Genet *10*, 2593-2601.

Murphy, P., Davidson, D.R., and Hill, R.E. (1989). Segment-specific expression of a homoeobox-containing gene in the mouse hindbrain. Nature *341*, 156-159.

Muzumdar, M.D., Tasic, B., Miyamichi, K., Li, L., and Luo, L. (2007). A global double-fluorescent Cre reporter mouse. Genesis *45*, 593-605.

Nadarajah, B., Brunstrom, J.E., Grutzendler, J., Wong, R.O., and Pearlman, A.L. (2001). Two modes of radial migration in early development of the cerebral cortex. Nat Neurosci *4*, 143-150.

Nadarajah, B., and Parnavelas, J.G. (2002). Modes of neuronal migration in the developing cerebral cortex. Nat Rev Neurosci *3*, 423-432.

Nagy, A. (2003). Manipulating the mouse embryo : a laboratory manual, 3rd edn (Cold Spring Harbor, NY, Cold Spring Harbor Laboratory Press).

Nambiar, R.M., Ignatius, M.S., and Henion, P.D. (2007). Zebrafish colgate/hdac1 functions in the non-canonical Wnt pathway during axial extension and in Wnt-independent branchiomotor neuron migration. Mech Dev *124*, 682-698.

Nardelli, J., Thiesson, D., Fujiwara, Y., Tsai, F.Y., and Orkin, S.H. (1999). Expression and genetic interaction of transcription factors GATA-2 and GATA-3 during development of the mouse central nervous system. Dev Biol *210*, 305-321.

Narimatsu, M., Bose, R., Pye, M., Zhang, L., Miller, B., Ching, P., Sakuma, R., Luga, V., Roncari, L., Attisano, L*., et al.* (2009). Regulation of planar cell polarity by Smurf ubiquitin ligases. Cell *137*, 295-307.

Ng, Y.S., Rohan, R., Sunday, M.E., Demello, D.E., and D'Amore, P.A. (2001). Differential expression of VEGF isoforms in mouse during development and in the adult. Dev Dyn *220*, 112-121.

Noctor, S.C., Flint, A.C., Weissman, T.A., Dammerman, R.S., and Kriegstein, A.R. (2001). Neurons derived from radial glial cells establish radial units in neocortex. Nature *409*, 714-720.

Ogawa, M., Miyata, T., Nakajima, K., Yagyu, K., Seike, M., Ikenaka, K., Yamamoto, H., and Mikoshiba, K. (1995). The reeler gene-associated antigen on Cajal-Retzius neurons is a crucial molecule for laminar organization of cortical neurons. Neuron *14*, 899-912.

Ohsawa, R., Ohtsuka, T., and Kageyama, R. (2005). Mash1 and Math3 are required for development of branchiomotor neurons and maintenance of neural progenitors. J Neurosci *25*, 5857-5865.

Ohshima, T., and Mikoshiba, K. (2002). Reelin signaling and Cdk5 in the control of neuronal positioning. Mol Neurobiol *26*, 153-166.

Ohshima, T., Ogawa, M., Takeuchi, K., Takahashi, S., Kulkarni, A.B., and Mikoshiba, K. (2002). Cyclin-dependent kinase 5/p35 contributes synergistically with Reelin/Dab1 to the positioning of facial branchiomotor and inferior olive neurons in the developing mouse hindbrain. J Neurosci *22*, 4036-4044.

Okada, Y., Takeda, S., Tanaka, Y., Belmonte, J.C., and Hirokawa, N. (2005). Mechanism of nodal flow: a conserved symmetry breaking event in left-right axis determination. Cell *121*, 633-644.

Papaioannou, V.E., and Behringer, R. (2005). Mouse phenotypes : a handbook of mutation analysis (Cold Spring Harbor. N.Y., Cold Spring Harbor Laboratory Press).

Park, M., and Moon, R.T. (2002). The planar cell-polarity gene stbm regulates cell behaviour and cell fate in vertebrate embryos. Nat Cell Biol *4*, 20-25.

Parrini, E., Ramazzotti, A., Dobyns, W.B., Mei, D., Moro, F., Veggiotti, P., Marini, C., Brilstra, E.H., Dalla Bernardina, B., Goodwin, L.*, et al.* (2006). Periventricular heterotopia: phenotypic heterogeneity and correlation with Filamin A mutations. Brain *129*, 1892-1906.

Pata, I., Studer, M., van Doorninck, J.H., Briscoe, J., Kuuse, S., Engel, J.D., Grosveld, F., and Karis, A. (1999). The transcription factor GATA3 is a downstream effector of Hoxb1 specification in rhombomere 4. Development *126*, 5523-5531.

Pattyn, A., Hirsch, M., Goridis, C., and Brunet, J.F. (2000). Control of hindbrain motor neuron differentiation by the homeobox gene Phox2b. Development *127*, 1349-1358.

Pattyn, A., Morin, X., Cremer, H., Goridis, C., and Brunet, J.F. (1997). Expression and interactions of the two closely related homeobox genes Phox2a and Phox2b during neurogenesis. Development *124*, 4065-4075.

Pattyn, A., Vallstedt, A., Dias, J.M., Sander, M., and Ericson, J. (2003). Complementary roles for Nkx6 and Nkx2 class proteins in the establishment of motoneuron identity in the hindbrain. Development *130*, 4149-4159.

Paudyal, A., Damrau, C., Patterson, V.L., Ermakov, A., Formstone, C., Lalanne, Z., Wells, S., Lu, X., Norris, D.P., Dean, C.H.*, et al.* (2010). The novel mouse mutant, chuzhoi, has disruption of Ptk7 protein and exhibits defects in neural tube, heart and lung development and abnormal planar cell polarity in the ear. BMC Dev Biol *10*, 87.

Pearlman, A.L., Faust, P.L., Hatten, M.E., and Brunstrom, J.E. (1998). New directions for neuronal migration. Curr Opin Neurobiol *8*, 45-54.

Pfaff, S.L., Mendelsohn, M., Stewart, C.L., Edlund, T., and Jessell, T.M. (1996). Requirement for LIM homeobox gene Isl1 in motor neuron generation reveals a motor neuron-dependent step in interneuron differentiation. Cell *84*, 309-320.

Poirier, K., Keays, D.A., Francis, F., Saillour, Y., Bahi, N., Manouvrier, S., Fallet-Bianco, C., Pasquier, L., Toutain, A., Tuy, F.P.*, et al.* (2007). Large spectrum of lissencephaly and pachygyria phenotypes resulting from de novo missense mutations in tubulin alpha 1A (TUBA1A). Hum Mutat *28*, 1055-1064.

Przyborski, S.A., Knowles, B.B., and Ackerman, S.L. (1998). Embryonic phenotype of Unc5h3 mutant mice suggests chemorepulsion during the formation of the rostral cerebellar boundary. Development *125*, 41-50.

Qu, Y., Glasco, D.M., Zhou, L., Sawant, A., Ravni, A., Fritzsch, B., Damrau, C., Murdoch, J.N., Evans, S., Pfaff, S.L*., et al.* (2010). Atypical Cadherins Celsr1-3 Differentially Regulate Migration of Facial Branchiomotor Neurons in Mice. J Neurosci *30*, 9392-9401.

Ravni, A., Qu, Y., Goffinet, A.M., and Tissir, F. (2009). Planar cell polarity cadherin celsr1 regulates skin hair patterning in the mouse. J Invest Dermatol *129*, 2507-2509.

Rohrschneider, M.R., Elsen, G.E., and Prince, V.E. (2007). Zebrafish Hoxb1a regulates multiple downstream genes including prickle1b. Dev Biol.

Rossel, M., and Capecchi, M.R. (1999). Mice mutant for both Hoxa1 and Hoxb1 show extensive remodeling of the hindbrain and defects in craniofacial development. Development *126*, 5027-5040.

Sadl, V.S., Sing, A., Mar, L., Jin, F., and Cordes, S.P. (2003). Analysis of hindbrain patterning defects caused by the kreisler(enu) mutation reveals multiple roles of Kreisler in hindbrain segmentation. Dev Dyn *227*, 134-142.

Samad, O.A., Geisen, M.J., Caronia, G., Varlet, I., Zappavigna, V., Ericson, J., Goridis, C., and Rijli, F.M. (2004). Integration of anteroposterior and dorsoventral regulation of Phox2b transcription in cranial motoneuron progenitors by homeodomain proteins. Development *131*, 4071-4083.

Sanchez-Alcaniz, J.A., Haege, S., Mueller, W., Pla, R., Mackay, F., Schulz, S., Lopez-Bendito, G., Stumm, R., and Marin, O. (2011). Cxcr7 controls neuronal migration by regulating chemokine responsiveness. Neuron *69*, 77-90.

Sander, M., Paydar, S., Ericson, J., Briscoe, J., Berber, E., German, M., Jessell, T.M., and Rubenstein, J.L. (2000). Ventral neural patterning by Nkx homeobox genes: Nkx6.1 controls somatic motor neuron and ventral interneuron fates. Genes Dev *14*, 2134-2139.

Schneider-Maunoury, S., Seitanidou, T., Charnay, P., and Lumsden, A. (1997). Segmental and neuronal architecture of the hindbrain of Krox-20 mouse mutants. Development *124*, 1215-1226.

Schwarz, Q., Gu, C., Fujisawa, H., Sabelko, K., Gertsenstein, M., Nagy, A., Taniguchi, M., Kolodkin, A.L., Ginty, D.D., Shima, D.T*., et al.* (2004). Vascular endothelial growth factor

controls neuronal migration and cooperates with Sema3A to pattern distinct compartments of the facial nerve. Genes Dev *18*, 2822-2834.

Seitanidou, T., Schneider-Maunoury, S., Desmarquet, C., Wilkinson, D.G., and Charnay, P. (1997). Krox-20 is a key regulator of rhombomere-specific gene expression in the developing hindbrain. Mech Dev *65*, 31-42.

Senzaki, K., Ogawa, M., and Yagi, T. (1999). Proteins of the CNR family are multiple receptors for Reelin. Cell *99*, 635-647.

Serafini, T., Colamarino, S.A., Leonardo, E.D., Wang, H., Beddington, R., Skarnes, W.C., and Tessier-Lavigne, M. (1996). Netrin-1 is required for commissural axon guidance in the developing vertebrate nervous system. Cell *87*, 1001-1014.

Shafer, B., Onishi, K., Lo, C., Colakoglu, G., and Zou, Y. (2011). Vangl2 Promotes Wnt/Planar Cell Polarity-like Signaling by Antagonizing Dvl1-Mediated Feedback Inhibition in Growth Cone Guidance. Dev Cell *20*, 177-191.

Shima, Y., Copeland, N.G., Gilbert, D.J., Jenkins, N.A., Chisaka, O., Takeichi, M., and Uemura, T. (2002). Differential expression of the seven-pass transmembrane cadherin genes Celsr1-3 and distribution of the Celsr2 protein during mouse development. Dev Dyn *223*, 321-332.

Shirasaki, R., Lewcock, J.W., Lettieri, K., and Pfaff, S.L. (2006). FGF as a target-derived chemoattractant for developing motor axons genetically programmed by the LIM code. Neuron *50*, 841-853.

Shnitsar, I., and Borchers, A. (2008). PTK7 recruits dsh to regulate neural crest migration. Development *135*, 4015-4024.

Sittaramane, V., Sawant, A., Wolman, M.A., Maves, L., Halloran, M.C., and Chandrasekhar, A. (2009). The cell adhesion molecule Tag1, transmembrane protein Stbm/Vangl2, and Lamininalpha1 exhibit genetic interactions during migration of facial branchiomotor neurons in zebrafish. Dev Biol *325*, 363-373.

Soker, S. (2001). Neuropilin in the midst of cell migration and retraction. Int J Biochem Cell Biol *33*, 433-437.

Song, H., Hu, J., Chen, W., Elliott, G., Andre, P., Gao, B., and Yang, Y. (2010). Planar cell polarity breaks bilateral symmetry by controlling ciliary positioning. Nature *466*, 378-382.

Song, M.R. (2007). Moving cell bodies: understanding the migratory mechanism of facial motor neurons. Arch Pharm Res *30*, 1273-1282.

Song, M.R., Shirasaki, R., Cai, C.L., Ruiz, E.C., Evans, S.M., Lee, S.K., and Pfaff, S.L. (2006). T-Box transcription factor Tbx20 regulates a genetic program for cranial motor neuron cell body migration. Development *133*, 4945-4955.

Srinivas, S., Watanabe, T., Lin, C.S., William, C.M., Tanabe, Y., Jessell, T.M., and Costantini, F. (2001). Cre reporter strains produced by targeted insertion of EYFP and ECFP into the ROSA26 locus. BMC Dev Biol *1*, 4.

Studer, M. (2001). Initiation of facial motoneurone migration is dependent on rhombomeres 5 and 6. Development *128*, 3707-3716.

Studer, M., Gavalas, A., Marshall, H., Ariza-McNaughton, L., Rijli, F.M., Chambon, P., and Krumlauf, R. (1998). Genetic interactions between Hoxa1 and Hoxb1 reveal new roles in regulation of early hindbrain patterning. Development *125*, 1025-1036.

Studer, M., Lumsden, A., Ariza-McNaughton, L., Bradley, A., and Krumlauf, R. (1996). Altered segmental identity and abnormal migration of motor neurons in mice lacking Hoxb-1. Nature *384*, 630-634.

Suzuki, S., Sano, K., and Tanihara, H. (1991). Diversity of the cadherin family: evidence for eight new cadherins in nervous tissue. Cell Regul *2*, 261-270.

Swiatek, P.J., and Gridley, T. (1993). Perinatal lethality and defects in hindbrain development in mice homozygous for a targeted mutation of the zinc finger gene Krox20. Genes Dev *7*, 2071-2084.

Tada, M., Concha, M.L., and Heisenberg, C.P. (2002). Non-canonical Wnt signalling and regulation of gastrulation movements. Semin Cell Dev Biol *13*, 251-260.

Takagi, S., Kasuya, Y., Shimizu, M., Matsuura, T., Tsuboi, M., Kawakami, A., and Fujisawa, H. (1995). Expression of a cell adhesion molecule, neuropilin, in the developing chick nervous system. Dev Biol *170*, 207-222.

Takeichi, M. (2007). The cadherin superfamily in neuronal connections and interactions. Nat Rev Neurosci *8*, 11-20.

Tanimukai, H., Sato, K., Kudo, T., Kashiwagi, Y., Tohyama, M., and Takeda, M. (1999). Regional distribution of presenilin-1 messenger RNA in the embryonic rat brain: comparison with beta-amyloid precursor protein messenger RNA localization. Neuroscience *90*, 27-39.

Thaler, J., Harrison, K., Sharma, K., Lettieri, K., Kehrl, J., and Pfaff, S.L. (1999). Active suppression of interneuron programs within developing motor neurons revealed by analysis of homeodomain factor HB9. Neuron *23*, 675-687.

Theil, T., Ariza-McNaughton, L., Manzanares, M., Brodie, J., Krumlauf, R., and Wilkinson, D.G. (2002). Requirement for downregulation of kreisler during late patterning of the hindbrain. Development *129*, 1477-1485.

Theveneau, E., Marchant, L., Kuriyama, S., Gull, M., Moepps, B., Parsons, M., and Mayor, R. (2010). Collective chemotaxis requires contact-dependent cell polarity. Dev Cell *19*, 39-53.

Tissir, F., Bar, I., Jossin, Y., De Backer, O., and Goffinet, A.M. (2005). Protocadherin Celsr3 is crucial in axonal tract development. Nat Neurosci *8*, 451-457.

Tissir, F., De-Backer, O., Goffinet, A.M., and Lambert de Rouvroit, C. (2002). Developmental expression profiles of Celsr (Flamingo) genes in the mouse. Mech Dev *112*, 157-160.

Tissir, F., and Goffinet, A.M. (2006). Expression of planar cell polarity genes during development of the mouse CNS. Eur J Neurosci *23*, 597-607.

Tiveron, M.C., Pattyn, A., Hirsch, M.R., and Brunet, J.F. (2003). Role of Phox2b and Mash1 in the generation of the vestibular efferent nucleus. Dev Biol *260*, 46-57.

Torban, E., Kor, C., and Gros, P. (2004a). Van Gogh-like2 (Strabismus) and its role in planar cell polarity and convergent extension in vertebrates. Trends Genet *20*, 570-577.

Torban, E., Wang, H.J., Groulx, N., and Gros, P. (2004b). Independent mutations in mouse Vangl2 that cause neural tube defects in looptail mice impair interaction with members of the Dishevelled family. J Biol Chem *279*, 52703-52713.

Torban, E., Wang, H.J., Patenaude, A.M., Riccomagno, M., Daniels, E., Epstein, D., and Gros, P. (2007). Tissue, cellular and sub-cellular localization of the Vangl2 protein during embryonic development: effect of the Lp mutation. Gene Expr Patterns *7*, 346-354.

Trupp, M., Arenas, E., Fainzilber, M., Nilsson, A.S., Sieber, B.A., Grigoriou, M., Kilkenny, C., Salazar-Grueso, E., Pachnis, V., and Arumae, U. (1996). Functional receptor for GDNF encoded by the c-ret proto-oncogene. Nature *381*, 785-789.

Tsai, L.H., and Gleeson, J.G. (2005). Nucleokinesis in neuronal migration. Neuron *46*, 383-388.

Tsai, L.H., Takahashi, T., Caviness, V.S., Jr., and Harlow, E. (1993). Activity and expression pattern of cyclin-dependent kinase 5 in the embryonic mouse nervous system. Development *119*, 1029-1040.

Tucker, E.S., Polleux, F., and LaMantia, A.S. (2006). Position and time specify the migration of a pioneering population of olfactory bulb interneurons. Dev Biol *297*, 387-401.

Umeshima, H., Hirano, T., and Kengaku, M. (2007). Microtubule-based nuclear movement occurs independently of centrosome positioning in migrating neurons. Proc Natl Acad Sci U S A *104*, 16182-16187.

Valiente, M., and Marin, O. (2010). Neuronal migration mechanisms in development and disease. Curr Opin Neurobiol *20*, 68-78.

Varela-Echavarria, A., Pfaff, S.L., and Guthrie, S. (1996). Differential expression of LIM homeobox genes among motor neuron subpopulations in the developing chick brain stem. Mol Cell Neurosci *8*, 242-257.

Veeman, M.T., Axelrod, J.D., and Moon, R.T. (2003). A second canon. Functions and mechanisms of beta-catenin-independent Wnt signaling. Dev Cell *5*, 367-377.

Vielmetter, J., Kayyem, J.F., Roman, J.M., and Dreyer, W.J. (1994). Neogenin, an avian cell surface protein expressed during terminal neuronal differentiation, is closely related to the human tumor suppressor molecule deleted in colorectal cancer. J Cell Biol *127*, 2009-2020.

Vivancos, V., Chen, P., Spassky, N., Qian, D., Dabdoub, A., Kelley, M., Studer, M., and Guthrie, S. (2009). Wnt activity guides facial branchiomotor neuron migration, and involves the PCP pathway and JNK and ROCK kinases. Neural Dev *4*, 7.

Voiculescu, O., Charnay, P., and Schneider-Maunoury, S. (2000). Expression pattern of a Krox-20/Cre knock-in allele in the developing hindbrain, bones, and peripheral nervous system. Genesis *26*, 123-126.

Voiculescu, O., Taillebourg, E., Pujades, C., Kress, C., Buart, S., Charnay, P., and Schneider-Maunoury, S. (2001). Hindbrain patterning: Krox20 couples segmentation and specification of regional identity. Development *128*, 4967-4978.

Wada, H., Iwasaki, M., Sato, T., Masai, I., Nishiwaki, Y., Tanaka, H., Sato, A., Nojima, Y., and Okamoto, H. (2005). Dual roles of zygotic and maternal Scribble1 in neural migration and convergent extension movements in zebrafish embryos. Development *132*, 2273-2285.

Wada, H., Tanaka, H., Nakayama, S., Iwasaki, M., and Okamoto, H. (2006). Frizzled3a and Celsr2 function in the neuroepithelium to regulate migration of facial motor neurons in the developing zebrafish hindbrain. Development *133*, 4749-4759.

Wallingford, J.B., Fraser, S.E., and Harland, R.M. (2002). Convergent extension: the molecular control of polarized cell movement during embryonic development. Dev Cell *2*, 695-706.

Wallingford, J.B., and Harland, R.M. (2002). Neural tube closure requires Dishevelled-dependent convergent extension of the midline. Development *129*, 5815-5825.

Wang, J., Mark, S., Zhang, X., Qian, D., Yoo, S.J., Radde-Gallwitz, K., Zhang, Y., Lin, X., Collazo, A., Wynshaw-Boris, A*., et al.* (2005). Regulation of polarized extension and

planar cell polarity in the cochlea by the vertebrate PCP pathway. Nat Genet *37*, 980-985.

Wang, Y., Guo, N., and Nathans, J. (2006). The role of Frizzled3 and Frizzled6 in neural tube closure and in the planar polarity of inner-ear sensory hair cells. J Neurosci *26*, 2147-2156.

Wang, Y., and Nathans, J. (2007). Tissue/planar cell polarity in vertebrates: new insights and new questions. Development *134*, 647-658.

Wang, Z., Gerstein, M., and Snyder, M. (2009). RNA-Seq: a revolutionary tool for transcriptomics. Nat Rev Genet *10*, 57-63.

Wilson-Pauwels, L., Akesson, E.J., and Stewart, P.A. (1988). Cranial nerves : anatomy and clinical comments (Toronto ; Philadelphia, B.C. Decker ; Saint Louis, Mo. : C.V. Mosby distributor).

Wilson, V., and Conlon, F.L. (2002). The T-box family. Genome Biol *3*, REVIEWS3008.

Wong, H.C., Bourdelas, A., Krauss, A., Lee, H.J., Shao, Y., Wu, D., Mlodzik, M., Shi, D.L., and Zheng, J. (2003). Direct binding of the PDZ domain of Dishevelled to a conserved internal sequence in the C-terminal region of Frizzled. Mol Cell *12*, 1251-1260.

Ybot-Gonzalez, P., Savery, D., Gerrelli, D., Signore, M., Mitchell, C.E., Faux, C.H., Greene, N.D., and Copp, A.J. (2007). Convergent extension, planar-cell-polarity signalling and initiation of mouse neural tube closure. Development *134*, 789-799.

Yen, W.W., Williams, M., Periasamy, A., Conaway, M., Burdsal, C., Keller, R., Lu, X., and Sutherland, A. (2009). PTK7 is essential for polarized cell motility and convergent extension during mouse gastrulation. Development *136*, 2039-2048.

Zheng, M., Leung, C.L., and Liem, R.K. (1998). Region-specific expression of cyclin-dependent kinase 5 (cdk5) and its activators, p35 and p39, in the developing and adult rat central nervous system. J Neurobiol *35*, 141-159.

Zhou, L., Bar, I., Achouri, Y., Campbell, K., De Backer, O., Hebert, J.M., Jones, K., Kessaris, N., de Rouvroit, C.L., O'Leary, D.*, et al.* (2008). Early forebrain wiring: genetic dissection using conditional Celsr3 mutant mice. Science *320*, 946-949.

VITA

Derrick Michael Glasco was born on October 10, 1982, in Aurora, Missouri, to Michael and Delilah Glasco. After spending the golden years of his childhood in Charleston, SC, and Orlando, FL, his family returned to Missouri. Derrick's interest in science was sparked during his sophomore year of high school while hospitalized for a spontaneous collapsed lung. After watching a video of his surgery and enjoying close interactions with his physicians, he decided to pursue a career in medicine. He graduated from Nevada High School in 2000 with an emphasis in health sciences, then went on to major in biology at Missouri Southern State University in Joplin, Missouri. Through many class discussions, he became most intrigued with the "unknowns" in biology; thus, he decided to pursue an academic career and completed a summer research internship in the Department of Biochemistry at Iowa State University in 2003. He then graduated with a B.S. in Biology and a minor in Chemistry in 2004 with multiple honors. After a short and much enjoyable hiatus as a Park Guide at George Washington Carver National Monument in Diamond, MO, he began his graduate studies at the University of Missouri in 2005 and was subsequently awarded his Ph.D. in Biological Sciences in 2011. In August 2011, he will begin his appointment as an Assistant Professor of Biology at Bob Jones University in Greenville, SC.